PB94-157658

REPORT NO.
UCB/EERC-93/07
DECEMBER 1993

EARTHQUAKE ENGINEERING RESEARCH CENTER

EARTHQUAKE ANALYSIS AND RESPONSE OF CONCRETE GRAVITY DAMS INCLUDING BASE SLIDING

by

JUAN W. CHAVEZ
GREGORY L. FENVES

Report to the National Science Foundation

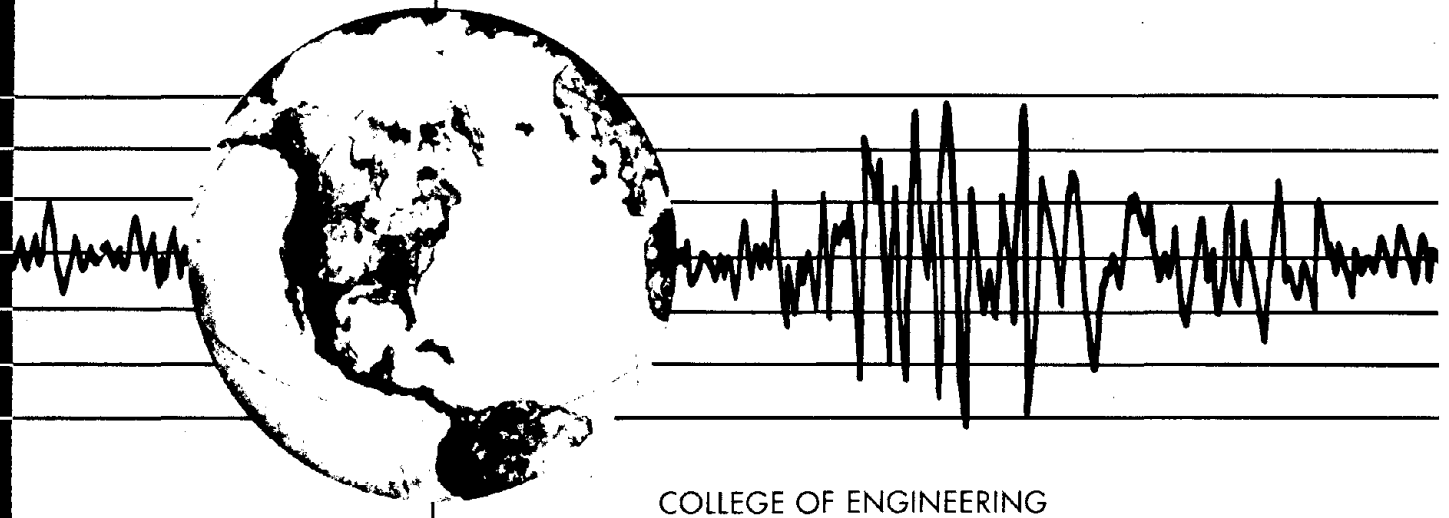

COLLEGE OF ENGINEERING

UNIVERSITY OF CALIFORNIA AT BERKELEY

ABSTRACT

The stability of a concrete gravity dam against sliding along the interface between the dam base and the foundation rock must be assured in a seismic safety evaluation. For this type of evaluation, a new numerical method is used to compute the earthquake response of gravity dams, including base sliding. The hybrid frequency-time domain procedure accounts for the nonlinear base sliding behavior of the dam and the frequency-dependent response of the impounded water and the flexible foundation rock.

The results of a parameter study of typical gravity dams show how the earthquake-induced sliding is affected by the different characteristics of the ground motion and dam system. Gravity dam monoliths may slide downstream, depending on the coefficient of friction for the interface zone and the peaks in the earthquake ground acceleration record. Although the dam remains stable after the earthquake, base sliding displacements may produce damage in the interface zone.

The cases investigated demonstrate that it is necessary to include the effects of dam-foundation rock interaction to obtain realistic estimates of the base sliding displacement for a dam. The assumption of rigid foundation rock overestimates the base sliding displacement. The sliding displacement is sensitive to the value of the coefficient of friction for the interface zone, especially for moderate to tall dams. Water compressibility and reservoir bottom absorption affect the base sliding displacement of dams on rigid foundation rock, but they are less important for dams on flexible foundation rock. Although base sliding may be interpreted as an isolation and damping mechanism for the dam, it has little effect on reducing the maximum stresses in the monolith.

ACKNOWLEDGEMENTS

The research reported herein has been sponsored by the National Science Foundation under Grant No. BCS-8896121. The Government has certain rights to this material. Any opinions, findings, and conclusions or recommendations expressed in this material are those of the authors and do not necessarily reflect the views of the National Science Foundation.

The authors wish to thank the program director, Dr. Shih-Chi Liu, for his continued support of this research.

TABLE OF CONTENTS

LIST OF FIGURES

LIST OF TABLES

Chapter 1

INTRODUCTION

Concrete gravity dams are important structures that are constructed to retain large quantities of water in a reservoir. The safety of a dam during severe load conditions, such as due to earthquake ground motion, must be verified because of the catastrophic consequences of a sudden release of the reservoir. One potential failure mode of a concrete gravity dam during an earthquake is extensive cracking and deformation in the zone between the base of the dam and the foundation rock. The interface zone is often a weak link in the transfer of seismic forces between the foundation rock and the dam monoliths. Failure of the zone can result in a relative displacement between the dam and the foundation rock, a displacement which is often called a base sliding displacement.

The earthquake safety evaluation of a dam involves many aspects, one of which is verifying that the dam will remain stable during and after an earthquake, in the sense that the base sliding displacement is not excessive. The traditional check of sliding stability involves computing a factor of safety against sliding based on a friction model of the interface zone and equivalent static loads that represent the dynamic effects of an earthquake on the dam. It has been observed that a static stability criterion is not appropriate for evaluating the base sliding displacement of a dam due to oscillatory and transient ground motion [Zhang and Chopra, 1991].

The development of mathematical models which are able to predict the earth-

quake response of concrete gravity dams, including interface zone deformation, is a complex problem. Since the dam-foundation rock interface is a complicated zone, for which it is difficult to collect data about, it is common to use a friction model for earthquake analysis [Danay and Adeghe, 1993]. The problem is also complicated because the response of the dam depends on interaction between the dam and compressible water, and between the dam and the flexible foundation rock region.

1.1 Studies on Sliding Response of Gravity Dams

To account for the dynamics of dam systems during an earthquake, various analyses of the base sliding response of concrete gravity dams have been performed. Leger and Katsouli [1989] studied the stability of concrete gravity dams using a finite element formulation for the dam, water, and foundation rock, and gap-friction elements to model the sliding at the base interface. The response was computed for a short time (3 sec) and the results indicated that the nonlinear behavior of the dam-foundation rock interface reduced the seismic response of the dam. Using the sliding block concept introduced by Newmark [1965], Danay and Adeghe [1993] developed an empirical formula, based on a statistical regression of many simplified dynamic analyses, for estimating the seismic slip of concrete gravity dams. The impounded water was assumed incompressible in this study, and the dam-rock interface was modeled by gap-friction elements. The study was restricted to short dams of height less than 60 m. Chopra and Zhang [1991] studied the sliding response of gravity dams on rigid foundation rock using a simplified model. Base sliding was shown to be more important than rocking of the dam in the cases considered.

Danay and Adeghe [1993], and Chopra and Zhang [1991], provided several methods to estimate the earthquake-induced base sliding displacement of gravity dams. The scope of results, however, are limited because the models did not include important factors, such as dam-foundation rock interaction and water compressibility. Leger and Katsouli [1989] included dam-foundation rock interaction, although water compressibility was not considered. Since these factors may have an important effect on the base sliding displacement, the present study includes dam-water interaction, with water compressibility and reservoir bottom absorption, and dam-foundation rock interaction.

1.2 Modeling of Dam Systems

There are several strategies for modeling and computing the nonlinear earthquake response of dam-reservoir-foundation rock systems, including base sliding. It is generally accepted that long dams respond to strong earthquakes as two-dimensional monoliths. In this study, tensile cracking and other nonlinear material behavior of the dam concrete are not included in the model. The arbitrary geometry and idealized linear elastic properties of a monolith are conveniently represented by a finite element discretization.

The interface zone between the dam base and the foundation rock is very complex. Rigorous modeling of the interface zone would require a sophisticated constitutive model that represents the cyclic behavior of the concrete and foundation rock and the actual interface conditions. Another approach is to consider the interface as a discrete joint between the dam monolith and the foundation rock region.

Joint elements at the interface may be used to approximate the behavior of the contact materials in a finite element analysis [Toki, Sato, and Miura, 1980]. Models using nonlinear gap-friction contact elements between the dam and foundation rock surface follow this approach [Leger and Katsouli, 1989]. An even simpler approach is to assume that the force-displacement relationship at the interface is governed by a friction model [Chopra and Zhang, 1991]. The advantage of the friction model is that it does not require detailed information about the constitution of the concrete and rock materials, but rather only an effective friction coefficient and cohesion force for the interface zone.

As for the water domain, it can be discretized by finite elements or boundary elements, with a choice for the response variable such as pressure [Saini, Bettess, and Zienkiewicz, 1978] or potential of velocity or displacement [Zienkiewicz, Paul, and Hinton, 1982]. However, these approaches require solving unsymmetric equations of motion. Staggered or partitioned solution algorithms, in which each domain is solved separately, can also be used [Park and Felippa, 1980].

Another formulation uses the displacement of the water as the response variable [Bathe and Hahn, 1979; Fenves and Vargas-Loli, 1988]. The advantage is that the fluid elements can be easily coupled to the dam elements and the equations of motion are symmetric. A time dependent radiation boundary condition is necessary to approximate the large upstream extent of the impounded water. Recent work [Tsai, Lee, and Ketter, 1990] has resulted in a time domain radiation boundary condition that can be used with a small discretized region of the water.

The water domain can be, alternatively, represented as continuous medium.

The frequency-dependent hydrodynamic pressures are computed in the frequency domain to account for the compressibility of water and reservoir bottom absorption. This formulation has been extensively used for the linear analysis of concrete gravity dams in the frequency domain [Chopra, 1967; Chopra, Chakrabarti, and Gupta 1980; Fenves and Chopra, 1984a]. The response of the fluid can also be computed by a convolution integral in the time domain, using the unit impulse functions for the water. The efficiency can be increased by recursive evaluation of the unit impulse functions [Wolf and Motosuka, 1989].

The foundation rock introduces flexibility and damping into the dam system. The energy dissipation arises from material damping and radiation damping. The foundation rock region can be modeled by finite elements or boundary elements, but again the radiation damping can be only approximated in the time domain. An alternative approach widely used is to consider the foundation rock as an viscoelastic half-plane for the computation of dam-foundation rock interaction effects in the frequency domain.

1.3 Methods of Analysis

Direct time integration methods [Newmark, 1959] are used to solve nonlinear equations of motion in which the properties of the system are independent of the excitation frequency. When the frequency-dependent characteristics of the hydrodynamic pressure and foundation rock interface forces are included in the linear analysis of dams, a frequency domain solution is preferable. For nonlinear models, such as due to base sliding, a frequency domain solution is not possible because the forces are

nonlinear functions of the past and present state of the system, so the superposition used in frequency domain analysis is not applicable. Thus, the step from linear to nonlinear models has a major consequence: the powerful frequency domain technique is no longer directly applicable. A time domain procedure is necessary to evaluate the nonlinear forces.

Several related iterative approaches have been used for the solution of nonlinear systems with frequency-dependent properties:

- The force correction method [Stricklin and Haisler, 1977] has been modified for frequency domain analysis of offshore structures [Lima and De-Lima, 1986].

- The alternating frequency (AFT) method [Cameron and Griffin, 1989] has been used to solve problems involving friction. The convolution integrals and convergence are evaluated in the frequency domain, and the nonlinear forces are evaluated in the time domain.

- The hybrid frequency-time domain (HFTD) approach [Kawamoto, 1983] has been applied for the solution of soil-structure problems [Darbre and Wolf, 1988]. In this approach, the equations of motion are solved in the frequency domain, including the frequency-dependent properties, and the nonlinear forces are evaluated in the time domain.

The hybrid frequency-time domain procedure is used in this study to compute the nonlinear earthquake response of gravity dams including sliding at the base. The nonlinear terms in the equations of motion are linearized, and the linearized equations,

including the frequency-dependent terms due to dam-water interaction and dam-foundation rock interaction, are solved in the frequency domain. Since the unbalanced forces are a function of the current state of the system, it is necessary to iterate to obtain a solution that satisfies the force-displacement relationship for the interface zone. The HFTD method has been applied for the nonlinear earthquake analysis of simplified models of concrete gravity dams [Fenves and Chávez, 1990].

1.4 Objective of Study

The first objective of this study is to develop the HFTD procedure for computing the nonlinear sliding response of concrete gravity dams during earthquakes. The model includes dam-water interaction, with water compressibility and reservoir bottom absorption, and dam-foundation rock interaction. The dam is modeled using finite elements, the water reservoir is modeled as a continuous, inviscid and compressible medium, and the foundation rock is modeled as a viscoelastic half-plane.

The second objective is to perform a detailed analysis of the earthquake response of a typical dam, Pine Flat, using the numerical procedure. The purpose of the case study is to investigate how the ground motion, foundation rock flexibility, and the coefficient of friction influences the base sliding of the dam and other response quantities.

The third objective is to perform a extensive parameter study on typical concrete gravity dams to further investigate how the sliding displacement is affected by other parameters, such as height of the dam, water compressibility, reservoir bottom materials, and modulus of elasticity of concrete.

1.5 Organization of Report

Chapter 2 describes the gravity dam model considered in this study. Assumptions regarding the model, particularly the characteristics of the dam-foundation rock interface are presented.

Chapter 3 presents the formulation of the analysis procedure to compute the earthquake response of the dam-water-foundation rock system including sliding at the interface. The computational procedure is based on the hybrid frequency-time domain (HFTD) method, in which the equations of motion are solved in the frequency domain and the determination of the sliding state is performed in the time domain.

Chapter 4 presents the implementation of the HFTD procedure including the algorithm for the iteration. It presents the idea of time segmentation to improve convergence of the solution.

Chapter 5 presents a detailed case study of the earthquake response of Pine Flat dam including base sliding. The effects of a range of properties for the dam and foundation rock and various earthquake ground motions on the response of the dam are investigated.

Chapter 6 presents a parameter study of the base sliding displacement of typical concrete gravity dams using a simplified dam model. The influence of the ground motion, water compressibility, coefficient of friction, modulus of elasticity of concrete, reservoir bottom absorption coefficient, and foundation rock flexibility, on the base sliding of dams with a range of heights is investigated.

Chapter 7 presents the conclusions regarding the influence of parameters that affect the earthquake-induced base sliding response of concrete gravity dams.

Chapter 2

IDEALIZATION OF THE DAM SYSTEM

2.1 Introduction

Conventional concrete gravity dams are constructed as monoliths separated by vertical expansion joints. For the large amplitude motion expected during strong earthquakes, the shear forces transmitted across the joints are small compared with the inertia forces and the monoliths will tend to vibrate independently [Rea, Liaw, and Chopra, 1975]. Consequently, a two-dimensional model of individual monoliths can be used to determine the response of long concrete gravity dams for moderate to strong earthquakes.

The idealized concrete gravity dam monolith considered in this study is shown in Figure 2.1. The two-dimensional monolith with rigid base is supported by flexible foundation rock and impounds a reservoir of compressible water. The dam is allowed to slide along the interface between the dam base and the foundation rock. The base interface with the foundation rock may be inclined, although this entails an approximation of the domains. Sliding of the dam is the only source of nonlinearity in the system. Other nonlinearities, such as concrete cracking, opening and sliding of joints, and water cavitation are not represented in the model.

The system is subjected to horizontal and vertical components of free-field earthquake ground motion acting at the base of the dam. The free-field ground accel-

eration is assumed to result from vertically propagating shear waves in the foundation rock, so kinematic interaction effects with the dam are neglected. Static loads, such as hydrostatic pressure, dead weight, and uplift forces, exist prior to and during the earthquake.

The interface between the dam monolith and the foundation rock region is a complex zone of shear keys, grout curtains, and roughened surfaces. Modeling the complex dam-foundation rock interface in an earthquake analysis would require a very detailed finite element model. In this study a simpler approach is adopted. The interface is assumed to be a straight surface in the two-dimensional model with the resistance to sliding governed by the Mohr-Coulomb law for friction resistance. This type of model allows quantification of the effects of sliding during an earthquake without requiring a detailed modeling of the interface zone.

Sliding occurs when the base shear force exceeds the shear strength of the base-foundation rock interface. Sliding of the dam along the interface is the dominant motion compared with rocking of the dam. Rocking of the monolith under the seismic loading is not considered in this study because rocking effects are small compared with the motion of the dam due to sliding. A preliminary study by Chopra and Zhang [1991], using a simplified model for gravity dams, showed that a dam slides downstream before it rocks because of the large hydrostatic force acting in that direction. Even when rocking is initiated, the rotation is small because of the relatively small height-to-width ratio of gravity dams.

The assumption of a rigid dam base at the interface with the foundation rock is appropriate for computing the earthquake response of concrete gravity dams be-

cause the base deformations have little influence on the dam response [Fenves and Chopra, 1984a]. The foundation rock surface extends to infinity in the downstream and upstream directions. When the interface is sloped, the model has discontinuities between the foundation rock and water domains. The discontinuity between the foundation rock and the bottom of the reservoir can be neglected provided that the angle of inclination, β, at the interface is small.

2.2 Dam Domain

The monolith is modeled using plane stress finite elements, allowing representation of a general geometry, and linear elastic, orthotropic material properties. The upstream face of the dam should be vertical, or near vertical. This condition is necessary because the hydrodynamic pressure acting on the dam is computed assuming the upstream face is vertical. The base of the dam is assumed rigid, and it should be straight, or near straight, at the angle of inclination, β. Under this condition, a single sliding displacement represents the sliding motion of the dam at the interface.

2.3 Water Domain

The water impounded in the reservoir is idealized as a two-dimensional domain extending to infinity in the upstream direction. The water is treated as an inviscid and compressible fluid. The upstream face of the dam is assumed vertical and the reservoir bottom is assumed horizontal for computing the hydrodynamic pressure. Because of water compressibility, the hydrodynamic pressure is dependent on the excitation frequency.

The bottom of a reservoir consists of highly variable layers of bedrock, silt and other sedimentary materials. The effect of the reservoir bottom materials has been the subject of several recent investigations. A simplified analysis, which neglects the coupling between the foundation rock and reservoir [Fenves and Chopra, 1984a], assumes that the reservoir bottom materials are accounted for by the wave reflection coefficient, α. In the absence of experimental data, a wave reflection coefficient of 0.9 for newer dams and 0.7 for older dams having more sediments has been recommended [Chopra, 1988].

Other models [Lotfi, Roesset, and Tassoulas, 1987; Bougacha and Tassoulas, 1991] represent the sediments as a soft, nearly incompressible, viscoelastic solid. In a recent study by Humar and Chandrashaker [1992], a rigorous model was used to represent the fluid-foundation rock effect including coupling between the dam-foundation rock and the rock below the reservoir. It was concluded that the simplified approach with the wave reflection coefficient is fairly accurate. This approach is used in the current study.

2.4 Foundation Rock Domain

The inclusion of dam-foundation rock interaction introduces flexibility at the base of the dam and provides additional damping mechanisms, through material damping and radiation. The foundation rock is idealized as a homogeneous, isotropic and viscoelastic half-plane for the purpose of computing the impedance functions that characterize the dam-foundation rock interaction. The half-plane idealization of the foundation rock region is only approximately correct for dams with an inclined

base because of the discontinuities at the surface. It is assumed, however, that this approximation is still applicable for dams with a base having a small angle, β, of inclination.

The impedance matrix for a viscoelastic half-plane is computed by using the approach by Dasgupta and Chopra [1979]. Other approaches [Wolf and Darbre, 1984; Alarcon, Dominguez, and Cano, 1980] use boundary element methods and Green's functions to analyze the problem. A layered soil or a hybrid modeling of a single-layer can be also used [Zong and Penzien, 1986].

2.5 Sliding Interface Characteristics

A Mohr-Coulomb friction model is used to model the behavior of the sliding interface between the dam base and the foundation rock surface. The sliding resistance at the interface depends on a cohesion force, the coefficient of friction, and the time varying normal force. As mentioned previously, dam rocking and uplift are not considered in the model. The possibility of water intrusion into open cracks at the base, which could lead to additional forces, is also not considered.

In reality, the cohesion force varies along the interface because the contact conditions between the dam and the foundation rock surface change during sliding. In the analysis, however, the cohesion is represented by a constant equivalent value, which may represent an average value between the cohesion force when there is no sliding, and the cohesion force for large values of sliding displacement. An assumption of zero cohesion represents the fact that little cohesive resistance can be expected during large earthquake-induced sliding of a dam.

The coefficient of friction is influenced by the contact conditions, direction and velocity of motion, and magnitude of the ground excitation [Zadnik and Paskalov, 1992]. A constant equivalent coefficient of friction is used in this study. Selection of an appropriate value for this coefficient of friction is difficult because of the complex nature of the interface zone. Values between 0.7 to 1.2 have been recommended [Chopra and Zhang, 1991; Danay and Adeghe, 1993] for use in seismic evaluation.

The normal forces are distributed along the base. They include the gravity forces, uplift forces, and time-varying normal forces due to the dynamic response. For the Mohr-Coulomb model, only the resultant normal force at the base is needed to determine the sliding state of the dam.

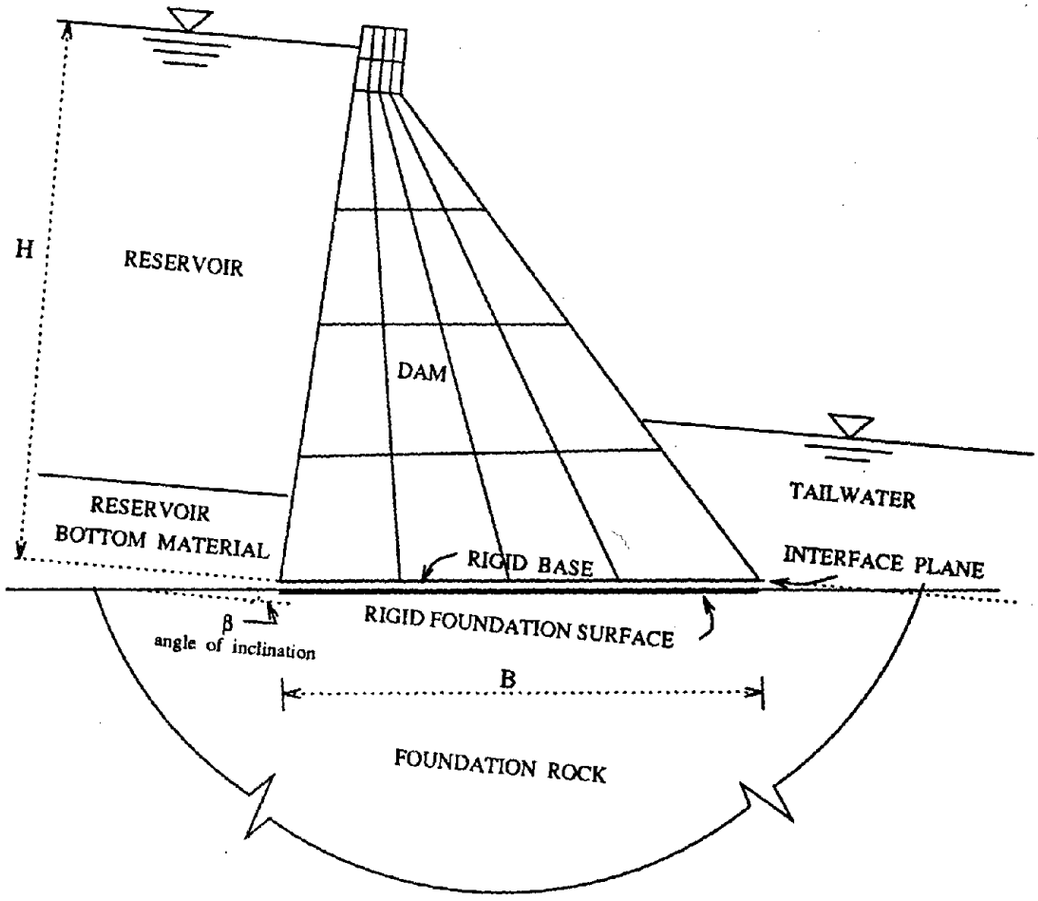

Figure 2.1. Dam-reservoir-foundation rock system with interface plane for sliding at the base.

Chapter 3

FORMULATION OF THE ANALYSIS METHOD

3.1 Introduction

The equations of motion for the dam-water-foundation rock system are formulated in this chapter, based on the substructure approach. Figure 3.1 shows the three substructures and the sliding interface. The equations of motion include the frequency-dependent hydrodynamic forces acting on the dam and the dam-foundation rock interaction forces. The sliding of the dam along the foundation rock surface produces additional inertia forces on the dam and introduces nonlinear behavior into the otherwise linear model.

The solution of the nonlinear equations of motion with frequency-dependent forces is computed using the hybrid frequency-time domain (HFTD) procedure [Kawamoto, 1983; Darbre and Wolf, 1988]. The chapter presents the application of the iterative procedure to the solution of the equations of motion for the dam system.

3.2 Equations of Motion for the Dam

The equations of motion for a finite element discretization of the dam with a rigid, but sliding, interface at the base are:

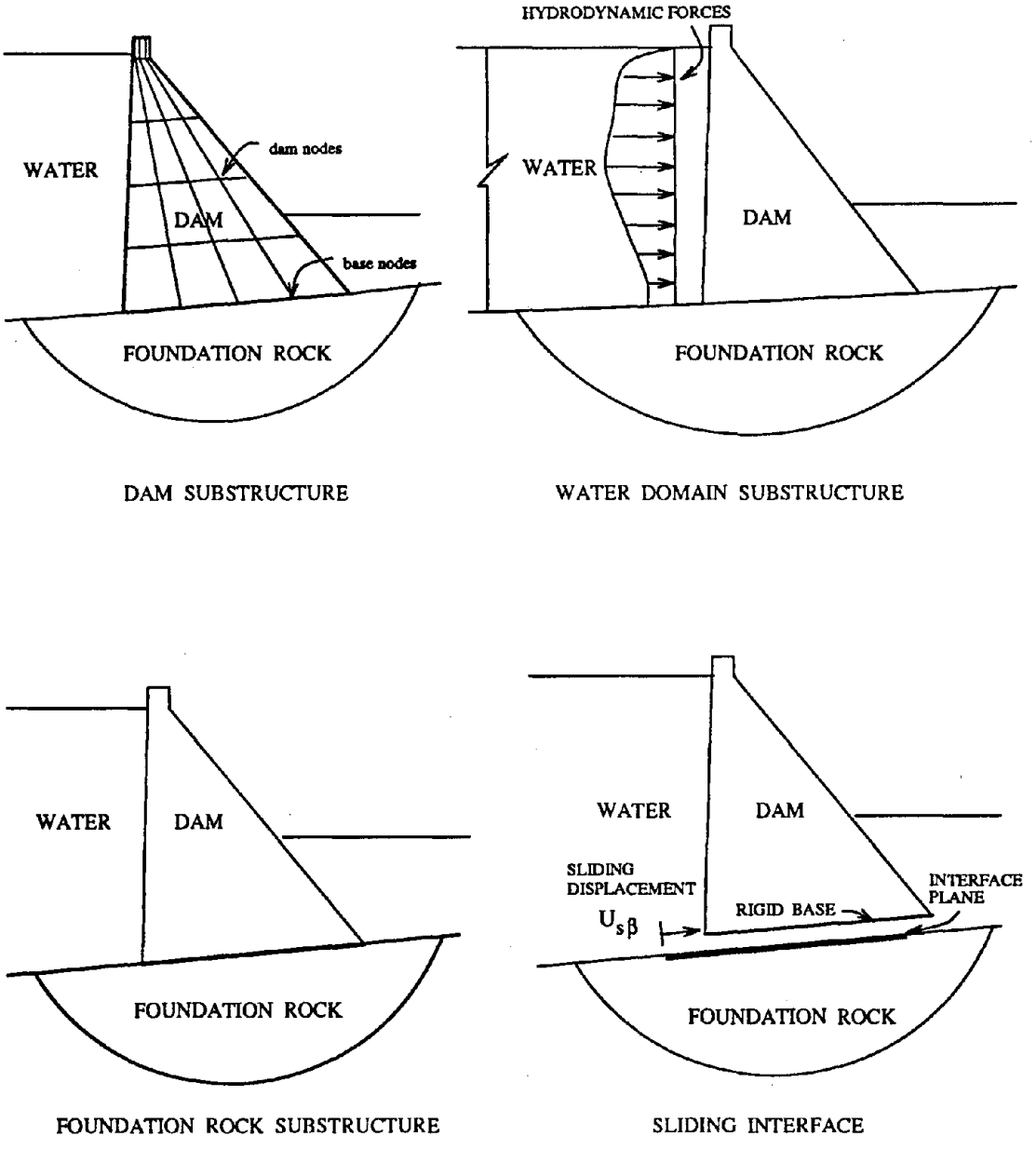

Figure 3.1. Substructures in dam-water-foundation rock system and sliding interface.

$$\mathbf{M\ddot{U}} + \mathbf{C\dot{U}} + \mathbf{KU} + \mathbf{MR\ddot{U}}_f + \mathbf{F}_{sd}(\ddot{U}_{s\beta}) = -\mathbf{MR\ddot{U}}_g(t) + \mathbf{P}(t) \tag{3.1}$$

$$\mathbf{R}^T\mathbf{M\ddot{U}} + \mathbf{M}_t\mathbf{\ddot{U}}_f + \mathbf{F}_f(t) + \mathbf{F}_{sb}(\ddot{U}_{s\beta}) = -\mathbf{M}_t\mathbf{\ddot{U}}_g(t) + \mathbf{R}^T\mathbf{P}(t) \tag{3.2}$$

The initial condition are "at rest"; the displacement and velocity are zero at time zero. As derived in Appendix B, equation 3.1 represents the equilibrium of forces for the nodal points of the dam above the base, and equation 3.2 represents equilibrium for the entire dam including all forces acting at the base. The quantities used in the equations of motion are defined in the following categories.

Response Quantities

- The vector **U** contains the time varying nodal point displacements relative to the rigid body motion of the dam base:

$$\mathbf{U} = [\ U_1^x \quad U_1^y \quad U_2^x \quad U_2^y \quad \ldots\ldots \quad U_n^x \quad U_n^y\ ]^T$$

  in which U_i^x and U_i^y are the x- and y-components of displacement for node i, and n is the number of nodes above the base.

- The vector $\mathbf{U}_f$ contains the rigid body displacements of the foundation rock surface relative to the free-field ground motion:

$$\mathbf{U}_f = [\ U_f^x \quad U_f^y \quad \Theta\ ]^T$$

  where U_f^x, U_f^y and Θ are the x-displacement, y-displacement, and rotation, respectively.

- The vector $\ddot{\mathbf{U}}_g(t)$ contains the specified x- and y-components of the free-field ground acceleration at the foundation rock surface:

$$\ddot{\mathbf{U}}_g(t) = [\, \ddot{U}_g^x(t) \quad \ddot{U}_g^y(t) \quad 0 \,]^T$$

- $U_{s\beta}(t)$ is the sliding displacement of the dam base relative to the foundation rock surface along the interface plane. It is positive when the dam slides in the downstream direction. $\ddot{U}_{s\beta}(t)$ is the sliding acceleration.

Dam Properties

- **M**, **C** and **K** are the mass, damping and stiffness matrices of the dam associated with the nodes above the base. The mass and stiffness matrices are symmetric and they are evaluated by standard finite element procedures. The damping matrix is expressed as a function of the stiffness matrix in the frequency domain, as will be shown later, to represent hysteretic damping in the dam.

- **R** is the influence matrix for rigid body motion of the dam about the center of the base:

$$\mathbf{R} = [\, \mathbf{1}^x \quad \mathbf{1}^y \quad \mathbf{h} \,]$$

where $\mathbf{1}^x$ and $\mathbf{1}^y$ are vectors containing unit values for the DOF in the x-direction and y-direction, respectively; and h contains the displacement components due to unit rotation about the center of the base.

- The matrix $\mathbf{M}_t$ contains the total translational mass and the rotational inertia of the dam about the center of the base. This matrix is not diagonal because

the center of the base is not the center of mass for the dam. This matrix is defined in Appendix B as follows:

$$\mathbf{M}_t = \left\{ \begin{array}{cc} \mathbf{R}_d^T & \mathbf{R}_b^T \end{array} \right\} \left[\begin{array}{cc} \mathbf{M}_{dd} & \mathbf{M}_{db} \\ \mathbf{M}_{bd} & \mathbf{M}_{bb} \end{array} \right] \left\{ \begin{array}{c} \mathbf{R}_d \\ \mathbf{R}_b \end{array} \right\} \tag{3.3}$$

where $\mathbf{M}_{dd}$, $\mathbf{M}_{bd}$, $\mathbf{M}_{db}$, and $\mathbf{M}_{bb}$ are the sub-matrices of the mass matrix for the dam, and $\mathbf{R}_d$ and $\mathbf{R}_b$ are the sub-matrices of the influence matrix $\mathbf{R}$ for the DOF in the dam (d) and on the base (b).

Interaction Forces

- The vector $\mathbf{P}(t)$ are the equivalent nodal forces for the hydrodynamic pressure acting on the dam. The upstream face of the dam is assumed vertical, so only the x-components for the nodes in contact with water are nonzero. The hydrodynamic forces are computed in the frequency domain by considering the water domain substructure.

- The dam-foundation rock interaction forces, $\mathbf{F}_f(t)$, at the base of the dam are:

$$\mathbf{F}_f(t) \;=\; [\; F_f^x(t) \quad F_f^y(t) \quad M_f(t) \;]^T$$

where $F_f^x(t)$, $F_f^y(t)$, and $M_f(t)$ are the forces in the x- and y-directions and moment about the center of the base, respectively, as shown in Figure 3.2 (a). For flexible foundation rock, the interaction forces are expressed as a function of the foundation displacements, $\mathbf{U}_f$, in the frequency domain.

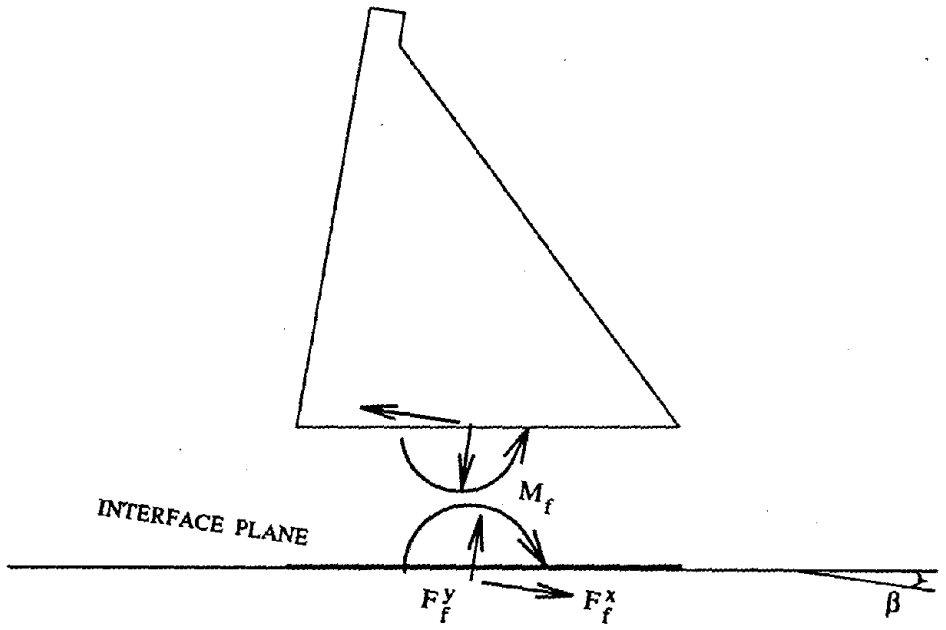

(a) BASE FORCES IN THE X-Y COORDINATE SYSTEM

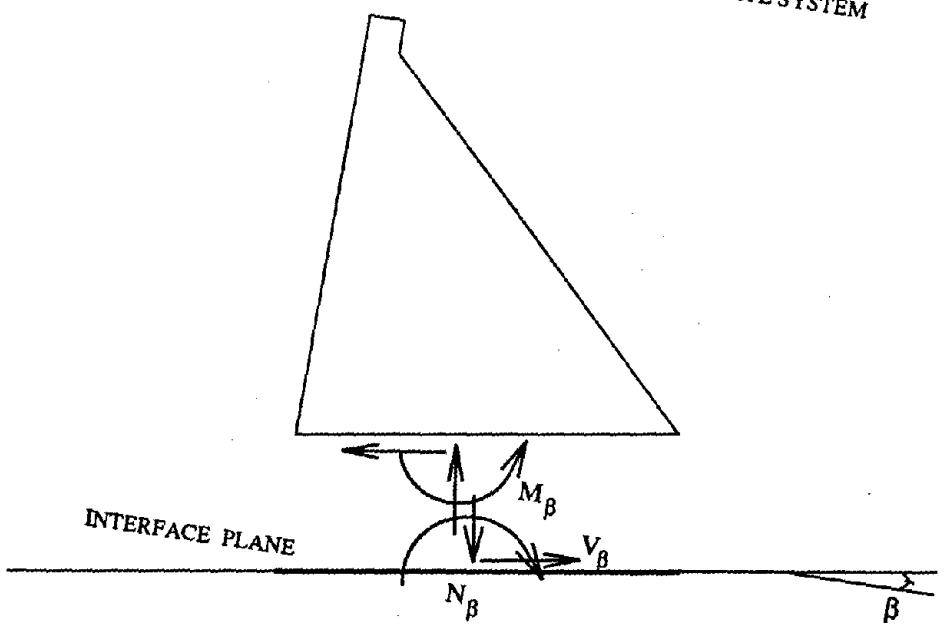

(b) BASE FORCES IN THE INTERFACE COORDINATE SYSTEM FOR SLIDING IN THE DOWNSTREAM DIRECTION

Figure 3.2. Forces at the base of the dam.

Inertia Forces due to Sliding

- The vectors $\mathbf{F}_{sd}$ and $\mathbf{F}_{sb}$ are the inertia forces of the dam due to sliding at the interface. $\mathbf{F}_{sd}$ is the vector of inertia forces for nodes above the base, and $\mathbf{F}_{sb}$ is the resultant inertia force at the base. These forces are a function of the sliding acceleration, $\ddot{U}_{s\beta}(t)$, in the interface plane:

$$\mathbf{F}_{sd}(\ddot{U}_{s\beta}) = \mathbf{MRT}_{\beta}\ddot{U}_{s\beta}(t)$$

$$\mathbf{F}_{sb}(\ddot{U}_{s\beta}) = \mathbf{M}_{t}\mathbf{T}_{\beta}\ddot{U}_{s\beta}(t)$$

where $\mathbf{T}_{\beta} = [\cos\beta \quad \sin\beta \quad 0]^{T}$ is the transformation between acceleration in the interface plane and in the x-y coordinate system.

3.3 Sliding Condition

The inertia forces due to sliding depend on the sliding acceleration, $\ddot{U}_{s\beta}(t)$, which is one of the unknown quantities in the response analysis. Thus, an additional equation is required to determine this acceleration. The approach used in this study assumes that the forces at the interface satisfy the Mohr-Coulomb law.

Given the dynamic forces at the base of the dam, $\mathbf{F}_{f}(t)$, defined in the x-y coordinate system, the components of the forces in the interface plane are:

$$\begin{Bmatrix} V_{\beta}(t) \\ N_{\beta}(t) \\ M_{\beta}(t) \end{Bmatrix} = \mathbf{T}^{T}\mathbf{F}_{f}(t)$$

where $V_{\beta}(t)$, $N_{\beta}(t)$, and $M_{\beta}(t)$ are the shear force, normal force, and moment, as shown in Figure 3.2 (b). The shear force, $V_{\beta}(t)$, is positive when the dam slides in

the downstream direction; the normal force, $N_\beta(t)$, is positive in compression. With this sign convention the transformation matrix $\mathbf{T}$ is:

$$\mathbf{T} = \begin{bmatrix} Cos\beta & Sin\beta & 0 \\ Sin\beta & -Cos\beta & 0 \\ 0 & 0 & 1 \end{bmatrix}$$

Considering the total shear and normal forces, $V^t_\beta(t)$ and $N^t_\beta(t)$, at the interface, the Mohr-Coulomb law relates them by:

$$V^t_\beta(t) \;=\; e(t)\,[c + \mu N^t_\beta(t)] \tag{3.4}$$

where the cohesion force, c, and the friction coefficient, μ, are specified properties of the interface. The quantity $e(t)$ defines the direction of the sliding. It is $+1$ when the dam is sliding in the downstream direction, -1 when the dam is sliding in the upstream direction, or zero when the dam is not sliding. The interface forces, $V^t_\beta(t)$ and $N^t_\beta(t)$, include the static resultant forces, $V_{\beta,st}$ and $N_{\beta,st}$, due to hydrostatic, uplift, and other static loads on the dam.

3.4 Reduction of Degrees-of-Freedom

The response of gravity dams to earthquake ground motion is dominated by a few modes of vibration. A Rayleigh-Ritz procedure is used to reduce the number of degrees-of-freedom to a small number of generalized coordinates. The displacement of the dam, $\mathbf{U}$, relative to the base is expressed as linear combinations of Ritz vectors:

$$\mathbf{U} \;=\; \mathbf{\Psi}\,\mathbf{Z} \tag{3.5}$$

where Ψ contains J Ritz vectors and $\mathbf{Z}$ is the vector of time-varying generalized coordinates:

$$\Psi = [\ \Psi_1 \quad \Psi_2 \quad \Psi_3 \quad ..... \quad \Psi_J\ ]$$

$$\mathbf{Z} = [\ Z_1 \quad Z_2 \quad Z_3 \quad ..... \quad Z_J\ ]^T$$

The Ritz vectors can be computed in J steps to represent the inertia, stiffness, and earthquake loads for the dam [Wilson, 1982]. The procedure generates mass orthogonalized vectors that most participate in the response to the free-field ground motion. The impounded water is not included in the generation of the Ritz vectors, and the foundation rock flexibility has no effect because of the assumed rigid base of the dam.

Substituting equation 3.5 into equations 3.1 and 3.2 and premultiplying equation 3.1 by Ψ^T gives the reduced equations of motion:

$$\mathbf{M^*\ddot{Z} + C^*\dot{Z} + K^*Z + L\ddot{U}_f + \Psi^T F_{sd}(\ddot{U}_{s\beta}) = -L\ddot{U}_g(t) + \Psi^T\ P}(t) \tag{3.6}$$

$$\mathbf{L^T\ddot{Z} + M_t\ddot{U}_f + F_f}(t) + \mathbf{F_{sb}}(\ddot{U}_{s\beta}) = -\mathbf{M_t\ddot{U}_g}(t) + \mathbf{R^TP}(t) \tag{3.7}$$

where $\mathbf{M^*}$, $\mathbf{C^*}$ and $\mathbf{K^*}$ are the generalized mass, damping and stiffness matrices of the dam, respectively; and the matrix $\mathbf{L}$ gives the participation of the Ritz vectors in rigid body motion of the dam base:

$$\mathbf{M^* = \Psi^T M\Psi} \qquad \mathbf{C^* = \Psi^T C\Psi} \qquad \mathbf{K^* = \Psi^T K\Psi} \qquad \mathbf{L = \Psi^T MR}$$

The Ritz vectors are orthonormalized such that the generalized mass, $\mathbf{M}^*$, is the identity matrix. The generalized stiffness matrix, $\mathbf{K}^*$, is a symmetric full matrix. The generalized damping matrix, $\mathbf{C}^*$, will be defined to represent frequency-independent hysteretic damping.

3.5 Hybrid Frequency-Time Domain Procedure

The hybrid frequency-time domain (HFTD) procedure [Kawamoto, 1983; Darbre and Wolf, 1988] is used to solve the nonlinear and frequency-dependent equations of motion, equations 3.6 and 3.7. The solution procedure can be divided into three stages: (a) linearization of the equations of motion, (b) solution of the linearized equations in the frequency domain, and (c) state determination in the time domain. Iteration over segments of time is required to converge to the exact solution.

3.5.1 Linearization

The inertia forces, $\mathbf{F}_{sd}$ and $\mathbf{F}_{sb}$, due to sliding are nonlinear functions of the response. Given the sliding acceleration history, $\ddot{U}_{s\beta}^{[k]}(t)$, for iteration k, the $k+1$ estimate of the inertia forces due to sliding is:

$$\mathbf{F}_{sd}^{[k+1]}(\ddot{U}_{s\beta}) = \mathbf{MRT}_\beta \ddot{U}_{s\beta}^{[k]}(t) \tag{3.8}$$

$$\mathbf{F}_{sb}^{[k+1]}(\ddot{U}_{s\beta}) = \mathbf{M}_l \mathbf{T}_\beta \ddot{U}_{s\beta}^{[k]}(t) \tag{3.9}$$

3.5.2 Solution

Substituting equations 3.8 and 3.9 into equations 3.6 and 3.7 gives the linearized equations of motion for the $k+1$ estimate of the response:

$$\mathbf{M}^*\ddot{\mathbf{Z}}^{[k+1]} + \mathbf{C}^*\dot{\mathbf{Z}}^{[k+1]} + \mathbf{K}^*\mathbf{Z}^{[k+1]} + \mathbf{L}\ddot{\mathbf{U}}_f^{[k+1]} =$$
$$-\mathbf{L}\ddot{\mathbf{U}}_g(t) - \mathbf{L}\mathbf{T}_\beta\ddot{U}_{s\beta}^{[k]}(t) + \mathbf{\Psi}^T[\mathbf{P}_g(t) + \mathbf{P}_s^{[k]}(t) + \mathbf{P}_{zf}^{[k+1]}(t)] \tag{3.10}$$

$$\mathbf{L}^T\ddot{\mathbf{Z}}^{[k+1]} + \mathbf{M}_t\ddot{\mathbf{U}}_f^{[k+1]} + \mathbf{F}_f^{[k+1]}(t) =$$
$$-\mathbf{M}_t\ddot{\mathbf{U}}_g(t) - \mathbf{M}_t\mathbf{T}_\beta\ddot{U}_{s\beta}^{[k]}(t) + \mathbf{R}^T[\mathbf{P}_g(t) + \mathbf{P}_s^{[k]}(t) + \mathbf{P}_{zf}^{[k+1]}(t)] \tag{3.11}$$

The $k+1$ estimate of the hydrodynamic force vector, $\mathbf{P}^{[k+1]}(t)$, has been written as:

$$\mathbf{P}^{[k+1]}(t) = \mathbf{P}_g(t) + \mathbf{P}_s^{[k]}(t) + \mathbf{P}_{zf}^{[k+1]}(t)$$

where $\mathbf{P}_g(t)$ is the hydrodynamic force due to free-field ground acceleration; $\mathbf{P}_s^{[k]}(t)$ is the hydrodynamic force due to the sliding acceleration for iteration k; and $\mathbf{P}_{zf}^{[k+1]}(t)$ is the hydrodynamic force due to deformation of the dam and foundation rock for iteration $k+1$.

The linearized equations of motion will be solved in the frequency domain.

3.5.3 State Determination

The base forces must be computed to determine the sliding state. For this purpose, equation 3.11 is rearranged and the base forces can be computed as follows:

$$\mathbf{F}_f^{[k+1]}(t) = \mathbf{F}^{[k+1]}(t) - \mathbf{M}_t\mathbf{T}_\beta\ddot{U}_{s\beta}^{[k+1]}(t) \tag{3.12}$$

where the base forces excluding the sliding inertia forces are:

$$\begin{aligned}\mathbf{F}^{[k+1]}(t) &= -\mathbf{L}^T\ddot{\mathbf{Z}}^{[k+1]}(t) - \mathbf{M}_t\ddot{\mathbf{U}}_f^{[k+1]}(t) - \mathbf{M}_t\ddot{\mathbf{U}}_g(t) \\ &\quad +\mathbf{R}^T[\mathbf{P}_g(t) + \mathbf{P}_s^{[k]}(t) + \mathbf{P}_{zf}^{[k+1]}(t)] \end{aligned} \tag{3.13}$$

The components of the force $\mathbf{F}_f^{[k+1]}(t)$ in the interface plane are obtained by premultiplying equation 3.12 by $\mathbf{T}^T$:

$$\begin{Bmatrix} V_\beta^{[k+1]}(t) \\ N_\beta^{[k+1]}(t) \\ M_\beta^{[k+1]}(t) \end{Bmatrix} = \begin{Bmatrix} V^{[k+1]}(t) \\ N^{[k+1]}(t) \\ M^{[k+1]}(t) \end{Bmatrix} - \begin{Bmatrix} m_V \\ m_N \\ m_M \end{Bmatrix} \ddot{U}_{s\beta}^{[k+1]}(t) \tag{3.14}$$

where $V^{[k+1]}(t)$, $N^{[k+1]}(t)$, and $M^{[k+1]}(t)$ are the shear force, normal force, and moment at the interface due to all effects except sliding:

$$\begin{Bmatrix} V^{[k+1]}(t) \\ N^{[k+1]}(t) \\ M^{[k+1]}(t) \end{Bmatrix} = \mathbf{T}^T\mathbf{F}^{[k+1]}(t) \tag{3.15}$$

m_V, m_N, and m_M are masses that represent the inertia forces at the interface plane due to unit sliding acceleration. They are defined as follows:

$$\begin{Bmatrix} m_V \\ m_N \\ m_M \end{Bmatrix} = \mathbf{T}^T\mathbf{M}_t\mathbf{T}_\beta$$

Applying the Mohr-Coulomb law from equation 3.4 for iteration $k+1$ gives:

$$[V_\beta^{[k+1]}(t) + V_{\beta,st}] = e^{[k]}(t)\ [c + \mu(N_\beta^{[k+1]}(t) + N_{\beta,st})] \tag{3.16}$$

The sliding acceleration that satisfies the Mohr-Coulomb law is obtained by substituting the terms for shear and normal forces from equation 3.14 into equation 3.16:

$$\ddot{U}_{s\beta}^{[k+1]}(t) = \frac{[V^{[k+1]}(t) + V_{\beta,st}] - \ e^{[k]}(t)\ [c + \mu(N^{[k+1]}(t) + N_{\beta,st})]}{m_R(t)} \tag{3.17}$$

where the effective mass, $m_R(t)$, resisting sliding acceleration is:

$$m_R(t) = m_V \ - m_S(t) \qquad\qquad m_S(t) = e^{[k]}(t)\ \mu\ m_N$$

The term $m_S(t)$ represents the change in effective mass (change in normal force) due to sliding acceleration.

The function $e^{[k]}(t)$ defines the sliding status of the dam. This quantity is evaluated by considering the equilibrium of forces at the dam interface at each time step. During the non-sliding phase, the sliding acceleration, $\ddot{U}_{s\beta}(t)$, is zero, and $e^{[k]}(t) = 0$. The dam slides when the total shear force at the base exceeds the resistance at the interface:

$$|V^{[k+1]}(t) + V_{\beta,st}| \geq |c + \mu(N^{[k+1]}(t) + N_{\beta,st})| \tag{3.18}$$

and the direction of sliding is given by:

$$e^{[k+1]}(t) \ = \ \frac{V^{[k+1]}(t) + V_{\beta,st}}{|V^{[k+1]}(t) + V_{\beta,st}|} \tag{3.19}$$

The sliding ends when the sliding velocity is zero, $\dot{U}_{s\beta}^{[k+1]}(t) = 0$, and at that time $e^{[k+1]}(t) = 0$. The sliding velocity is computed by integrating the sliding acceleration.

3.6 Frequency Domain Solution

Equations 3.10 and 3.11 contain frequency-dependent terms due to hydrodynamic forces, $\mathbf{P}_g$, $\mathbf{P}_s$ and $\mathbf{P}_z$, and dam-foundation rock interaction forces, $\mathbf{F}_f$. Therefore it is necessary to transform the equations of motion to the frequency domain for computing the $k+1$ estimate of response.

The transformation of the response and force quantities is accomplished by using the Fourier transforms:

$$\bar{\mathbf{G}}_c(\omega) = \int_0^{T_p} \mathbf{G}_c(t) e^{-i\omega t} dt \tag{3.20a}$$

$$\mathbf{G}_c(t) = \frac{1}{2\pi} \int_{-\infty}^{\infty} \bar{\mathbf{G}}_c(\omega) e^{i\omega t} d\omega \tag{3.20b}$$

where T_p is the duration of the response including the quiet zone. $\mathbf{G}_c(t)$ and $\bar{\mathbf{G}}_c(\omega)$ represent any response quantity and its transformation, respectively.

3.6.1 Dam Substructure

The frequency-domain form of equations 3.10 and 3.11 is:

$$\begin{aligned}
&[-\omega^2\mathbf{M}^* + (1+i\eta)\mathbf{K}^*]\ \bar{\mathbf{Z}}^{[k+1]}(\omega) - \omega^2\mathbf{L}\bar{\mathbf{U}}_f^{[k+1]}(\omega) \ = \\
&\quad -\mathbf{L}\bar{\ddot{\mathbf{U}}}_g(\omega) - \mathbf{L}\mathbf{T}_\beta \bar{\ddot{U}}_{s\beta}^{[k]}(\omega) + \mathbf{\Psi}^T[\bar{\mathbf{P}}_g(\omega) + \bar{\mathbf{P}}_s^{[k]}(\omega) + \bar{\mathbf{P}}_{zf}^{[k+1]}(\omega)]
\end{aligned} \tag{3.21}$$

$$\begin{aligned}
&-\omega^2\mathbf{L}^T\bar{\mathbf{Z}}^{[k+1]}(\omega) - \omega^2\mathbf{M}_t\bar{U}_f^{[k+1]}(\omega) + \bar{\mathbf{F}}_f^{[k+1]}(\omega) = \\
&\quad -\mathbf{M}_t\bar{\ddot{\mathbf{U}}}_g(\omega) - \mathbf{M}_t\mathbf{T}_\beta\bar{\ddot{U}}_{s\beta}^{[k]}(\omega) + \mathbf{R}^T[\bar{\mathbf{P}}_g(\omega) + \bar{\mathbf{P}}_s^{[k]}(\omega) + \bar{\mathbf{P}}_{zf}^{[k+1]}(\omega)]
\end{aligned} \tag{3.22}$$

where $\bar{\mathbf{Z}}^{[k+1]}(\omega)$ is the transform of the generalized displacements; $\bar{\mathbf{U}}_f^{[k+1]}(\omega)$ is the transform of the foundation displacements; $\bar{\mathbf{F}}_f(\omega)$ is the transform of the forces at the base due to dam-foundation rock interaction; and $\bar{\mathbf{P}}_g(\omega)$, $\bar{\mathbf{P}}_s^{[k]}(\omega)$, $\bar{\mathbf{P}}_{zf}^{[k+1]}(\omega)$ are

the transforms of the hydrodynamic forces. Hysteretic damping in the dam is modeled by a frequency-independent, stiffness proportional damping factor, η, so $\omega \mathbf{C}^* = \eta \mathbf{K}^*$.

3.6.2 Foundation Rock Substructure

At the rigid foundation rock surface, the relationship between the foundation displacements, $\mathbf{U}_{f\beta}(\omega)$, and interaction forces, $\mathbf{F}_{f\beta}(\omega)$, in the interface coordinate system are represented by a complex frequency-dependent impedance matrix, $\mathbf{K}_{f\beta}(\omega)$:

$$\bar{\mathbf{F}}_{f\beta}(\omega) = \mathbf{K}_{f\beta}(\omega)\, \bar{\mathbf{U}}_{f\beta}(\omega) \tag{3.23}$$

The foundation rock is modeled as a homogeneous, isotropic, and viscoelastic half-plane to compute the the impedance matrix, $\mathbf{K}_{f\beta}(\omega)$ [Dasgupta and Chopra, 1977]. The constraint of a rigid base gives an impedance matrix with the three rigid body modes for the foundation rock interface. Figure 3.3 shows the frequency-dependent terms in the impedance matrix.

In the x-y coordinate system, the relationship between the base interaction forces, $\mathbf{F}_f(\omega)$, and foundation displacements, $\mathbf{U}_f(\omega)$, is:

$$\bar{\mathbf{F}}_f(\omega) = \mathbf{K}_f(\omega)\bar{\mathbf{U}}_f(\omega) \tag{3.24}$$

where the impedance matrix in the x-y coordinate system is:

$$\mathbf{K}_f(\omega) = \mathbf{T}_f^T \mathbf{K}_{f\beta}(\omega)\mathbf{T}_f \tag{3.25}$$

$$K_{f\beta} = E_{fr} \begin{bmatrix} \bar{K}_{11} & 0 & B\,\bar{K}_{13} \\ 0 & \bar{K}_{22} & 0 \\ B\,\bar{K}_{31} & 0 & B^2\bar{K}_{33} \end{bmatrix}$$

$$\bar{K}_{ij} = K_{ij} + i\, a_o C_{ij}$$

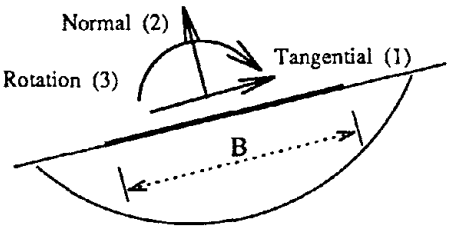

C_s = shear velocity at the foundation rock

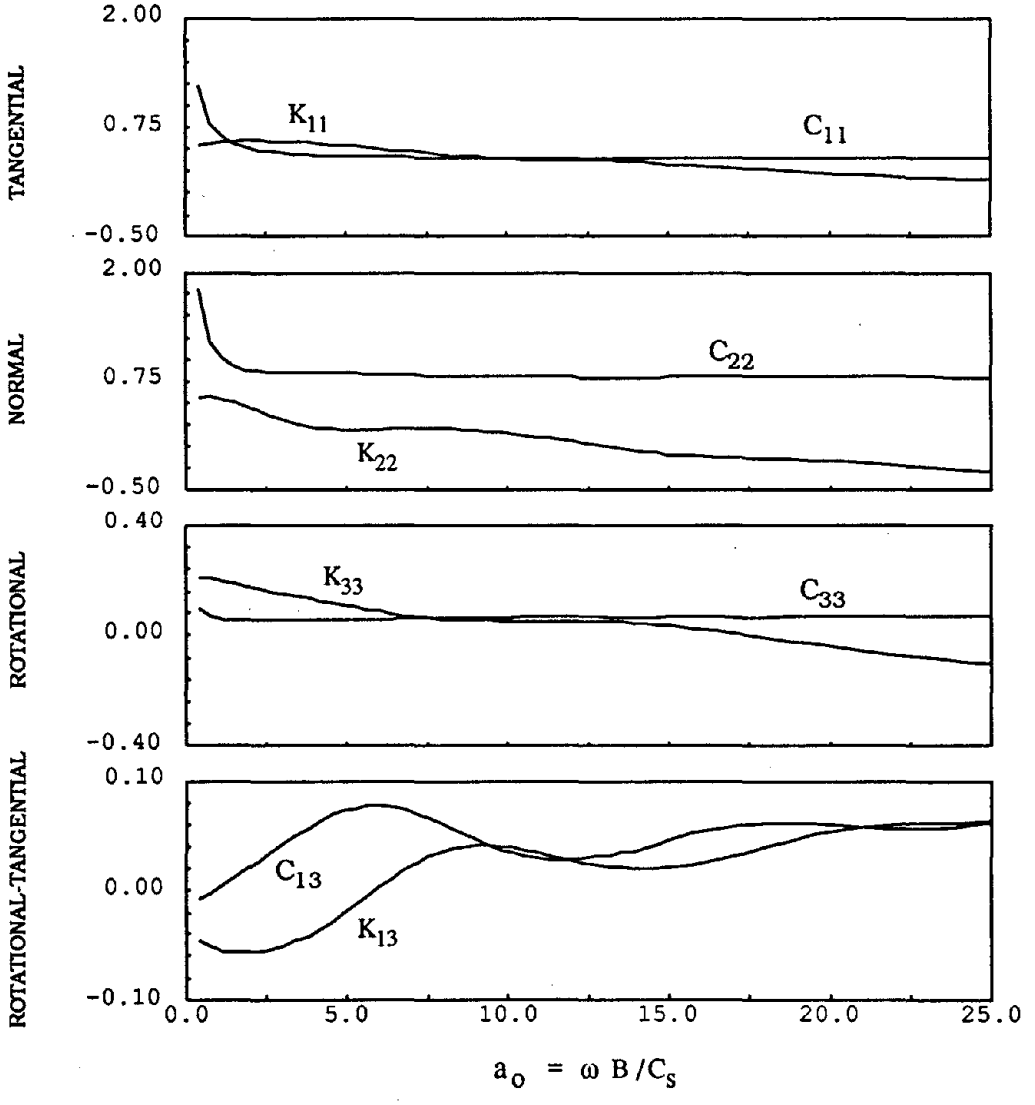

$a_o = \omega\, B / C_s$

Figure 3.3. Impedance functions for rigid base on viscoelastic half-plane ($\eta_f = 0.10$).

and the transformation matrix is:

$$\mathbf{T}_f = \begin{bmatrix} Cos\beta & Sin\beta & 0 \\ -Sin\beta & Cos\beta & 0 \\ 0 & 0 & 1 \end{bmatrix}$$

3.6.3 Water Substructure

The hydrodynamic forces on the dam are defined in the frequency domain. For iteration $k+1$, the forces are:

$$\bar{\mathbf{P}}^{[k+1]}(\omega) = \bar{\mathbf{P}}_g(\omega) + \bar{\mathbf{P}}_s^{[k]}(\omega) + \bar{\mathbf{P}}_{zf}^{[k+1]}(\omega) \tag{3.26}$$

As indicated in equations 3.21 and 3.22, $\bar{\mathbf{P}}^{[k+1]}(\omega)$ is premultiplied by $\mathbf{\Psi}^T$ and $\mathbf{R}^T$ in the equations of motion. The transformed hydrodynamic force vectors are defined in Appendix C as follows:

$$\mathbf{\Psi}^T\bar{\mathbf{P}}_g(\omega) = \mathbf{B}_{\Psi g}(\omega)\bar{\ddot{\mathbf{U}}}_g(\omega) \tag{3.27a}$$

$$\mathbf{\Psi}^T\bar{\mathbf{P}}_s^{[k]}(\omega) = \mathbf{B}_{\Psi s}(\omega)\mathbf{T}_\beta\bar{\ddot{U}}_{s\beta}^{[k]}(\omega) \tag{3.27b}$$

$$\mathbf{\Psi}^T\bar{\mathbf{P}}_{zf}^{[k+1]}(\omega) = \mathbf{B}_{\Psi z}(\omega)\bar{\ddot{\mathbf{Z}}}^{[k+1]}(\omega) + \mathbf{B}_{\Psi f}(\omega)\bar{\ddot{\mathbf{U}}}_f^{[k+1]}(\omega) \tag{3.27c}$$

$$\mathbf{R}^T\bar{\mathbf{P}}_g(\omega) = \mathbf{B}_{Rg}(\omega)\bar{\ddot{\mathbf{U}}}_g(\omega) \tag{3.27d}$$

$$\mathbf{R}^T\bar{\mathbf{P}}_s^{[k]}(\omega) = \mathbf{B}_{Rs}(\omega)\mathbf{T}_\beta\bar{\ddot{U}}_{s\beta}^{[k]}(\omega) \tag{3.27e}$$

$$\mathbf{R}^T\bar{\mathbf{P}}_{zf}^{[k+1]}(\omega) = \mathbf{B}_{Rz}(\omega)\bar{\ddot{\mathbf{Z}}}^{[k+1]}(\omega) + \mathbf{B}_{Rf}(\omega)\bar{\ddot{\mathbf{U}}}_f^{[k+1]}(\omega) \tag{3.27f}$$

The complex-valued matrices $\mathbf{B}_{\Psi z}(\omega)$ and $\mathbf{B}_{\Psi f}(\omega)$ are the added mass and damping due to deformation of the dam and foundation rock, respectively; the matrices $\mathbf{B}_{Rz}(\omega)$

and $\mathbf{B}_{Rf}(\omega)$ represent the added mass and damping due to rigid body displacements of the dam and foundation rock. The complex-valued vectors $\mathbf{B}_{\Psi g}(\omega)$, $\mathbf{B}_{\Psi s}(\omega)$, $\mathbf{B}_{Rg}(\omega)$, and $\mathbf{B}_{Rs}(\omega)$ are added loads due to free-field ground motion and sliding at the base.

3.6.4 Dam-Water-Foundation Rock System

Substituting equation 3.24 and equation 3.27 into equation 3.21 and 3.22, and expressing the free-field ground motion vector in terms of its components, the equations of motion for the entire system are:

$$\mathbf{S}(\omega)\bar{\mathbf{X}}^{[k+1]}(\omega) = \mathbf{L}^x(\omega)\bar{\ddot{U}}_g^x(\omega) + \mathbf{L}^y(\omega)\bar{\ddot{U}}_g^y(\omega) + \mathbf{L}^s(\omega)\bar{\ddot{U}}_{s\beta}^{[k]}(\omega) \tag{3.28}$$

The response vector $\bar{\mathbf{X}}^{[k+1]}(\omega)$ is:

$$\bar{\mathbf{X}}^{[k+1]}(\omega) = \left\{ \begin{array}{c} \bar{\mathbf{Z}}^{[k+1]}(\omega) \\ \bar{\mathbf{U}}_f^{[k+1]}(\omega) \end{array} \right\}$$

The dynamic stiffness matrix, $\mathbf{S}(\omega)$, is symmetric and defined as:

$$\mathbf{S}(\omega) = \left[\begin{array}{ll} -\omega^2\mathbf{M}^* + (1+i\eta)\mathbf{K}^* + \omega^2\mathbf{B}_{\Psi z}(\omega) & -\omega^2\mathbf{L} + \omega^2\mathbf{B}_{\Psi f}(\omega) \\ -\omega^2\mathbf{L}^T + \omega^2\mathbf{B}_{Rz}(\omega) & -\omega^2\mathbf{M}_t + \mathbf{K}_f(\omega) + \omega^2\mathbf{B}_{Rf}(\omega) \end{array} \right]$$

The load vectors $\mathbf{L}^x(\omega)$, $\mathbf{L}^y(\omega)$, and $\mathbf{L}^s(\omega)$ are:

$$\mathbf{L}^x(\omega) = \left\{ \begin{array}{l} -L_{11} + B_{01}(\omega) \\ -L_{21} + B_{02}(\omega) \\ \cdots \\ -L_{J1} + B_{0J}(\omega) \\ - - - - - - - \\ -M_{t11} + B_{00}(\omega) \\ -M_{t21} \\ -M_{t31} + B_{0\theta} \end{array} \right\}$$

$$\mathbf{L}^y(\omega) = \left\{ \begin{array}{l} -L_{12} + B_{y1}(\omega) \\ -L_{22} + B_{y2}(\omega) \\ \cdots \\ -L_{J2} + B_{yJ}(\omega) \\ - - - - - - - \\ -M_{t12} + B_{y0}(\omega) \\ -M_{t22} \\ -M_{t32} + B_{y\theta} \end{array} \right\}$$

$$\mathbf{L}^s(\omega) = \left\{ \begin{array}{l} -L_{12} \\ -L_{22} \\ .. \\ -L_{J2} \\ - - - \\ -M_{t12} \\ -M_{t22} \\ -M_{t32} \end{array} \right\} \sin\beta + \mathbf{L}^x(\omega)\cos\beta$$

where the coefficients L_{ij} and $M_{t_{ij}}$ are components of $\mathbf{L}$ and $\mathbf{M}_t$ defined previously; and $B_{00}(\omega)$, $B_{0\theta}(\omega)$, $B_{0j}(\omega)$, $B_{y\theta}(\omega)$, and $B_{yj}(\omega)$ $(j = 1,..,J)$, are complex-valued functions that are components of $\mathbf{B}_{\Psi_g}(\omega)$, $\mathbf{B}_{R_g}(\omega)$, $\mathbf{B}_{\Psi_s}(\omega)$, and $\mathbf{B}_{R_s}(\omega)$. .

3.7 Summary of Solution Procedure

The HFTD procedure requires iteration in the frequency domain and in the time domain. The important steps and equations are:

- Solve the linearized equations, equation 3.28, in the frequency domain to determine generalized displacements of the dam and foundation displacements:

$$\mathbf{S}(\omega)\bar{\mathbf{X}}^{[k+1]}(\omega) = \mathbf{L}^{x}(\omega)\bar{\ddot{U}}_{g}^{x}(\omega) + \mathbf{L}^{y}(\omega)\bar{\ddot{U}}_{g}^{y}(\omega) + \mathbf{L}^{s}(\omega)\bar{\ddot{U}}_{s\beta}^{[k]}(\omega)$$

- Evaluate the forces at the sliding interface in the time domain:

$$\left\{ \begin{array}{c} V^{[k+1]}(t) \\ N^{[k+1]}(t) \\ M^{[k+1]}(t) \end{array} \right\} = \mathbf{T}^{T}\mathbf{F}^{[k+1]}(t)$$

  the base force vector $\mathbf{F}^{[k+1]}(t)$ is in the x-y coordinate system.

- Evaluate the sliding acceleration:

$$\ddot{U}_{s\beta}^{[k+1]}(t) = \frac{[V^{[k+1]}(t) + V_{\beta,st}] - e^{[k]}(t)\,[c + \mu(N^{[k+1]}(t) + N_{\beta,st})]}{m_R(t)}$$

- Determine the sliding direction:

$$e^{[k+1]}(t) = \frac{V^{[k+1]}(t) + V_{\beta,st}}{|V^{[k+1]}(t) + V_{\beta,st}|}$$

  A positive value indicates sliding in the downstream direction. The dam will change from sliding to non-sliding phase when the sliding velocity, $\dot{U}_{s\beta}^{[k+1]}(t) = 0$, and at that step $e^{[k+1]}(t) = 0$.

The implementation of the steps in the solution procedure is detailed in Chapter 4.

Chapter 4

IMPLEMENTATION OF THE SOLUTION PROCEDURE

4.1 Introduction

The hybrid frequency-time domain (HFTD) procedure is used to solve the nonlinear, frequency-dependent equations of motion governing the earthquake sliding response of a dam-water-foundation rock system. Each iteration for the solution involves three stages:

- Linearization of equations of motion: the nonlinear system is linearized by transferring the nonlinear inertia forces due to sliding to the right-hand side of the equations of motion.
- Solution of the linearized equations of motion in frequency domain: the linearized equations of motion are solved in the frequency domain to account for the frequency-dependent effects of dam-water interaction and dam-foundation rock interaction.
- State determination in time domain: the Mohr-Coulomb law is applied to determine the sliding response. The sliding acceleration, which produces the nonlinear force, is evaluated at each time step.

The three stages are repeated until convergence of the solution is achieved for the total duration of response. The HFTD procedure converges in a time progressive

manner. The iterative procedure is performed for one segment of time until convergence is achieved in that segment. The number of iterations, and therefore the computation time, is influenced by the number of segments, the length of segments, and by the extent of the nonlinear response.

A large part of the computation and storage involves evaluating the complex-valued frequency response functions due to hydrodynamic terms and the computation of frequency response functions. An interpolation procedure is used to reduce the storage of the frequency response functions. For nonlinear problems, the interpolation procedure must be performed at each iteration to compute the frequency response functions for all frequencies, so there is little reduction in computation time.

4.2 Segmentation of Time

The iterative solution of equation 3.28 and the Fourier transform of the response functions gives the displacement history $\mathbf{X}^{[k+1]}(t)$. Early applications of the HFTD procedure exhibited slow convergence of the solution [Kawamoto, 1983]. Observation of the iterates show that convergence begins at time zero ($t = 0$) and progresses in time with each iteration. This has led to a procedure in which the total duration of response is divided into segments of time and the solution is obtained over one segment at a time [Darbre and Wolf, 1988]. After convergence is achieved in a segment, the solution proceeds to the next segment. The segmentation procedure is illustrated in Figure 4.1. The following is necessary in the implementation of the segmentation approach:

- A quiet zone, as shown in Figure 4.1(a), is appended to the free-field ground acceleration histories to satisfy the initial conditions in the frequency domain solution. The length of the quiet zone is determined from the fundamental frequency and damping for the dam system.

- The unbalanced forces are the inertia forces due to the sliding acceleration. A transition function must be appended to these forces, as shown in Figure 4.1(b), to avoid suddenly unloading the system at the end of a segment causing large oscillations in response due to the sudden change in load. The transition function used in this study is based on a sinusoidal shape function [Darbre and Wolf, 1988].

- The response is computed for the complete history, but only the response in the current segment is updated. Dam displacements and sliding accelerations obtained from converged solutions of previous segments are not changed. An example of the updating of displacements in an iteration is shown in Figure 4.1(c).

The estimate of the unbalanced force for the first iteration in a segment influences the number of iterations required to achieve convergence. From experience with application of the method, the fastest convergence is obtained by setting the unbalanced force to zero for the first iteration, implying there is no sliding for the segment.

The Fourier transforms are computed over the entire duration of response (including the quiet zone). Other approaches have been devised so as to avoid the use of the quiet zone. A recent study uses the so-called exponential window method for this

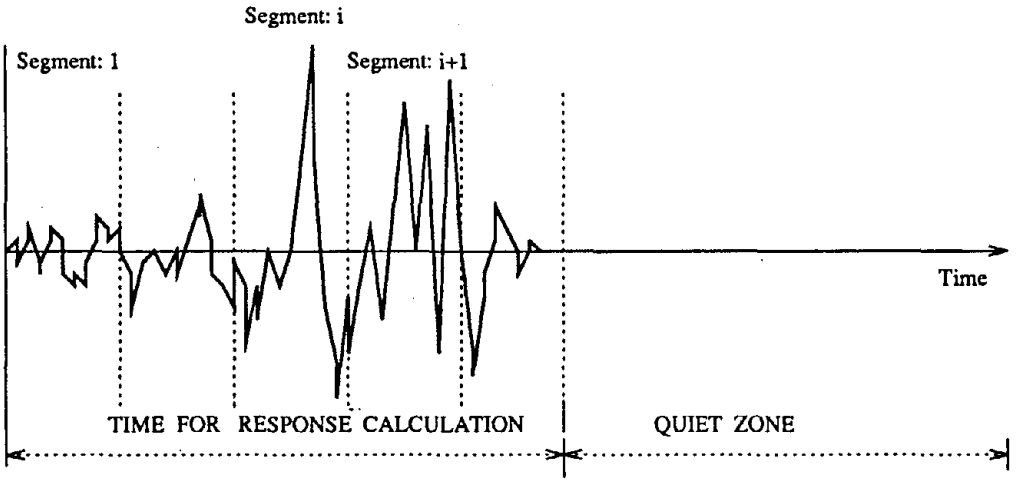

(a) GROUND ACCELERATION

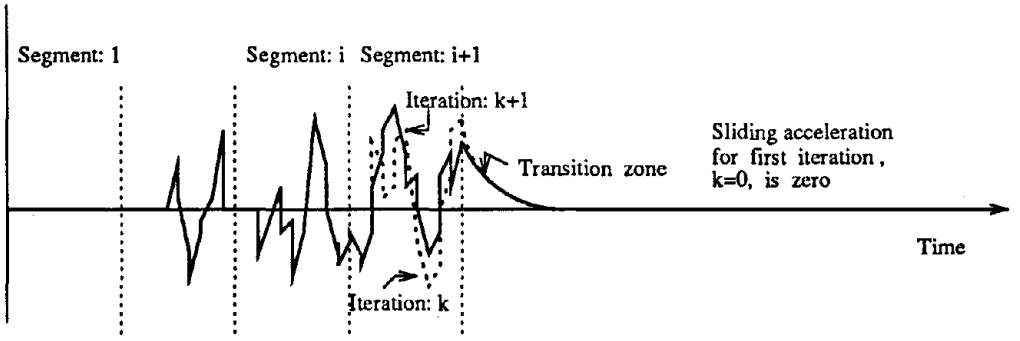

(b) SLIDING ACCELERATION

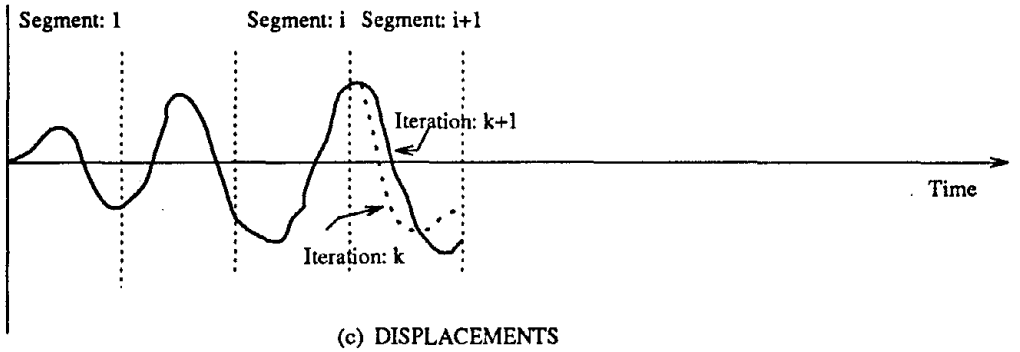

(c) DISPLACEMENTS

Figure 4.1. Hybrid frequency-time domain procedure for iterative solution of segment $i+1$.

purpose [Kausel and Roesset, 1992]. When the frequency response functions are evaluated by interpolation, however, small errors in the computation of the interpolated functions produce large errors in the solution, rendering the technique ineffective.

4.3 Stability Criterion

A necessary condition for the convergence of the HFTD procedure is based on the concept of spectral stability. This condition, formulated by Darbre and Wolf [1988], is the stability criterion for the HFTD procedure. The criterion requires that the spectral ratio, $\sigma(\omega)$, must be less than unity, where the spectral ratio is defined by:

$$\sigma(\omega) = max[\lambda_i(\omega)]$$

in which $\lambda_i(\omega)$ are the eigenvalues of the matrix:

$$\mathbf{I} - \mathbf{S}_o(\omega)^{-1}\mathbf{S}(\omega)$$

$\mathbf{S}_o(\omega)$ is the elastic stiffness matrix of the system, and $\mathbf{S}(\omega)$ is the dynamic stiffness matrix of the dam system, defined previously. Since the material properties are elastic, $\mathbf{S}_o(\omega) = \mathbf{S}(\omega)$, theoretically the spectral ratio is always zero and the HFTD procedure is expected to converge. From the practical point of view, however the sliding acceleration produces highly nonlinear force components, and it is necessary to use relatively short segments for an acceptable rate of convergence. Stability of the HFTD approach is also confirmed by the study performed by Trujillo [1982] for the force correction method [Stricklin and Haisler, 1977], which is similar to the HFTD procedure.

4.4 Convergence Criteria and Accuracy of Solution

The criteria for terminating the iterations in a segment affects the accuracy of the solution. The convergence criteria adopted in this study involve the generalized displacements of the dam, foundation displacements, and sliding acceleration. Convergence for a segment is achieved when the maximum difference between successive iterations of the response quantities is less than a tolerance at every time step in the segment. Thus the iteration terminates when:

$$[\Delta Z_j(t)] \leq \epsilon_{zj} \tag{4.1a}$$

$$[\Delta U_f^l(t)] \leq \epsilon_{fl} \tag{4.1b}$$

$$[\Delta \ddot{U}_{s\beta}(t)] \leq \epsilon_{s\beta} \tag{4.1c}$$

in which the error function $[\Delta A]$, for A representing either Z_j, U_f^l or $\ddot{U}_{s\beta}$, is defined as:

$$[\Delta A(t)] = max \frac{|A^{[k+1]}(t) - A^{[k]}(t)|}{|A^{[k+1]}(t)|}$$

and ϵ_{zj}, ϵ_{fl}, and $\epsilon_{s\beta}$ are the specified tolerances, and $j = 1, 2, ..., J$.

A further check of accuracy of the solution is performed at the end of the solution procedure by computing the energy balance for the system. Appendix E gives the energy balance equations that are used for this purpose. The equation that must be satisfied is:

$$E_i = E_s + E_f + E_d$$

where E_i is the input energy to the system due to ground motion, E_s, E_f, and E_d represent the energy and work due to sliding displacement, foundation displacement, and dam deformation, respectively.

4.5 Solution of Linearized Equations

The vector containing the generalized displacements and foundation displacements is computed from equation 3.28, as follows:

$$\bar{\mathbf{X}}^{[k+1]}(\omega) = \left\{ \begin{array}{c} \bar{\mathbf{Z}}^{[k+1]}(\omega) \\ \bar{\mathbf{U}}_f^{[k+1]}(\omega) \end{array} \right\} = \bar{\mathbf{Y}}^x(\omega)\bar{\ddot{U}}_g^x(\omega) + \bar{\mathbf{Y}}^y(\omega)\bar{\ddot{U}}_g^y(\omega) + \bar{\mathbf{Y}}^s(\omega)\bar{\ddot{U}}_{s\beta}^{[k]}(\omega) \quad (4.2)$$

where $\bar{\mathbf{Y}}^l(\omega)$ is the frequency response function for unit harmonic motion base acceleration. It is obtained from the solution of:

$$\mathbf{S}(\omega)\bar{\mathbf{Y}}^l(\omega) = \mathbf{L}^l(\omega) \qquad l = x, y, s \quad (4.3)$$

To minimize storage, the frequency response functions, $\bar{\mathbf{Y}}^l(\omega)$, are computed for a few frequencies, and the responses for other frequencies are obtained by interpolation. The interpolation scheme is summarized in Appendix D [Tajirian, 1981; Fok and Chopra, 1985].

4.6 Evaluation of Base Forces

The base forces for iteration $k+1$ are evaluated in the frequency domain and then transformed to the time domain. The interface forces from equation 3.15,

expressed in the frequency domain, are:

$$\left\{ \begin{array}{c} \bar{V}^{[k+1]}(\omega) \\ \bar{N}^{[k+1]}(\omega) \\ \bar{M}^{[k+1]}(\omega) \end{array} \right\} = \mathbf{T}^T \bar{\mathbf{F}}^{[k+1]}(\omega) \tag{4.4}$$

where the transform $\bar{\mathbf{F}}^{[k+1]}(\omega)$ comes from equation 3.13:

$$\begin{aligned} \bar{\mathbf{F}}^{[k+1]}(\omega) \;=\; & [-\mathbf{M}_t + \mathbf{B}_{Rg}(\omega)]\bar{\ddot{\mathbf{U}}}_g(\omega) + \mathbf{B}_{Rs}(\omega)\mathbf{T}_\beta \bar{\ddot{U}}_{s\beta}^{[k]}(\omega) + \\ & [-\mathbf{L}^T + \mathbf{B}_{Rz}(\omega)]\bar{\ddot{\mathbf{Z}}}^{[k+1]}(\omega) + [-\mathbf{M}_t + \mathbf{B}_{Rf}(\omega)]\bar{\ddot{\mathbf{U}}}_f^{[k+1]}(\omega) \end{aligned} \tag{4.5}$$

After rearranging terms, equation 4.4 can be expressed as:

$$\begin{aligned} \left\{ \begin{array}{c} \bar{V}^{[k+1]}(\omega) \\ \bar{N}^{[k+1]}(\omega) \\ \bar{M}^{[k+1]}(\omega) \end{array} \right\} = & \mathbf{A}_g^x(\omega)\bar{\ddot{U}}_g^x(\omega) \;+\; \mathbf{A}_g^y(\omega)\bar{\ddot{U}}_g^y(\omega) + \\ & \mathbf{A}_s(\omega)\bar{\ddot{U}}_{s\beta}^{[k]}(\omega) + \mathbf{A}_x(\omega)\bar{\ddot{\mathbf{X}}}^{[k+1]}(\omega) \end{aligned} \tag{4.6}$$

The matrices $\mathbf{A}_g^x(\omega)$ and $\mathbf{A}_g^y(\omega)$, the first two column vectors of the array $\mathbf{T}^T[-\mathbf{M}_t + \mathbf{B}_{Rg}(\omega)]$, are the base forces due to harmonic ground acceleration in the x- and y-directions, respectively. The matrix $\mathbf{A}_s(\omega) = \mathbf{T}^T\mathbf{B}_{Rs}(\omega)\mathbf{T}_\beta$ contains the base forces due to harmonic sliding acceleration. The matrix $\mathbf{A}_x(\omega)$ contains the base forces due to harmonic dam deformation and foundation displacement. These matrices are defined as:

$$\mathbf{A}_g^x(\omega) = \left[\begin{array}{c} -M_{T_{11}} + T_{11}B_{00}(\omega) \\ -M_{T_{21}} + T_{12}B_{00}(\omega) \\ -M_{T_{31}} + T_{33}B_{y\theta}(\omega) \end{array} \right] \tag{4.7a}$$

$$\mathbf{A}_g^y(\omega) = \left[\begin{array}{c} -M_{T_{12}} + T_{11}B_{y0}(\omega) \\ -M_{T_{22}} + T_{12}B_{y0}(\omega) \\ -M_{T_{32}} + T_{33}B_{y\theta}(\omega) \end{array} \right] \tag{4.7b}$$

$$\mathbf{A}_s(\omega) = \begin{bmatrix} T_{11}B_{00}(\omega)\cos\beta \\ T_{12}B_{00}(\omega)\cos\beta \\ T_{33}B_{0\theta}(\omega)\cos\beta \end{bmatrix} \tag{4.7c}$$

$$\mathbf{A}_x(\omega) = [-\mathbf{T}^T\mathbf{L}^T + \mathbf{T}^T\mathbf{B}_{Rz}(\omega) \quad -\mathbf{T}^T\mathbf{M}_t + \mathbf{T}^T\mathbf{B}_{Rf}(\omega)] \tag{4.7d}$$

where the coefficients $M_{T_{ij}}$ and T_{ij} are individual elements of the matrices $\mathbf{T}^T\mathbf{M}_t$ and $\mathbf{T}$, respectively. The matrices $\mathbf{A}_g^x(\omega)$, $\mathbf{A}_g^y(\omega)$, $\mathbf{A}_s(\omega)$, and $\mathbf{A}_x(\omega)$ are evaluated by the same interpolation procedure used for the frequency response functions.

Equation 4.6 can be modified by using equation 4.2 to express the acceleration vector, $\bar{\bar{\mathbf{X}}}^{[k+1]}(\omega)$, in terms of ground acceleration and sliding acceleration for iteration k. After performing this substitution the following equation for the base forces is obtained:

$$\begin{Bmatrix} \bar{V}^{[k+1]}(\omega) \\ \bar{N}^{[k+1]}(\omega) \\ \bar{M}^{[k+1]}(\omega) \end{Bmatrix} = \mathbf{C}_x(\omega)\bar{\bar{U}}_g^x(\omega) + \mathbf{C}_y(\omega)\bar{\bar{U}}_g^y(\omega) + \mathbf{C}_s(\omega)\bar{\bar{U}}_{s\beta}^{[k]}(\omega) \tag{4.8}$$

where the vectors $\mathbf{C}_x(\omega)$, $\mathbf{C}_y(\omega)$, and $\mathbf{C}_s(\omega)$ are defined as:

$$\mathbf{C}_x(\omega) = \mathbf{A}_g^x(\omega) - \omega^2\mathbf{A}_x(\omega)\bar{\mathbf{Y}}^x(\omega) \tag{4.9a}$$

$$\mathbf{C}_y(\omega) = \mathbf{A}_g^y(\omega) - \omega^2\mathbf{A}_x(\omega)\bar{\mathbf{Y}}^y(\omega) \tag{4.9b}$$

$$\mathbf{C}_s(\omega) = \mathbf{A}_s(\omega) - \omega^2\mathbf{A}_x(\omega)\bar{\mathbf{Y}}^s(\omega) \tag{4.9c}$$

The use of equation 4.8 to calculate the interface forces is very convenient during the iterative HFTD procedure. All terms in this equation are known at the beginning of the computation and remain unchanged, except for the transform of the sliding acceleration, $\bar{\bar{U}}_{s\beta}^{[k]}$, which is the only function that must be computed and updated in each iteration.

4.7 Fourier Transforms

The transformations between frequency domain and time domain are performed in discrete form, using response values computed at M discrete points over the period T_p. The maximum frequency that is represented in the transformation is $\omega_{max} = \frac{\pi}{\Delta t}$, where Δt is the time interval. The following notation for the discrete Fourier pair transform is used in the specification of the solution procedure:

$$IDF[G] \equiv G_m = \frac{1}{M} \sum_{r=0}^{M-1} G_r e^{-2i\pi mr/M} \qquad m = 0, 1, ..., M-1$$

$$DFT[G] \equiv G_r = \sum_{m=0}^{M-1} G_m e^{2i\pi mr/M} \qquad r = 0, 1, ..., M-1$$

A efficient Fourier transform package, FFTPACK [Swarztrauber, 1985], is used in the implementation. The program computes and saves the exponents at the beginning and uses them for each transformation, providing considerable savings in computation.

4.8 Algorithm for the Solution Procedure

This section presents the algorithm for the solution procedure. The total duration of response is divided into segments. The functions $\mathbf{C}_l(\omega)$, defined in equation 4.9, are computed prior to the beginning of the iterative solution.

The solution procedure for a segment $i+1$, given the computed solution for segment i, proceeds as follows:

1. Initialize solution for segment $i+1$.

   (a) Transform the components of ground acceleration to the frequency domain. Even though the ground acceleration is constant, it is convenient to evaluate the transformation for segment $i+1$ with a subsequent quiet zone of zeroes:

   $$\bar{\ddot{U}}_g^l(\omega) = IDF[\ddot{U}_g^l(t)] \qquad l = x, y$$

   (b) The sliding acceleration for the segment is initialized to zero: $U_{s\beta}^{[0]}(t) = 0$.

   (c) Initialize the counter for iteration: $k = 0$.

2. Increment iteration counter: $k = k + 1$.

3. Compute the Fourier transform of the sliding acceleration:

   $$\bar{\ddot{U}}_{s\beta}^{[k]}(\omega) = IDF[\ddot{U}_{s\beta}^{[k]}(t)]$$

4. Compute displacements.

   (a) Compute the displacements for iteration $k+1$, in frequency domain, using equation 4.2:

   $$\bar{\mathbf{X}}^{[k+1]}(\omega) = \bar{\mathbf{Y}}^x(\omega)\bar{\ddot{U}}_g^x(\omega) + \bar{\mathbf{Y}}^y(\omega)\bar{\ddot{U}}_g^y(\omega) + \bar{\mathbf{Y}}^s(\omega)\bar{\ddot{U}}_{s\beta}^{[k]}(\omega)$$

   The frequency response functions, $\bar{\mathbf{Y}}^x(\omega)$, $\bar{\mathbf{Y}}^y(\omega)$ and $\bar{\mathbf{Y}}^s(\omega)$, are evaluated using the interpolation procedure.

   (b) Transform the displacements for iteration $k+1$ to the time domain:

   $$\mathbf{X}^{[k+1]}(t) = DFT[\bar{\mathbf{X}}^{[k+1]}(\omega)]$$

5. Compute interface forces.

   (a) Compute the base forces in the frequency domain according to equation 4.8:

$$\left\{ \begin{array}{c} \bar{V}^{[k+1]}(\omega) \\ \bar{N}^{[k+1]}(\omega) \\ \bar{M}^{[k+1]}(\omega) \end{array} \right\} = \mathbf{C}_x(\omega)\bar{\ddot{U}}_g^x(\omega) + \mathbf{C}_y(\omega)\bar{\ddot{U}}_g^y(\omega) + \mathbf{C}_s(\omega)\bar{\ddot{U}}_{s\beta}^{[k]}(\omega)$$

   (b) Transform the base forces to the time domain:

$$\left\{ \begin{array}{c} V^{[k+1]}(t) \\ N^{[k+1]}(t) \\ M^{[k+1]}(t) \end{array} \right\} = DFT[\left\{ \begin{array}{c} \bar{V}^{[k+1]}(\omega) \\ \bar{N}^{[k+1]}(\omega) \\ \bar{M}^{[k+1]}(\omega) \end{array} \right\}]$$

6. Dam initiates sliding phase.

   (a) When the dam at a given step is in the non-sliding phase, $e^{[k]}(t) = 0$, compute the total shear force at the base of the dam and the friction resisting force:

$$V_\beta^{t[k+1]}(t) = V^{[k+1]}(t) + V_{\beta,st}$$

$$V_{friction}^{[k+1]}(t) = c + \mu[N^{[k+1]}(t) + N_{\beta,st}]$$

   (b) Apply the Mohr-Coulomb law to determine if the dam will start to slide. If the total shear force is greater than the resisting friction force:

$$|V_\beta^{t[k+1]}(t)| \geq |V_{friction}^{[k+1]}(t)|$$

   then the dam slides and the direction of sliding is given by:

$$e^{[k+1]}(t) = \frac{V^{[k+1]}(t) + V_{\beta,st}}{|V^{[k+1]}(t) + V_{\beta,st}|}$$

7. Dam continues in sliding phase.

   (a) The dam is in the sliding phase when $e^{[k]}(t) = \pm 1$. A new estimate of the sliding acceleration is computed using equation 3.17:

$$\ddot{U}_{s\beta}^{[k+1]}(t) = \frac{(V^{[k+1]}(t) + V_{\beta,st}) - e^{[k]}(t)\,[c + \mu(N^{[k+1]}(t) + N_{\beta,st})]}{m_R(t)}$$

   (b) The dam will continue sliding, $e^{[k+1]}(t) = e^{[k]}(t)$, and the sliding velocity and sliding displacement are obtained by integration of the sliding acceleration. A linear variation of sliding acceleration between time steps is assumed for this calculation.

8. Dam returns to non-sliding phase.

   (a) When the dam is in the sliding phase, it is necessary to check if sliding stops, according to sliding velocity. If the sliding velocity does not change sign between two consecutive steps, then the dam continues in the sliding phase. If there is a change in sign or if the sliding velocity is equal to zero, then the dam has changed from sliding to a non-sliding phase.

   (b) This change in state occurs between two time steps. Since the calculation is performed only at discrete steps, the stick condition can only be enforced approximately. The approach used to determine the change in the sliding state is shown in Figure 4.2. When the dam stops sliding, the sliding velocity at that step is assumed to be zero. The sliding acceleration is corrected for this condition, and the sliding displacement is obtained by integrating the sliding velocity.

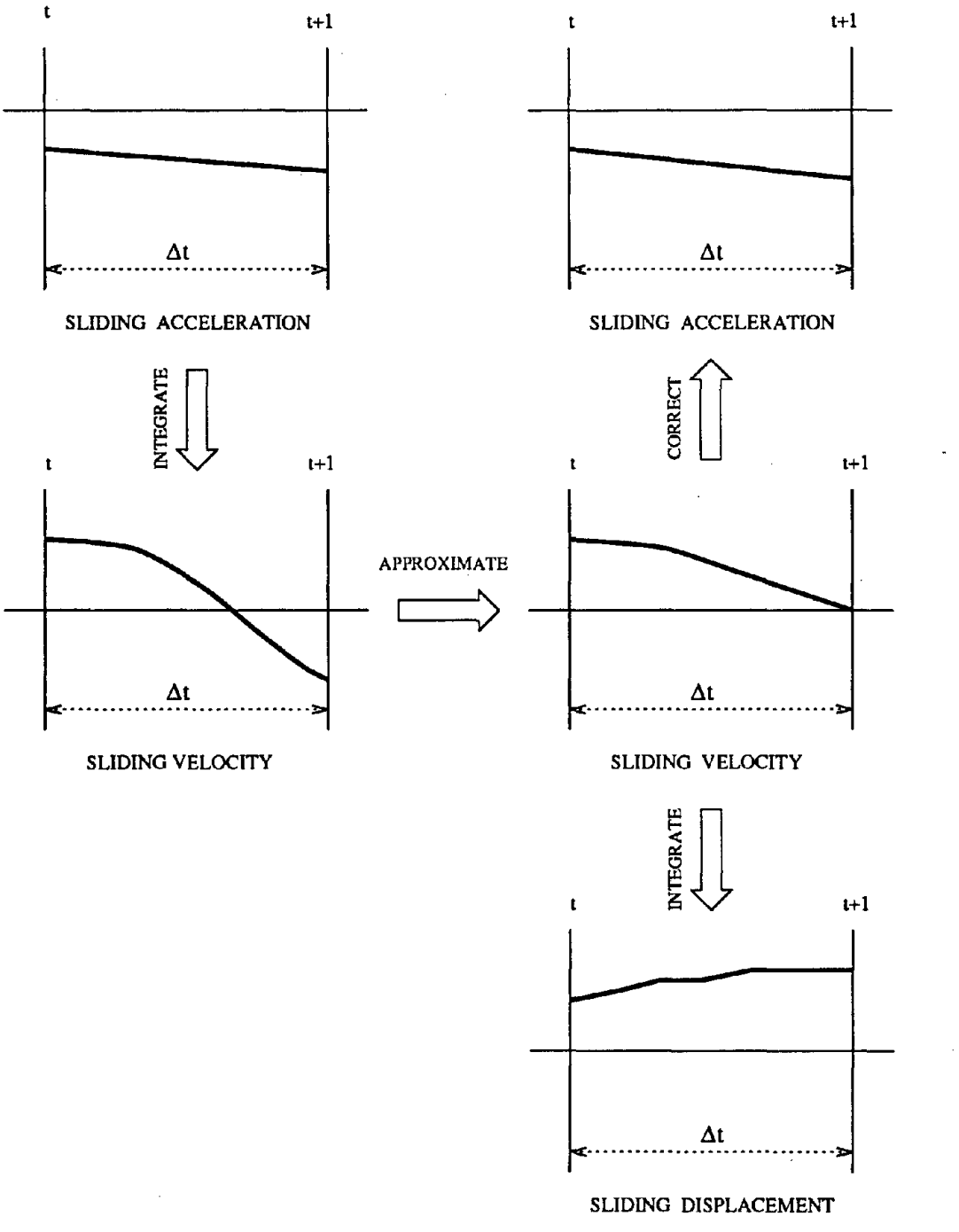

Figure 4.2. Change of state from sliding to non-sliding according to sliding velocity.

9. Check of convergence.

   (a) Apply equation 4.1 to compute the error functions for the solution, and check the convergence at each time step.

   (b) If convergence has not been achieved, go to step 2 for the next iteration. The calculations for the next iteration begin with the step where convergence was last achieved in the current segment.

   (c) If convergence has been achieved for all time steps within the segment, start the solution for the next segment at step 1.

4.9 Computer Program

A computer program, EAGD-SLIDE, implements the solution procedure for the earthquake-induced sliding response of concrete gravity dams including the dam-water interaction and the dam-foundation rock interaction. The program is available from the National Information Service for Earthquake Engineering (NISEE). [1]

All input data are in free-format. Input includes properties of dam, reservoir, foundation rock and parameters for the application of the HFTD procedure. The output includes time histories of dam displacements, time history of sliding displacement and interface forces, time history of energy quantities. Maximum response quantities, including maximum principal stresses in the dam and time of occurrence, are also evaluated.

[1] NISEE, 404A Davis Hall, University of California at Berkeley, Berkeley, CA, 94720.

Chapter 5

EARTHQUAKE RESPONSE OF PINE FLAT DAM

5.1 Introduction

The analysis procedure presented in Chapters 3 and 4 is used to compute the earthquake response of Pine Flat dam. The emphasis of this study is the nonlinear response of the dam due to sliding at the base. Previous studies have investigated the linear response of this dam [Fenves and Chopra, 1984a, 1984b]. The purpose of the current study is to: (a) demonstrate the applicability of the HFTD procedure for evaluating the earthquake response of concrete gravity dams, including the effects of dam-water interaction, dam-foundation rock interaction, and sliding at the dam-foundation rock interface; and (b) determine how sliding affects the response of a typical concrete dam.

Various cases of the dam system subjected to selected ground motions are considered to show the influence of the parameters on the sliding response of the dam, such as: the number of Ritz vectors used in the solution, the value of the coefficient of friction, the foundation rock flexibility, and the angle of base inclination. The influence of different ground motions and the influence of the amplitude of the ground acceleration on the response of the dam are also considered.

5.2 Properties of Pine Flat Dam

Pine Flat dam is a 561 m (1840 ft) long concrete gravity dam near Fresno, California. The tallest of the thirty-seven monoliths is 122 m (400 ft) high, and each monolith is 12 m (40 ft) to 15 m (50 ft) wide. The tallest monolith has a typical cross section for gravity dams. A two-dimensional, plane stress finite element idealization for the monolith is shown in Figure 5.1. The model consists of 36 nine-node quadrilateral elements and 171 nodes.

The angle of inclination at the base, β, is 0^o for most of the cases studied, although it is changed to 5^o sloping downstream and -5^o sloping upstream, as shown in Figure 5.2, for studying the influence of the base inclination on the sliding response. The cohesion force at the base is assumed to be zero and the coefficient of friction varies from 0.8 to 1.2. These values represent the friction properties at the interface as recommended in previous studies [Danay and Adeghe, 1993; Chopra and Zhang, 1991].

The dam concrete is assumed to be isotropic, homogeneous and elastic with the following properties: modulus of elasticity = 22.4 GPa (3.25 million psi), unit weight = 24.3 kN/m^3 (155 pcf), and Poisson's ratio = 0.2. A constant hysteretic damping factor of 0.10, which corresponds to 5 percent of critical viscous damping at resonance, is used to model the energy dissipation in the dam.

The foundation rock is idealized as a homogeneous, isotropic, viscoelastic half-plane with the following properties: Poisson's ratio = 0.33, unit weight = 25.9 kN/m^3 (165 pcf), and hysteretic damping coefficient = 0.10. The modulus of elasticity for

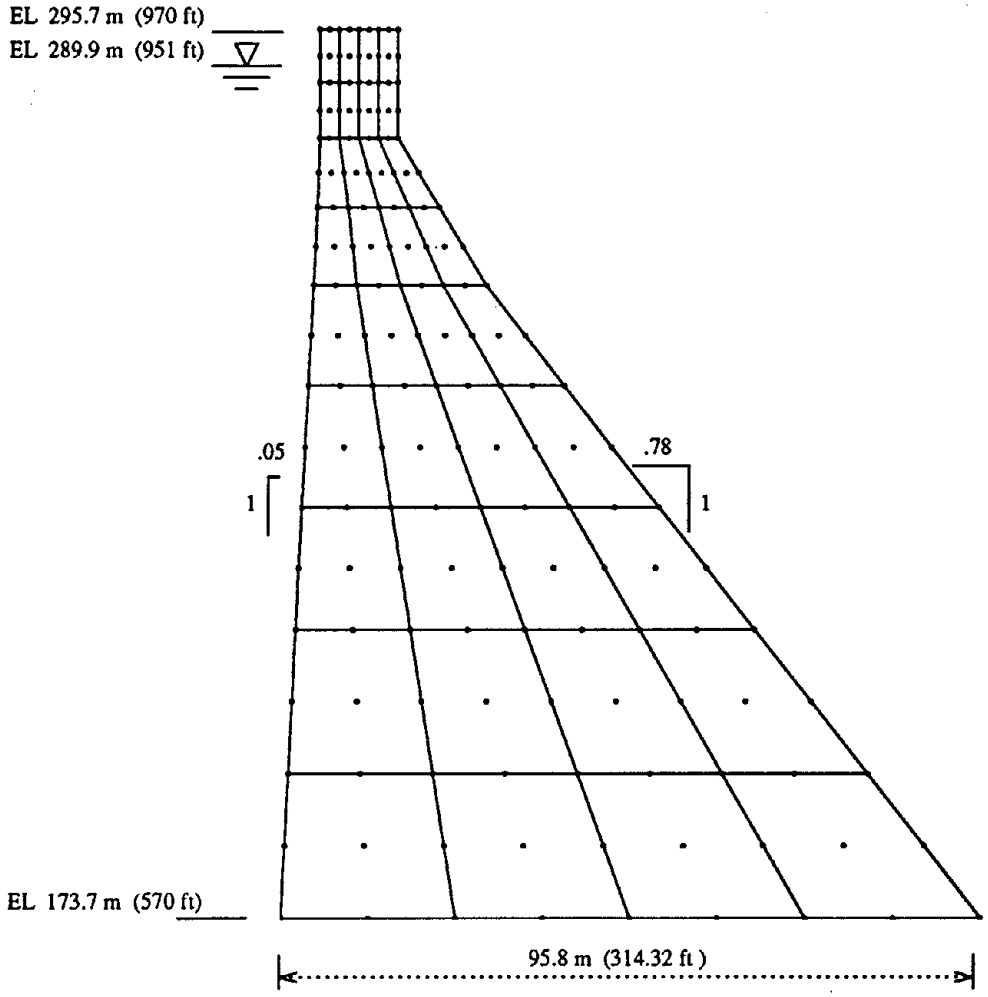

Figure 5.1. Finite element idealization of tallest monolith of Pine Flat dam.

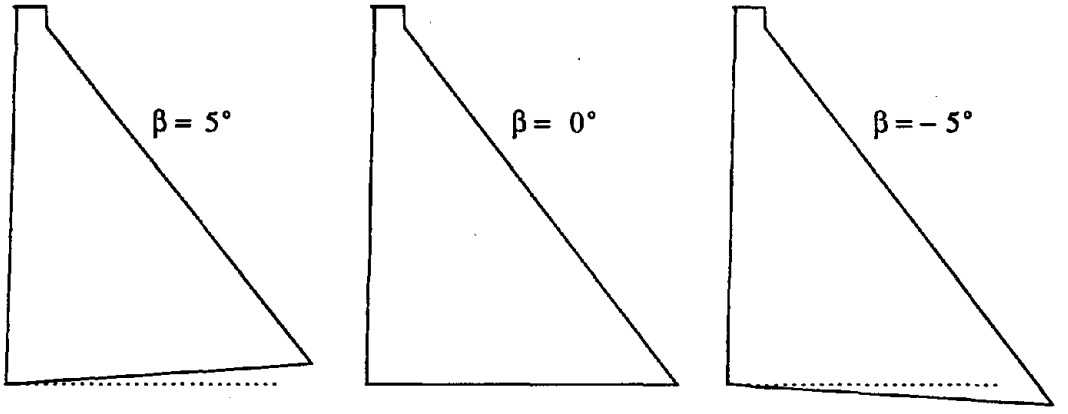

Figure 5.2. Inclination of dam base.

the foundation rock is varied to consider the effects of the foundation rock flexibility on the dam response. The following ratios between the modulus of elasticity of the concrete dam, E_{cd}, and the modulus of elasticity of the foundation rock, E_{fr}, are used: $E_{fr}/E_{cd} = \infty$, 4, 1, 0.25. The first case corresponds to a dam with rigid foundation rock, and the last case is a very flexible, although not untypical, foundation rock.

The impounded water has a depth of H = 116.2 m (381 ft) and the following properties: unit weight = 9.8 kN/m^3 (62.4 pcf), wave velocity = 1440 m/sec (4720 ft/sec). The wave reflection coefficient for the reservoir bottom materials is $\alpha = 1$ for most of the cases (rigid reservoir bottom), but a value of $\alpha = 0.9$ is used for the cases subjected to vertical ground motion. The resultant uplift force at the base is evaluated assuming a triangular distribution of internal pressure from 1.14 MPa (24 ksf) at the upstream face to zero at the downstream face. To account for drainage only 40 percent of the resultant uplift force is considered in the earthquake analysis.

5.3 Earthquake Ground Motions

The primary ground motion used for the evaluation of the earthquake response of Pine Flat dam is the Taft record, S69E horizontal and vertical components, obtained at the Lincoln School Tunnel in the 1952 Kern County earthquake. This ground motion contains a wide spectrum of frequencies and it has been used for many studies of concrete gravity dams [Chopra, Chakrabarti, and Gupta, 1980; Fenves and Chopra, 1984a]. The second ground motion is the El Centro record, S00E component, obtained in the 1940 Imperial Valley earthquake. This record has been widely used for the analysis of many structures. It has large velocity pulses that may affect the sliding of a dam. Another ground motion used is the Pacoima record, S16E component, recorded at Pacoima dam during the 1971 San Fernando earthquake. This record contains a large peak acceleration which can induce sliding of a dam. Table 5.1 lists the earthquakes used in the study and Figure 5.3 shows the acceleration histories normalized with respect to their individual peak accelerations.

A large peak ground acceleration does not necessarily produce a large response of a structure. In the case of dam sliding, however, the value of peak acceleration

Table 5.1. Ground motion records and peak ground accelerations.

Ground Motion	Component	Peak Acceleration (g)
Taft	S69E	0.18
Taft	VRT	0.11
El Centro	S00E	0.35
Pacoima	S16E	1.17

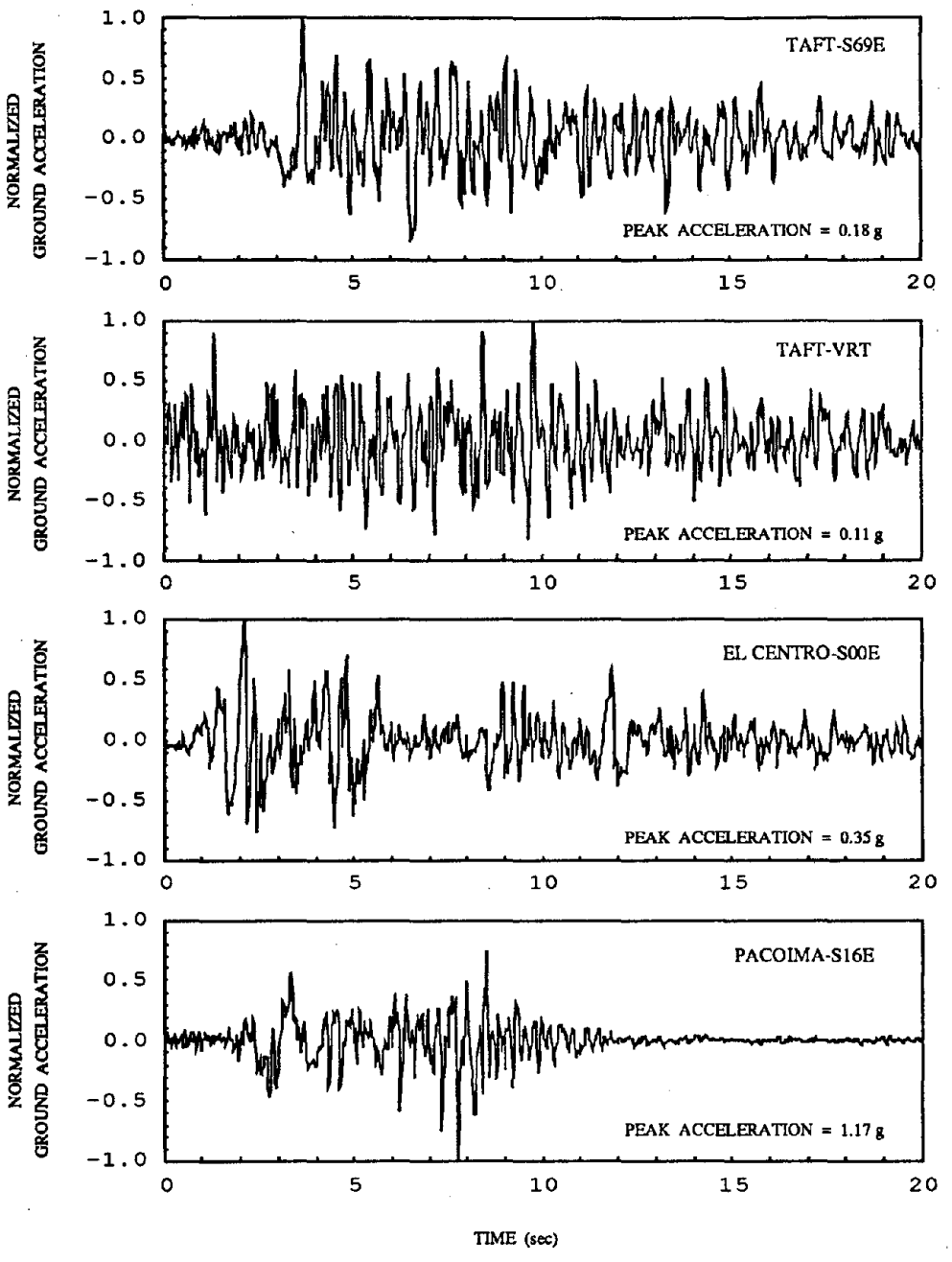

Figure 5.3. Ground acceleration records, normalized to individual peak ground accelerations.

determines whether sliding initiates and the amount of sliding displacement [Chopra and Zhang, 1991]. For most of the analysis, the horizontal components of ground motion are scaled to a peak acceleration of 0.4g, which is a typical value for moderate to strong earthquakes. The vertical component of Taft ground motion is scaled to a peak acceleration of 0.26g, which is two-thirds of the scaled horizontal peak acceleration. Additional analysis are performed using the S69E component of the Taft ground motion scaled to a peak acceleration of 0.6g to study the influence of the ground motion amplitude on the response of the dam.

5.4 Analysis Parameters

The analysis is performed using a time step of 0.01 sec. This time step is adequate for the nonlinear sliding analysis, and it is comparable to time steps used for analysis of the linear response. The response is computed for the first 20 sec of each ground motion. A quiet zone of 20.46 sec is appended to the first 20 sec of the acceleration data for a total duration of 40.46 sec. This corresponds to $2^{12} = 4096$ time steps for the discrete Fourier transforms. The maximum frequency represented is 50 Hz which is beyond the frequencies included in the processed ground motion acceleration records.

The total duration of response is divided into segments of equal length. Each segment consists of 20 time steps. The convergence of the solution is relatively fast using these short segments. The normal force is assumed to be constant during the determination of siding state, so the change in normal forces due to dam deformation is not considered. This is necessary to ensure convergence of the solution for all cases.

5.5 Cases Analyzed and Description of Response Quantities

The tallest monolith of Pine Flat dam is analyzed for several cases to evaluate the effects of: (a) the number of Ritz vectors used in the solution procedure, (b) the earthquake ground motion and its amplitude, (c) the coefficient of friction, (d) the flexibility of the foundation rock, (e) the vertical component of ground acceleration, and (f) the angle of inclination, β, at the base. Dam-water interaction with compressible water is included for all cases. Empty reservoir cases are not presented because the dam with empty reservoir does not slide for any of the ground motions and parameters considered. The cases analyzed and the maximum values of responses are summarized in Tables 5.2, 5.3, and 5.4.

The response results consist of time histories of displacements, forces, and energy quantities, and contours of maximum principal stresses. For each case, time history responses are presented for:

- Horizontal displacement of dam crest with respect to the base, indicating the level of dam deformation.
- Sliding displacement at the interface, $U_{s\beta}(t)$. Sliding displacement is positive in the downstream direction.
- Base shear force, $V_\beta(t)$. Sliding initiates when the base shear force exceeds the friction resistance at the base.
- Eccentricity ratio for base forces, which is defined as:

$$\text{eccentricity ratio} = -\frac{M_\beta(t)/N_\beta(t)}{B/2}$$

Table 5.2. Cases for earthquake analysis of Pine Flat dam on rigid foundation rock and maximum values of response. Peak ground acceleration is 0.4g for horizontal ground motion and 0.26g for vertical ground motion.

Ground Motion	Parameters				Maximum Response			
	α	β (°)	μ	J Ritz vect.	Dam def. (mm)	Base slide disp. (mm)	Stress upstream face (MPa)	Stress downstream face (MPa)
Taft-S69E	1.0	0	1.0	1	79	116	6.0	5.0
	1.0	0	1.0	5	80	124	5.0	5.0
El Centro-S00E	1.0	0	1.0	1	67	58	5.0	3.5
	1.0	0	1.0	5	74	58	5.0	4.0
Pacoima-S16E	1.0	0	1.0	1	77	36	5.0	5.0
	1.0	0	1.0	5	83	32	5.0	5.0
Taft-S69E	1.0	0	0.8	5	64	291	5.0	4.0
	1.0	0	0.9	5	73	187	5.0	4.0
	1.0	0	1.0	5	80	124	5.0	5.0
	1.0	0	1.2	5	86	38	6.0	5.0
	1.0	0	∞	5	87	0	7.0	5.0
Taft-S69E	1.0	5	1.0	5	75	53	5.0	7.0
	1.0	-5	1.0	5	76	201	5.0	4.0
Taft-S69E	0.9	0	1.0	5	78	115	5.0	5.0
Taft-VRT	0.9	0	1.0	5	48	0	3.5	3.5
Taft-S69E, VRT	0.9	0	1.0	5	80	112	6.0	5.0

Table 5.3. Cases for earthquake analysis of Pine Flat dam on flexible foundation rock and maximum values of response. Peak ground acceleration is 0.4g.

Ground Motion	Parameters					Maximum Response			
	E_{fr}/E_{cd}	α	β (°)	μ	J Ritz vect.	Dam def. (mm)	Base slide disp. (mm)	Stress upstream face (MPa)	Stress downstream face (MPa)
Taft	∞	1	0	1.0	5	80	124	6.0	5.0
S69E	4.00	1	0	1.0	5	80	113	5.0	4.0
	1.00	1	0	1.0	5	76	38	4.5	3.0
	0.25	1	0	1.0	5	94	3	3.0	2.5
Taft	0.25	1	0	0.8	5	93	62	2.0	2.5
S69E	0.25	1	0	0.9	5	93	21	2.5	2.5
	0.25	1	0	1.0	5	94	3	3.0	2.5
	0.25	1	0	1.2	5	98	0	3.0	2.5
	0.25	1	0	∞	5	98	0	3.0	2.5

Table 5.4. Cases for earthquake analysis of Pine Flat dam on flexible foundation rock and maximum values of response. Peak ground acceleration is 0.6g.

Ground Motion	Parameters					Maximum Response			
	E_{fr}/E_{cd}	α	β (°)	μ	J Ritz vect.	Dam def. (mm)	Base slide disp. (mm)	Stress upstream face (MPa)	Stress downstream face (MPa)
Taft	1.00	1	0	0.8	5	107	502	5.0	5.0
S69E	1.00	1	0	1.0	5	103	168	5.0	5.0
	1.00	1	0	1.2	5	113	64	6.0	5.0
Taft	0.25	1	0	0.8	5	128	228	2.5	4.0
S69E	0.25	1	0	1.0	5	140	56	3.5	4.0
	0.25	1	0	1.2	5	140	7	4.0	4.0

When the absolute value of this ratio exceeds one it means that the resultant base force is outside of the base and the dam will start rocking. A ratio greater than +1 indicates rocking about the heel, and a ratio less than -1 indicates rocking about the toe of the dam.

- Energy quantities, as defined in Appendix E, show the energy balance between the input energy and the work performed due to sliding of the base, displacement of the foundation, and dam deformation. The energy balance identifies the sources of dissipation of energy and verifies the accuracy of the solution.

The contours of maximum principal stresses do not include stresses due to the static loads. The stress contours are used to evaluate the effects of the parameters on the dynamic response only.

5.6 Response of Dam on Rigid Foundation Rock

The response of the dam on rigid foundation rock, $E_{fr}/E_{cd} = \infty$, shows the influence of basic parameters on the response: number of Ritz vectors, angle of base inclination, vertical ground motion, and coefficient of friction. The peak horizontal ground acceleration is scaled to 0.4g, and the peak vertical ground accelerations is scaled to 0.26g for these analysis.

5.6.1 Influence of Number of Ritz Vectors

The dam is analyzed using one and five Ritz vectors to investigate the influence of the number of Ritz vectors on the computed response of the dam to the Taft S69E

ground motion. As shown in Figures 5.4 and 5.5, the crest deformation time history and the base sliding time history are similar when one and five vectors are used. The maximum crest displacement is the same for both cases, but the maximum base sliding displacement is 7 percent greater when five vectors are used compared with one vector. The higher modes produce some additional base shear force and sliding, but do not affect significantly the dam deformation. Figure 5.10(a) shows that the analysis with one vector slightly overestimates the maximum principal stresses compared with the analysis including five vectors.

The response of the dam subjected to the El Centro S00E ground motion is shown in Figures 5.6 and 5.7. The maximum crest deformation is 10 percent greater when five vectors are included compared with one vector, but the base sliding displacement is the same for both cases. Sliding can be interpreted as an isolation mechanism that reduces higher modes participation. For this ground motion, however, the sliding is small, so the higher modes of vibration are not isolated and tend to contribute more to the deformation of the dam. The maximum principal stresses also increase slightly at the upstream and downstream faces when five vectors are used instead of one, as shown in Figure 5.10(b).

The response of the dam subjected to the Pacoima S16E ground motion is shown in Figures 5.8 and 5.9. The maximum crest deformation is comparable to the deformation observed for the Taft and El Centro ground motions, but the base sliding displacement is significantly less. The maximum crest deformation is 8 percent greater when five vectors are used compared with one vector. The larger crest displacement occurs during the first 8 sec of response, when there is no sliding, so the contribution

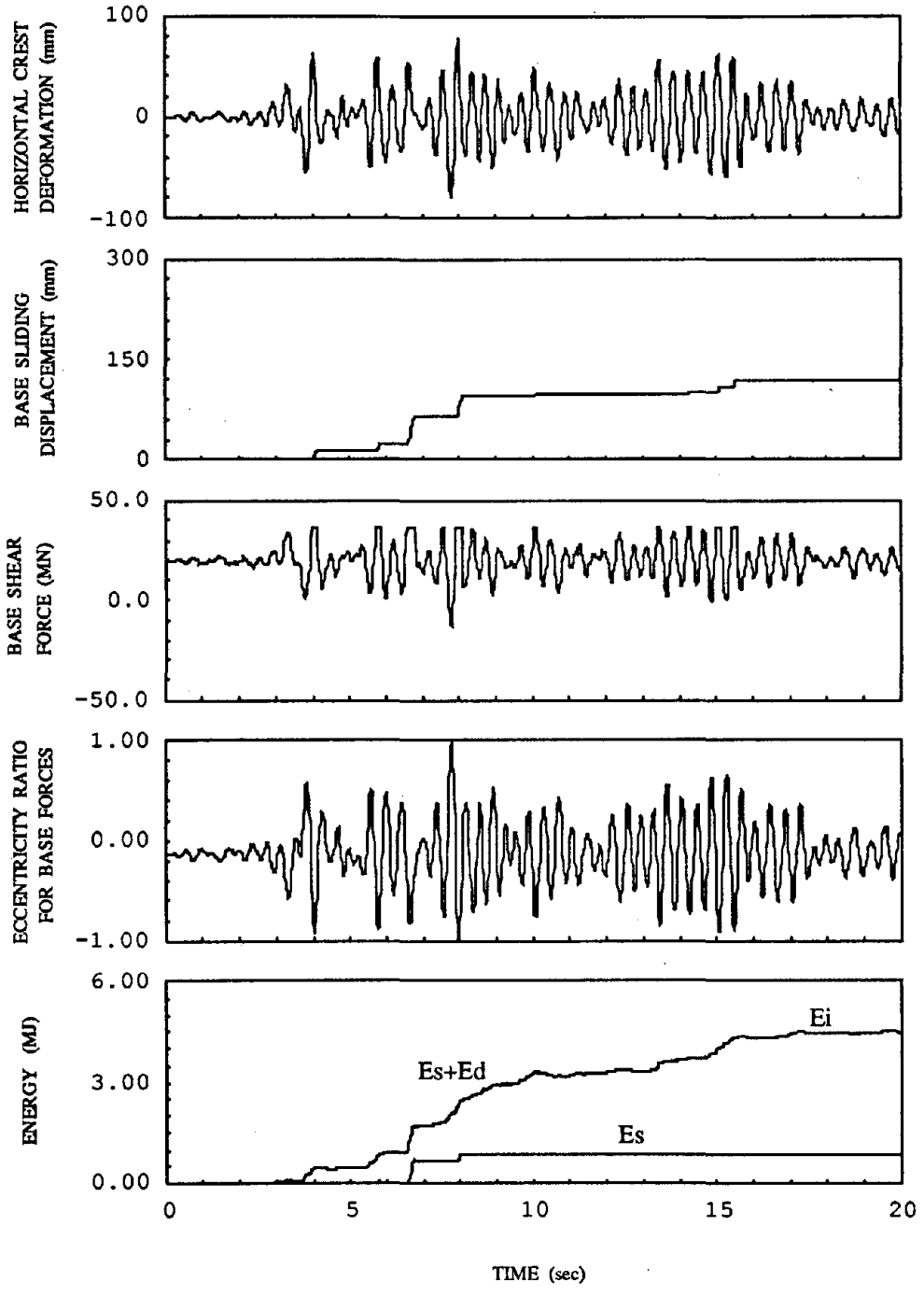

Figure 5.4. Response of Pine Flat dam with rigid foundation rock, horizontal interface, $\alpha = 1$, $\mu = 1$, subjected to the horizontal S69E component of Taft ground motion with peak ground acceleration = 0.4g. One Ritz vector is used in the analysis.

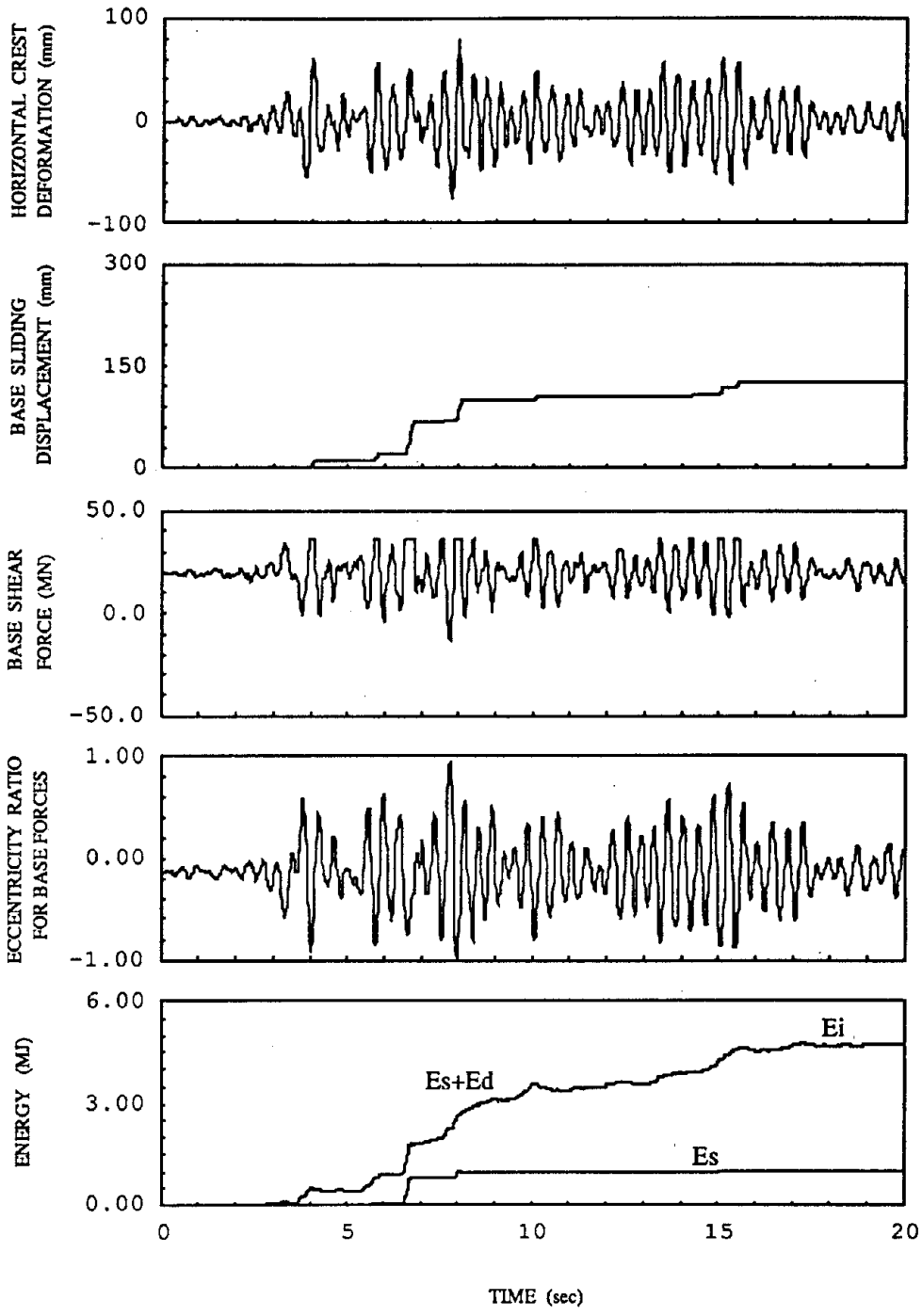

Figure 5.5. Response of Pine Flat dam with rigid foundation rock, horizontal interface, $\alpha = 1, \mu = 1$, subjected to the horizontal S69E component of Taft ground motion with peak ground acceleration = 0.4g. Five Ritz vectors are used in the analysis.

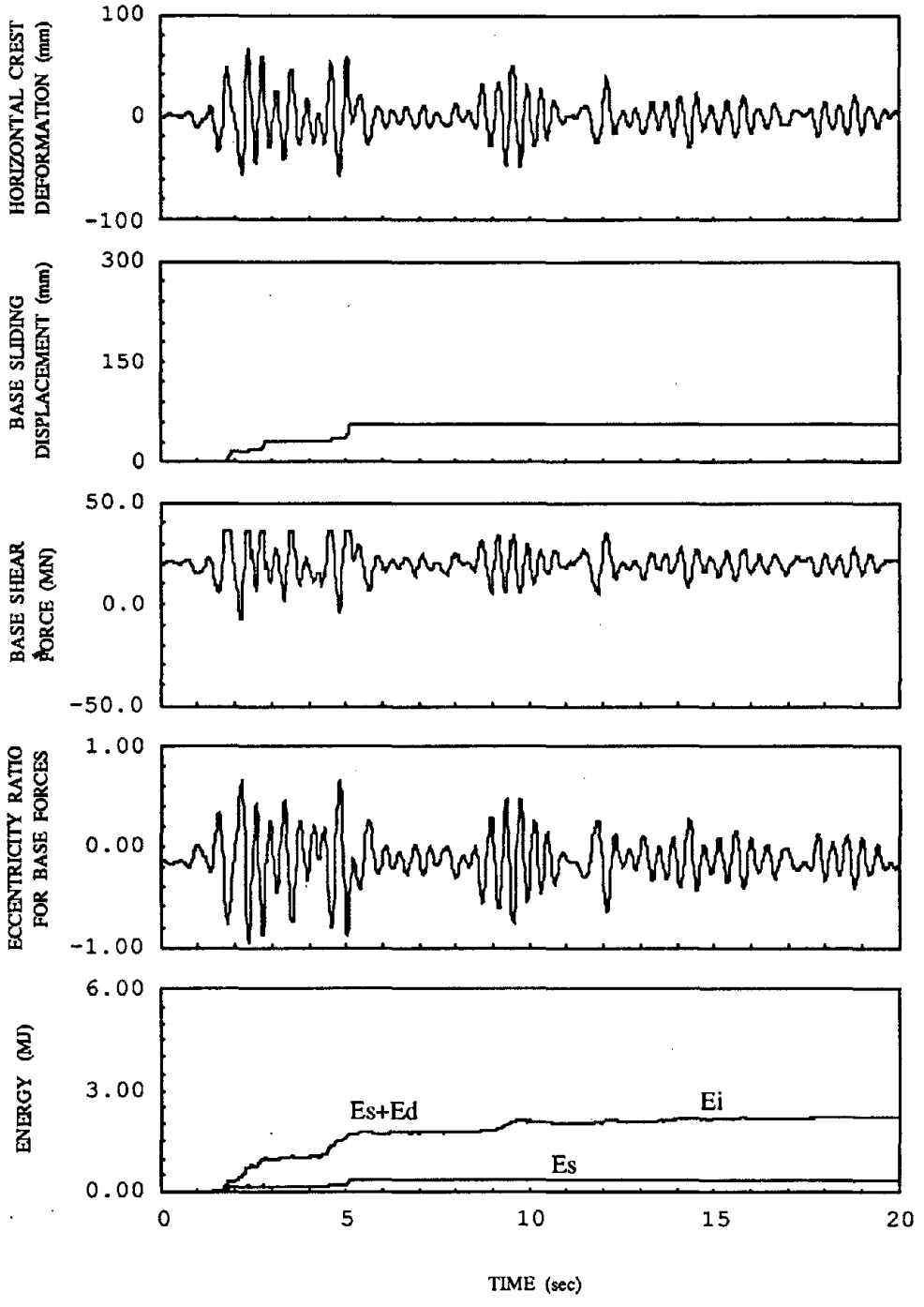

Figure 5.6. Response of Pine Flat dam with rigid foundation rock, horizontal interface, $\alpha = 1$, $\mu = 1$, subjected to the horizontal S00E component of El Centro ground motion with peak ground acceleration = 0.4g. One Ritz vector is used in the analysis.

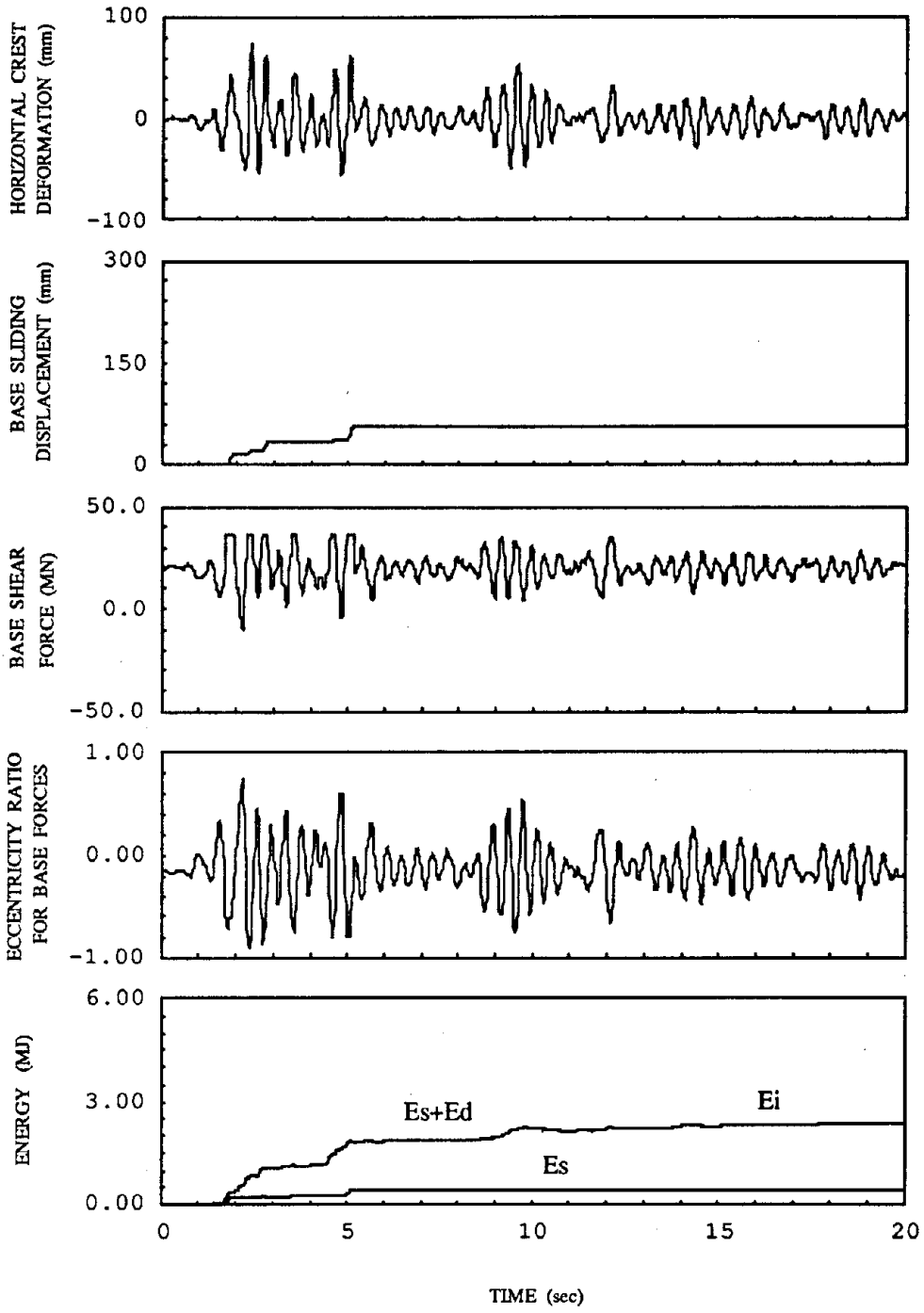

Figure 5.7. Response of Pine Flat dam with rigid foundation rock, horizontal interface, $\alpha = 1$, $\mu = 1$, subjected to the horizontal S00E component of El Centro ground motion with peak ground acceleration = 0.4g. Five Ritz vectors are used in the analysis.

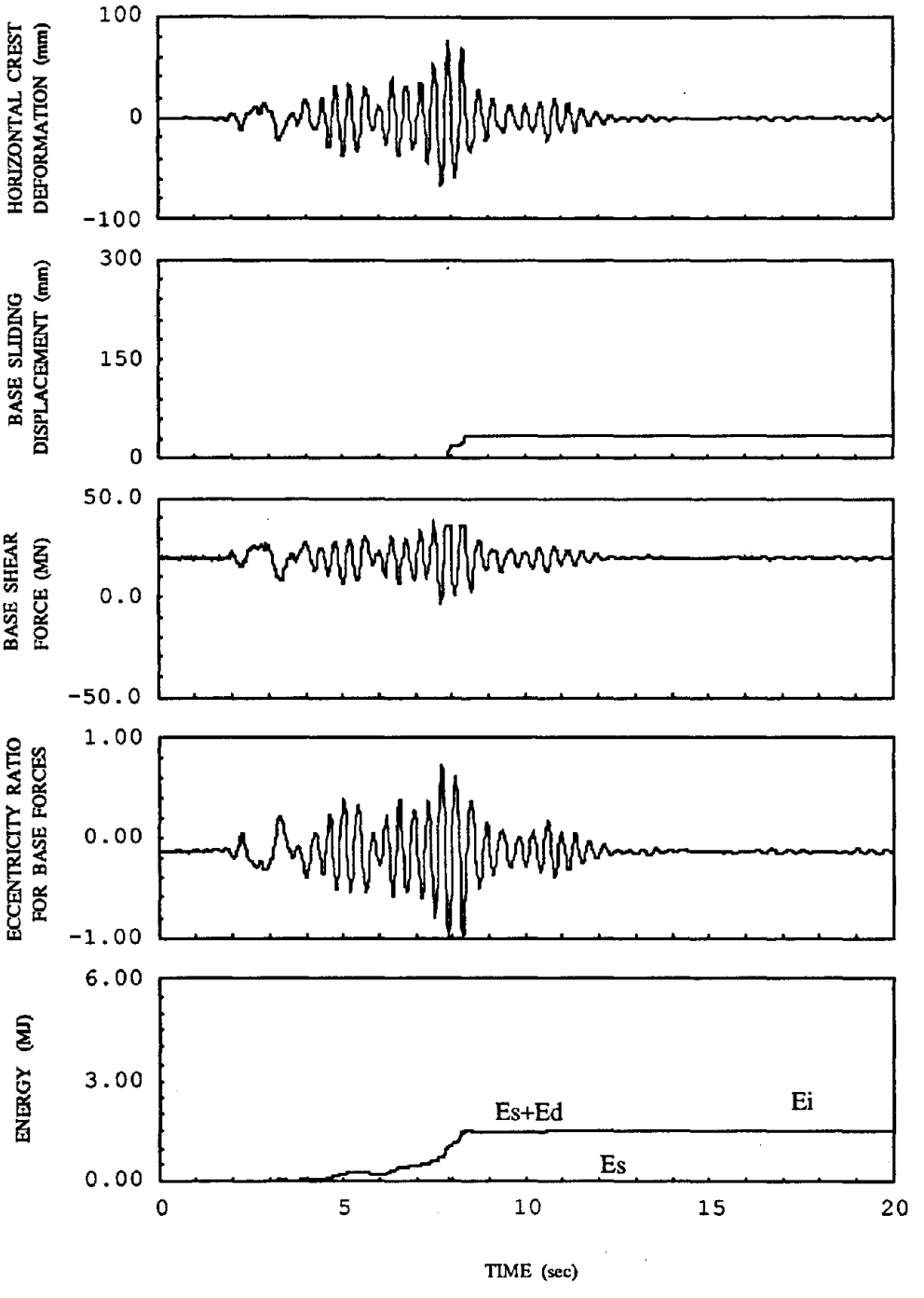

Figure 5.8. Response of Pine Flat dam with rigid foundation rock, horizontal interface, $\alpha = 1$, $\mu = 1$, subjected to the horizontal S16E component of Pacoima ground motion with peak ground acceleration = 0.4g. One Ritz vector is used in the analysis.

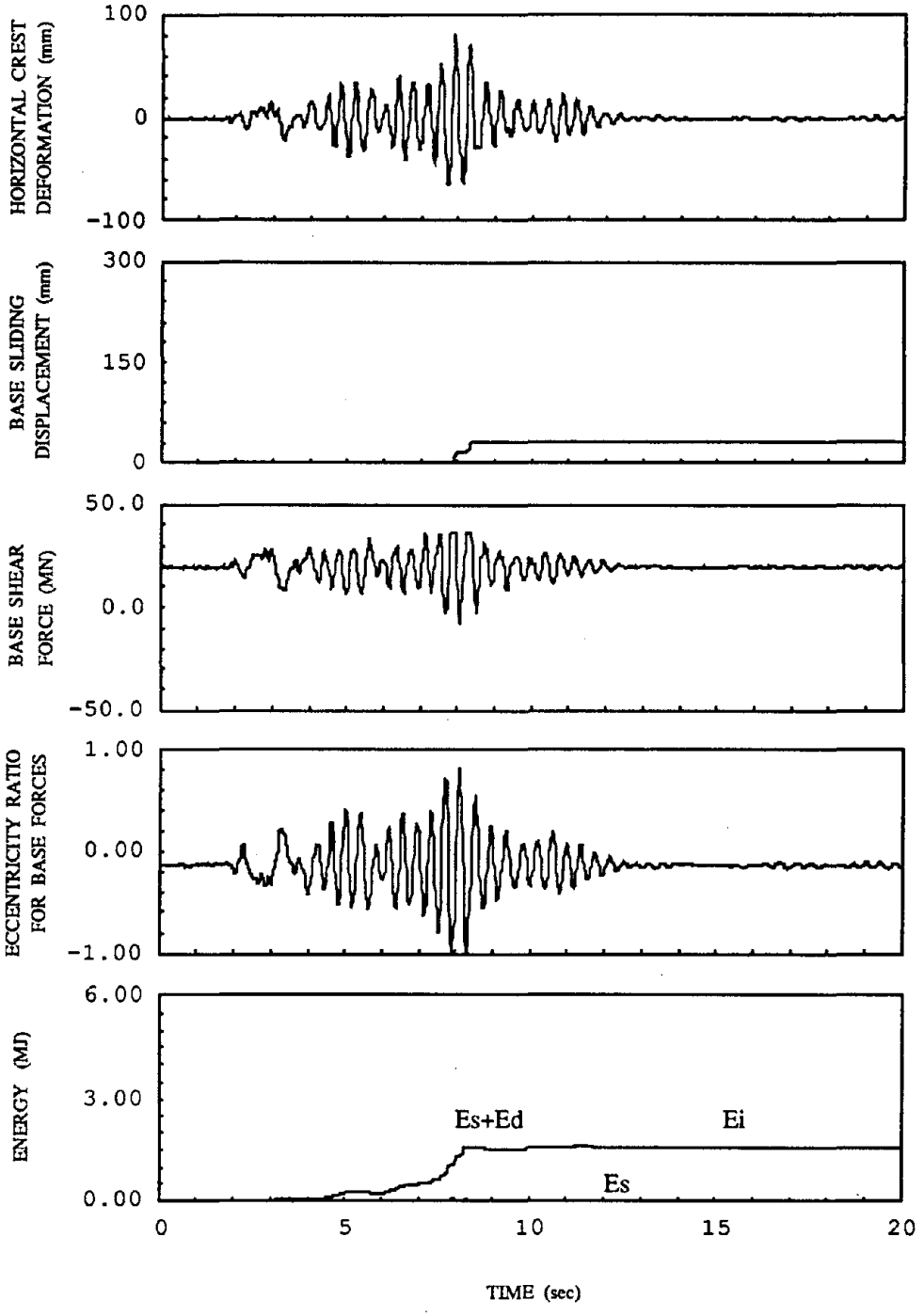

Figure 5.9. Response of Pine Flat dam with rigid foundation rock, horizontal interface, $\alpha = 1$, $\mu = 1$, subjected to the horizontal S16E component of Pacoima ground motion with peak ground acceleration = 0.4g. Five Ritz vectors are used in the analysis.

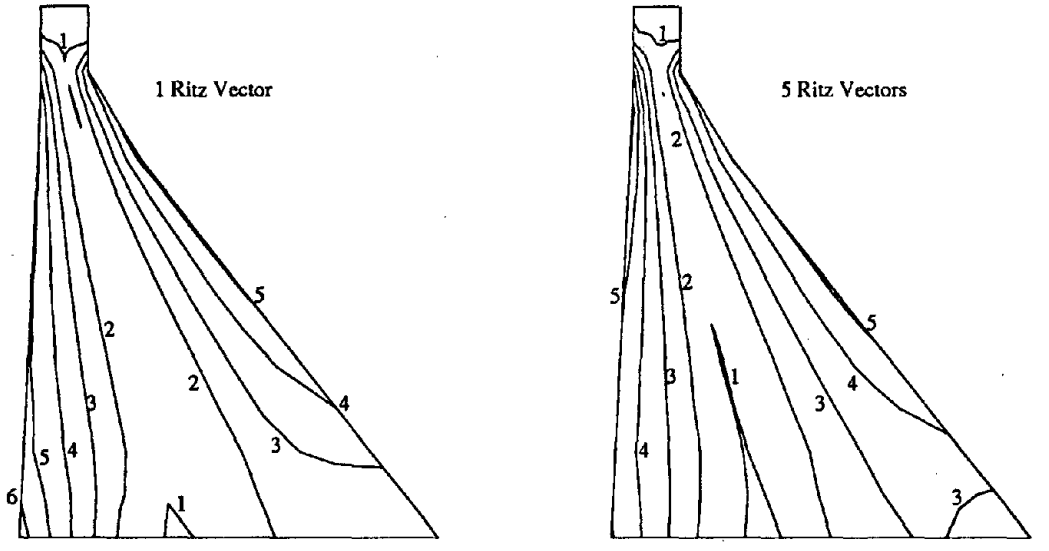

(a) Taft S69E

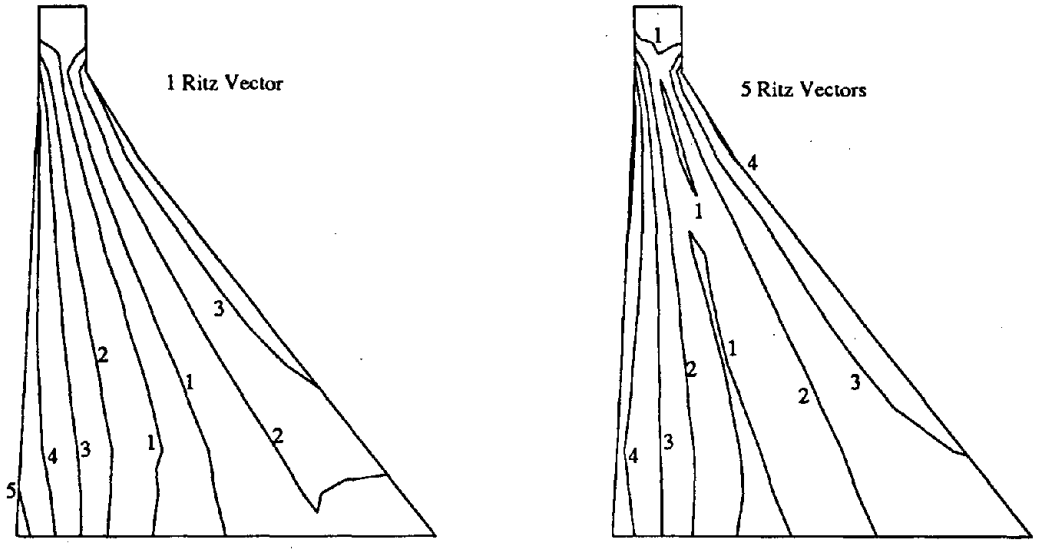

(b) El Centro S00E

Figure 5.10. Envelope of maximum principal stresses (in MPa) in Pine Flat dam with rigid foundation rock, horizontal interface, $\alpha = 1$ and $\mu = 1$, subjected to the horizontal S69E component of Taft, and to the horizontal S00E component of El Centro, ground motions with peak accelerations = 0.4g. Static effects not included.

of higher modes to the deformation of the dam is important. Contrary to the other cases, however, the base sliding displacement is slightly greater when one vector is used. The sliding occurs around 8 sec, near the time of the large pulse in the ground motion, otherwise the response is linear. Although not shown, the maximum stresses are the same in both cases.

These results indicate that higher Ritz vectors slightly affect the response of the dam. The differences in maximum dam crest deformations are on the order of 7 to 10 percent, depending on the ground motion. In general, the higher mode vectors tend to increase, although slightly, the sliding at the base. Therefore, five Ritz vectors will be used for the other cases.

5.6.2 Influence of Ground Motion

The characteristics of the ground motion affect significantly the sliding response of the dam. The response of the dam for the three ground motions, Taft S69E, El Centro S00E and Pacoima S16E, is shown in Figures 5.5, 5.7 and 5.9.

As shown in Figure 5.11, the base sliding due to the Taft ground motion is greater, by almost a factor of two, than the sliding due to the El Centro ground motion, and it is three times greater than the sliding due to the Pacoima ground motion. Taft produces larger sliding displacement because of the greater number of acceleration peaks over the long duration compared with the other records. Several sliding events occur at these peaks. El Centro produces sliding events that occur in the first 5 sec of response, when the ground motion is strongest. Pacoima produces two sliding events at around 8 sec, corresponding to the the large acceleration pulse in the

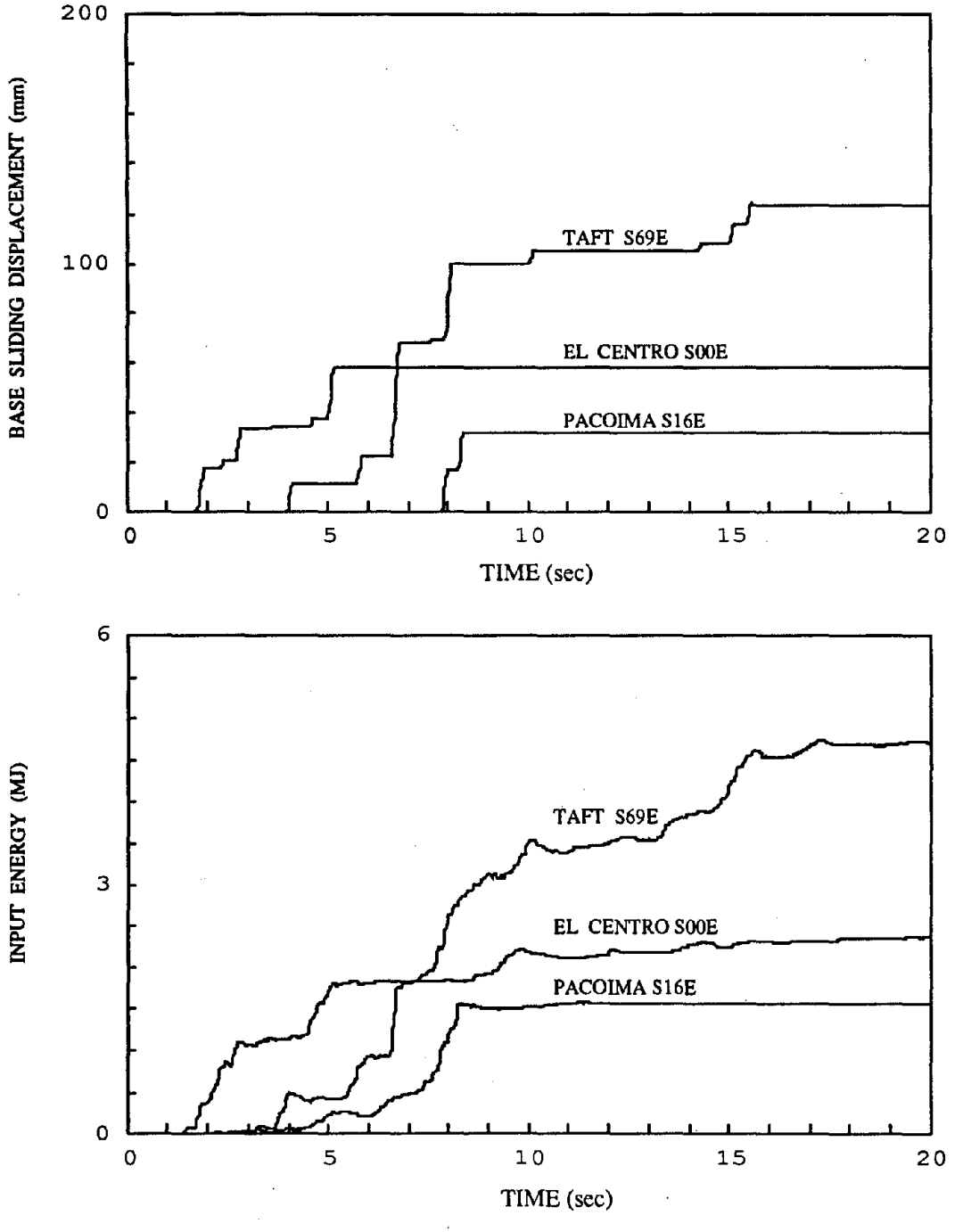

Figure 5.11. Sliding displacement and input energy for Pine Flat dam with rigid foundation rock, horizontal interface, $\alpha = 1$, $\mu = 1$, subjected to three ground motions with peak ground accelerations = 0.4g.

record. For all cases sliding accumulates in the downstream direction. Because of the few peaks in the El Centro and Pacoima records, the dam does not accumulate large base sliding displacement. The maximum crest deformation and maximum stresses are approximately the same for the three ground motions.

The input energy for the Taft ground motion is greater than the input energy for the El Centro and Pacoima ground motions, as shown in Figure 5.11. The input energy is an important parameter to evaluate the influence of the ground motion in the response of structures [Uang and Bertero, 1988], so it is expected that Taft ground motion produces the largest base sliding displacement of the dam. Therefore this ground motion is used to study in more detail the earthquake response of Pine Flat dam.

The eccentricity ratio for the base forces indicates the possibility of rocking of the dam during the earthquake. Taft produces three peaks with absolute values close to unity, as shown in Figure 5.5, although only one peak is greater than unity (at 8 sec), indicating initiation of rocking at this one instant of time. El Centro produces smaller eccentricity ratios and therefore the dam does not rock. Pacoima ground motion produces a large eccentricity ratio when the dam starts sliding and remains small thereafter.

5.6.3 Influence of the Coefficient of Friction

The most important parameter affecting the sliding of the dam is the value of the coefficient of friction, μ. Figures 5.12, 5.13, 5.5 and 5.14 show the time history responses of the dam with $\mu = 0.8,\ 0.9,\ 1.0$, and 1.2, respectively. Figure 5.15 shows

the linear response without sliding ($\mu = \infty$).

The maximum crest deformation increases almost linearly with the coefficient of friction, from 64 mm for $\mu = 0.8$ to 86 mm for $\mu = 1.2$. The crest deformation for $\mu = \infty$ (no sliding) is 87 mm. The maximum principal stresses, shown in Figure 5.16, increase at the upstream and downstream faces of the dam with larger values of μ, as expected, because dam stresses depend on the deformation of the dam.

The base sliding displacement is very sensitive to the coefficient of friction. Sliding initiates at early stages for smaller coefficients of friction. For $\mu = 0.8$ the sliding initiates at 3 sec, and for $\mu = 0.9$ and 1.0, sliding initiates at 4 sec. The maximum sliding displacement of the dam decreases nonlinearly with the increase of the coefficient of friction, from 291 mm for $\mu = 0.8$ to 38 mm for $\mu = 1.2$. The sliding displacement for $\mu = 0.8$ is one and one-half times that for $\mu = 0.9$, and more than twice that for $\mu = 1.0$. For $\mu = 1.2$ there are two small sliding events between 6.5 to 8 sec, and the response is very similar to the linear response of the dam shown in Fig 5.15. A slight decrease in the coefficient of friction may produce a large increase in the sliding displacement. For example reducing μ from 1.0 to 0.9, increases the sliding displacement by about 50 percent.

The eccentricity ratio (in absolute value) for the base forces decreases almost linearly with the value of μ. The eccentricity ratios for $\mu = 0.8$ and $\mu = 0.9$ are less than one. There is one peak close to one for $\mu = 1.0$ at 8 sec, and various peaks near one for $\mu = 1.2$. Thus rocking is not important for any of the cases with a peak ground acceleration of 0.4g.

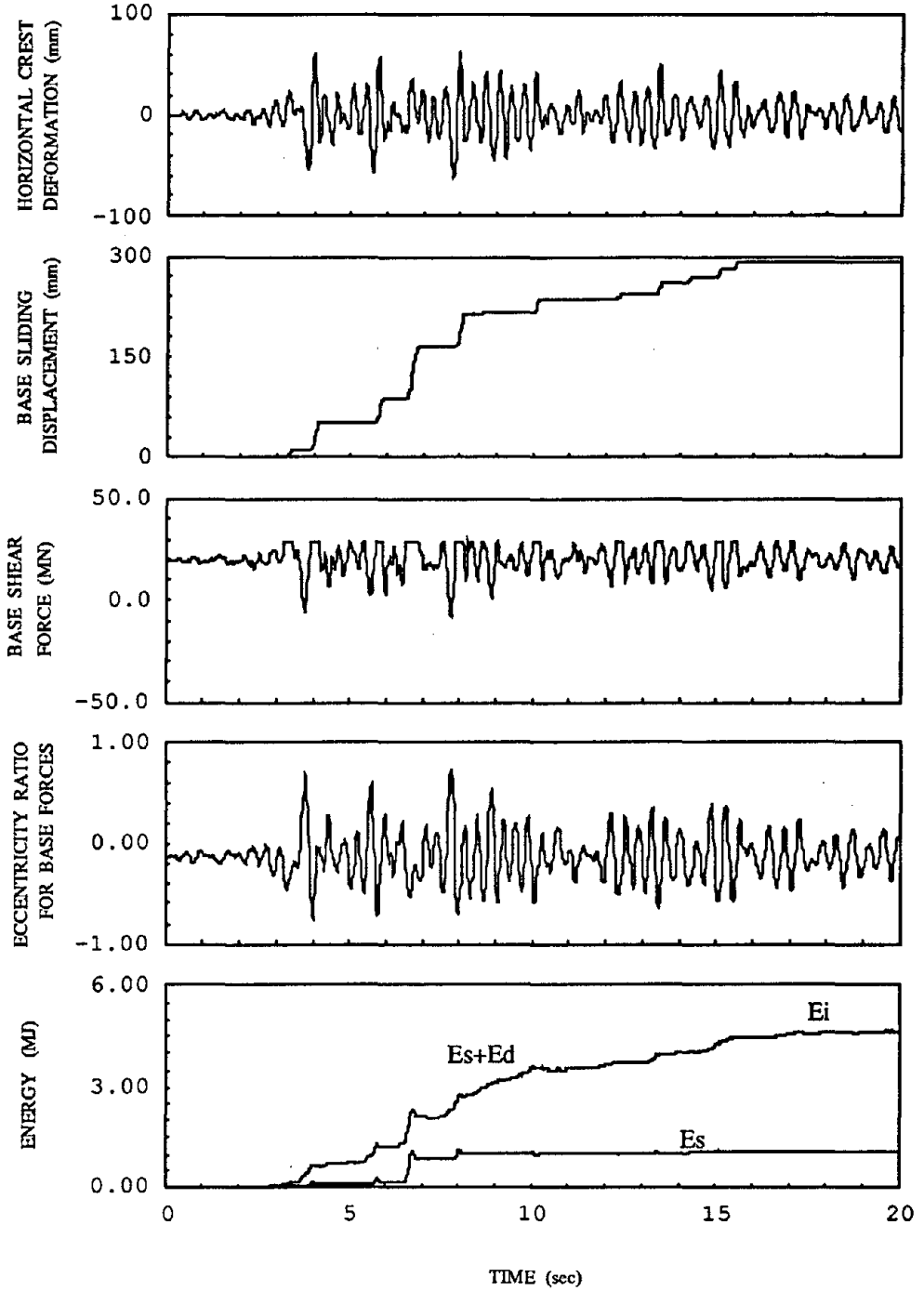

Figure 5.12. Response of Pine Flat dam with rigid foundation rock, horizontal interface, $\alpha = 1$, $\mu = 0.8$, subjected to the horizontal S69E component of Taft ground motion with peak ground acceleration = 0.4g.

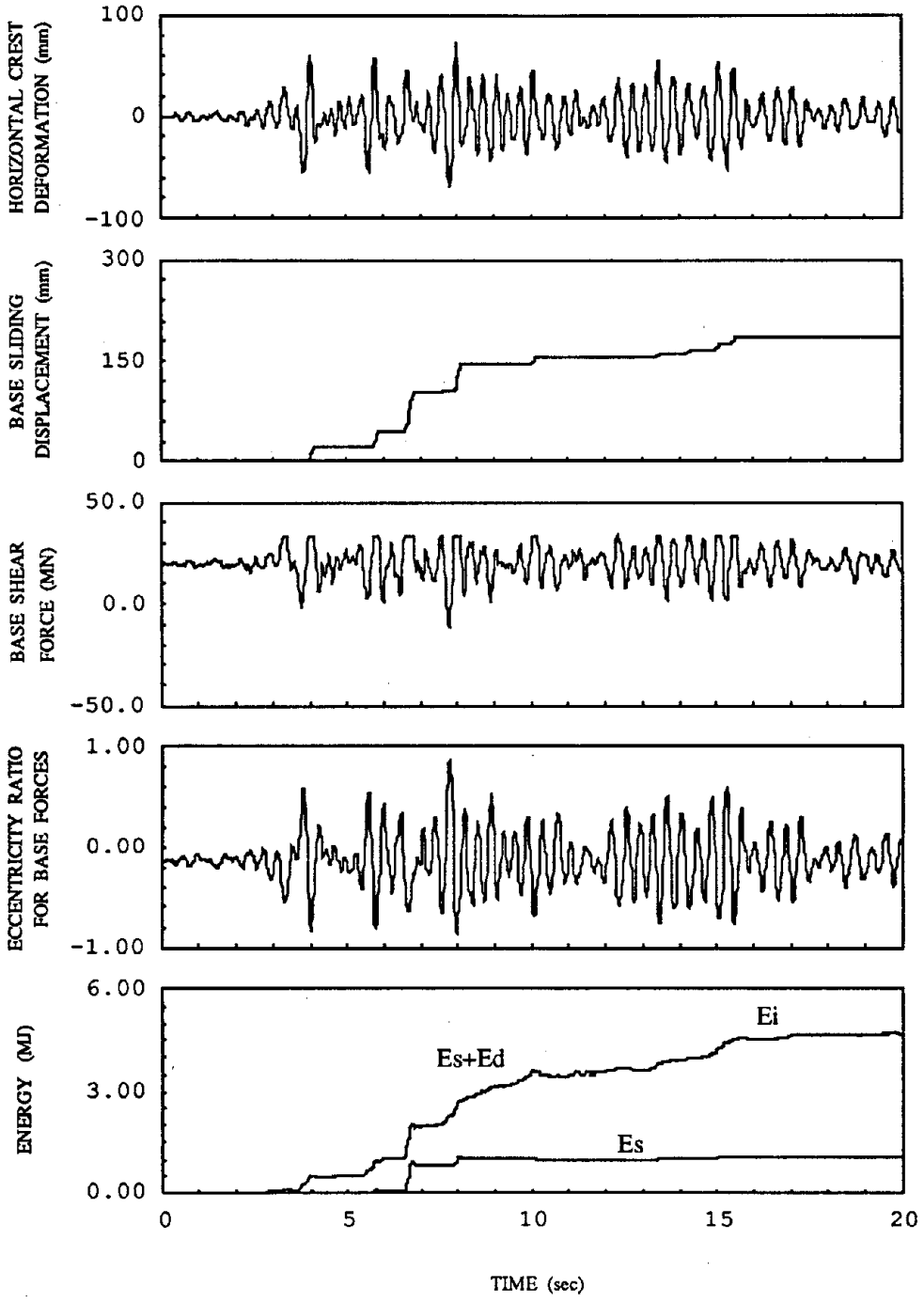

Figure 5.13. Response of Pine Flat dam with rigid foundation rock, horizontal interface, $\alpha = 1$, $\mu = 0.9$, subjected to the horizontal S69E component of Taft ground motion with peak ground acceleration = 0.4g.

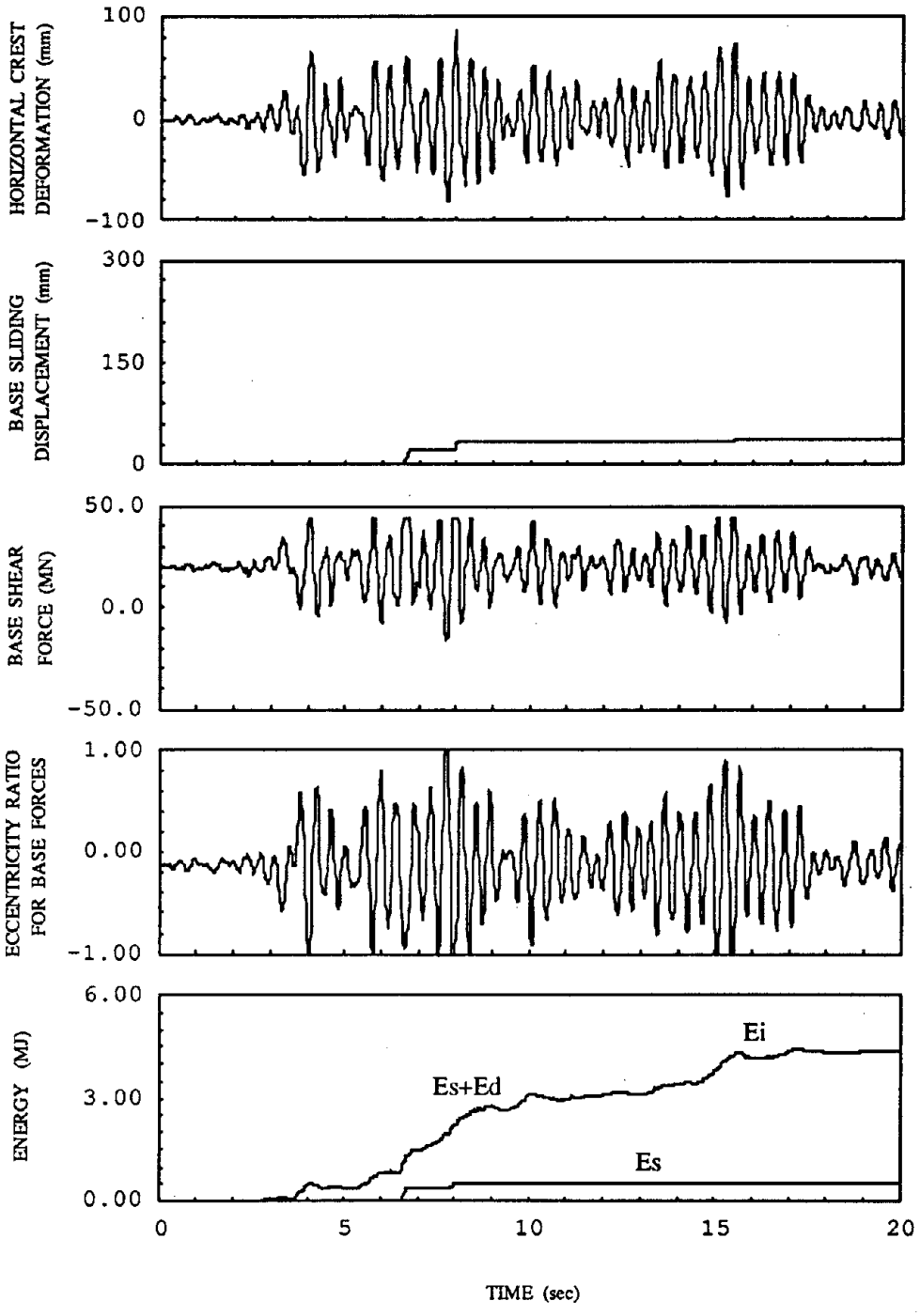

Figure 5.14. Response of Pine Flat dam with rigid foundation rock, horizontal interface, $\alpha = 1$, $\mu = 1.2$, subjected to the horizontal S69E component of Taft ground motion with peak ground acceleration = 0.4g.

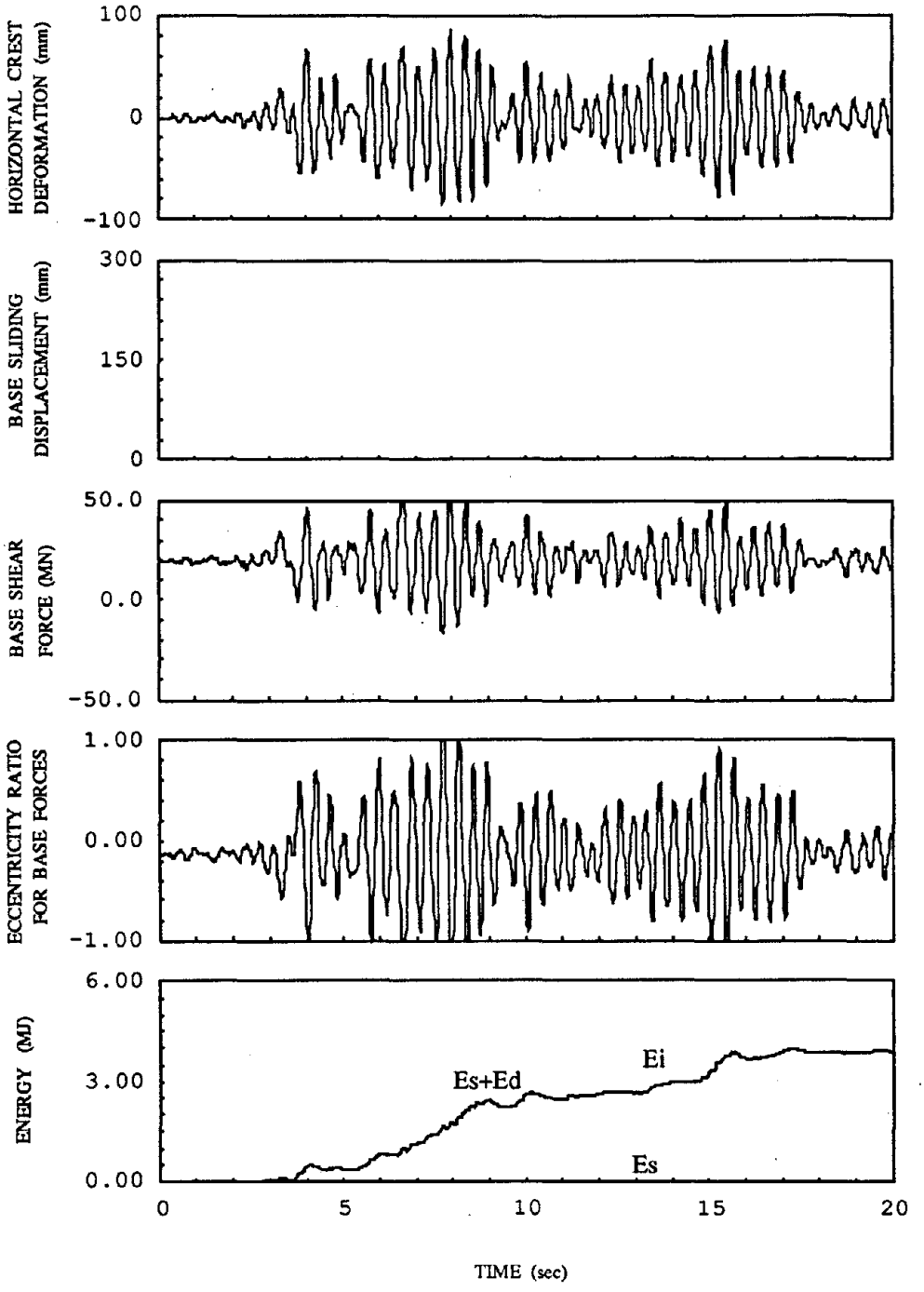

Figure 5.15. Response of Pine Flat dam with rigid foundation rock, horizontal interface, $\alpha = 1$, $\mu = \infty$, subjected to the horizontal S69E component of Taft ground motion with peak ground acceleration = 0.4g.

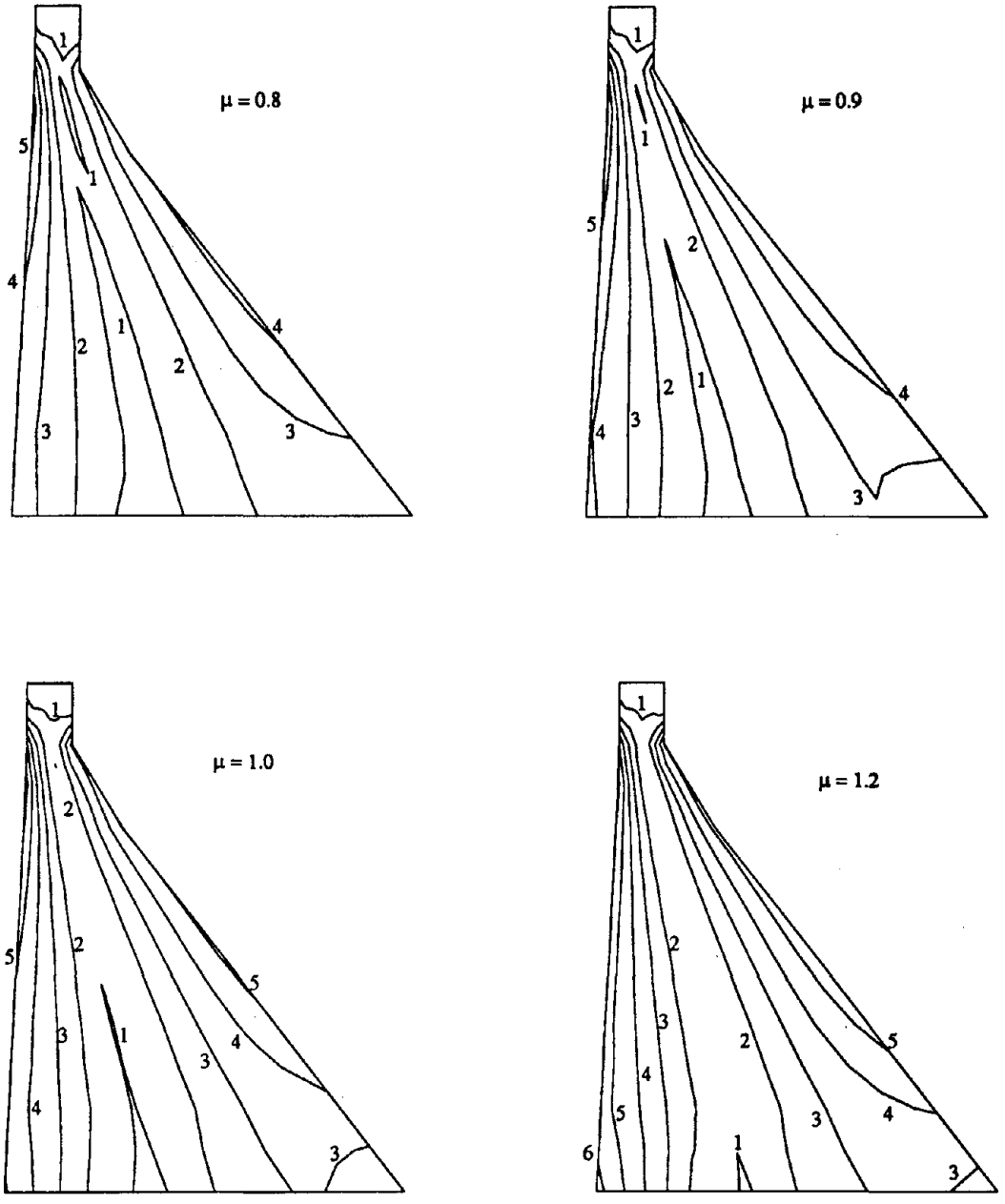

Figure 5.16. Envelope of maximum principal stresses (in MPa) in Pine Flat dam with rigid foundation rock, horizontal interface, $\alpha = 1$, subjected to the horizontal S69E component of Taft ground motion with peak ground acceleration = 0.4g. Static effects not included.

The input energy is similar for μ between 0.8 to 1.0, and slightly increases for $\mu = 1.2$. A large percentage of the input energy is due to deformation of the dam, E_d. The energy dissipated by sliding of the dam, E_s, is much less and it is almost not affected by the value of the coefficient of friction. For these cases, sliding is not an effective energy dissipation mechanism. An increase of the sliding displacement with a decrease in μ reduces dam deformation and the maximum principal stresses. Therefore, the sliding of the dam on rigid foundation rock can be interpreted as an isolation mechanism for the dam.

5.6.4 Influence of the Angle of Interface Inclination

The sliding displacement of the dam is affected by the angle, β, of the interface because the inclination affects the static normal force and shear force. The responses of the dam are shown in Figures 5.17 and 5.18 for two values of β. The crest deformation for $\beta = 5°$, sloping downstream, is larger than the crest deformation for $\beta = -5°$, sloping upstream, although the maximum crest deformation for both cases is almost the same.

The base sliding displacement is considerably affected by the value of β. The maximum base sliding for $\beta = 5°$ is almost four times that for $\beta = -5°$. When the angle of inclination is $-5°$ (sloping upstream) there is a component of gravity force that contributes to the base shear force in the downstream direction, inducing additional sliding downstream.

The maximum principal stresses, shown in Figure 5.19, are slightly less for the case of the dam sloping upstream ($\beta = -5°$) because of smaller deformation of the

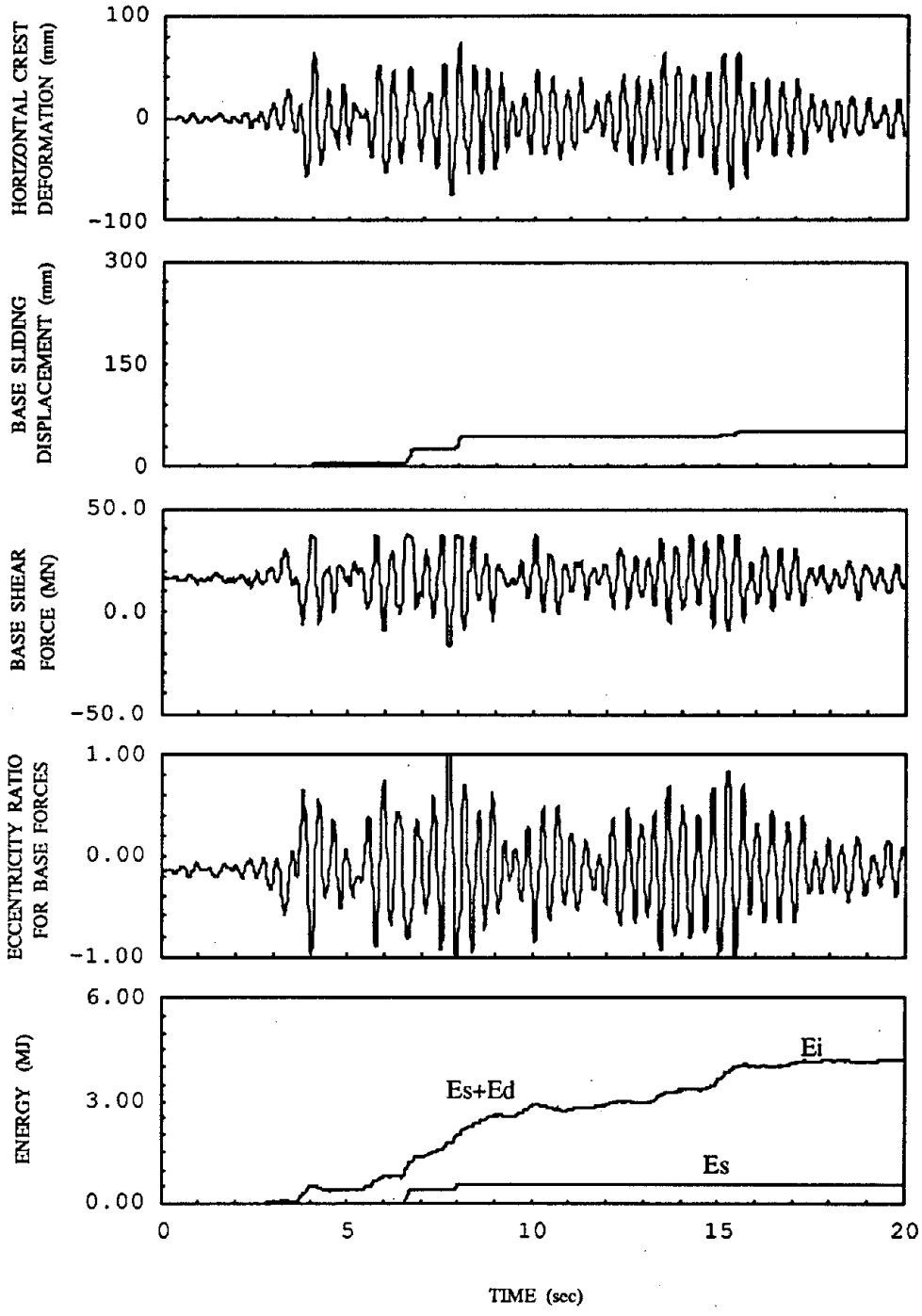

Figure 5.17. Response of Pine Flat dam with rigid foundation rock, angle of interface = 5°, $\alpha = 1$, $\mu = 1$, subjected to the horizontal S69E component of Taft ground motion with peak ground acceleration = 0.4g.

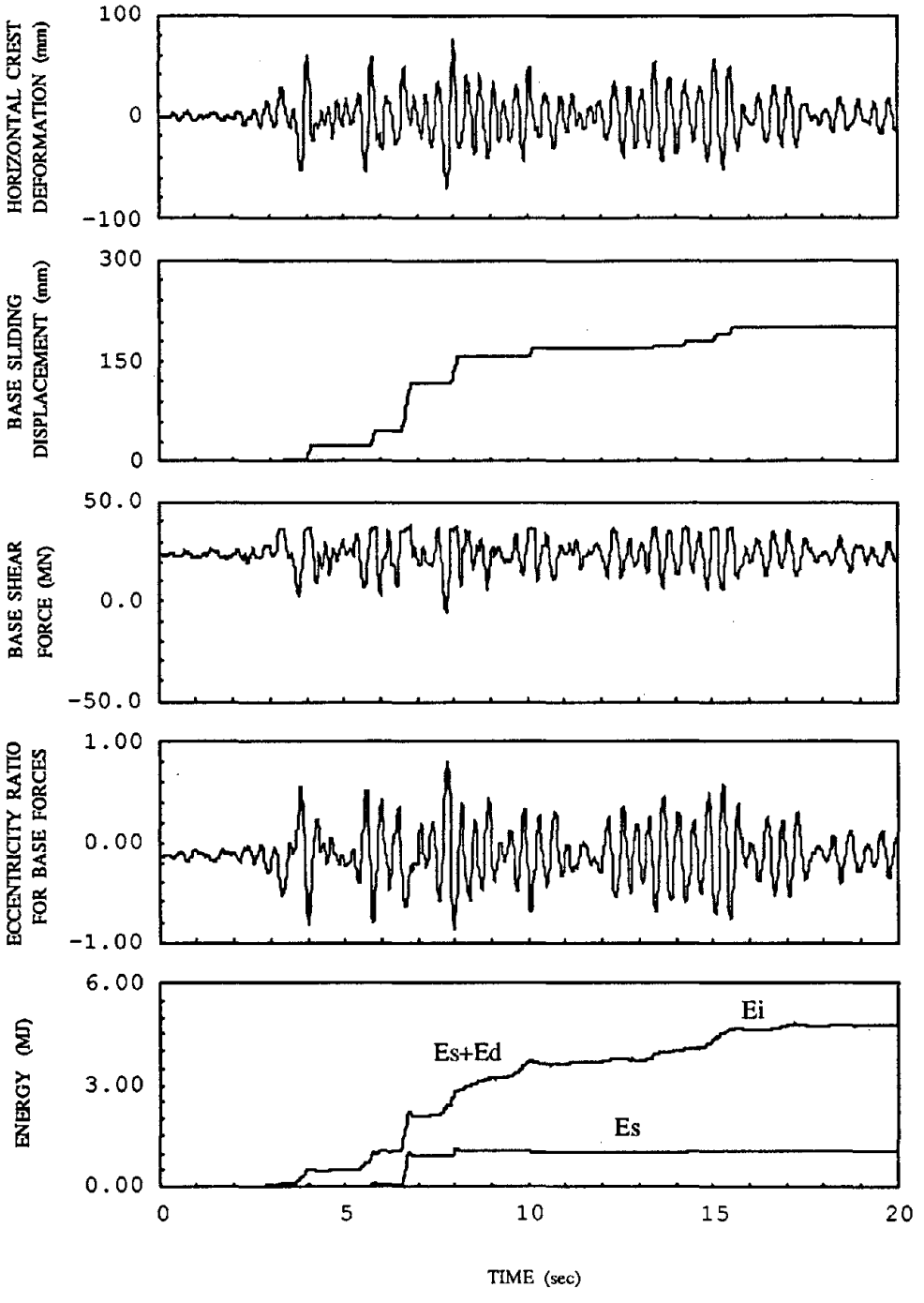

Figure 5.18. Response of Pine Flat dam with rigid foundation rock, angle of interface $= -5°$, $\alpha = 1$, $\mu = 1$, subjected to the horizontal S69E component of Taft ground motion with peak ground acceleration = 0.4g.

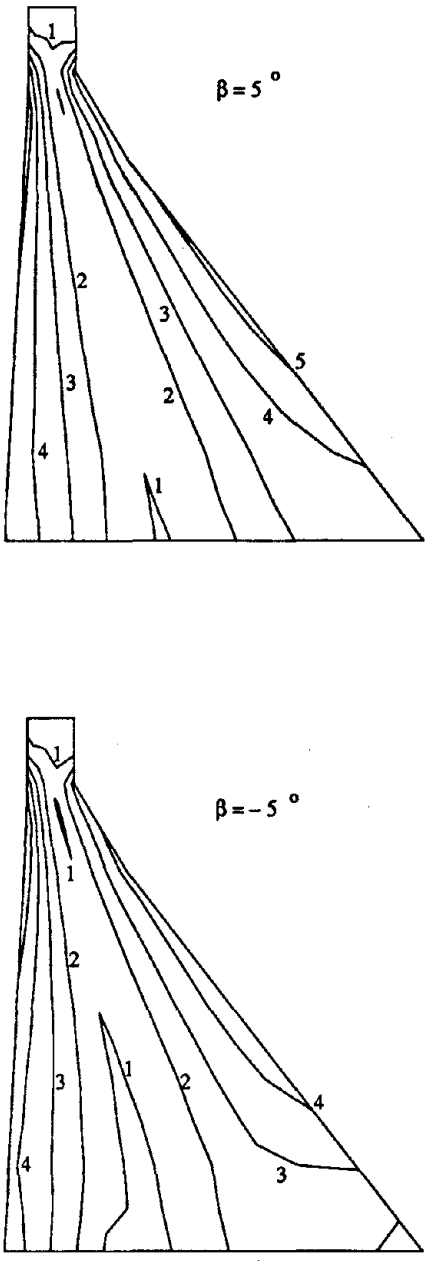

Figure 5.19. Envelope of maximum principal stresses (in MPa) in Pine Flat dam with rigid foundation rock, horizontal interface, $\alpha = 1$, $\mu = 1$, subjected to the horizontal S69E component of Taft ground motion with peak ground acceleration = 0.4g. Static effects not included.

dam from the isolation effect of sliding. Similarly, the tendency to rock is less for the dam sloping upstream ($\beta = -5°$) than for the dam sloping upstream ($\beta = 5°$).

5.6.5 Influence of Vertical Ground Motion

The response of the dam to vertical ground motion is computed to evaluate its significance on the sliding response of the dam. Figure 5.20 shows the response of the dam when it is subjected to the Taft S69E horizontal component of ground motion, Figure 5.21 shows the response due to the vertical component of the Taft ground motion, and Figure 5.22 shows the response of the dam subjected simultaneously to the horizontal and vertical components of the Taft ground motion. The reservoir bottom coefficient is $\alpha = 0.9$ for these three cases.

When the dam is subjected to the horizontal component of ground motion (peak acceleration = 0.4g), the maximum crest deformation is 78 mm. The maximum crest deformation for vertical ground motion alone (peak acceleration = 0.26 g) is 48 mm. The maximum crest deformation is 80 mm considering both components of ground motion, simultaneously. The history of crest displacements to the individual components are not in phase, so the contribution of the vertical ground motion to the total response is not large. The principal stress contours for the three cases are shown in Figure 5.23. The stresses increase with the vertical ground motion, which has been shown for the linear response of gravity dams [Fenves and Chopra, 1984a].

As for sliding, the maximum base sliding displacement due to horizontal ground motion is 115 mm. The dam does not slide due to the vertical ground motion only. The maximum base sliding due to the combined vertical and horizontal components

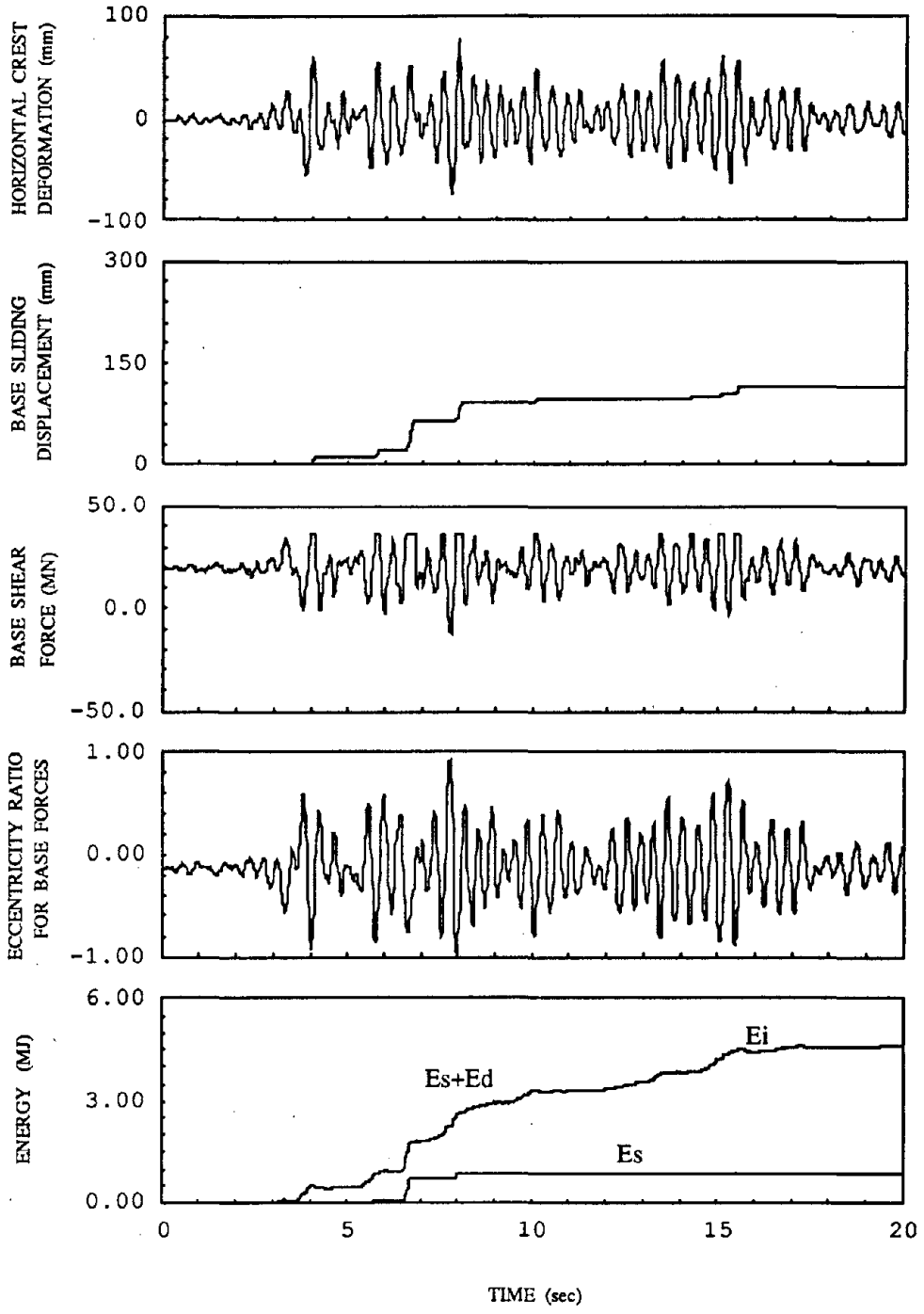

Figure 5.20. Response of Pine Flat dam with rigid foundation rock, horizontal interface, $\alpha = 0.9$, $\mu = 1$, subjected to the horizontal S69E component of Taft ground motion with peak ground acceleration = 0.4g.

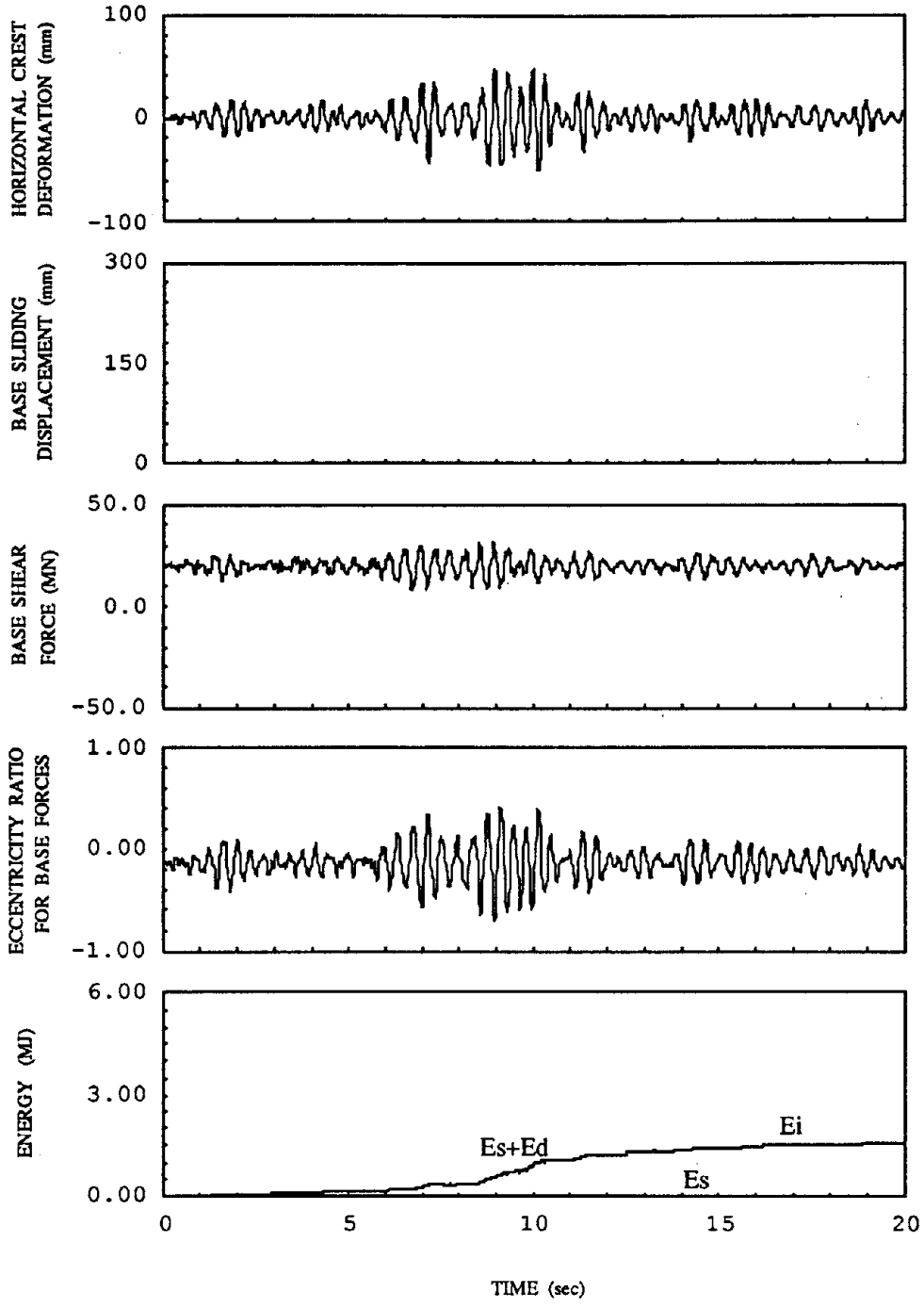

Figure 5.21. Response of Pine Flat dam with rigid foundation rock, horizontal interface, $\alpha = 0.9$, $\mu = 1$, subjected to the vertical component of Taft ground motion with peak ground acceleration = 0.26g.

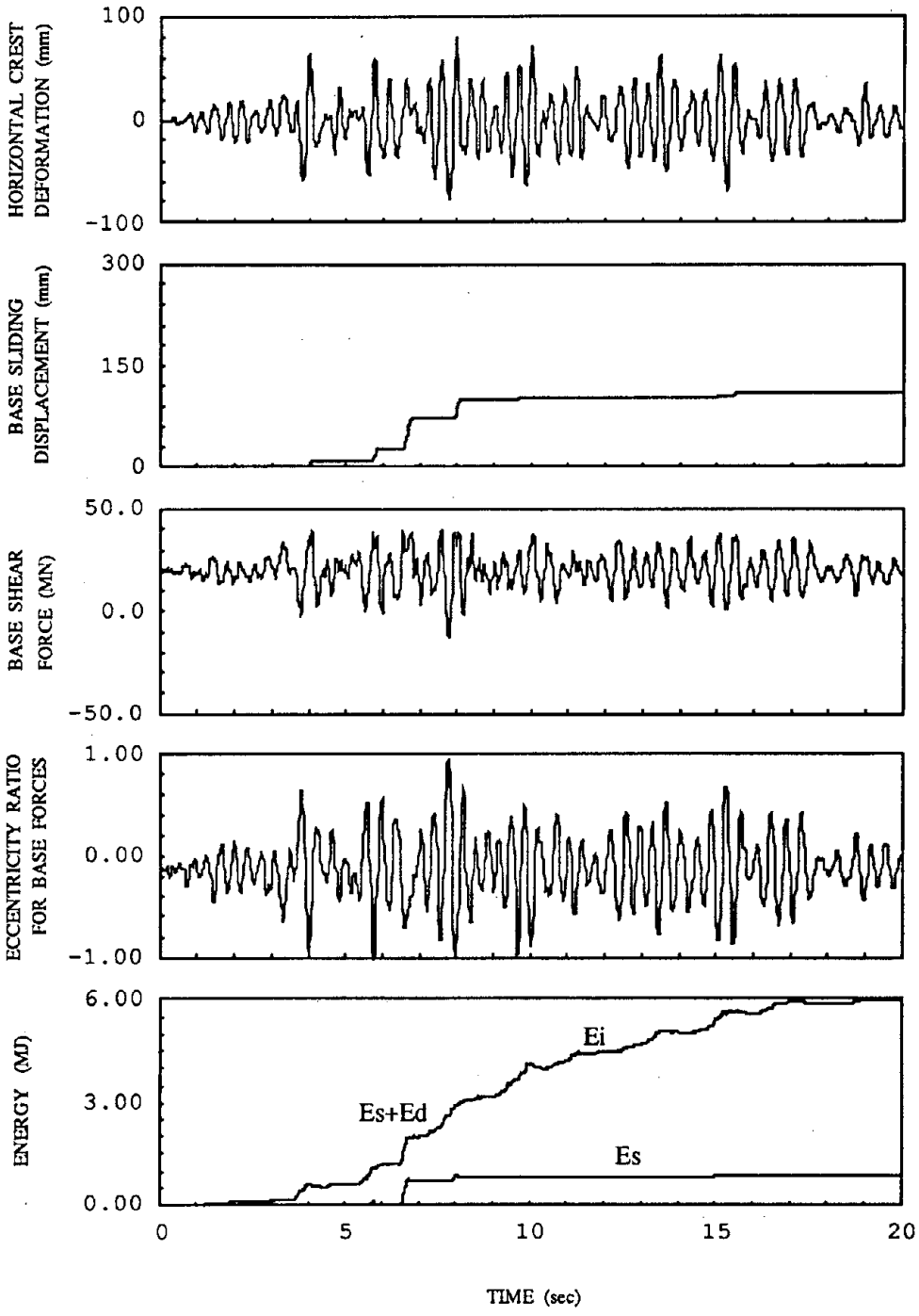

Figure 5.22. Response of Pine Flat dam with rigid foundation rock, horizontal interface, $\alpha = 0.9$, $\mu = 1$, subjected to the horizontal S69E and vertical components of Taft ground motion with peak ground accelerations = 0.40g and 0.26g, respectively.

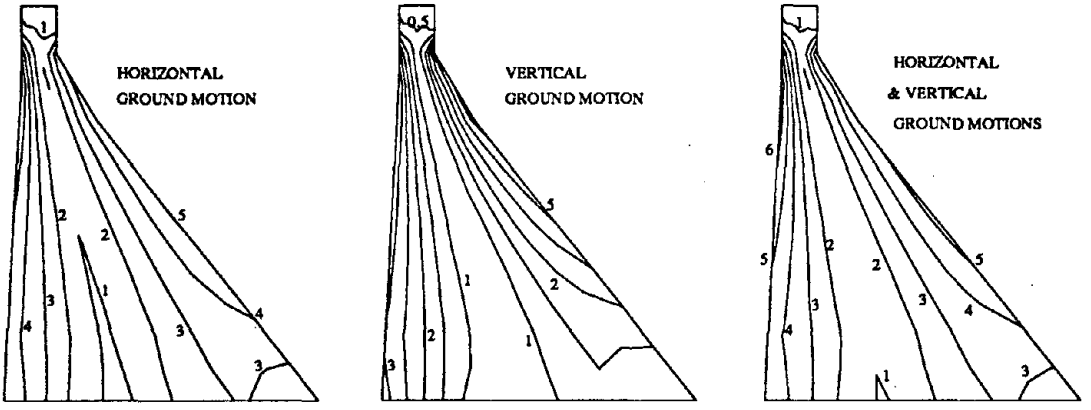

Figure 5.23. Envelope of maximum principal stresses (in MPa) in Pine Flat dam with rigid foundation rock, horizontal interface, $\alpha = 0.9$, $\mu = 1$, subjected to the horizontal S69E and vertical components of Taft ground motion with peak ground accelerations = 0.40g and 0.26g, respectively. Static effects not included.

of ground motion is 112 mm, showing that for this case the vertical ground motion has little effect on sliding. Since the responses to the ground motion components are not in phase, the maximum values of response occurs at different times.

The vertical ground motion also has little effect on the initiation of rocking of the dam. Rocking under vertical ground motion alone is not likely to occur. As for the input energy due to vertical ground motion, it will be mostly dissipated through dam deformation.

5.7 Response of Dam on Flexible Foundation Rock

5.7.1 Influence of Foundation Rock Flexibility

The response of the dam to the S69E Taft ground motion, with a peak ground acceleration of 0.4g, for $\mu = 1$ and different levels of foundation rock flexibility is shown in Figures 5.24 to 5.26. The flexibility of the foundation rock reduces the sliding response of the Pine Flat dam.

The crest deformation for $E_{fr}/E_{cd} = 4$, shown in Figure 5.24, is similar to the crest deformation for the dam on rigid foundation rock (Figure 5.5). There are few differences in displacements and for practical purposes a foundation rock with a moduli ratio $E_{fr}/E_{cd} = 4$ can be considered rigid. For more flexible foundation rocks, $E_{fr}/E_{cd} = 1$ and $E_{fr}/E_{cd} = 0.25$, the dam crest displacement, shown in Figures 5.25 and 5.26, increases slightly as the moduli ratio E_{fr}/E_{cd} decreases and the system becomes more flexible. The maximum crest deformation varies between 76 mm for $E_{fr}/E_{cd} = 1$ and 94 mm for $E_{fr}/E_{cd} = 0.25$. The crest displacements are influenced

by dam-foundation rock interaction, because the flexibility of the foundation rock reduces the fundamental resonant frequency of the system and adds additional damping mechanisms.

The sliding of the dam with a moduli ratio $E_{fr}/E_{cd} = 4$ is similar to the sliding of the dam on rigid foundation rock. There are six sliding events in the downstream direction. The last one occurs at 15 seconds. The maximum sliding displacement is 113 mm, which is 10 percent less than that of the dam on rigid foundation rock. The maximum sliding for $E_{fr}/E_{cd} = 1$ decreases by a factor of three to 38 mm. The base sliding displacement decreases substantially as the foundation rock becomes more flexible because the increase in effective damping due to energy radiation and material damping of the foundation rock reduces the base shear forces. There are only three sliding events and the last sliding occurs at 7 sec. There is very small sliding for the case of a very flexible foundation rock with a moduli ratio $E_{fr}/E_{cd} = 0.25$.

The decrease in sliding and base force is due to the large energy dissipation of the flexible foundation rock, as shown by the histories of energy terms in Figures 5.24 to 5.26. For a flexible foundation rock, $E_{fr}/E_{cd} = 0.25$, the energy dissipated by the foundation rock is almost 80 percent of the total input energy transmitted to the system. However, for a stiff foundation rock, $E_{fr}/E_{cd} = 4$, 70 percent of the energy is dissipated by damping of the dam.

The envelopes of maximum principal stresses are shown in Figure 5.27. The maximum stresses for $E_{fr}/E_{cd} = 4$ are equal to the stresses for a dam on rigid foundation rock. The maximum stresses decrease as the foundation rock becomes more flexible for the reasons discussed previously.

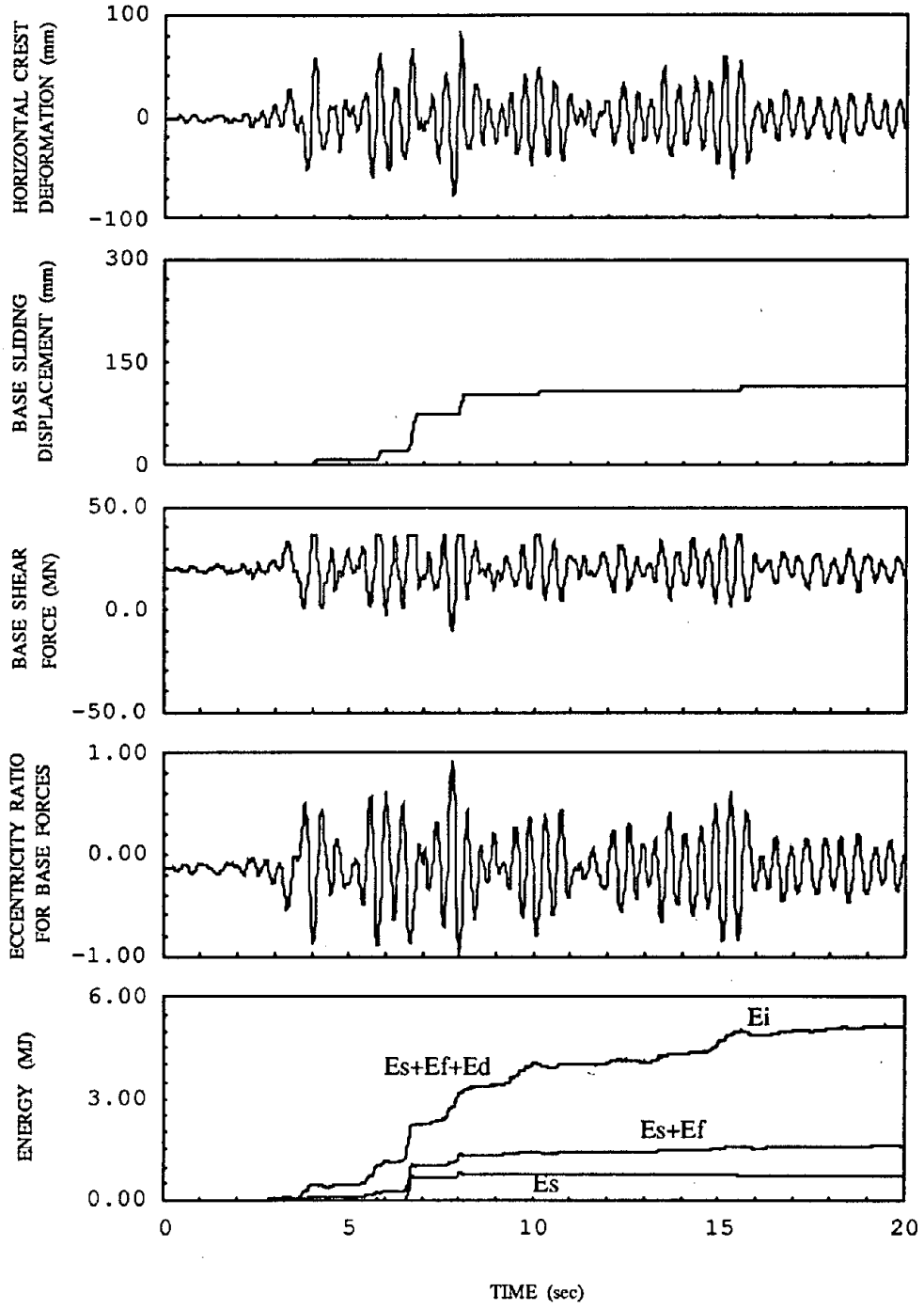

Figure 5.24. Response of Pine Flat dam with flexible foundation rock, $E_{fr}/E_{cd} = 4$, horizontal interface, $\alpha = 1$, $\mu = 1$, subjected to the horizontal S69E component of Taft ground motion with peak ground acceleration = 0.4g.

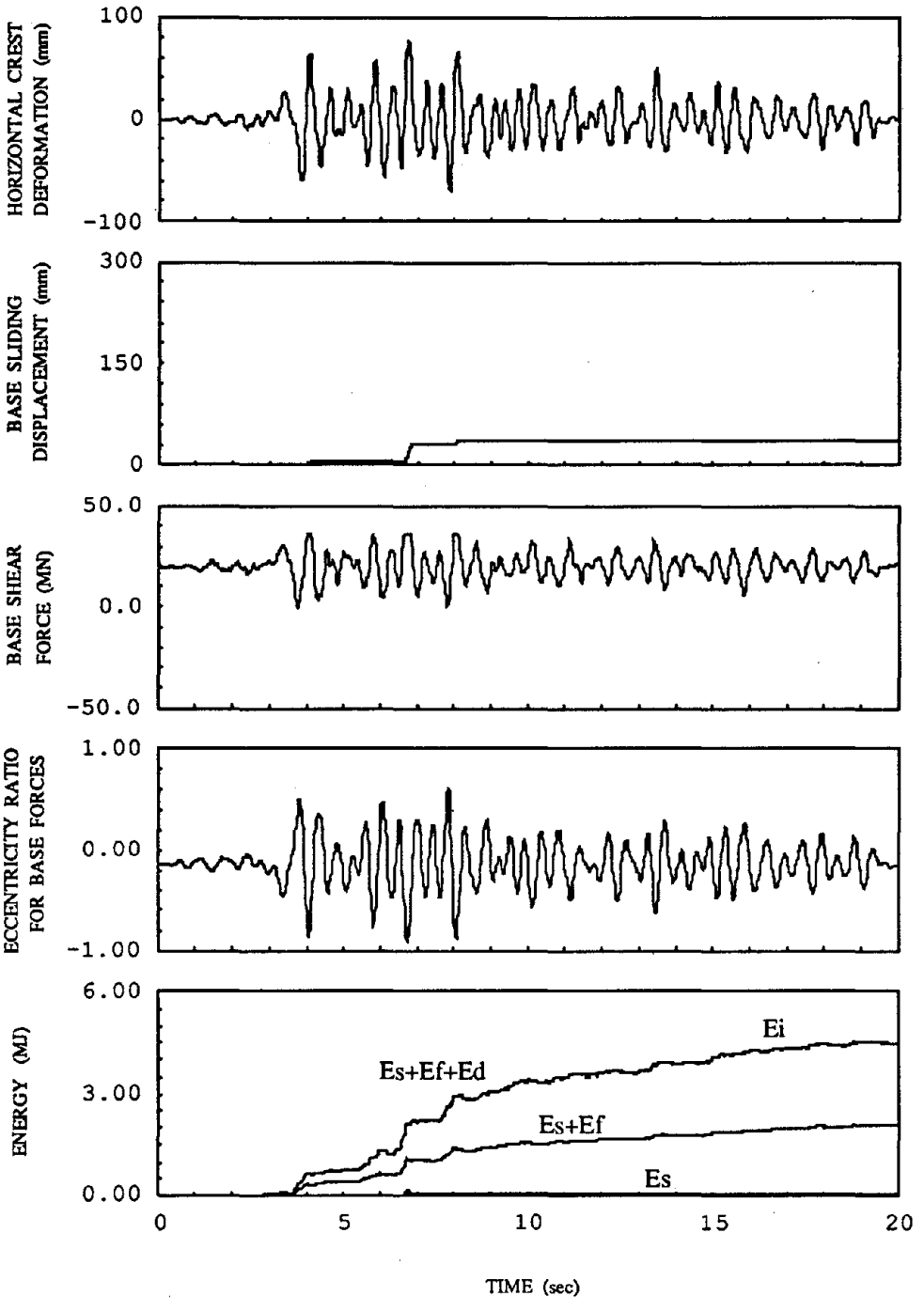

Figure 5.25. Response of Pine Flat dam with flexible foundation rock, $E_{fr}/E_{cd} = 1$, horizontal interface, $\alpha = 1$, $\mu = 1$, subjected to the horizontal S69E component of Taft ground motion with peak ground acceleration = 0.4g.

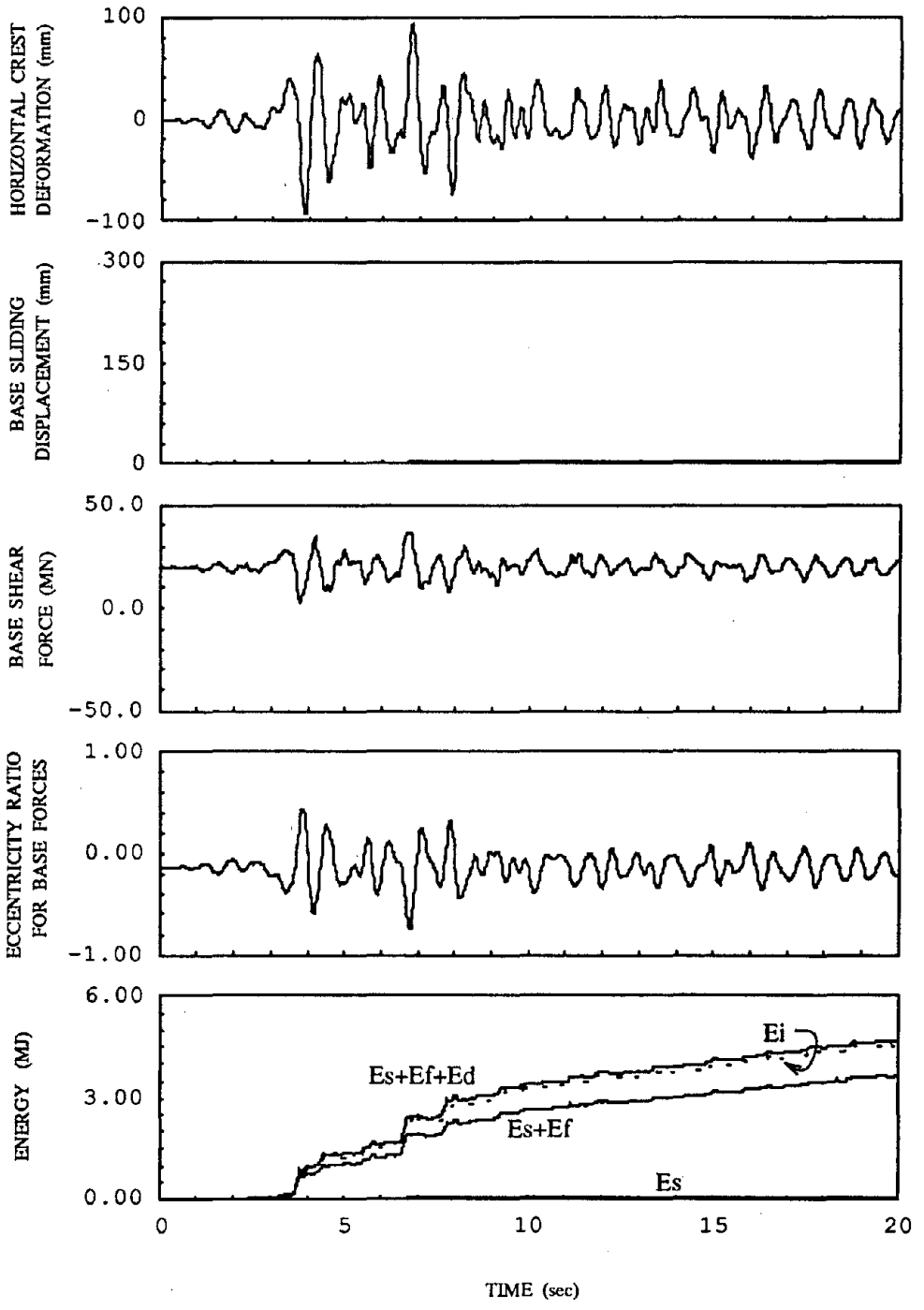

Figure 5.26. Response of Pine Flat dam with flexible foundation rock, $E_{fr}/E_{cd} = 0.25$, horizontal interface, $\alpha = 1$, $\mu = 1$, subjected to the horizontal S69E component of Taft ground motion with peak ground acceleration = 0.4g.

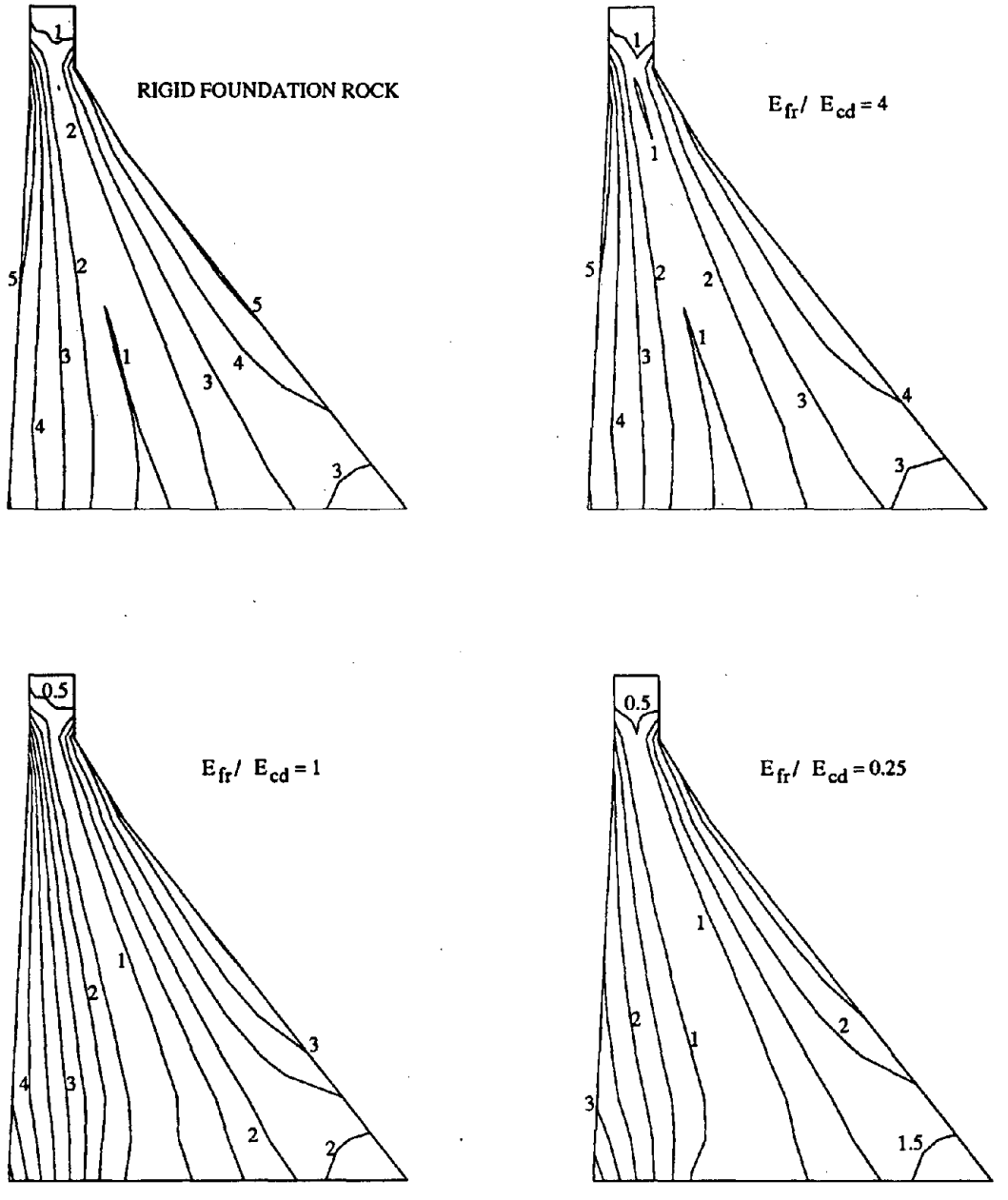

Figure 5.27. Envelope of maximum principal stresses (in MPa) in Pine Flat dam with flexible foundation rock, horizontal interface, $\alpha = 1$, $\mu = 1$, subjected to the horizontal S69E component of Taft ground motion with peak ground acceleration = 0.40g. Static effects not included.

The maximum eccentricity ratio of base forces decreases almost linearly as the foundation rock becomes more flexible. For $E_{fr}/E_{cd} = 4$, there is one peak value of the eccentricity ratio close to unity at 8 seconds. For $E_{fr}/E_{cd} = 1$, the maximum eccentricity ratio is less than 0.9, and for $E_{fr}/E_{cd} = 0.25$ the maximum eccentricity ratio is 0.75. For this ground motion the dam will not rock when the dam is supported on a flexible foundation rock.

5.7.2 Influence of the Coefficient of Friction

The responses of the dam on a flexible foundation rock with a moduli ratio $E_{fr}/E_{cd} = 0.25$ and different values of the coefficient of friction are shown in Figures 5.28 to 5.30. The crest dam deformation history is very similar for the different values of the coefficient of friction. The maximum crest deformation varies between 93 mm for $\mu = 0.8$ to 98 mm for $\mu = 1.2$.

The sliding of the dam on flexible foundation rock is very small compared with the sliding of the dam on rigid foundation rock. For $\mu = 0.8$ there are two sliding events and the maximum sliding displacement is 62 mm. For $\mu = 0.9$ there is only one sliding event and the maximum sliding displacement is 21 mm. For $\mu = 1$ there is little sliding, and for $\mu = 1.2$ there is no sliding. Although the sliding of the dam on flexible foundation rock is a nonlinear function of μ, the coefficient of friction is less important for a dam on flexible foundation rock because energy dissipation in the foundation rock reduces the response and limits the base shear force causing sliding.

The eccentricity ratios vary slightly with the different values of μ. The maximum ratios (absolute value) increase almost linearly from 0.6 for $\mu = 0.8$ to 0.8 for

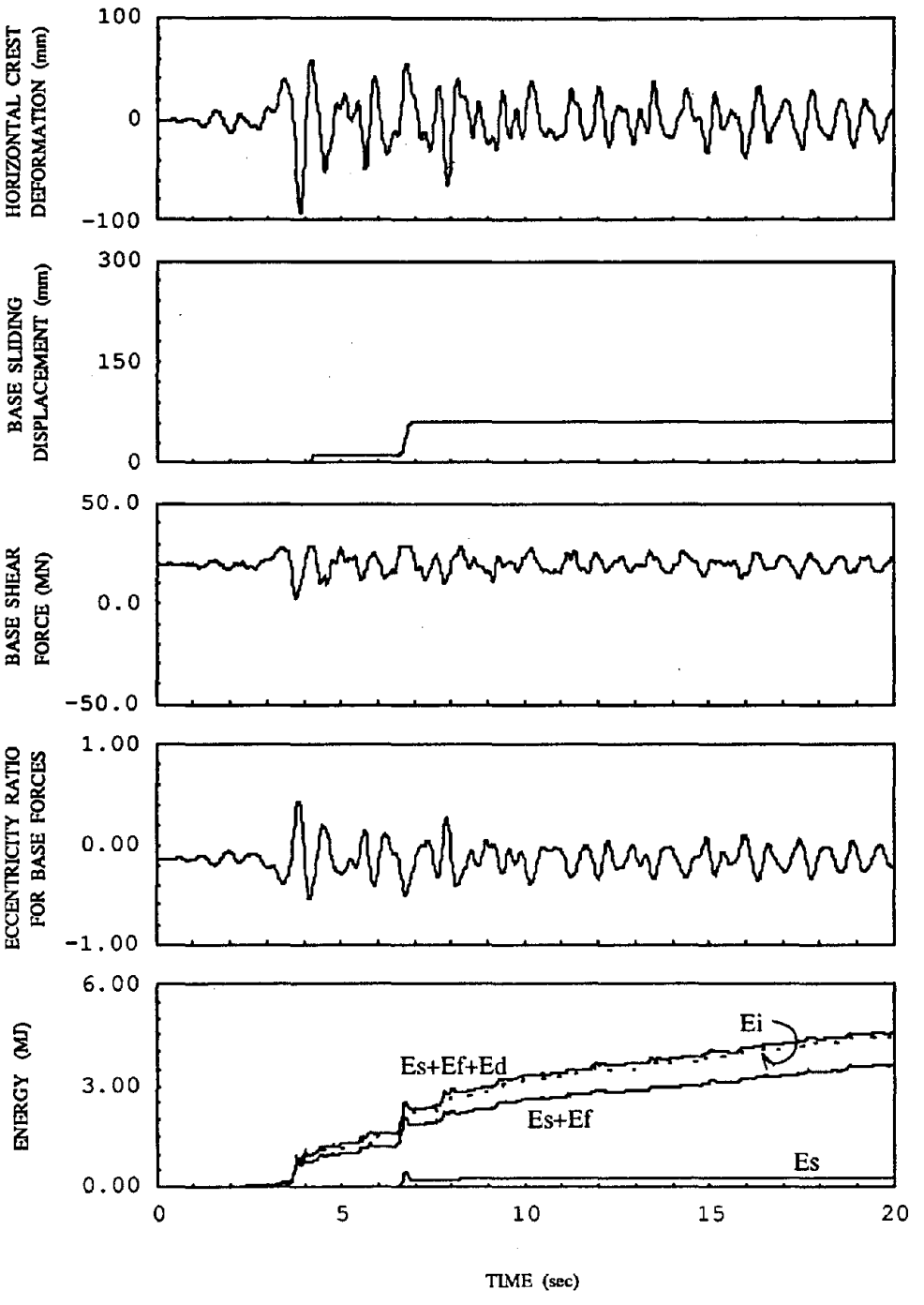

Figure 5.28. Response of Pine Flat dam with flexible foundation rock, $E_{fr}/E_{cd} = 0.25$, horizontal interface, $\alpha = 1$, $\mu = 0.8$, subjected to the horizontal S69E component of Taft ground motion with peak ground acceleration = 0.4g.

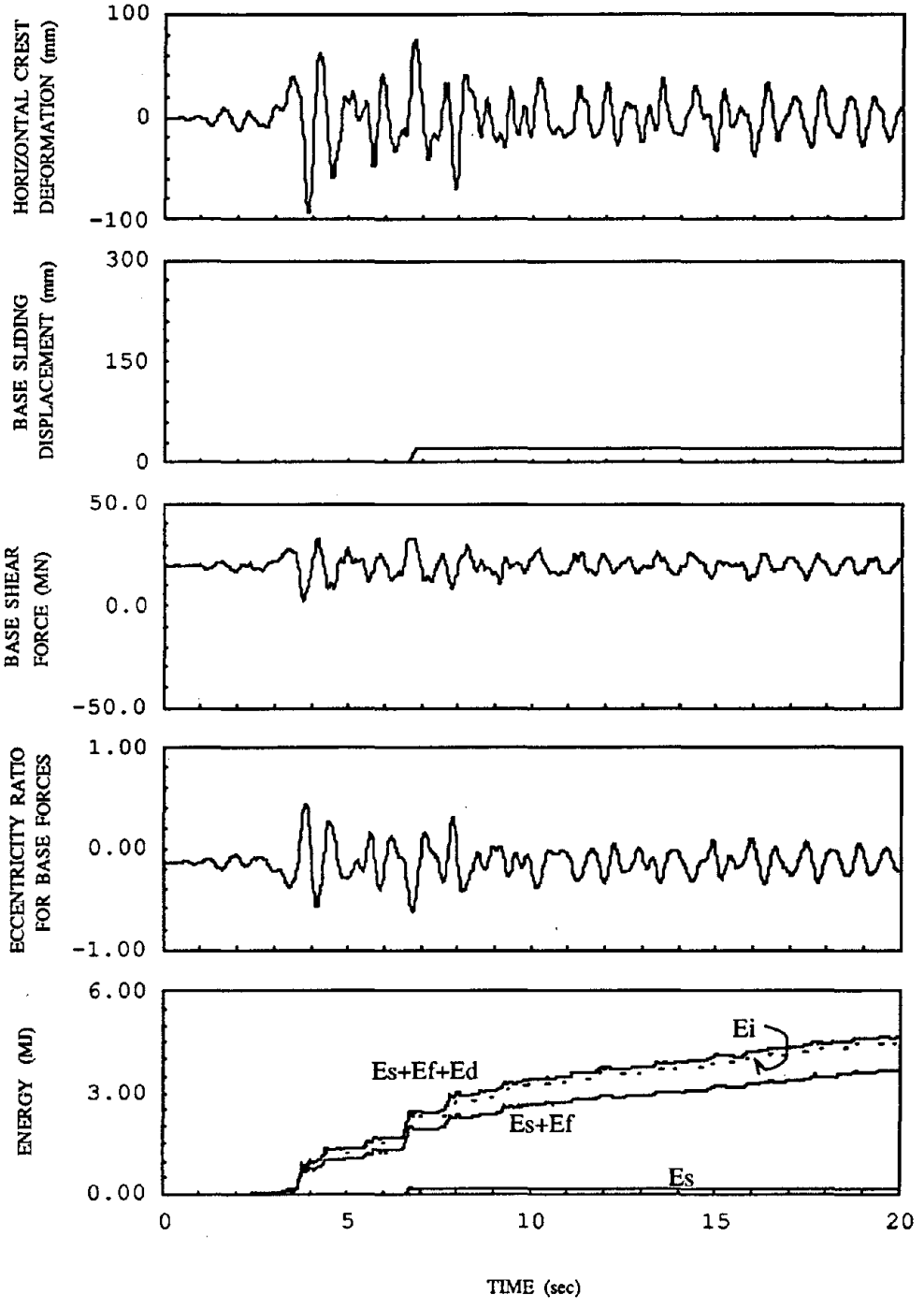

Figure 5.29. Response of Pine Flat dam with flexible foundation rock, $E_{fr}/E_{cd} = 0.25$, horizontal interface, $\alpha = 1$, $\mu = 0.9$, subjected to the horizontal S69E component of Taft ground motion with peak ground acceleration = 0.4g.

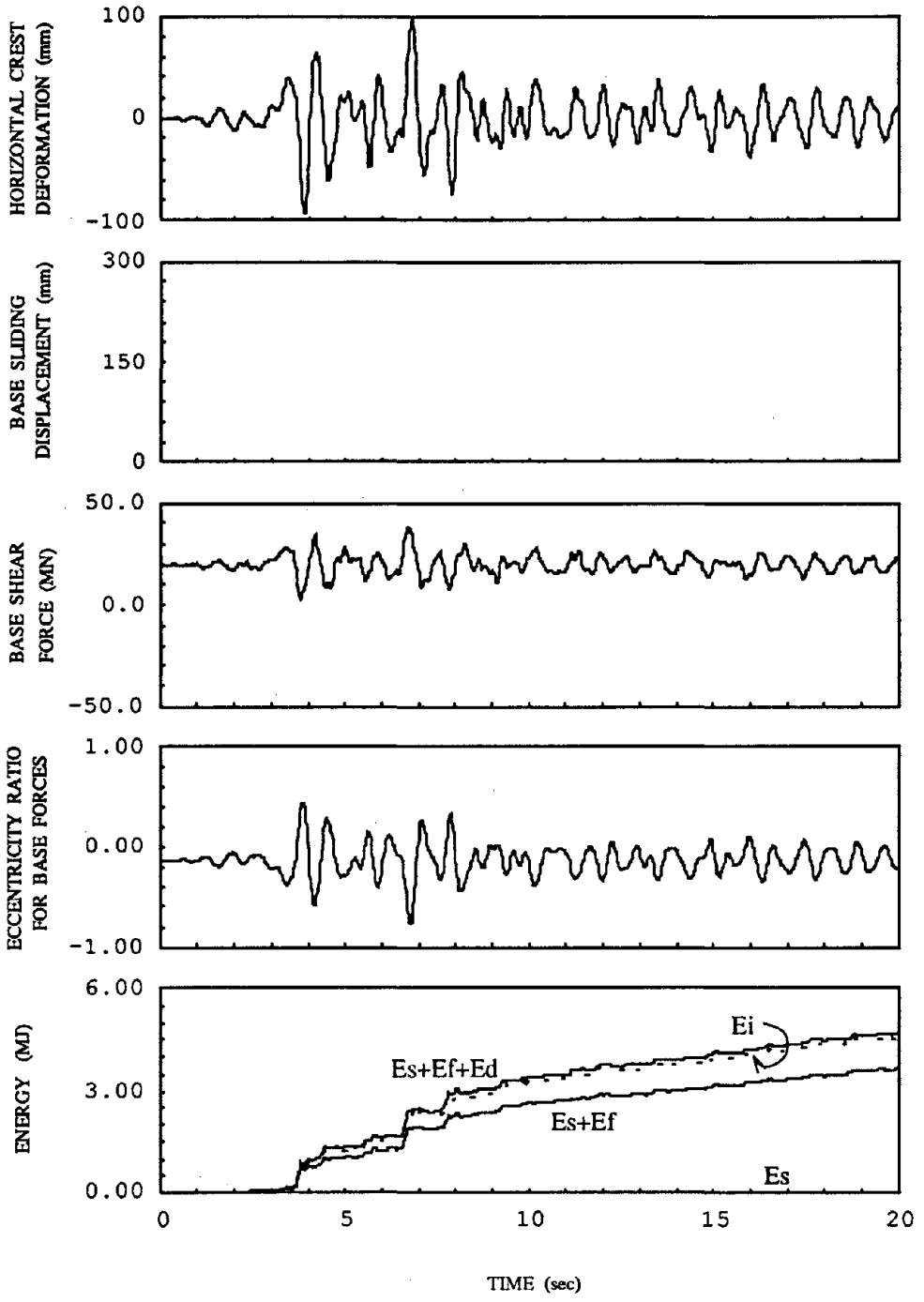

Figure 5.30. Response of Pine Flat dam with flexible foundation rock, $E_{fr}/E_{cd} = 0.25$, horizontal interface, $\alpha = 1$, $\mu = 1.2$, subjected to the horizontal S69E component of Taft ground motion with peak ground acceleration = 0.4g.

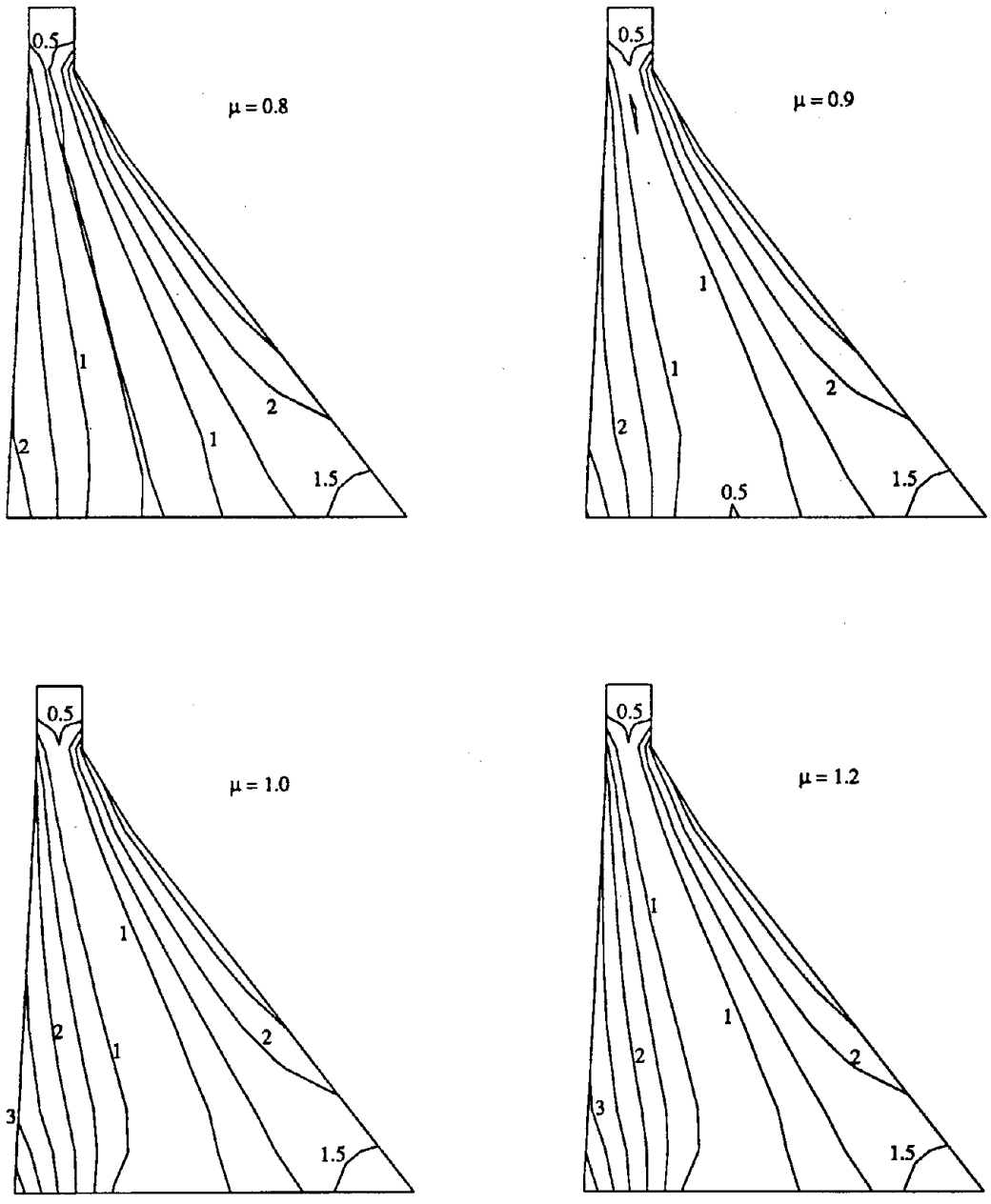

Figure 5.31. Envelope of maximum principal stresses (in MPa) in Pine Flat dam with flexible foundation rock, $E_{fr}/E_{cd} = 0.25$, horizontal interface, $\alpha = 1$, subjected to the horizontal S69E component of Taft ground motion with peak ground acceleration = 0.4g. Static effects not included.

$\mu = 1.2$. Therefore the dam will not rock for these cases. The maximum stresses, shown in Figure 5.31, which depend on the dam deformation, increase slightly with the value of μ.

5.8 Influence of Amplitude of Ground Acceleration

The peak ground acceleration is an important factor in the sliding response of the dam. Increasing the peak acceleration induces larger sliding displacement of the dam. The responses of Pine Flat dam to the S69E Taft ground motion with a peak ground acceleration of 0.6g and three values of the coefficient of friction, $\mu = 0.8$, 1.0, and 1.2 on flexible foundation rock with moduli ratios of $E_{fr}/E_{cd} = 1$ and $E_{fr}/E_{cd} = 0.25$ are shown in Figures 5.32 to 5.34, and in Figures 5.37 to 5.38, respectively.

The crest displacement increases as the moduli ratio decreases and the system becomes more flexible. The maximum crest deformation varies between 107 mm to 113 mm for $E_{fr}/E_{cd} = 1$, and between 128 mm to 140 mm for $E_{fr}/E_{cd} = 0.25$. The crest deformation for the dam subjected to the Taft ground motion with a peak ground acceleration of 0.6g is about 40 percent greater than the deformation for the dam subjected to Taft ground motion with a peak acceleration of 0.4g. Thus, the increase in maximum crest deformation varies almost linearly with the increase in peak ground acceleration.

The base sliding displacement is more sensitive to the amplitude of the ground acceleration. For the Pine Flat dam on flexible foundation rock with a moduli ratio $E_{fr}/E_{cd} = 1$ the sliding initiates around 3 sec for $\mu = 0.8$ and around 4 sec for $\mu = 1.0$

and 1.2. The maximum base sliding displacement for $\mu = 0.8$ is 502 mm, a large value because for this moduli ratio the foundation rock is relatively rigid and the response is very dependent on the value of the coefficient of friction. For larger values of μ, the sliding displacement decreases to 168 mm for $\mu = 1.0$ and to 64 mm for $\mu = 1.2$.

For the dam on flexible foundation rock with a moduli ratio $E_{fr}/E_{cd} = 0.25$, the amplitude of the ground acceleration is still important, although due to the flexibility of the foundation rock, the base sliding displacement is smaller compared with the case when $E_{fr}/E_{cd} = 1$. For $\mu = 0.8$, the maximum base sliding displacement is 228 mm, almost four times that of the dam subjected to the same ground motion with a peak acceleration of 0.4g. For $\mu = 1.0$ the base sliding displacement is reduced to 56 mm, and for $\mu = 1.2$ there is almost no sliding.

An increase in ground acceleration amplitude also increases the eccentricity ratio (in absolute value) for the base forces. For $E_{fr}/E_{cd} = 1$ there are two peaks (around 8 sec) for $\mu = 1$ and five peaks (at different times) for $\mu = 1.2$ exceeding unity. For $E_{fr}/E_{cd} = 0.25$ the eccentricity ratios are all less than one. Thus, rocking will not occur for a dam on very flexible foundation rock, although it could become important for a dam on a more rigid foundation rock subjected to a ground motion with a large peak ground acceleration.

The input energy increases by almost a factor of two when the amplitude of the Taft ground acceleration increases from 0.4g to 0.6g, and for the cases analyzed, sliding seems not to be an important dissipator of energy. For very flexible foundation rock, $E_{fr}/E_{cd} = 0.25$, most of the energy is dissipated in the foundation rock.

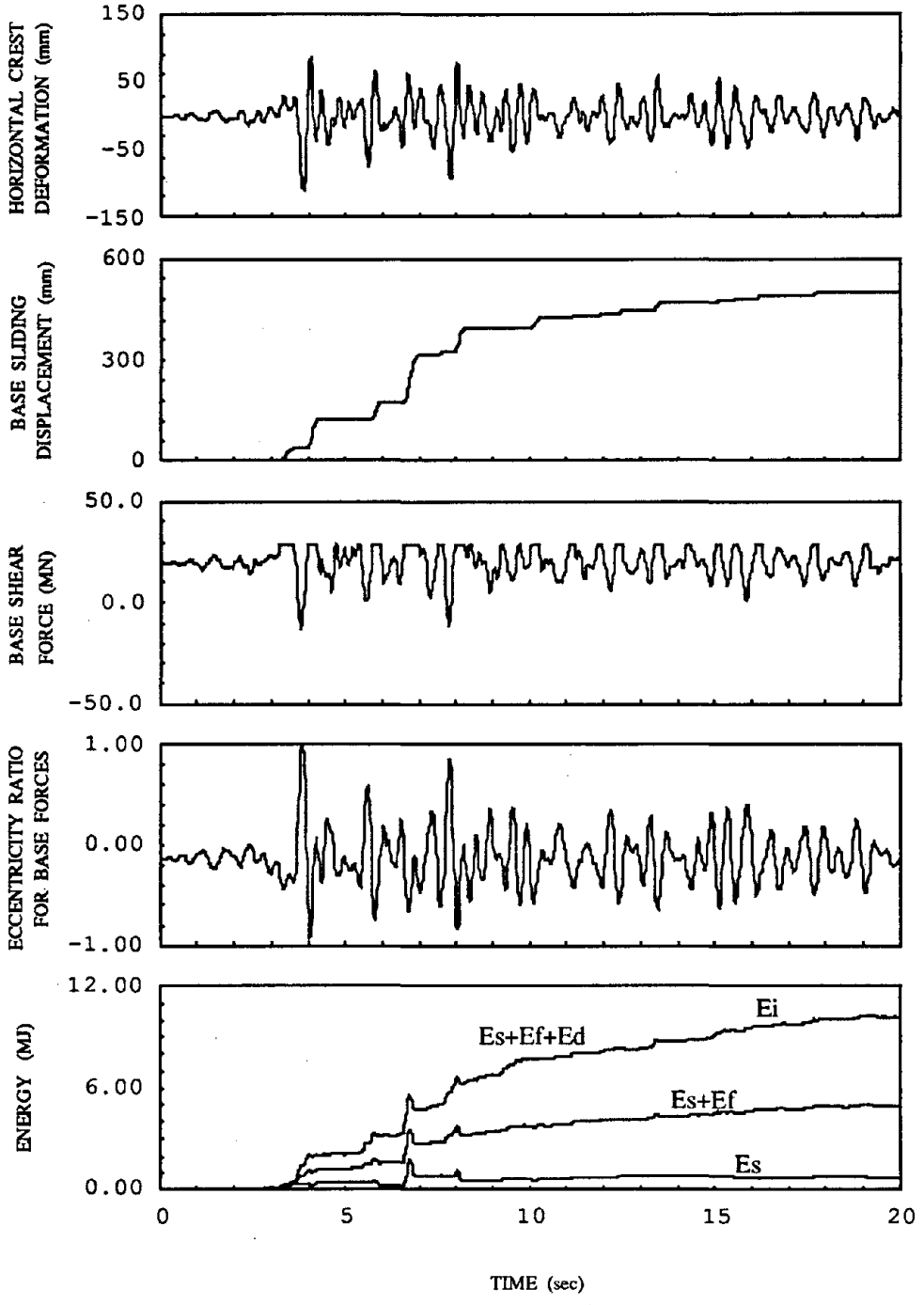

Figure 5.32. Response of Pine Flat dam with flexible foundation rock, $E_{fr}/E_{cd} = 1$, horizontal interface, $\alpha = 1$, $\mu = 0.8$, subjected to the horizontal S69E component of Taft ground motion with peak ground acceleration = 0.6g.

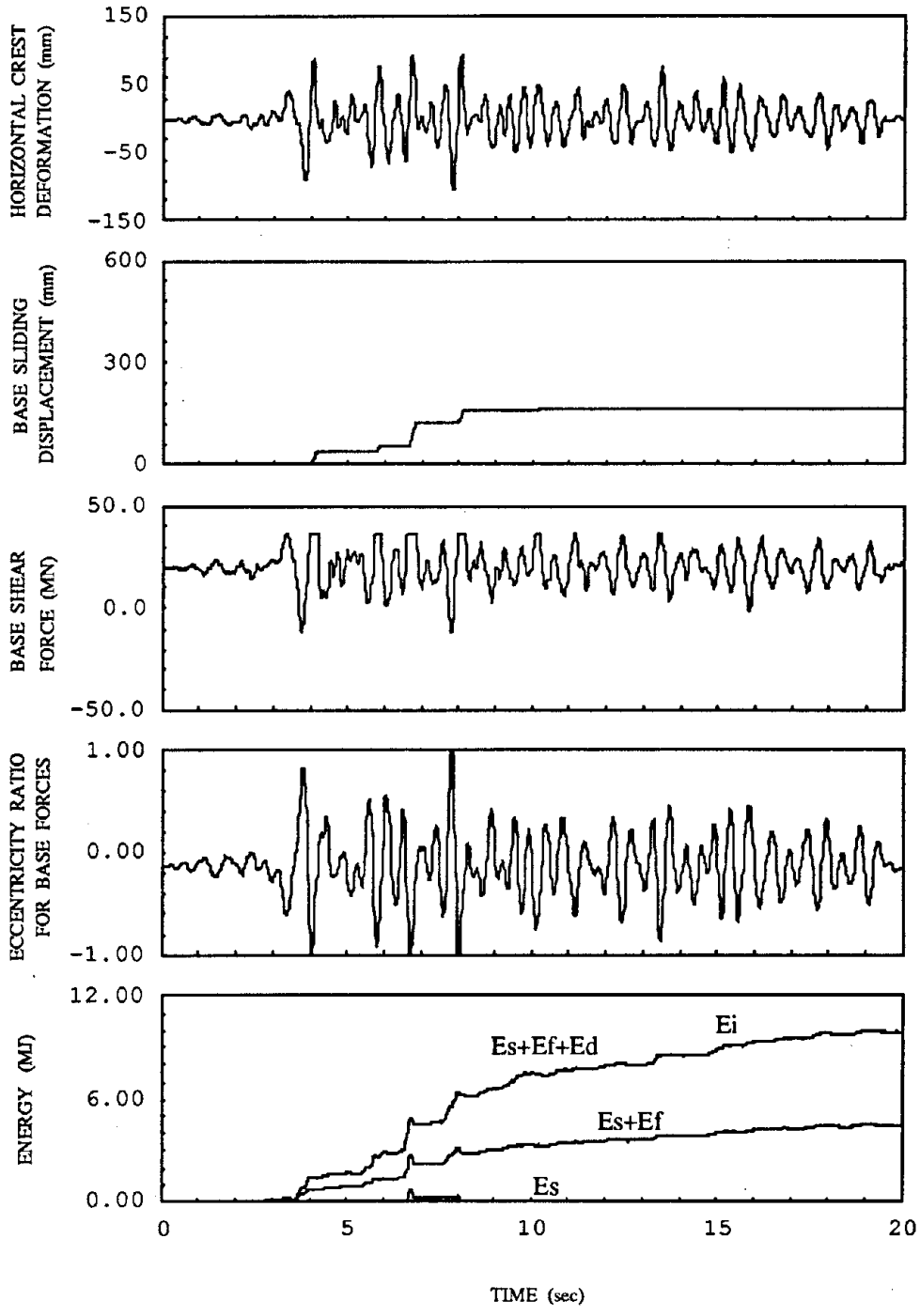

Figure 5.33. Response of Pine Flat dam with flexible foundation rock, $E_{fr}/E_{cd} = 1$, horizontal interface, $\alpha = 1$, $\mu = 1$, subjected to the horizontal S69E component of Taft ground motion with peak ground acceleration = 0.6g.

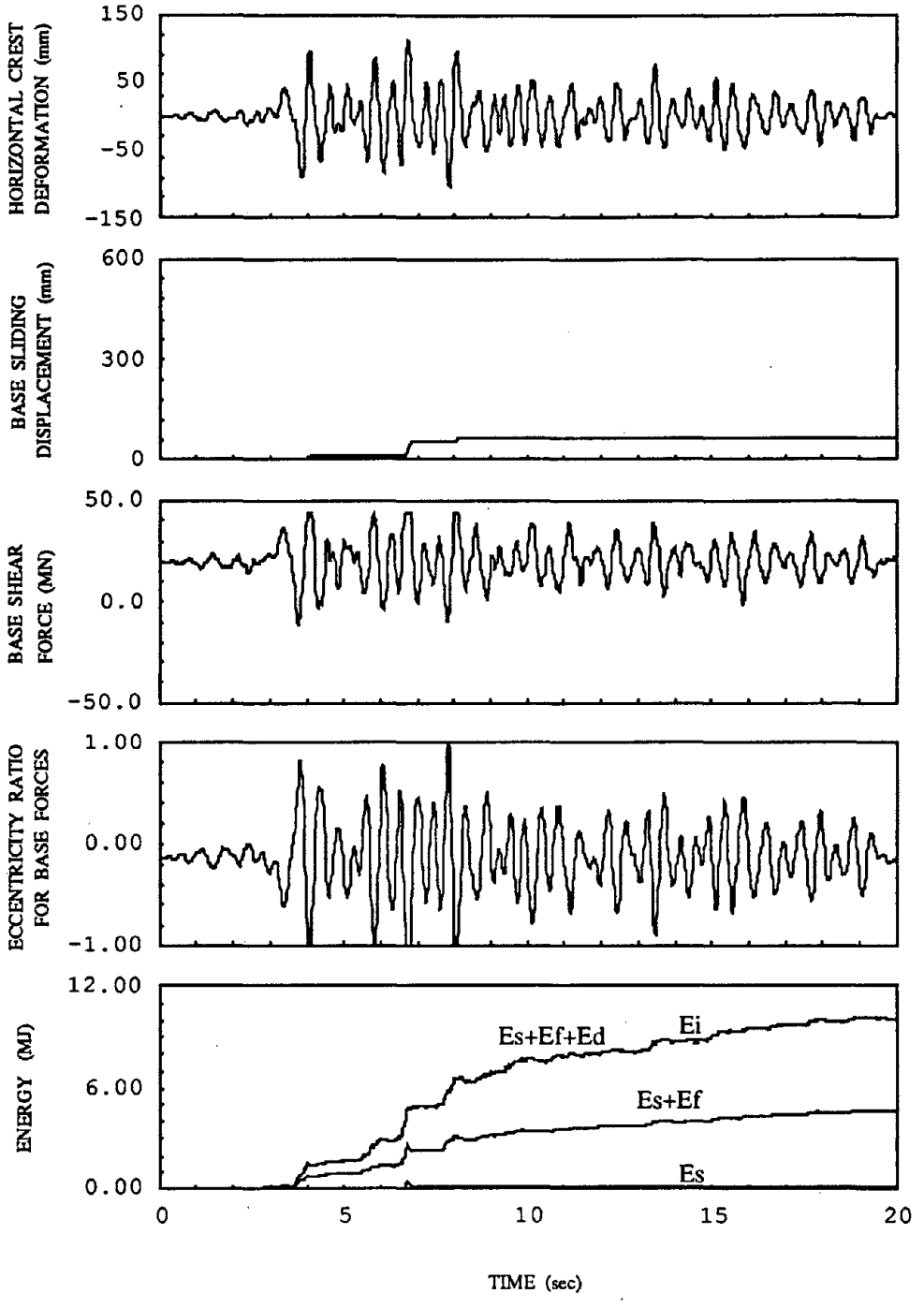

Figure 5.34. Response of Pine Flat dam with flexible foundation rock, $E_{fr}/E_{cd} = 1$, horizontal interface, $\alpha = 1$, $\mu = 1.2$, subjected to the horizontal S69E component of Taft ground motion with peak ground acceleration = 0.6g.

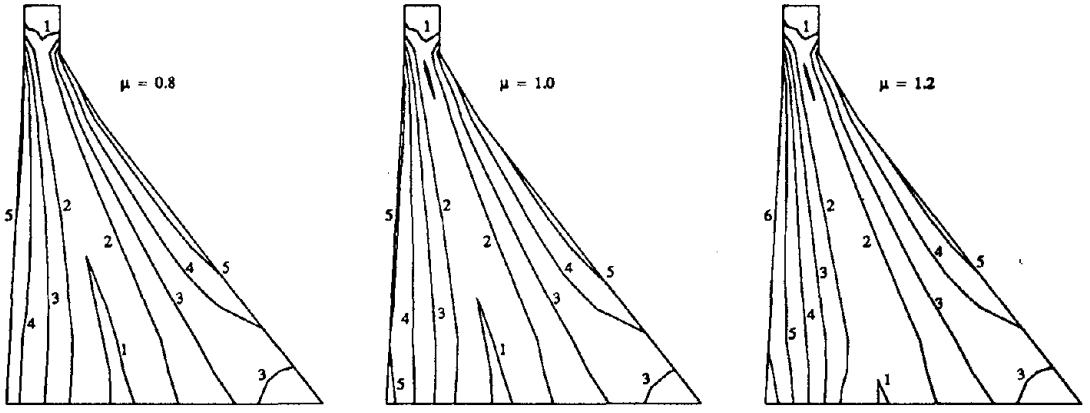

Figure 5.35. Envelope of maximum principal stresses (in MPa) in Pine Flat dam with flexible foundation rock, $E_{fr}/E_{cd} = 1$, horizontal interface, $\alpha = 1$, subjected to the horizontal S69E component of Taft ground motion with peak ground acceleration = 0.6g. Static effects not included.

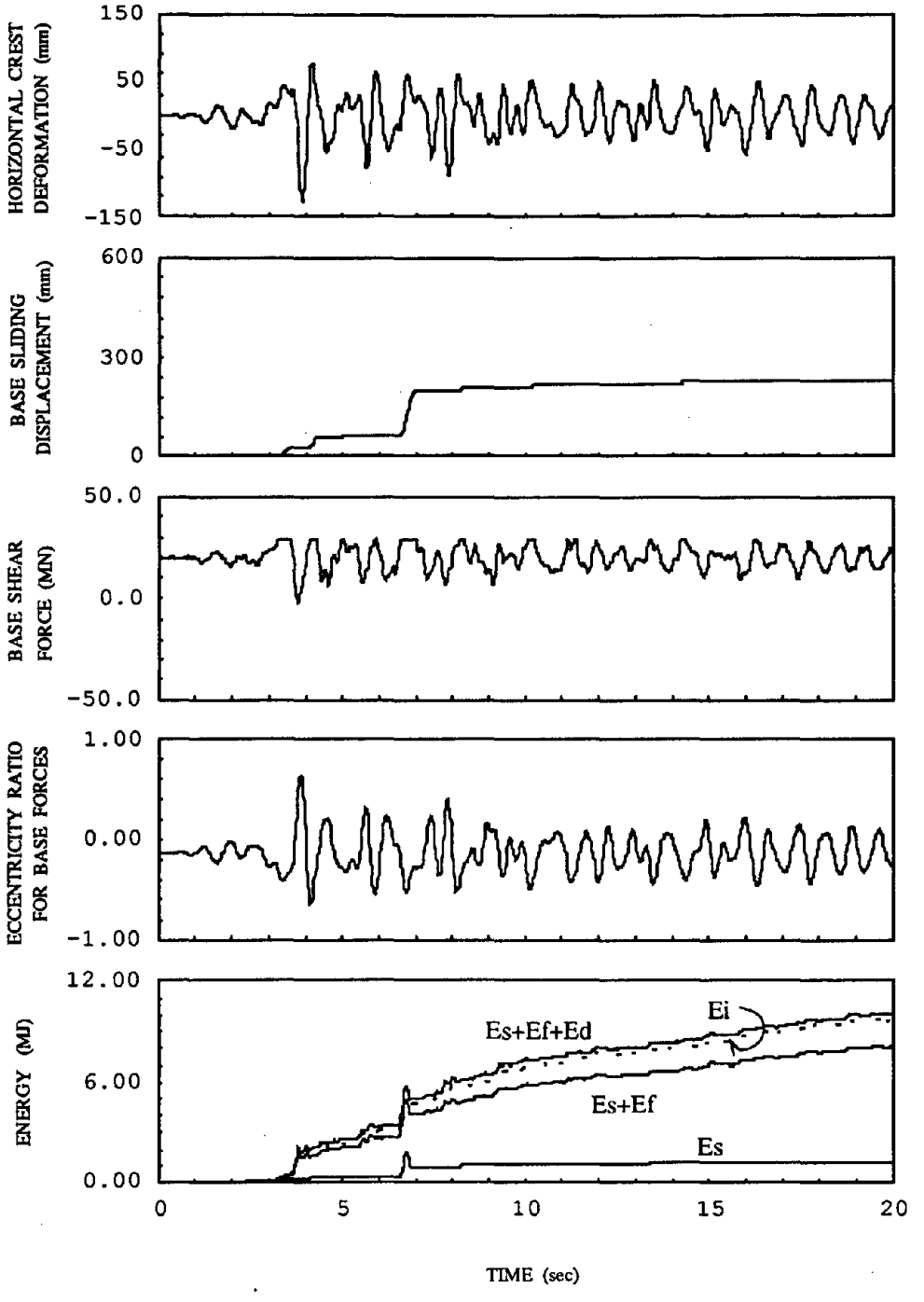

Figure 5.36. Response of Pine Flat dam with flexible foundation rock, $E_{fr}/E_{cd} = 0.25$, horizontal interface, $\alpha = 1$, $\mu = 0.8$, subjected to the horizontal S69E component of Taft ground motion with peak ground acceleration = 0.6g.

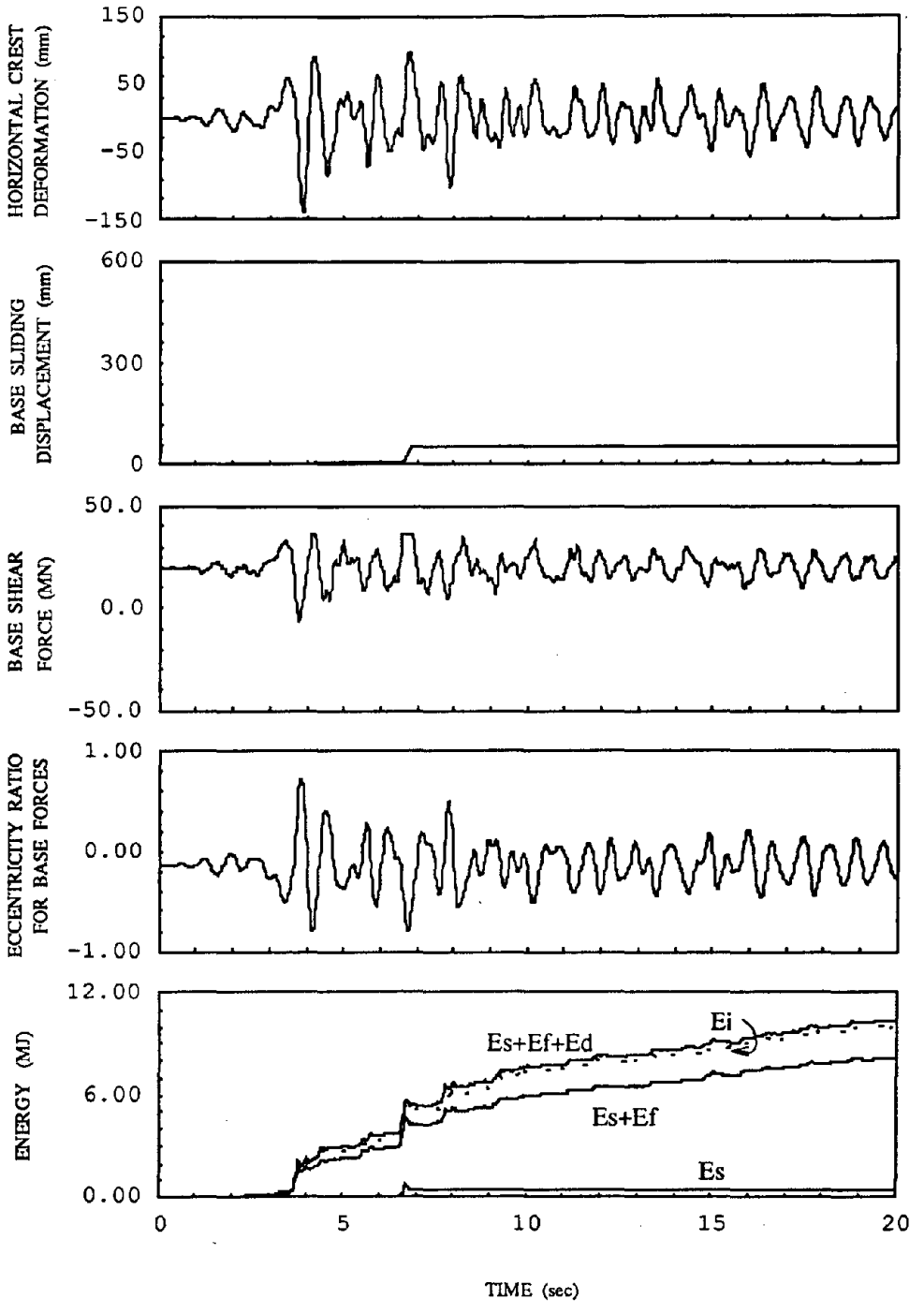

Figure 5.37. Response of Pine Flat dam with flexible foundation rock, $E_{fr}/E_{cd} = 0.25$, horizontal interface, $\alpha = 1$, $\mu = 1$, subjected to the horizontal S69E component of Taft ground motion with peak ground acceleration = 0.6g.

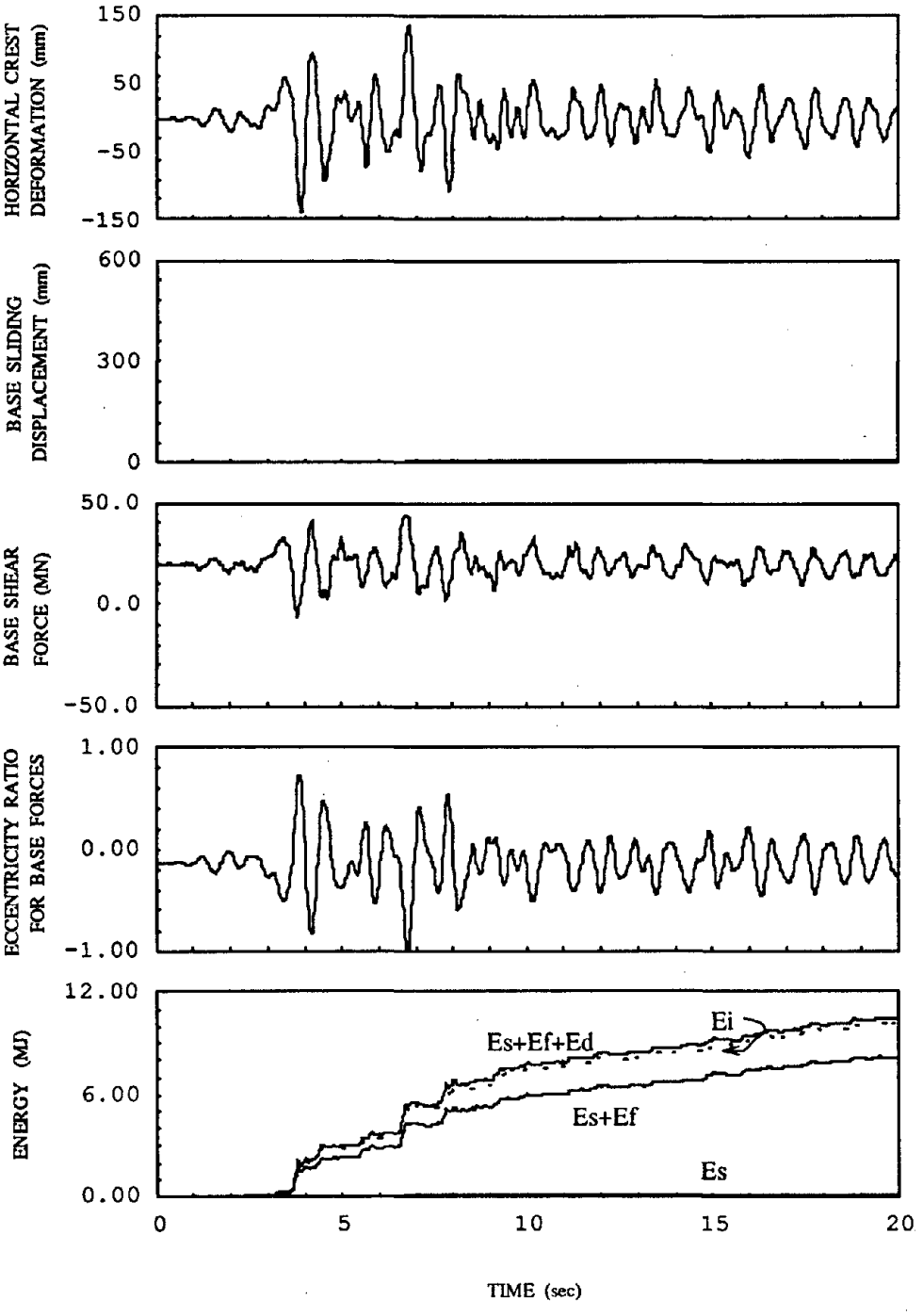

Figure 5.38. Response of Pine Flat dam with flexible foundation rock, $E_{fr}/E_{cd} = 0.25$, horizontal interface, $\alpha = 1$, $\mu = 1.2$, subjected to the horizontal S69E component of Taft ground motion with peak ground acceleration = 0.6g.

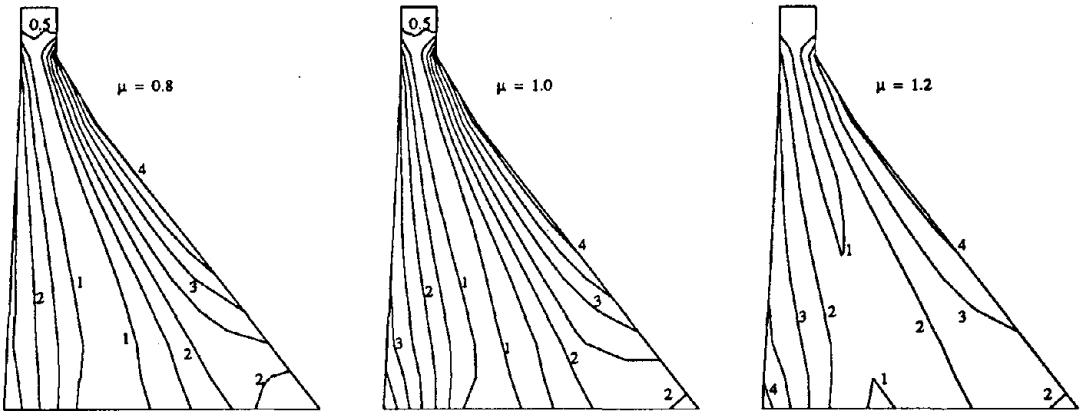

Figure 5.39. Envelope of maximum principal stresses (in MPa) in Pine Flat dam with flexible foundation rock, $E_{fr}/E_{cd} = 0.25$, horizontal interface, $\alpha = 1$, subjected to the horizontal S69E component of Taft ground motion with peak ground acceleration = 0.6g. Static effects not included.

The maximum principal stresses, shown in Figures 5.35 and 5.39, increase with the increase of peak ground acceleration to 0.6g compared with the stresses due to a peak acceleration of 0.4g. An increase in principal stresses of about 60 percent is observed at the downstream face of the dam on a flexible foundation rock with a moduli ratio $E_{fr}/E_{cd} = 0.25$.

5.9 Summary of Response Trends

The case study of Pine Flat dam, which is representative of concrete gravity dams of moderate height, indicates the following:

1. The sliding response of the dam is affected by the ground motion record. A ground motion with many acceleration peaks, such as the Taft record, will produce several sliding events. For the cases analyzed, sliding accumulates in the downstream direction with large acceleration peaks and therefore Taft produces the largest sliding compared with the sliding produced by the El Centro and Pacoima ground motions. This trend is confirmed by comparing the input energy for the three ground motions, in which the Taft ground motion produces the largest input energy to the system.

2. The amplitude of the ground motion affects considerably the base sliding displacement of the dam. The influence is more pronounced for dams on rigid foundation rock compared with dams on flexible foundation rock, because in the latter case damping in the foundation rock region reduces the response.

3. The contribution of vertical ground motion to the sliding response depends on the dynamic properties of the dam system and on the characteristics of the ground motion considered. For the cases analyzed the vertical ground motion has little effect in the sliding displacement of the dam.

4. Sliding at the base of the dam acts as an isolation mechanism that slightly decreases the deformation of the dam, producing smaller stresses compared with a dam prevented from sliding.

5. For dams on rigid foundation rock, the base sliding displacement is very sensitive to the coefficient of friction. A slight decrease in the value of the coefficient of friction produces a large increase in the sliding displacement. On the other hand, dam deformation and maximum principal stresses are not very sensitive to the coefficient of friction.

6. The coefficient of friction is less important for dams on flexible foundation rock compared with dams on rigid foundation rock. The base sliding displacement decreases substantially as the foundation rock becomes more flexible because the increase in effective damping from the foundation rock reduces the response and limits the base shear force causing sliding. For the flexible founadtion rock cases analyzed sliding is not an effective energy dissipation mechanism.

7. The analysis of Pine Flat dam (with a 95 percent full reservoir) indicates that rocking of the dam is not likely to occur when the dam is subjected to ground motions of moderate amplitude (0.4g), but it may may be necessary to consider rocking for larger amplitude ground motions (0.6g).

Chapter 6

PARAMETER STUDY OF A SIMPLIFIED DAM MODEL

6.1 Introduction

The sliding stability of a concrete gravity dam during a design earthquake must be evaluated to assess the seismic safety of the dam. Current design practice attempts to evaluate sliding stability with an equivalent static analysis to give a factor of safety against sliding. However, the application of this procedure has been questioned as to whether it represents the transient characteristics of the sliding response.

The study of Pine Flat dam, in Chapter 5, showed that the sliding response depends on the ground motion and it is sensitive to the coefficient of friction. The sliding displacement of this dam is notably reduced due to dam-foundation rock interaction. It is desirable to estimate how these factors affect the sliding response of dams with different dynamic properties and different heights.

The parameter study of a typical dam monolith investigates the factors that influence the sliding response of typical concrete dams to horizontal ground motion. The results are presented in the form of sliding displacement spectra. The analysis include the effects of water compressibility and foundation rock flexibility, which were not considered in previous studies [Danay and Adeghe, 1993; Chopra and Zhang, 1991]. These effects, as shown for Pine Flat dam, may influence considerably the sliding response of a dam.

The parameter study is performed using the procedure presented in Chapters 3 and 4. However, the analysis is simplified by using only one generalized coordinate to represent the motion of the dam in its fundamental vibration mode. The procedure accounts for the important factors affecting the earthquake response, including the dynamic properties of the dam, dam-water interaction, and dam-foundation rock interaction. The sliding displacements computed using the simplified model are a good approximation of the displacements obtained by using five generalized coordinates in the analysis.

6.2 Typical Dam Monolith

A typical concrete gravity dam monolith, shown in Figure 6.1, is used to investigate the sliding response. The monolith of height H_s has a rigid base and it rests on a flexible foundation rock. The mass concrete is assumed to be homogeneous, with linear and isotropic properties. The interface plane is assumed to be horizontal and sliding occurs along this plane. The impounded water has a constant depth H and it is idealized as extending to infinity in the upstream direction. The foundation rock is idealized as a homogeneous, isotropic, and linear viscoelastic half-plane.

One generalized coordinate is used to represent the deformation of the dam. The assumed mode shape for the dam is:

$$\Psi_1(y) = a\left(\frac{y}{H_s}\right) + (1-a)\left(\frac{y}{H_s}\right)^2 \tag{6.1}$$

with $a = 0.18$ representing the flexural and shear deformation of the dam [Chopra,

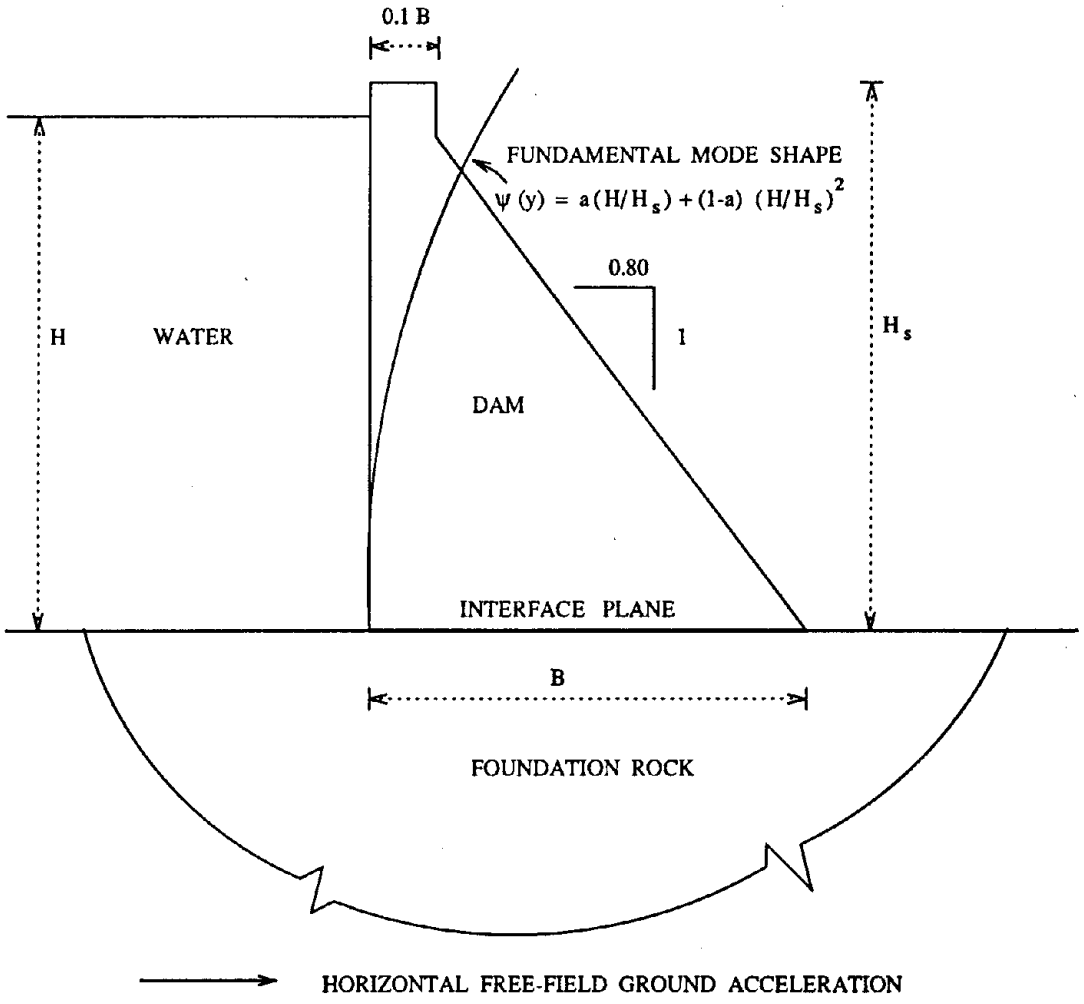

Figure 6.1. Simplified model of typical gravity dam monolith.

1967]. The fundamental period of the dam can be approximated by [Chopra, 1967]:

$$T = 0.38\frac{H_s}{\sqrt{E_{cd}}} \tag{6.2}$$

where E_{cd} is the modulus of elasticity of the concrete in MPa, and H_s is in meters.

As an example, a 100 m high typical dam is analyzed using the finite element model presented in Chapters 3 and 4 with five modes of vibration and using the simplified model. The dam is subjected to the Taft S69E ground motion, and two cases are considered: dam on rigid foundation rock, and dam on flexible foundation rock. The responses of the two models are shown in Figure 6.2. The crest displacement obtained with the simplified model is approximately the same as that of the finite element model for both the rigid and flexible foundation rock cases. The sliding displacements are also similar. The sliding events are well represented by the simplified model, although for these cases of the simplified model overestimates the sliding of the finite element model by 6 and 15 percent for the rigid and flexible foundation rock cases, respectively.

6.3 Parameter Study

The height of the dam is varied from 25 m (82 ft) to 175 m (574 ft) to consider a wide range of dams. The geometry of the monolith is scaled proportionally, according to Figure 6.1. The concrete has a modulus of elasticity, E_{cd}, of 27.6 GPa (4 million psi) for most of the cases analyzed, although values of 20.7 GPa (3 million psi) and 34.5 GPa (5 million psi) are used when the effect of the modulus of elasticity is examined. The unit weight of concrete is 24.3 kN/m^3 (155 pcf) and the Poisson's

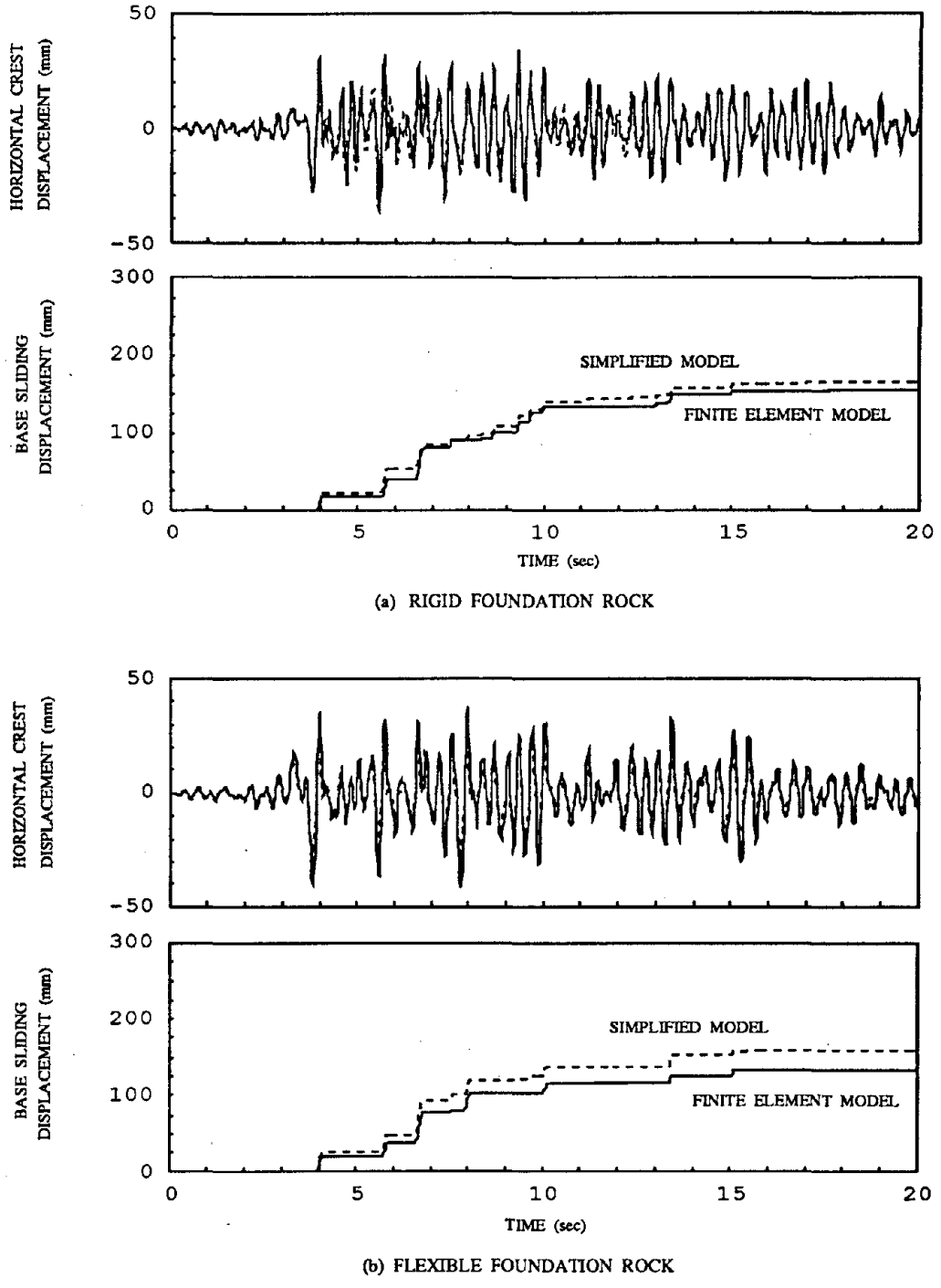

Figure 6.2. Response of a 100 m high typical dam with full reservoir of compressible water, $\alpha = 1$, $\mu = 1$, subjected to the horizontal S69E component of Taft ground motion, on rigid and flexible foundation rock with a moduli ratio $E_{fr}/E_{cd} = 1$.

ratio is 0.2. A constant hysteretic damping factor of 0.10 for the dam is used for all cases.

The unit weight of water is 9.8 kN/m^3 (62.4 pcf). The velocity of wave propagation is 1440 m/sec (4720 ft/sec). The wave reflection coefficient for the reservoir bottom materials is unity, indicating no reservoir bottom absorption for most cases. Wave reflection coefficients of 0 and 0.5 are used to study the influence of the reservoir bottom materials on the base sliding response of the dam.

The dam does not slide for any case with an empty reservoir, $H/H_s = 0$, or a half-full reservoir, $H/H_s = 0.5$. This indicates the important effect of the impounded water on the earthquake-induced sliding of the dam. Thus a full reservoir is used for all cases.

The modulus of elasticity of the foundation rock, E_{fr}, is varied to consider various rock sites. The following moduli ratios are used: $E_{fr}/E_{cd} = \infty$, 1, and 0.25. The unit weight of the foundation rock is 25.9 kN/m^3 (165 pcf) and the Poisson's ratio is 0.33. A hysteretic damping coefficient of 0.10 is assumed for the foundation rock.

A coefficient of friction of unity is used in most of the cases to determine the sliding response of the dam, although values of $\mu = 0.8$, 0.9, 1.0, and 1.2 are used to study the effect of the coefficient of friction on the sliding displacement. The cohesion force at the interface is assumed to be zero.

The parameter study considers the response of the dam to horizontal free-field ground acceleration. The dam is subjected to the Taft S69E ground motion

for most of the cases. Additional cases of the dam subjected to the El Centro S00E and Pacoima S16E ground motions show the influence of the ground motion on the dam response. The ground motions are normalized to have a peak acceleration of 0.4g which represents a moderate design-earthquake. The peak ground acceleration is varied over 0.3g, 0.5g, and 0.6g to study the effect of ground motion amplitude on the sliding response of the dam.

6.4 Influence of Ground Motion

The sliding displacement of the dam due to each ground motion record varies with the height of the dam and the flexibility of the foundation rock, as shown in Figure 6.3. Each ground motion excites the dam system in a different manner depending on the response spectrum for ground motion, the fundamental vibration period of the system, and the number and amplitude of acceleration peaks.

The sliding displacement is, for most cases, largest when the dam is subjected to the Taft S69E ground motion. This applies to dams on rigid foundation rock with a height less than 160 m (525 ft) and to dams on flexible foundation rock with a moduli ratio $E_{fr}/E_{cd} = 0.25$, with a height less than 90 m (295 ft). In general, the sliding decreases as the foundation rock becomes more flexible. The peaks of the sliding displacement spectra are shifted to shorter dams as the foundation rock becomes more flexible because the vibration period of the system lengthens due to dam-foundation rock interaction.

The sliding displacement of dams subjected to the El Centro S00E ground motion is the largest for very tall dams on rigid foundation rock and for moderately

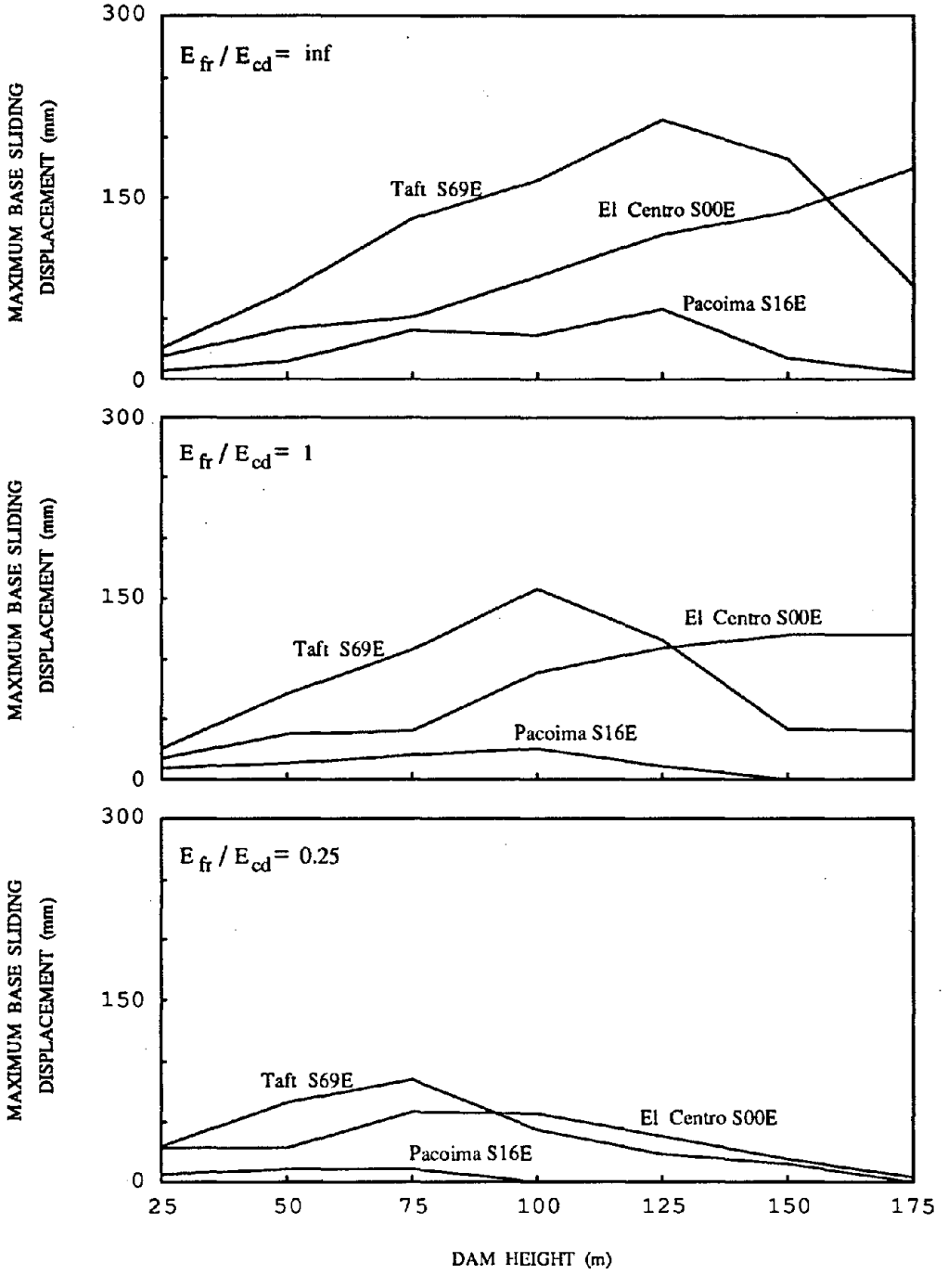

Figure 6.3. Maximum base sliding displacement of a typical dam with full reservoir of compressible water, $\alpha = 1$, $\mu = 1$, subjected to three ground motions with peak ground acceleration = 0.4g.

tall dams on flexible foundation rock, with a moduli ratio $E_{fr}/E_{cd} = 1$, because the period of the system for these cases is in the highly amplified region of the response spectrum. For very flexible foundation rock, $E_{fr}/E_{cd} = 0.25$, the damping due to dam-foundation rock interaction decreases the response for the tall dams subjected to all three ground motions.

The sliding displacement of dams subjected to the Pacoima S16E ground motion is the smallest, because the ground motion acceleration record has only one large pulse that produces sliding, so the accumulated sliding displacement is small. The sliding decreases with the increasing flexibility of the foundation rock and the increasing height of the dam. There is almost no sliding of the dam on flexible foundation rock with a moduli ratio of $E_{fr}/E_{cd} = 0.25$.

The Taft S69E ground motion will be used for the rest of the parameter study because for the most of the cases the sliding displacement is approximately twice that of the El Centro ground motion and three to four times that of the Pacoima ground motion.

6.5 Influence of Peak Ground Acceleration

The initiation of sliding is influenced by the peak ground acceleration and the occurrence of subsequent sliding events depends also on peaks in the ground acceleration record. Figure 6.4 shows the maximum sliding displacement for a dam subjected to the Taft S69E ground motion scaled to four levels of peak ground acceleration: 0.3g, 0.4g, 0.5g and 0.6g.

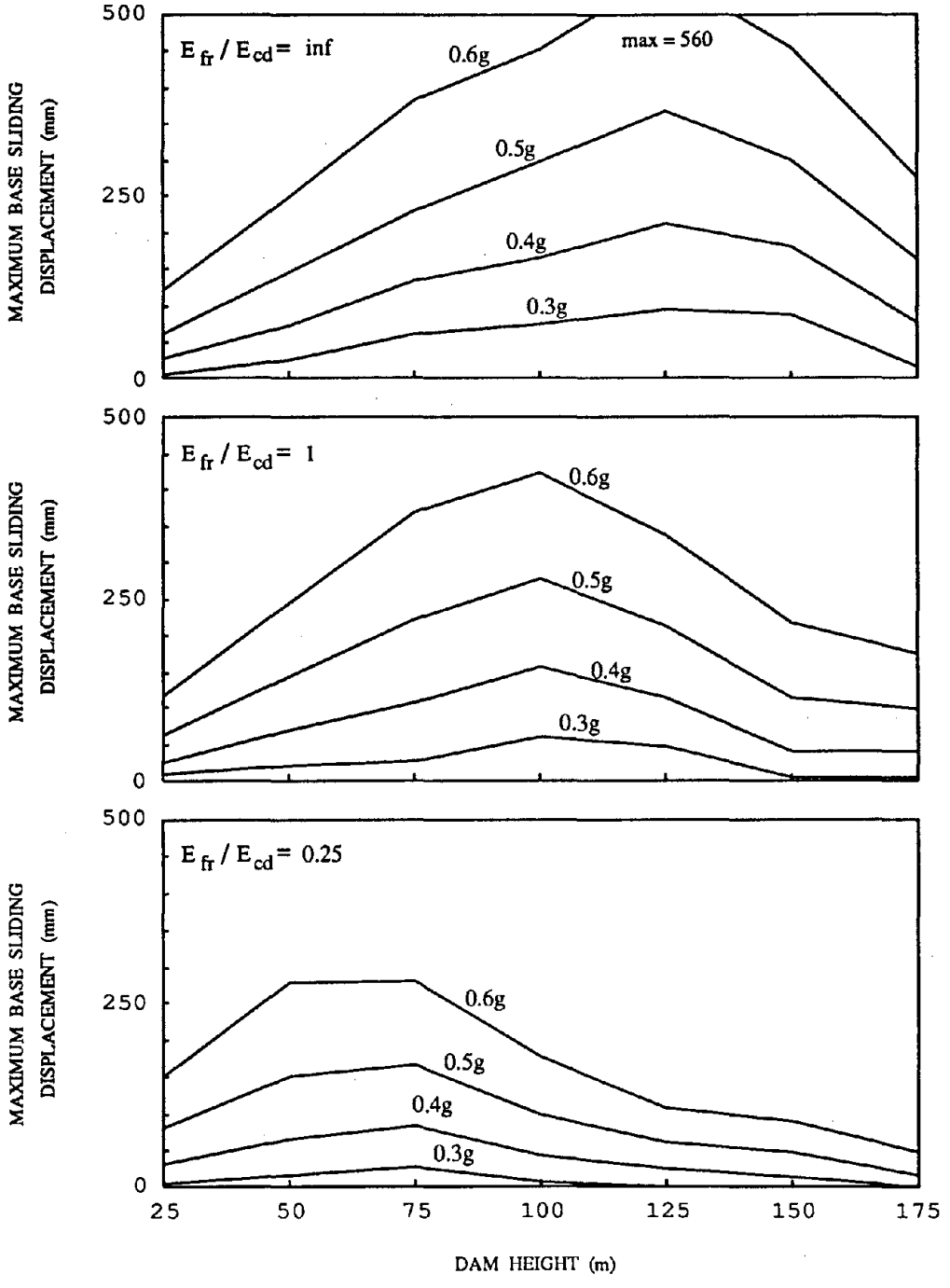

Figure 6.4. Influence of peak ground acceleration on the maximum base sliding displacement of a typical dam with full reservoir of compressible water, $\alpha = 1$, $\mu = 1$, subjected to the horizontal S69E component of Taft ground motion.

The sliding displacement increase nonlinearly with increasing peak ground acceleration. For a rigid foundation rock, the increase in sliding displacement is roughly about 120 percent when the peak ground acceleration increases from 0.3g to 0.4g. The sliding increases about 90 percent when the peak ground acceleration increases from 0.4g to 0.5g. The sliding increases about 50 percent when the peak ground acceleration increases from 0.5g to 0.6g. For flexible foundation rock the increase in sliding displacement is greater as the foundation rock becomes more flexible, although the maximum sliding displacement decreases.

The sliding response of the dam is not influenced by the peak ground acceleration alone. The value of the coefficient of friction also affects the maximum displacement. However, these results show that the maximum sliding displacement is substantially affected by the peak ground acceleration.

6.6 Influence of the Coefficient of Friction

The sliding displacement is sensitive to the value of the coefficient of friction. Figure 6.5 shows the maximum sliding displacement of a dam subjected to the Taft S69E ground motion for four values of coefficient of friction, μ = 0.8, 0.9, 1.0, and 1.2. For the same value of μ, a dam on rigid foundation rock slides more than a dam on flexible foundation rock. The maximum sliding displacement occurs for tall dams, H_s=125 m (410 ft) on rigid foundation rock, and for shorter dams, H_s=75 m (246 ft), on flexible foundation rock. The shifting of the peaks of maximum sliding displacement is due to the lengthening of the period of the dam system as the dam becomes taller and the foundation rock becomes more flexible.

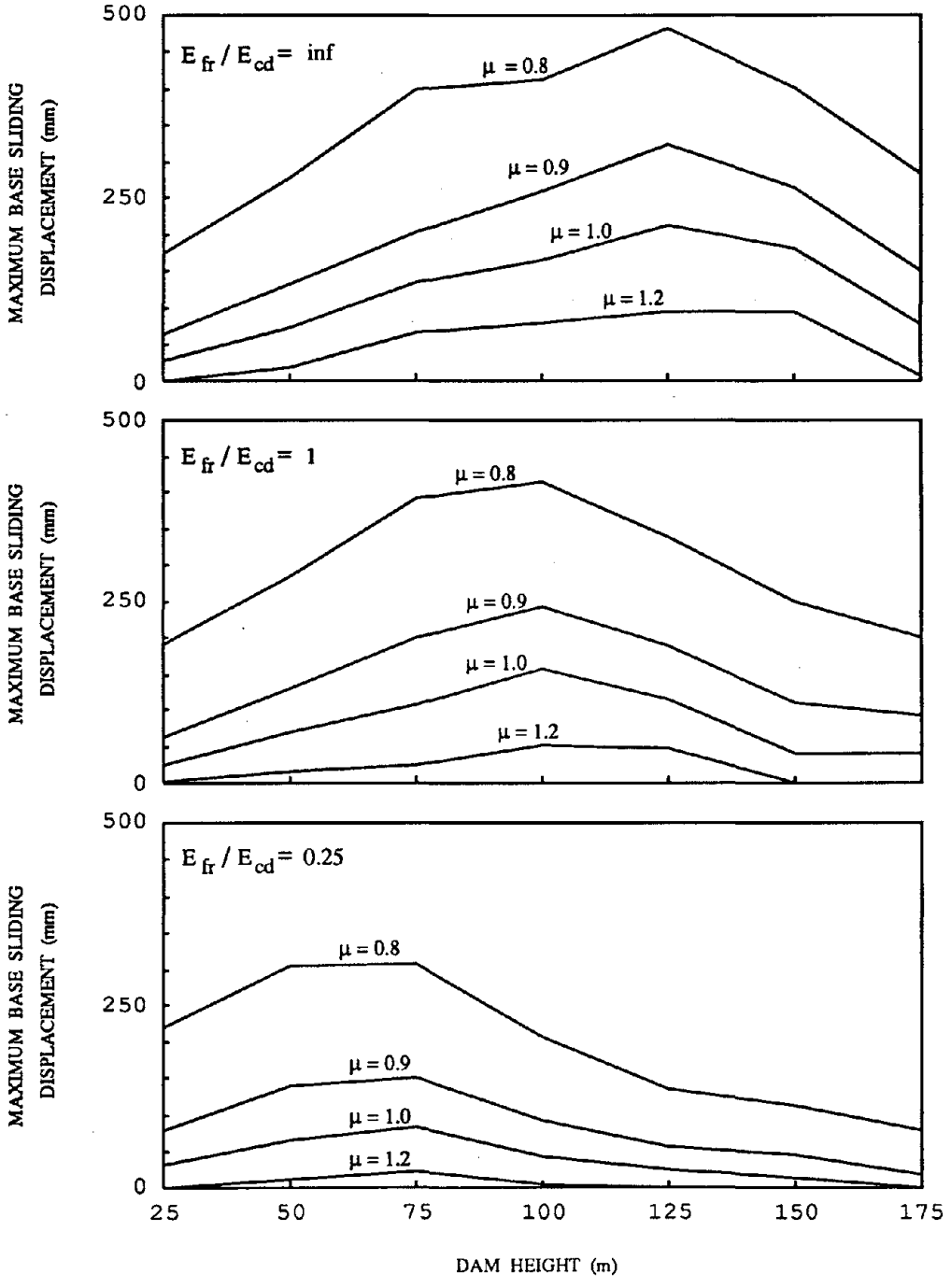

Figure 6.5. Influence of the coefficient of friction on the maximum base sliding displacement of a typical dam with full reservoir of compressible water, $\alpha = 1$, subjected to the horizontal S69E component of Taft ground motion with peak ground acceleration = 0.4g.

The maximum sliding displacement increases nonlinearly as the coefficient of friction decreases. The relative increase in sliding displacement with μ is largest for short dams and flexible foundation rock, although the largest sliding displacements are obtained for tall dams on rigid foundation rock. For example, for a 125 m (410 ft) tall dam on rigid foundation rock the maximum sliding increases by a factor of two from 215 mm for $\mu = 1$ to 480 mm for $\mu = 0.8$. For a 75 m (246 ft) tall dam on flexible foundation rock, with a moduli ratio $E_{fr}/E_{cd} = 0.25$, the maximum sliding displacement increases three times from 84 mm for $\mu = 1$ to 309 mm for $\mu = 0.8$.

Base sliding may be interpreted as an isolation mechanism because it limits the base shear force transmitted to the dam. Figure 6.6 shows the relationship between the sliding displacement and crest displacement, which is related to the maximum stresses, for selected values of dam height. The crest displacement decreases with an increase in sliding displacement for dams taller than 100 m (328 ft) on rigid foundation rock. However, there is no reduction in the crest displacement when the foundation rock is flexible. It may be concluded that sliding isolation of the dam is not an important factor with flexible foundation rock because the foundation rock itself provides a substantial amount of isolation and energy dissipation.

6.7 Influence of Foundation Rock Flexibility

The flexibility of the foundation rock introduces material and radiation damping in the dam-water-foundation rock system and thus reduces the response. This is shown in Figure 6.7, where foundation rock flexibility generally reduces the base sliding displacement for various levels of peak ground acceleration. The influence of the

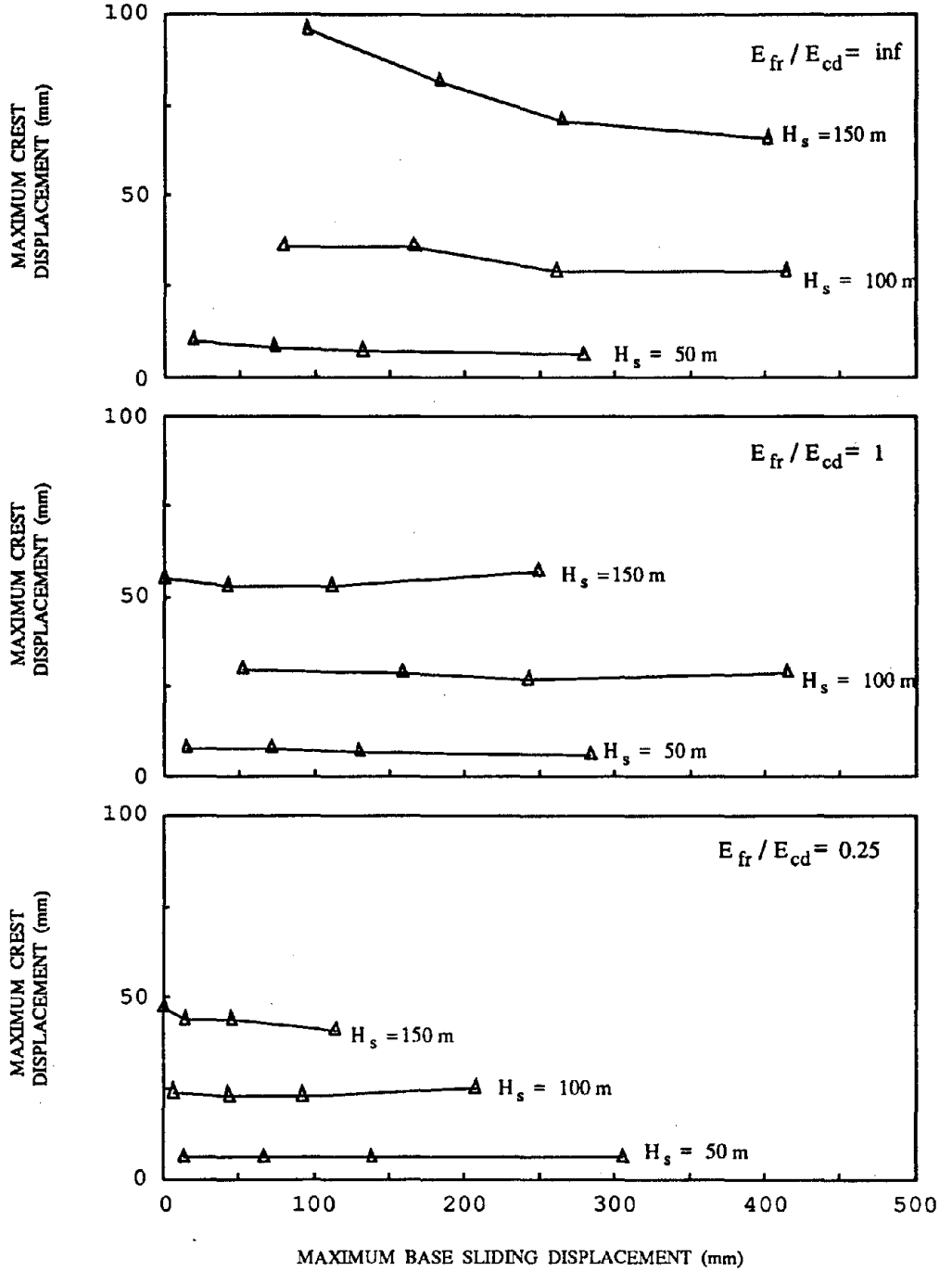

Figure 6.6. Relationship between maximum base sliding displacement and maximum crest displacement of a typical dam with full reservoir of compressible water, $\alpha = 1$, $\mu = 1$, subjected to the horizontal S69E component of Taft ground motion with peak ground acceleration = 0.4g.

foundation rock flexibility is sensitive to the dam height. For tall dams the maximum base displacement is reduced as the foundation rock becomes more flexible, and for short dams the maximum base sliding displacement is independent of the foundation rock flexibility. This is because the fundamental period of the dam system lengthens with the increase in dam height and flexibility of the foundation rock, and larger values of response are obtained when this period is in the amplified region of the response spectrum for the ground motion.

Figure 6.8. shows the decrease in sliding displacement with flexible foundation rock for three heights of the dam, H_s = 50 m, 100 m, and 150 m, and a range of the coefficient of friction. For the 50 m (164 ft) tall dam the flexible foundation rock has no effect on the sliding displacement of the dam. This corroborates the assumptions in previous studies that neglected the influence of flexibility of foundation rock when analyzing short dams [Adeghe and Danay, 1993]. As the height of the dam increases, the influence of the foundation rock flexibility becomes important. For the 100 m (328 ft) tall dam the sliding displacement for the dam on rigid foundation rock decreases approximately by one-half when the dam is on flexible foundation rock with a moduli ratio $E_{fr}/E_{cd} = 0.25$. For the 150 m (492 ft) tall dam the sliding displacement for the dam on rigid foundation rock decreases by more than a factor of three when the dam is on flexible foundation rock with a moduli ratio $E_{fr}/E_{cd} = 0.25$, depending on the value of coefficient of friction. This trend was observed in the earthquake response of the 122 m (400 ft) tall Pine Flat dam presented in Chapter 5.

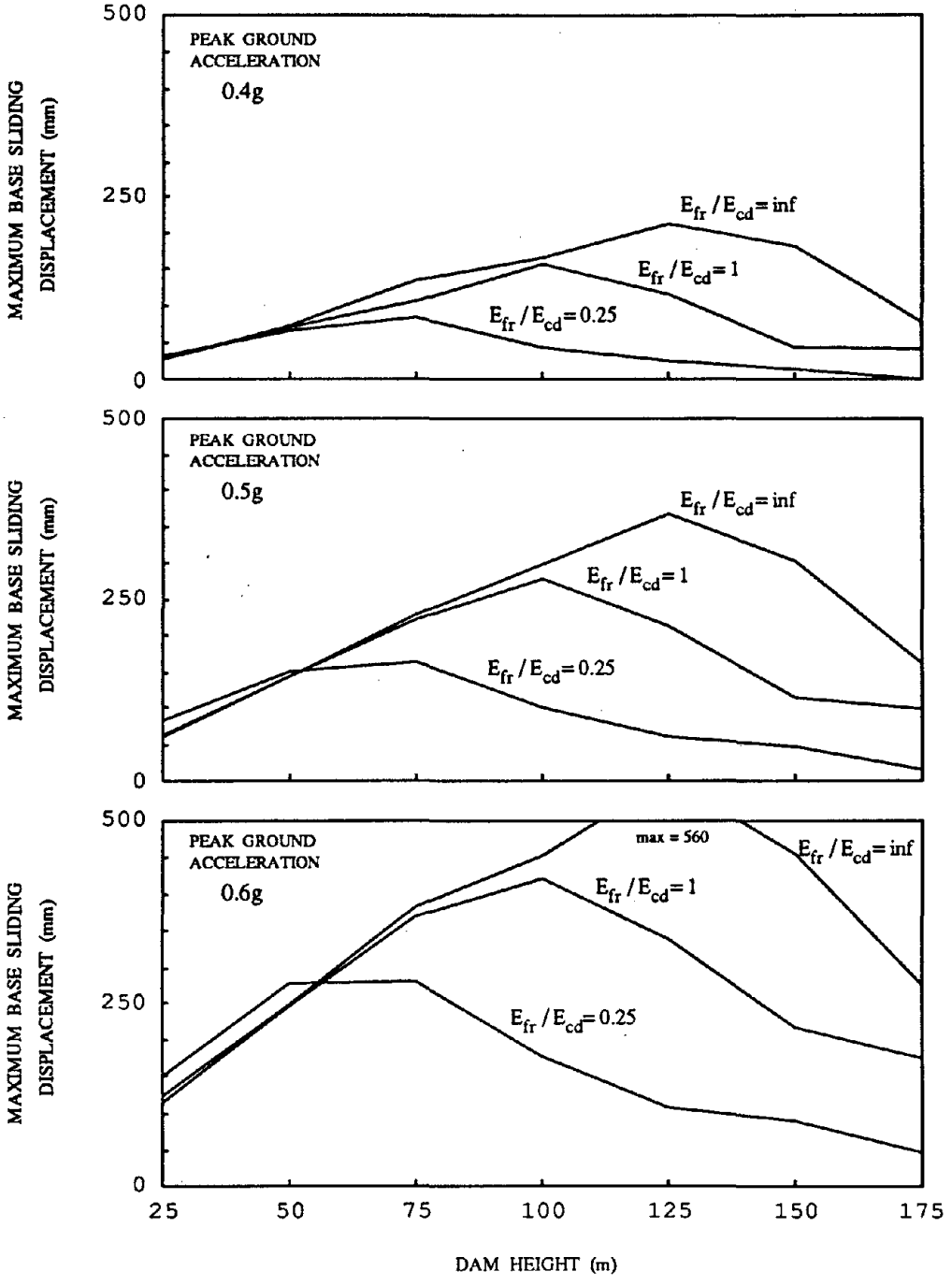

Figure 6.7. Influence of foundation rock flexibility on the maximum base sliding displacement of a typical dam with full reservoir of compressible water, $\alpha = 1$, $\mu = 1$, subjected to the horizontal S69E component of Taft ground motion.

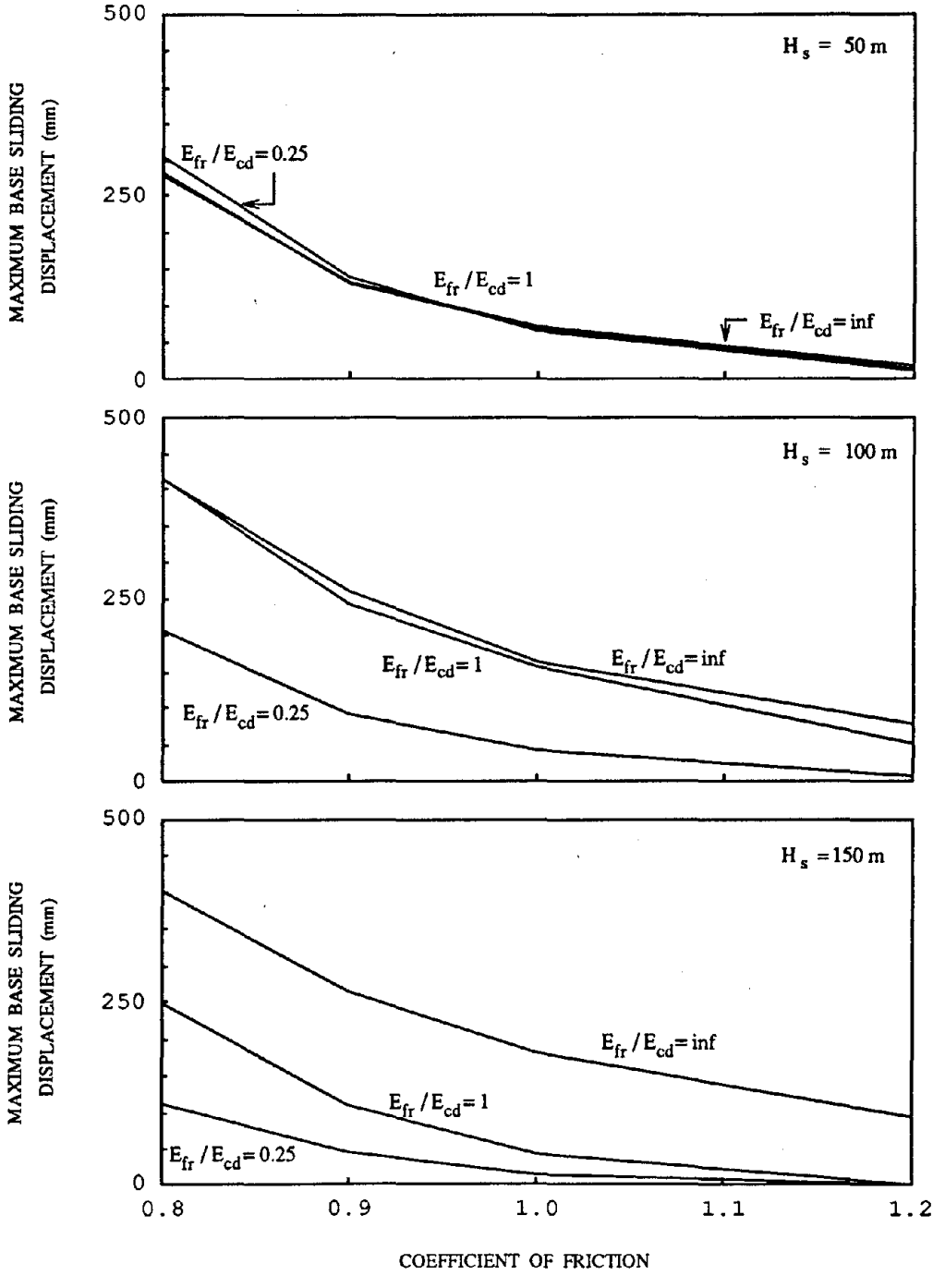

Figure 6.8. Influence of foundation rock flexibility on the maximum base sliding displacement of a typical dam with full reservoir of compressible water, $\mu = 1$, subjected to the horizontal S69E component of Taft ground motion with peak ground acceleration = 0.4g.

6.8 Influence of Water Compressibility

The maximum sliding displacement for a dam on rigid or flexible foundation rock is greater when the water is considered to be compressible compared with the case of incompressible water, as shown in Figure 6.9. Water compressibility has the most effect when the dam is on rigid foundation rock, especially for dams less than 150 m (492 ft) tall. In this range of dam heights, the sliding displacement obtained with incompressible water is as much as 40 percent less than the displacement with compressible water. The effects of compressibility are less for dams on flexible foundation rock because the foundation rock damping generally reduces the importance of dam-water interaction. This trend has been observed for the linear earthquake response of dams without sliding [Fenves and Chopra, 1984a].

6.9 Influence of Reservoir Bottom Materials

The effects of the reservoir bottom materials on the sliding response of a typical dam with full reservoir of water subjected to the Taft S69E ground motion are shown in Figure 6.10. The wave reflection coefficient $\alpha = 0$ represents a very absorptive reservoir bottom and $\alpha = 1$ corresponds to a rigid reservoir bottom.

The sliding displacement is reduced by the reservoir bottom materials because of the added damping due to absorption. The reduction in the sliding displacement is largest when the dam is on rigid foundation rock. Reductions in sliding displacement of 50 percent or more occur when the reservoir bottom becomes very absorptive. The effect of reservoir bottom absorption is less important when the foundation rock is

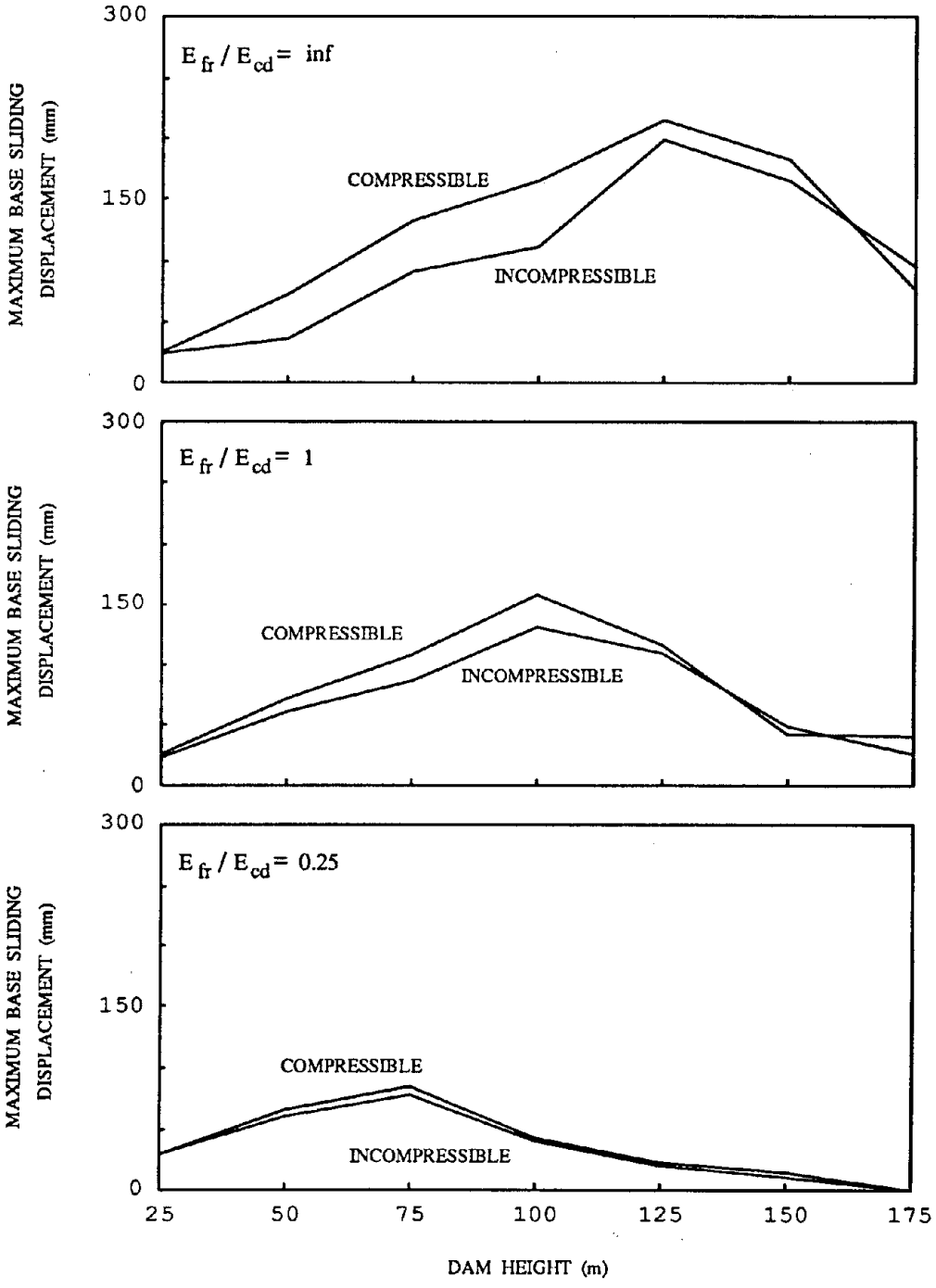

Figure 6.9. Influence of water compressibility on the maximum base sliding displacement of a typical dam with full reservoir, $\alpha = 1$, $\mu = 1$, subjected to the horizontal S69E component of Taft ground motion with peak ground acceleration = 0.4g.

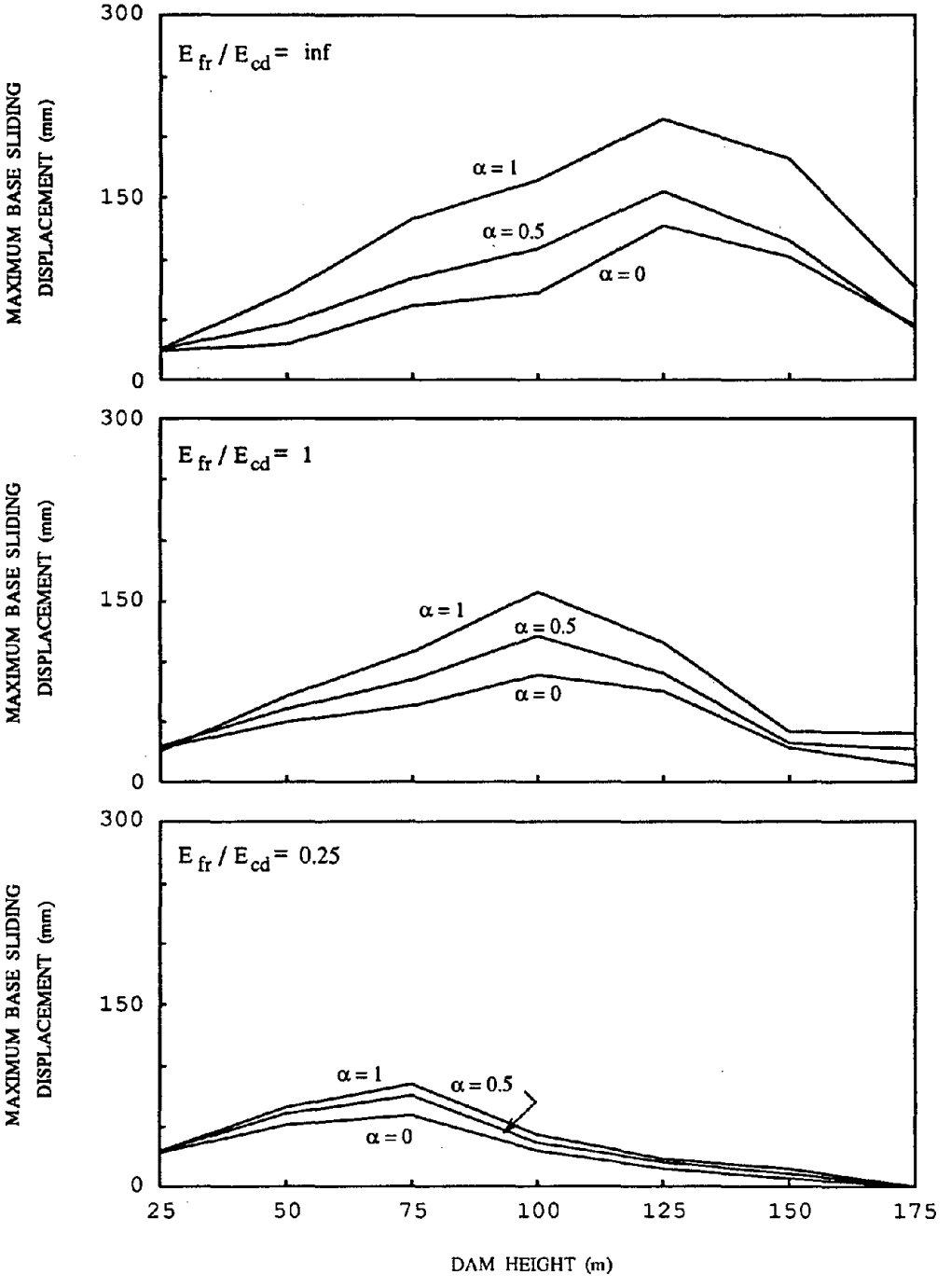

Figure 6.10. Influence of reservoir bottom absorption on the maximum base sliding displacement of a typical dam with full reservoir of compressible water, $\mu = 1$, subjected to the horizontal S69E component of Taft ground motion with peak ground acceleration = 0.4g.

flexible because of the decreased importance of dam-water interaction with the flexible foundation rock.

6.10 Influence of Modulus of Elasticity of Dam Concrete

The modulus of elasticity of the dam concrete affects the fundamental period of the dam-water-foundation rock system and hence influences the sliding response of the dam. Figure 6.11 shows the maximum sliding displacements for three values of the modulus of elasticity for the concrete, E_{cd}. The effect of the modulus varies with the height of the dam and the flexibility of the foundation rock because they also affect the fundamental vibration period of the system.

The results show that the sliding displacement increases with the modulus of elasticity for dams taller than 125 m (410 ft) on rigid foundation rock. The sliding displacement decreases for larger values of E_{cd} for dams shorter than 125 m (410 ft). A dam with this height has a fundamental period close to the dominant period range for the Taft ground motion.

The effect of the modulus of elasticity of the dam, E_{cd}, is lessened by the dam-foundation rock interaction, especially for shorter dams. For moderately flexible foundation rock ($E_{fr}/E_{cd} = 1$), the value of E_{cd} is not important for dams shorter than 100 m (328 ft), and sliding increases with E_{cd} for taller dams. For more flexible foundation rock, the sliding displacement is small and the modulus of elasticity does not affect significantly the response of the dam.

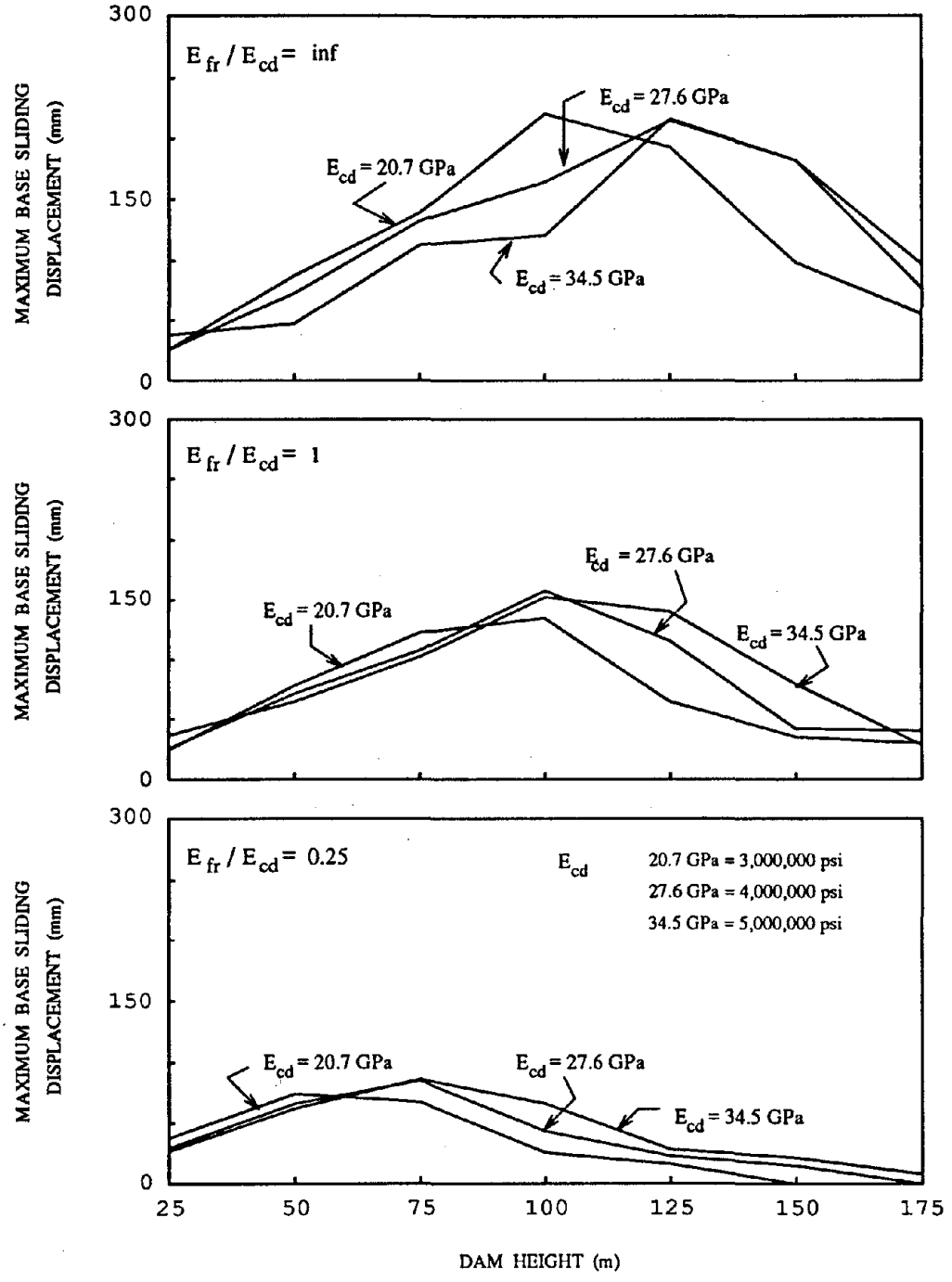

Figure 6.11. Influence of the modulus of elasticity of concrete on the maximum base sliding displacement of a typical dam with full reservoir of compressible water, $\mu = 1$, subjected to the horizontal S69E component of Taft ground motion with peak ground acceleration = 0.4g.

6.11 Summary of Parameter Study

The results from the parameter study of a typical concrete gravity dam are used to quantify the base sliding response. The most important trends are the following:

- The base sliding displacement of the dam is, for most cases, largest when the dam is subjected to the Taft S69E ground motion compared with the other records considered. For the different ground motions, the sliding decreases as the foundation rock becomes more flexible. Base sliding also varies with the height of the dam. The initiation of sliding and the occurrence of subsequent sliding events depend on peaks in the ground acceleration record.

- The choice of the earthquake record and the level of peak ground acceleration affects significantly the base sliding response of the dam. The sliding displacement increases by a factor of four when the peak ground acceleration increases from 0.3g to 0.5g for the cases considered.

- The maximum base sliding displacement is very dependent on dam-foundation rock interaction, especially for moderate to tall dams. For short dams the flexible foundation rock has little effect in the sliding displacement of the dam.

- The sliding response is also sensitive to the value of coefficient of friction. This is especially true for moderate or tall dams.

- Water compressibility and reservoir bottom absorption are important for the sliding response of dams on rigid foundation rock. Their effects are less important for dams on flexible foundation rock.

Chapter 7

CONCLUSIONS AND RECOMMENDATIONS

An accurate numerical procedure for the earthquake analysis of concrete gravity dams including sliding at the base has been developed using the hybrid frequency-time domain method. Each domain in the system, dam, impounded water, and foundation rock, is modeled as a separate substructure in the formulation of the equations of motion. The formulation accounts for the nonlinear sliding at the base of the dam and the frequency-dependent interaction effects between the dam and water and between the dam and foundation rock. The numerical procedure has been implemented in a new computer program, EAGD-SLIDE, which can be used to evaluate the earthquake response of a gravity dam, specifically addressing the questions about the base sliding displacement and the sliding stability.

The two-dimensional response of a monolith to horizontal and vertical free-field ground motion is modeled. The nonlinear sliding behavior in the complex interface zone is represented by the Mohr-Coulomb relationship for friction resistance of a material. According to the relationship, the interface zone is characterized by a coefficient of friction and a cohesion strength. Other sources of sliding resistance, such as three-dimensional response of the dam or resistance of adjacent monoliths, are neglected in the model. Consequently, the sliding displacement obtained from earthquake response analysis of a dam may be considered an upper bound on the base displacement experienced by the actual dam.

Since the sliding model only has one degree-of-freedom (the base sliding displacement) directly affected by the nonlinear Mohr-Coulomb relationship, the convergence of the iterative solution procedure is relatively fast. Additional efforts to improve computational efficiency of the solution procedure involve computation of the base forces in terms of the sliding displacement and interpolation of the frequency response functions. Segmentation of time is an essential requirement for rapid convergence of the solution. At present there are no general rules for selecting the duration of each segment, although short segments are required for convergence when large base sliding occurs.

The earthquake response of Pine Flat dam, including base sliding, and the sliding displacement of typical concrete gravity dams to various earthquake ground motions have been computed using the numerical procedure. Base sliding does not occur for dams with reservoirs less than one-half full. For dams with full reservoirs, the earthquake-induced base sliding occurs in the downstream direction only because the combination of hydrostatic forces and dynamic forces exceed the friction strength of the interface zone. Although rocking of the dam about the base is not included in the formulation, it is clear from the resultant of base forces that earthquake-induced rocking (or overturning) of gravity dams is not an important consideration. For most of the cases considered, the resultant base force acts within the dam base, so rocking does not occur.

Earthquake-induced base sliding accumulates only in the downstream direction. The maximum sliding displacement is influenced by the duration and characteristics of the free-field ground motion. A ground motion with a large number of

important peak accelerations, such as the Taft record, induces more sliding than a ground motion with a single large pulse, such as the Pacoima record. The amplitude of the peak ground acceleration also influences the amount of base sliding. A moderate ground motion (peak ground acceleration of 0.3g to 0.4g) produces considerably less sliding than that produced by a strong ground motion (peak ground acceleration of 0.5g to 0.6g).

The response of dams to horizontal ground motion was computed for most of the cases. For the limited cases in which the dam was subjected to horizontal and vertical ground motion, the vertical ground motion had almost no effect on the sliding displacement of the dam, although it slightly increased the maximum stresses in the dam compared with the case of horizontal ground motion only.

In all the cases considered, the cohesion strength of the interface was assumed to be zero because of the damage caused by base sliding. With zero cohesion, the sliding displacement is sensitive to the value of the coefficient of friction. In the range of coefficients considered, from 0.80 to 1.20, the sliding displacement increases as the coefficient of friction decreases. This trend is particularly pronounced for low values of coefficients, such as 0.80. Taller dams will be more affected by the coefficient of friction than shorter dams.

In contrast with earlier studies of earthquake-induced base sliding of dams, the current study has included the effects of dam-foundation rock interaction, namely the flexibility and energy dissipation in the foundation rock region. Since dam-foundation rock interaction reduces the earthquake response of a gravity dam in general, primarily because of the increased energy dissipation, it also reduces the amount of base

sliding. The assumption of rigid foundation rock can significantly overestimate the amount of base sliding compared with more realistic estimates obtained from including dam-foundation rock interaction. Dam-foundation rock interaction effects are more important for tall dams than for short dams.

The response of a typical dam demonstrates that water compressibility and reservoir bottom absorption are important factors in determining the base sliding of dams on rigid foundation rock. For dams on flexible foundation rock, their effects on sliding displacement are less important.

Base sliding may be interpreted as an isolation and energy dissipation mechanism for dams. The response results indicate, however, that the sliding displacements are not large enough to substantially reduce the deformations and stresses in the dam. This is particularly true for dams on flexible foundation rock.

Although the dams may slide at the base during a strong earthquake ground motion, the dam remains stable during and after the earthquake. For the 122 m tall Pine Flat dam on flexible foundation rock with a modulus equal to that of the dam concrete and a coefficient of friction of 1.0, the earthquake induced sliding displacement is 168 mm when excited by the Taft ground motion scaled to a peak ground acceleration of 0.6g. For this extreme case the sliding displacement is 0.14 percent of the dam height, a comparatively small value that does not indicate unstable response. Well designed and constructed dams should be able to tolerate this amount of deformation at the foundation rock interface. Although the base sliding may cause local damage to keys, drains, and grout curtains, it does not necessarily indicate loss of the reservoir. For smaller values of the coefficient of friction, the base sliding dis-

placement may be excessive, indicating that remedial treatment of the interface zone is necessary for seismic safety of the dam.

The friction model used for the dam-foundation rock interface zone is a simple approach that is useful for estimating the earthquake-induced sliding of a dam at the base. There are, however, uncertainties in establishing the appropriate value of the coefficient of friction for an earthquake evaluation, which may considerably affect the computed response. The simple friction model does not consider the nonlinear behavior of the materials in the interface zone. More elaborate models can be developed, but there is a lack of experimental data to justify overly sophisticated models. Given the uncertainties in the earthquake evaluation of a dam, it is believed that the approach adopted in this study provides important information about the base sliding displacements and stability of concrete gravity dams in earthquakes.

REFERENCES

Alarcon, E., Dominguez, J., and Del Cano, F. (1980). "Dynamic Stiffness of Foundations," *Proceedings of the 2nd International Seminar, Recent Advances in BEM*, edited by C.A. Brebia, pp. 264-288.

Bathe, K.J., and Hahn, W.F. (1979). "On Transient Analysis of Fluid-Structure Systems," *Computer and Structures*, Vol. 11, pp. 383-391.

Bougacha, S., and Tassoulas, J.L. (1991). "Effects of Sedimentary Material on the Response of Concrete Gravity Dams," *Earthquake Engineering and Structural Dynamics*, Vol. 20, pp. 849-858.

Cameron, T.M., and Griffin, J.H. (1989). "An Alternating Frequency/Time Domain Method for Calculating the Steady-State Response of Nonlinear Dynamic Systems," *Journal of Applied Mechanics*, Vol. 56, pp. 149-153.

Chopra, A.K. (1967). "Hydrodynamic Pressures on Dams During Earthquakes," *Journal of the Engineering Mechanics Division*, ASCE, Vol. 93, EM6, pp. 205-223.

Chopra, A.K. (1988). "Earthquake Response Analysis of Concrete Dams," *Advanced Dam Engineering*, Chapter 15, edited by R. Jansen, Van Nostrand Reinhold, New York.

Chopra, A.K., Chakrabarti, P., and Gupta, S. (1980). "Earthquake Response of Concrete Gravity Dams Including Hydrodynamic and Foundation Interaction

Effects," *Report No. UCB/EERC-80/01*, Earthquake Engineering Research Center, University of California, Berkeley, California.

Chopra, A.K., and Zhang, L. (1991). "Base Sliding Response of Concrete Gravity Dams to Earthquakes," *Report No. UCB/EERC-91/05*, Earthquake Engineering Research Center, University of California, Berkeley, California.

Danay, A., and Adeghe, L.N. (1993). "Seismic Induced Slip of Concrete Gravity Dams," *Journal of Structural Engineering*, ASCE, Vol. 119, No. 1, pp. 108-129.

Darbre, G.R and Wolf, J.P. (1988). "Criterion of Stability and Implementation Issues of Hybrid Frequency-Time Domain Procedure for Non-Linear Dynamic Analysis," *Earthquake Engineering and Structural Dynamics*, Vol. 16, pp. 569-581.

Dasgupta, G., and Chopra, A.K. (1979). "Dynamic Stiffness Matrices for Viscoelastic Half Planes," *Journal of the Engineering Mechanics Division*, ASCE, Vol. 105, No. EM5, pp. 729-745.

Fenves, G., and Chávez, J. (1990). "Hybrid Frequency-Time Domain Analysis of Nonlinear Fluid-Structure Systems," *Fourth U.S. National Conference on Earthquake Engineering*, Vol. 2, pp. 97-106, Palm Springs.

Fenves, G., and Chopra, A.K. (1984a). "Earthquake Analysis and Response of Concrete Gravity Dams," *Report No. UCB/EERC-84/10*, Earthquake Engineering Research Center, University of California, Berkeley, California.

Fenves, G. and Chopra, A.K. (1984b). "EAGD-84: A Computer Program for Earth-

quake Analysis of Concrete Gravity Dams," *Report No. UCB/EERC-84/11*, Earthquake Engineering Research Center, University of California, Berkeley, California.

Fenves, G., and Vargas-Loli, L. (1988). "Nonlinear Dynamic Analysis of Fluid-Structure Systems," *Journal of Engineering Mechanics*, ASCE, Vol. 114, No. 2, pp. 219-240.

Fok, K.-L., and Chopra, A.K. (1985). "Earthquake Analysis and Response of Concrete Arch Dams," *Report No. UCB/EERC-85/07*, Earthquake Engineering Research Center, University of California, Berkeley, California.

Humar, J.L., and Chandrashaker, R. (1992). "Treatment of Interaction Effects in the Seismic Response of Gravity Dams," *Proceedings of the Tenth World Conference on Earthquake Engineering*, Vol. 8, pp. 4657-4662, Barcelona.

Kawamoto, J.D. (1983). "Solution of Nonlinear Dynamic Structural Systems by a Hybrid Frequency-Time Domain Approach," *Ph.D. Dissertation*, Massachusetts Institute of Technology, Cambridge, Massachusetts.

Kausel E., and Roesset, J.M. (1992). "Frequency Domain Analysis of Undamped Systems," *Journal of Engineering Mechanics*, ASCE, Vol. 118, No. 4, pp. 721-734.

Leger, P., and Katsouli, M. (1989). "Seismic Stability of Concrete Gravity Dams," *Earthquake Engineering and Structural Dynamics*, Vol. 18, pp. 889-902.

Lima, A.L., and De Lima, E. (1986) "Nonlinear Dynamic Analysis in Frequency Domain Without Using Equivalent Linearization Techniques," *Segundo Sim-*

posio sobre Aplicaciones del Metodo de los Elementos Finitos en Ingenieria, pp 63-72, Barcelona.

Lotfi, V., Roesset, J.M., and Tassoulas, J.L. (1987). "A Technique for the Analysis of the Response of Dams to Earthquakes," *Earthquake Engineering and Structural Dynamics*, Vol. 15, pp. 463-489.

Newmark, N.M. (1959). "A Method of Computation for Structural Dynamics," *Journal of Engineering Mechanics Division*, ASCE, Vol. 85, pp. 67-94.

Newmark, N.M. (1965). "Effect of Earthquakes on Dams and Embankments," *Geotechnique*, Vol. 15, No. 2, pp. 139-160.

Park, K.C, and Felippa, C.A. (1980). "Partitioned Transient Analysis Procedures for Coupled-Field Problems: Accuracy Analysis," *Journal of Applied Mechanics*, Vol. 47, pp. 919-926.

Rea, D., Liaw, C.Y., and Chopra, A.K. (1975). "Mathematical Models for the Dynamic Analysis of Concrete Gravity Dams," *Earthquake Engineering and Structural Dynamics*, Vol. 3, No. 3, pp. 249-258.

Saini, S.S., Bettess, P., and Zienkiewicz, O.C. (1978). "Coupled Hydrodynamic Response of Concrete Dams Using Finite and Infinity Elements," *Earthquake Engineering and Structural Dynamics*, Vol. 6, No. 4, pp. 363-374.

Stricklin, J., and Haisler, W. (1977). "Formulation and Solution Procedures for Nonlinear Structural Analysis," *Computers and Structures*, Vol. 7, pp 125-136.

Swarztrauber, P. (1985). "A Package of Fortran Subprograms for the Fast Fourier

Transforms of Periodic and Other Symmetric Sequences," National Center for Atmospheric Research, Boulder, Colorado.

Tajirian, F.F. (1981). "Impedance Matrices and Interpolation Techniques for 3-D Interaction Analysis by the Flexible Volume Method," *Ph.D Dissertation*, Department of Civil Engineering, University of California, Berkeley, California.

Trujillo, D.M. (1982). "Stability Analysis of an Extrapolated Force Correction Method for Nonlinear Structural Dynamics," *Journal of Applied Mechanics*, Vol. 49, pp. 203-205

Toki, K., Sato, T., and Miura, F. (1980). "Separation and Sliding Between Soil and Structure During Strong Ground Motions," *Earthquake Engineering and Structural Dynamics*, Vol. 9, pp. 263-277.

Tsai, Ch.S., Lee, G.C., and Ketter, L. (1990). "A Semi-analytical Method for Time-Domain Analysis of Dam-Reservoir Interactions," *International Journal for Numerical Methods in Engineering*, Vol. 29, pp. 913-933.

Uang, C.-M., and Bertero, V.V. (1988). "Use of Energy as a Design Criterion in Earthquake-Resistant Design," *Report UCB/EERC-88/18*, Earthquake Engineering Research Center, University of California, Berkeley, California.

Wilson, E. (1982). "New Approaches for the Dynamic Analysis of Large Structural Systems," *Report No. UCB/EERC-82/04*, Earthquake Engineering Research Center, University of California, Berkeley, California.

Wolf, J.P., and Darbre G.R. (1984). "Dynamic Stiffness Matrix of Soil by the Bound-

ary Element Method," *Earthquake Engineering and Structural Dynamics*, Vol. 12, pp. 401-416.

Wolf, J.P, and Motosuka, M. (1989). "Recursive Evaluation of Interaction Forces of Unbounded Soil in the Time-Domain," *Earthquake Engineering and Structural Dynamics*, Vol. 18, pp. 345-363.

Zadnik, B., and Paskalov, T. (1992). "Dam Stability and Time-Dependent Coefficient of Friction," *Proceedings of the Tenth World Conference on Earthquake Engineering*, Vol. 8, pp. 4633-4638, Barcelona.

Zienkiewicz, O.C, Paul, D.K., and Hinton, E. (1982). "Cavitation in Fluid-Structure Response (With Particular Reference to Dams Under Earthquake Loading)," *Earthquake Engineering and Structural Dynamics*, Vol. 11, pp. 463-481.

Zong, T., and Penzien. J. (1986). "Hybrid Modeling of a Single Layer Half-Space System in Soil-Structure Interaction," *Earthquake Engineering and Structural Dynamics*, Vol. 14, pp. 517-530.

Appendix A

NOTATION

The following symbols are used in the definition of the notation:

- Subscript $a = z, f, s, g$ is associated with generalized accelerations, foundation accelerations, sliding acceleration, and ground acceleration, respectively.
- Subscript $l = x, y$ is associated with the $x-$ and $y-$components of ground acceleration.
- $\bar{W}(\omega)$ is the Fourier transform of $W(t)$ where W is a scalar or vector quantity.

$A_n(\omega)$	complex-valued function defined in equation C.33
$A_y(\omega)$	complex-valued function defined in equation C.35
$\mathbf{A}_g^l(\omega)$	frequency-dependent vector defined in equation 4.7
$\mathbf{A}_s(\omega)$, $\mathbf{A}_x(\omega)$	frequency-dependent vector defined in equation 4.7
b	constant used in interpolation of the frequency response functions
B	length of the base of the dam
$B_{0a}(\omega)$	hydrodynamic frequency response function defined in equation C.30
$B_{kl}(\omega)$	hydrodynamic frequency response function defined in equation C.32
$B_{\theta a}(\omega)$	hydrodynamic frequency response function defined in equation C.31

$B_{ay}(\omega)$	hydrodynamic frequency response function defined in equation C.34
$\mathbf{B}_{Ra}(\omega)$	matrix of hydrodynamic complex-valued response functions defined in equations C.23 to C.29
$\mathbf{B}_{\Psi a}(\omega)$	matrix of hydrodynamic complex-valued functions defined in equations C.22 to C.28
c	cohesion force at the base interface
C	wave propagation velocity for impounded water
C_s	shear wave velocity for the foundation rock
$\mathbf{C}$	damping matrix for the dam
$\mathbf{C}^*$	generalized damping matrix for the dam
$\mathbf{C}_l(\omega)$, $\mathbf{C}_s(\omega)$	frequency-dependent vector defined in equation 4.9
$e(t)$	function defining the sliding direction of the dam
E_{cd}	modulus of elasticity of the concrete dam
E_{fr}	modulus of elasticity of the foundation rock
E_d, E_s, E_f	components of energy balance equation for dam base, defined in equation E.7, associated with dam deformation, sliding displacement, and foundation displacements, respectively
$\mathbf{F}(t)$	base forces excluding sliding
$\mathbf{F}_{sd}$	inertia force for nodes above the base of the dam, due to sliding at the interface

$\mathbf{F}_{sb}$	resultant inertia force at the base of the dam due to sliding
$\mathbf{F}_f(t)$	$[F_f^x(t) \;\; F_f^y(t) \;\; M_f(t)]$, dam-foundation rock interaction forces
$h(y)$	continuous form of h, for the $x-$component of nodal displacements due to unit rotation about the center of the base
h	vector component of $\mathbf{R}$, $x-$ and $y-$components of nodal displacements due to unit rotation about the center of the base
H	depth of the impounded water
H_s	height of the upstream face of the dam
$I_{on}(\omega)$	integral defined in equation C.15
$I_{\theta n}(\omega)$	integral defined in equation C.16
$I_{jn}(\omega)$	integral defined in equation C.17
J	number of Ritz vectors
$J_o(\omega)$	integral defined in equation C.36
$J_\theta(\omega)$	integral defined in equation C.37
$J_j(\omega)$	integral defined in equation C.38, $j = 1, J$
$\mathbf{K}$	stiffness matrix for the dam
$\mathbf{K}^*$	generalized stiffness matrix for the dam
$\mathbf{K}_f(\omega)$	impedance matrix of the foundation rock in the x-y coordinate system
$\mathbf{K}_{f\beta}(\omega)$	impedance matrix of the foundation rock in the interface coordinate system

$\mathbf{L}$	matrix of participation factors
$\mathbf{L}^l(\omega)$	vector of forces associated with $l-$component of ground acceleration
$\mathbf{L}^s(\omega)$	vector of forces associated with sliding acceleration
m_V, m_N, m_M	masses associated with inertia forces due to sliding acceleration
$m_R(t)$	effective mass resisting sliding acceleration
$m_S(t)$	variation of effective mass due to to sliding
$M(t)$	moment at the center of the base interface due to dynamic loads, excluding sliding effect
$M_\beta(t)$	moment at the base interface due to dynamic loads
$\mathbf{M}$	mass matrix for the dam
$\mathbf{M}^*$	generalized mass matrix for the dam
$\mathbf{M}_t$	matrix of total translational mass and rotational inertia of the dam about the center of the base
$N(t)$	normal force at the base due to dynamic loads, excluding forces due to sliding acceleration
$N_\beta(t)$	normal force at the base interface due to dynamic loads
$N_\beta{}^t(t)$	total normal force at the base interface including static loads
$N_{\beta,st}$	resultant normal force at the base interface due to static loads
$p(x,y,t)$	hydrodynamic pressure

$\bar{p}(y,\omega)$	frequency response function for the hydrodynamic pressure at the upstream face of the dam
$\bar{p}_o^l(y,\omega)$	frequency response function for hydrodynamic pressure for a rigid dam due to the l-component of ground motion
$\bar{p}_o^\theta(y,\omega)$	frequency response function for hydrodynamic pressure on a rigid dam rotating about the center of the base
$\bar{p}_j(y,\omega)$	frequency response function for hydrodynamic pressure due to dam deformation
$\mathbf{P}(t)$	vector of equivalent nodal forces due to hydrodynamic pressures acting on the upstream face of the dam
$\bar{\mathbf{P}}(\omega)$	frequency response function for the vector of hydrodynamic forces
$\mathbf{P}_g(t)$	hydrodynamic force due to free-field ground acceleration
$\mathbf{P}_s(t)$	hydrodynamic force due to sliding acceleration
$\mathbf{P}_{zf}(t)$	hydrodynamic force due to dam and foundation acceleration
q	compliance of the reservoir bottom materials
$\mathbf{Q}_a(\omega)$	vector of response frequency functions for the hydrodynamic pressure at the upstream face of the dam
$\mathbf{R}$	$[1^x\ 1^y\ \mathbf{h}]$ influence matrix for rigid body motion of the dam about the center of the base
$\mathbf{S}(\omega)$	dynamic stiffness matrix

$\mathbf{S}_o(\omega)$	elastic stiffness matrix
T_p	duration of response
$\mathbf{T}$	transformation matrix for base forces
$\mathbf{T}_f$	transformation matrix for the foundation rock impedance matrix
$\mathbf{T}_\beta$	transformation matrix for sliding
$U_{s_\beta}(t)$	sliding displacement of the dam base relative to the foundation
$\ddot{U}_{s\beta}(t)$	sliding acceleration at the base interface
$\mathbf{U(t)}$	vector of dam displacements relative to rigid body motion of the base
$\mathbf{U}_f(t)$	vector of rigid body displacements of the foundation surface relative to the free-field motion
$\mathbf{U}_g(t)$	vector of free-field displacements due to ground motion
$\ddot{\mathbf{U}}_g(t)$	free-field ground acceleration vector
$V(t)$	shear force at the base interface due to dynamic loads, excluding forces due to sliding
$V_{friction}(t)$	friction resisting force at interface
$V_\beta(t)$	shear force at the base interface due to dynamic loads
$V_\beta{}^t(t)$	total shear force at the base interface including static loads
$V_{\beta,st}$	shear force at the base interface due to static forces
$\mathbf{X}(t)$	vector of generalized displacements and foundation displacements

$\bar{\mathbf{Y}}^I(\omega)$	frequency response function for unit harmonic ground motion
$\bar{\mathbf{Y}}^s(\omega)$	frequency response fucntion for unit harmonic sliding acceleration
$\mathbf{Z}$	vector of generalized displacements
α	wave reflection coefficient for the reservoir bottom
β	angle of inclination of the base of the dam
ϵ_{zj}, ϵ_{fl}, $\epsilon_{s\beta}$	tolerance for convergence of generalized displacements, rigid body displacements, and sliding acceleration, respectively
η	constant hysteretic damping factor for the dam
μ	coefficient of friction at the base interface
$\mu_n(\omega)$	eigenvalue for n^{th} natural vibration mode of the impounded water
ρ	water density
σ	spectral ratio
$\Psi_j^x(y)$	continuous form of Ψ for the $x-$displacements of the dam
ω	harmonic excitation frequency
ω_1	fundamental natural vibration frequency of the dam on rigid foundation rock with a empty reservoir
ω_{max}	maximum excitation frequency considered in the analysis
$\mathbf{\Psi}$	$[\mathbf{\Psi}_1\mathbf{\Psi}_2...\mathbf{\Psi}_J]$ matrix of Ritz vectors
$\Theta(t)$	rotation of the foundation surface at the center of the base of the dam

Δt	time step for response computation
$\Delta\omega$	increment of frequency evaluated during interpolation procedure
$\Delta\omega_{min}$	minimum increment of frequency used in interpolation
$\Delta\omega_{max}$	maximum increment of frequency used in interpolation
Ω_j	frequencies for interpolation of response functions
$\Upsilon_n(y,\omega)$	eigenfunction for n^{th} vibration mode of the impounded water
$\mathbf{1}^l$	vector component of $\mathbf{R}$ for displacements in direction l.

Appendix B

EQUATIONS OF MOTION FOR THE DAM

The equations of static equilibrium and the equations of motion, equations 3.1 and 3.2, for the dam are derived in this appendix. The nodal points in the finite element model of the dam are divided into two groups: nodes above the base, denoted by the subscript d, and nodes on the rigid base, denoted by the subscript b. The water domain and foundation rock domain are represented by interaction forces acting on the dam.

B.1 Kinematics

Assuming no sliding occurs under static loads, the static displacements of the dam are:

$$\left\{ \begin{array}{c} \mathbf{U}^t_{d,stat} \\ \mathbf{U}^t_{b,stat} \end{array} \right\} = \left\{ \begin{array}{c} \mathbf{U}_{d,stat} \\ \mathbf{0} \end{array} \right\} + \left\{ \begin{array}{c} \mathbf{R}_d \\ \mathbf{R}_b \end{array} \right\} \mathbf{U}_{f,stat} \tag{B.1}$$

where the vectors $\mathbf{U}^t_{d,stat}$ and $\mathbf{U}^t_{b,stat}$ are the total displacement of the nodal points above the base and on the base, respectively; $\mathbf{U}_{d,stat}$ is the vector of displacements of the dam with respect to the base; $\mathbf{U}_{f,stat}$ is the vector of foundation displacements; $\mathbf{R}_d$ and $\mathbf{R}_b$ are the influence matrices for the nodal points above the base and on the base, respectively.

Considering the response to earthquake ground motion, the total dam displacements are:

$$\begin{Bmatrix} \mathbf{U}_d^t(t) \\ \mathbf{U}_b^t(t) \end{Bmatrix} = \begin{Bmatrix} \mathbf{U}_d(t) \\ \mathbf{0} \end{Bmatrix} + \begin{Bmatrix} \mathbf{R}_d \\ \mathbf{R}_b \end{Bmatrix} \mathbf{U}_f(t) + \begin{Bmatrix} \mathbf{R}_d \\ \mathbf{R}_b \end{Bmatrix} \mathbf{U}_g(t) + \begin{Bmatrix} \mathbf{R}_d \\ \mathbf{R}_b \end{Bmatrix} \mathbf{T}_\beta U_{s\beta}(t) + \begin{Bmatrix} \mathbf{U}_{d,stat}^t \\ \mathbf{U}_{b,stat}^t \end{Bmatrix} \tag{B.2}$$

where $\mathbf{U}_d^t(t)$ and $\mathbf{U}_b^t(t)$ are the vectors of total displacements of the dam; $\mathbf{U}_d(t)$ is the vector of dam displacements with respect to the base due to dynamic loads; $\mathbf{U}_f(t)$ is the vector of displacements of the foundation surface with respect to the free-field ground motion; $\mathbf{U}_g(t)$ is the vector of free-field ground displacements; $U_{s\beta}(t)$ is the sliding displacement of the base at the interface plane; and $\mathbf{T}_\beta$ is the vector transforming the sliding displacement at the interface plane to the global x-y coordinate system.

The condition of rigid body displacements of the dam means that there are no external forces under rigid body motion. Thus the following relationships between the influence matrices, $\mathbf{R}_d$ and $\mathbf{R}_b$, and the stiffness matrix of the dam, expressed in partitioned form, are satisfied:

$$\mathbf{K}_{dd}\mathbf{R}_d + \mathbf{K}_{db}\mathbf{R}_b = \mathbf{0} \tag{B.3}$$

$$\mathbf{K}_{bd}\mathbf{R}_d + \mathbf{K}_{bb}\mathbf{R}_b = \mathbf{0} \tag{B.4}$$

B.2 Equations of Static Equilibrium

Considering only the static loads, the equilibrium equations for the dam are:

$$\begin{bmatrix} \mathbf{K}_{dd} & \mathbf{K}_{db} \\ \mathbf{K}_{bd} & \mathbf{K}_{bb} \end{bmatrix} \begin{Bmatrix} \mathbf{U}^t_{d,stat} \\ \mathbf{U}^t_{b,stat} \end{Bmatrix} = \begin{Bmatrix} \mathbf{P}_{d,stat} \\ \mathbf{P}_{b,stat} \end{Bmatrix} + \begin{Bmatrix} \mathbf{0} \\ \mathbf{P}_{b,u} \end{Bmatrix} + \begin{Bmatrix} \mathbf{0} \\ \mathbf{P}_{bf,stat} \end{Bmatrix} \tag{B.5}$$

where $\mathbf{P}_{d,stat}$ and $\mathbf{P}_{b,stat}$ are the external static loads applied to the dam including the hydrostatic forces; $\mathbf{P}_{b,u}$ is the vector of uplift forces acting at the base; and $\mathbf{P}_{bf,stat}$ is the vector of forces at the nodes of the base exerted by the foundation.

Substituting the first partition of equation B.1 into the first partition of equation B.5, and applying the rigid body conditions from equation B.3 gives:

$$\mathbf{K}_{dd}\, \mathbf{U}_{d,stat} \;=\; \mathbf{P}_{d,stat} \tag{B.6}$$

The solution of this equation gives the static displacements of the dam with respect to the rigid base. Static stresses of the dam depend on these displacements only and are independent of the base displacements.

Substituting the second partition of equation B.1 into the second partition of equation B.5, applying the rigid body conditions from equation B.4, and using equation B.6 gives:

$$\mathbf{K}_{bd}[\mathbf{K}_{dd}{}^{-1}\mathbf{P}_{d,stat}] = \mathbf{P}_{b,stat} + \mathbf{P}_{bf,stat} + \mathbf{P}_{b,u}$$

Premultiplying this equation by $\mathbf{R}_b^T$, applying the rigid body conditions from equations B.3 and B.4, and using the condition of symmetry for the stiffness matrix gives:

$$-\mathbf{R}_b^T\mathbf{P}_{bf,stat} = [\mathbf{R}_d^T\mathbf{P}_{d,stat} + \mathbf{R}_b^T\mathbf{P}_{b,stat}] + \mathbf{R}_b^T\mathbf{P}_{b,u} \tag{B.7}$$

where $-\mathbf{R}_b^T\mathbf{P}_{bf,stat}$, the resultant of static forces at the base of the dam, is equal to the sum of the resultants of the external loads and the uplift forces.

B.3 Equations of Motion

Considering static and dynamic response, the equations of motion for the dam are:

$$\begin{bmatrix} \mathbf{M}_{dd} & \mathbf{M}_{db} \\ \mathbf{M}_{bd} & \mathbf{M}_{bb} \end{bmatrix} \begin{Bmatrix} \ddot{\mathbf{U}}_d^t(t) \\ \ddot{\mathbf{U}}_b^t(t) \end{Bmatrix} + \begin{bmatrix} \mathbf{C}_{dd} & \mathbf{C}_{db} \\ \mathbf{C}_{bd} & \mathbf{C}_{bb} \end{bmatrix} \begin{Bmatrix} \dot{\mathbf{U}}_d^t(t) \\ \dot{\mathbf{U}}_b^t(t) \end{Bmatrix} + \begin{bmatrix} \mathbf{K}_{dd} & \mathbf{K}_{db} \\ \mathbf{K}_{bd} & \mathbf{K}_{bb} \end{bmatrix} \begin{Bmatrix} \mathbf{U}_d^t(t) \\ \mathbf{U}_b^t(t) \end{Bmatrix}$$

$$= \begin{Bmatrix} \mathbf{P}_d(t) \\ \mathbf{P}_b(t) \end{Bmatrix} + \begin{Bmatrix} \mathbf{0} \\ \mathbf{P}_{bf}(t) \end{Bmatrix} + \begin{Bmatrix} \mathbf{P}_{d,stat} \\ \mathbf{P}_{b,stat} + \mathbf{P}_{bf,stat} + \mathbf{P}_{b,u} \end{Bmatrix} \tag{B.8}$$

(B.9)

where $\mathbf{M}_{dd}$, $\mathbf{M}_{db}$, $\mathbf{M}_{bd}$, $\mathbf{M}_{bb}$, and $\mathbf{C}_{dd}$, $\mathbf{C}_{db}$, $\mathbf{C}_{bd}$, $\mathbf{C}_{bb}$ are the partitions of the mass and damping matrices of the dam, respectively; $\mathbf{P}_d(t)$ and $\mathbf{P}_b(t)$ are the hydrodynamic forces acting on the upstream face of the dam, above the base and on the base, respectively; and $\mathbf{P}_{bf}(t)$ is the vector of interaction forces at the foundation.

Assuming that the damping matrix is proportional to the stiffness matrix, the rigid body motion requirements from equations B.3 and B.4 are also valid for the damping matrix:

$$\mathbf{C}_{dd}\mathbf{R}_d + \mathbf{C}_{db}\mathbf{R}_b = \mathbf{0} \tag{B.10}$$

$$\mathbf{C}_{bd}\mathbf{R}_d + \mathbf{C}_{bb}\mathbf{R}_b = \mathbf{0} \tag{B.11}$$

B.3.1 Equations of Motion for Dam

Substituting the first partition of equation B.2 into the first partition of equation B.8, and applying equation B.3 gives:

$$\mathbf{M}_{dd}\ddot{\mathbf{U}}_d^t(t) + \mathbf{M}_{db}\ddot{\mathbf{U}}_b^t(t) + \mathbf{C}_{dd}\dot{\mathbf{U}}_d(t) + \mathbf{K}_{dd}\mathbf{U}_d(t) = \mathbf{P}_d(t)$$

$\mathbf{M}_{db}\ddot{\mathbf{U}}_b^t(t)$ contains the inertia forces at the dam nodes due to rigid body acceleration of the masses at the base. These forces are small compared with the other forces in the equation of motion, so they can be neglected. Thus, the equations of motion for the dam are:

$$\mathbf{M}_{dd}\ddot{\mathbf{U}}_d^t(t) + \mathbf{C}_{dd}\dot{\mathbf{U}}_d(t) + \mathbf{K}_{dd}\mathbf{U}_d(t) = \mathbf{P}_d(t) \tag{B.12}$$

Substituting the first partition of equation B.2 into equation B.12 gives:

$$\begin{aligned}\mathbf{M}_{dd}\ddot{\mathbf{U}}_d(t) + \mathbf{C}_{dd}\dot{\mathbf{U}}_d(t) + \mathbf{K}_{dd}\mathbf{U}_d(t) + \mathbf{M}_{dd}\mathbf{R}_d\ddot{\mathbf{U}}_f(t) + \mathbf{M}_{dd}\mathbf{R}_d\mathbf{T}_\beta\ddot{U}_{s\beta}(t) \\ = -\mathbf{M}_{dd}\mathbf{R}_d\ddot{\mathbf{U}}_g(t) + \mathbf{P}_d(t)\end{aligned} \tag{B.13}$$

Defining the inertia force due to sliding as,

$$\mathbf{F}_{sd}(\ddot{U}_{s\beta}) = \mathbf{M}_{dd}\mathbf{R}_d\mathbf{T}_\beta\ddot{U}_{s\beta}(t)$$

and dropping the subscripts d for convenience, equation B.13 becomes equation 3.1:

$$\mathbf{M}\ddot{\mathbf{U}} + \mathbf{C}\dot{\mathbf{U}} + \mathbf{K}\mathbf{U} + \mathbf{M}\mathbf{R}\ddot{\mathbf{U}}_f + \mathbf{F}_{sd}(\ddot{U}_{s\beta}) = -\mathbf{M}\mathbf{R}\ddot{\mathbf{U}}_g(t) + \mathbf{P}(t) \tag{B.14}$$

B.3.2 Equilibrium of Forces at Base

Substituting equation B.2 into equation B.8 and applying the rigid body conditions from equations B.3, B.4, B.10 and B.11 gives:

$$\begin{bmatrix} \mathbf{M}_{dd} & \mathbf{M}_{db} \\ \mathbf{M}_{bd} & \mathbf{M}_{bb} \end{bmatrix} \begin{Bmatrix} \ddot{\mathbf{U}}_d^t(t) \\ \ddot{\mathbf{U}}_b^t(t) \end{Bmatrix} + \begin{bmatrix} \mathbf{C}_{dd} & \mathbf{C}_{db} \\ \mathbf{C}_{bd} & \mathbf{C}_{bb} \end{bmatrix} \begin{Bmatrix} \dot{\mathbf{U}}_d(t) \\ \mathbf{0} \end{Bmatrix} + \begin{bmatrix} \mathbf{K}_{dd} & \mathbf{K}_{bd} \\ \mathbf{K}_{db} & \mathbf{K}_{bb} \end{bmatrix} \begin{Bmatrix} \mathbf{U}_d(t) \\ \mathbf{0} \end{Bmatrix} = \begin{Bmatrix} \mathbf{P}_d(t) \\ \mathbf{P}_b(t) \end{Bmatrix} + \begin{Bmatrix} \mathbf{0} \\ \mathbf{P}_{bf}(t) \end{Bmatrix}$$

Premultiplying this equation by $\{\mathbf{R}_d^T \ \mathbf{R}_b^T\}$, applying equations B.2 again, and the rigid body conditions from equations B.10 and B.11 gives:

$$\begin{Bmatrix} \mathbf{R}_d^T & \mathbf{R}_b^T \end{Bmatrix} \begin{bmatrix} \mathbf{M}_{dd} & \mathbf{M}_{db} \\ \mathbf{M}_{bd} & \mathbf{M}_{bb} \end{bmatrix} \begin{Bmatrix} \ddot{\mathbf{U}}_d(t) \\ \mathbf{0} \end{Bmatrix} + \mathbf{M}_t \left\{ \ddot{\mathbf{U}}_f(t) + \ddot{\mathbf{U}}_g(t) + \mathbf{T}_\beta \ddot{U}_{s\beta}(t) \right\} = \mathbf{R}_b^T \mathbf{P}_{bf}(t) + \mathbf{R}_t^T \mathbf{P}_t(t) \qquad \text{(B.15)}$$

The vector $\mathbf{F}_f(t) = -\mathbf{R}_b^T \mathbf{P}_{bf}(t)$ contains the interaction forces between the dam and the foundation. The total mass of the dam and the total force at the base are defined as:

$$\mathbf{M}_t = \begin{Bmatrix} \mathbf{R}_d^T & \mathbf{R}_b^T \end{Bmatrix} \begin{bmatrix} \mathbf{M}_{dd} & \mathbf{M}_{db} \\ \mathbf{M}_{bd} & \mathbf{M}_{bb} \end{bmatrix} \begin{Bmatrix} \mathbf{R}_d \\ \mathbf{R}_b \end{Bmatrix} \qquad \text{(B.16)}$$

$$\mathbf{R}_t^T \mathbf{P}_t(t) = \mathbf{R}_d^T \mathbf{P}_d(t) + \mathbf{R}_b^T \mathbf{P}_b(t) \qquad \text{(B.17)}$$

equation B.15 can be further rewritten as follows:

$$\mathbf{R}_d^T \mathbf{M}_{dd} \ddot{\mathbf{U}}(t) + \mathbf{R}_b^T \mathbf{M}_{bd} \ddot{\mathbf{U}}_d(t) + \mathbf{M}_t \ddot{\mathbf{U}}_f(t) + \mathbf{M}_t \mathbf{T}_\beta \ddot{U}_{s\beta}(t) + \mathbf{F}_f(t) = -\mathbf{M}_t \ddot{\mathbf{U}}_g(t) + \mathbf{R}_t^T \mathbf{P}_t(t) \qquad \text{(B.18)}$$

The coupling term $\mathbf{R}_b^T \mathbf{M}_{bd} \ddot{\mathbf{U}}_d(t)$ is small compared with the other forces, so it is neglected. Similarly the contribution of $\mathbf{R}_b^T \mathbf{P}_b(t)$ to the hydrodynamic forces is small and it is neglected. After rearranging terms, equation B.18 becomes:

$$\mathbf{R}_d^T \mathbf{M}_{dd} \ddot{\mathbf{U}}(t) + \mathbf{M}_t \ddot{\mathbf{U}}_f(t) + \mathbf{M}_t \mathbf{T}_\beta \ddot{U}_{s\beta}(t) + \mathbf{F}_f(t) = -\mathbf{M}_t \ddot{\mathbf{U}}_g(t) + \mathbf{R}_d \mathbf{P}_d(t) \quad \text{(B.19)}$$

Defining the inertia force at the base due to sliding as,

$$\mathbf{F}_{sb}(\ddot{U}_{s\beta}) = \mathbf{M}_t \mathbf{T}_\beta \ddot{U}_{s\beta}(t)$$

and after dropping the subscripts d for convenience, equation B.19 becomes equation 3.2:

$$\mathbf{R}^T \mathbf{M} \ddot{\mathbf{U}} + \mathbf{M}_t \ddot{\mathbf{U}}_f + \mathbf{F}_f(t) + \mathbf{F}_{sb}(\ddot{U}_{s\beta}) = -\mathbf{M}_t \ddot{\mathbf{U}}_g(t) + \mathbf{R}^T \mathbf{P}(t) \quad \text{(B.20)}$$

Equations B.14 and B.20 are the equations of motion for the dam system subjected to the free-field ground motion.

Appendix C

HYDRODYNAMIC FORCES

The hydrodynamic forces on the dam due to dam-water interaction are derived in this appendix. The impounded water is idealized as a two-dimensional domain of depth H extending infinitely in the upstream direction. The boundary with the dam is assumed to be vertical, and the boundary with the foundation rock is assumed to be horizontal. The water is treated as a compressible, irrotational, inviscid fluid with small displacement motion [Fenves and Chopra, 1984a].

C.1 Wave Equation

For the assumptions described above, the hydrodynamic pressure is governed by the wave equation:

$$\nabla^2 p = \frac{1}{C^2}\frac{\partial^2 p}{\partial t^2} \tag{C.1}$$

where $p(x, y, t)$ is the hydrodynamic pressure (in excess of hydrostatic pressure), and C is the wave propagation velocity for water. The hydrodynamic pressure is generated by horizontal acceleration of the upstream face of the dam and vertical acceleration of the reservoir bottom. When this pressure is expressed in the frequency domain, as complex-valued frequency response function for hydrodynamic pressure,

$$p(x, y, t) = \bar{p}(x, y, \omega)e^{i\omega t}$$

the wave equation becomes the Helmholtz equation:

$$\frac{\partial^2 \bar{p}}{\partial x^2} + \frac{\partial^2 \bar{p}}{\partial y^2} + \frac{\omega^2}{C^2}\bar{p} = 0 \tag{C.2}$$

C.2 Boundary Conditions

Considering that the origin of the x-y coordinate system is defined at the bottom of the upstream face of the dam, and that the x-axis is positive in the downstream direction, the following boundary conditions must be satisfied:

1. At the free surface, the effect of surface waves is neglected and hence the pressure is zero.

$$\bar{p}(x, H, \omega) = 0 \tag{C.3}$$

2. At the upstream face of the dam, the horizontal acceleration of the water is the same as the total horizontal acceleration of the dam. Considering each acceleration component:

   - free-field ground acceleration:

$$\frac{\partial \bar{p}(0, y, \omega)}{\partial x} = -\rho\ \delta_{xl} \bar{\ddot{U}}^{l}_{g}(\omega) \qquad\qquad l = x, y \tag{C.4a}$$

   - foundation acceleration:

$$\frac{\partial \bar{p}(0, y, \omega)}{\partial x} = -\rho\ [\bar{\ddot{U}}^{x}_{f}(\omega) + h(y)\bar{\ddot{\Theta}}(\omega)] \tag{C.4b}$$

   - sliding acceleration:

$$\frac{\partial \bar{p}(0, y, \omega)}{\partial x} = -\rho \cos\beta\ \bar{\ddot{U}}_{s\beta}(\omega) \tag{C.4c}$$

- dam deformation:

$$\frac{\partial \bar{p}(0,y,\omega)}{\partial x} = -\rho \sum_{j=1}^{J} \Psi_j^x(y) \bar{\bar{Z}}_j(\omega) \qquad (C.4d)$$

where ρ is the water density; δ_{xl} is the Kronecker delta function; β is the angle of inclination of the interface; $\bar{\bar{U}}_g^l(\omega)$ is the Fourier transform of the l-component of ground motion; $\bar{\bar{U}}_f^x(\omega)$ and $\bar{\bar{\Theta}}(\omega)$ are the Fourier transforms of the translational acceleration in the x-direction and rotational acceleration of the center of the base of the dam with respect to the free-field acceleration; $\Psi_j^x(y)$ is the continuous form of $\boldsymbol{\Psi}$ associated with the x-components of the Ritz vectors for the dam; similarly, $h(y)$ is the continuous form of $\mathbf{h}$ for dam displacements in the x-direction produced by rotation of the base; and J is the number of Ritz vectors considered in the analysis.

3. At the reservoir bottom, the vertical motion of the fluid, including the interaction between the water and reservoir bottom, depends on the vertical component of ground acceleration only.

$$[\frac{\partial}{\partial y} - i\omega q]\bar{p}(x,0,\omega) = -\rho\, \bar{\bar{U}}_g^y(\omega) \qquad (C.5)$$

where q is the compliance of the reservoir bottom materials. The compliance is defined in terms of the wave reflection coefficient, α:

$$\alpha = \frac{1 - qC}{1 + qC}$$

The coefficient α is defined as the ratio of the amplitude of the reflected hydrodynamic pressure wave to the amplitude of a vertically propagating pressure

wave incident on the reservoir bottom. $\alpha = 1$ represents a rigid reservoir bottom, and $\alpha = 0$ is a very absorptive reservoir bottom material.

4. The hydrodynamic pressure must be finite in the upstream direction.

C.3 Solution for Hydrodynamic Pressure

The solution of equation C.2 with the boundary conditions in equations C.3 to C.5 and the radiation condition gives the frequency response function for hydrodynamic pressure at the upstream face of the dam:

$$\bar{\mathbf{p}}(y,\omega) = \bar{\mathbf{p}}_g(y,\omega)\ddot{\bar{\mathbf{U}}}_g(\omega) + \bar{\mathbf{p}}_f(y,\omega)\ddot{\bar{\mathbf{U}}}_f(\omega) + \bar{\mathbf{p}}_s(y,\omega)\mathbf{T}_\beta\ddot{\bar{U}}_{s\beta}(\omega) + \bar{\mathbf{p}}_z(y,\omega)\ddot{\bar{\mathbf{Z}}}(\omega) \tag{C.6}$$

The hydrodynamic pressure vectors associated with ground acceleration, foundation acceleration, sliding acceleration, and dam acceleration, respectively, are defined as:

$$\bar{\mathbf{p}}_g(y,\omega) = [\ \bar{p}_o^x(y,\omega) \quad \bar{p}_o^y(y,\omega) \quad 0\ ] \tag{C.7}$$

$$\bar{\mathbf{p}}_f(y,\omega) = [\ \bar{p}_o^x(y,\omega) \quad 0 \quad \bar{p}_o^\theta(y,\omega)\ ] \tag{C.8}$$

$$\bar{\mathbf{p}}_s(y,\omega) = [\ \bar{p}_o^x(y,\omega) \quad 0 \quad 0\ ] \tag{C.9}$$

$$\bar{\mathbf{p}}_z(y,\omega) = [\ \bar{p}_1(y,\omega) \quad \bar{p}_2(y,\omega) \quad \ldots\ldots \quad \bar{p}_J(y,\omega)\ ] \tag{C.10}$$

Each frequency response function is defined as follows [Fenves and Chopra, 1984]:

$$\bar{p}_o^x(y,\omega) = -2\rho H \sum_{n=1}^{\infty} \frac{\mu_n^2(\omega)}{H[\mu_n^2(\omega) - (\omega q)^2] + i(\omega q)} \frac{I_{on}(\omega)}{\sqrt{\mu_n^2(\omega) - \omega^2/C^2}} \Upsilon_n(y,\omega) \tag{C.11}$$

$$\bar{p}_o^y(y,\omega) = \frac{\rho C}{\omega}\frac{1}{\cos\frac{\omega H}{C} + iqC\sin\frac{\omega H}{C}}\sin\frac{\omega(H-y)}{C} \tag{C.12}$$

$$\bar{p}_o^\theta(y,\omega) = -2\rho H\sum_{n=1}^{\infty}\frac{\mu_n^2(\omega)}{H[\mu_n^2(\omega)-(\omega q)^2]+i(\omega q)}\frac{I_{\theta n}(\omega)}{\sqrt{\mu_n^2(\omega)-\omega^2/C^2}}\Upsilon_n(y,\omega) \tag{C.13}$$

$$\bar{p}_j(y,\omega) = -2\rho H\sum_{n=1}^{\infty}\frac{\mu_n^2(\omega)}{H[\mu_n^2(\omega)-(\omega q)^2]+i(\omega q)}\frac{I_{jn}(\omega)}{\sqrt{\mu_n^2(\omega)-\omega^2/C^2}}\Upsilon_n(y,\omega) \tag{C.14}$$

$\bar{p}_o^x(y,\omega)$, $\bar{p}_o^y(y,\omega)$, and $\bar{p}_o^\theta(y,\omega)$ are the hydrodynamic pressures due to rigid body motion of the dam; and $\bar{p}_j(y,\omega)$ is the hydrodynamic pressure due to deformation of the upstream face of the dam corresponding to the j^{th} Ritz vector. The coefficients I_{on}, $I_{\theta n}$, and I_{jn} are:

$$I_{on}(\omega) = \frac{1}{H}\int_0^H \Upsilon_n(y,\omega)dy \tag{C.15}$$

$$I_{\theta n}(\omega) = \frac{1}{H}\int_0^H h(y)\Upsilon_n(y,\omega)dy \tag{C.16}$$

$$I_{jn}(\omega) = \frac{1}{H}\int_0^H \Psi_j^x(y)\Upsilon_n(y,\omega)dy \tag{C.17}$$

The eigenvalues, $\mu_n(\omega)$, and the eigenfunctions, $\Upsilon_n(y,\omega)$, of the impounded water are given by:

$$e^{2i\mu_n(\omega)H} = -\frac{\mu_n(\omega)-\omega q}{\mu_n(\omega)+\omega q} \tag{C.18}$$

$$\Upsilon_n(y,\omega) = \frac{1}{2\mu_n(\omega)}\left(\,[\mu_n(\omega)+\omega q]e^{i\mu_n(\omega)y} + [\mu_n(\omega)-\omega q]e^{-i\mu_n(\omega)y}\,\right) \tag{C.19}$$

C.4 Hydrodynamic Force Vectors

The frequency response function for the vector of hydrodynamic forces, $\bar{\mathbf{P}}(\omega)$, at the upstream face of the dam is obtained by integrating the hydrodynamic pressures from equation C.6:

$$\bar{\mathbf{P}}(\omega) = \bar{\mathbf{Q}}_g(\omega)\ddot{\bar{\mathbf{U}}}_g(\omega) + \bar{\mathbf{Q}}_f(\omega)\ddot{\bar{\mathbf{U}}}_f(\omega) + \bar{\mathbf{Q}}_s(\omega)\mathbf{T}_\beta\ddot{\bar{U}}_{s\beta}(\omega) + \bar{\mathbf{Q}}_z(\omega)\ddot{\bar{\mathbf{Z}}}(\omega) \qquad \text{(C.20)}$$

where $\bar{\mathbf{Q}}_g(\omega)$, $\bar{\mathbf{Q}}_f(\omega)$, $\bar{\mathbf{Q}}_s(\omega)$, and $\bar{\mathbf{Q}}_z(\omega)$ are the equivalent nodal forces in the x-direction for the pressures at the upstream face of the dam. Considering the finite element discretization of the dam the force vector is assembled from the virtual work integrals for the wet elements at the upstream face:

$$\bar{\mathbf{Q}}_l(\omega) = \sum_e \int \mathbf{N}^T \bar{\mathbf{p}}_a(y,\omega)dy \qquad a = g, f, s, z \qquad \text{(C.21)}$$

where $\mathbf{N}$ contains the shape functions for the elements.

C.5 Hydrodynamic Response Functions

The hydrodynamic response functions needed in equations of motion are the force vectors $\bar{\mathbf{Q}}(\omega)$ premultiplied by the transformations $\mathbf{\Psi}^T$ and $\mathbf{R}^T$. These complex-value functions have the following properties:

1. The matrices $\mathbf{\Psi}^T\bar{\mathbf{Q}}_z(\omega)$ and $\mathbf{R}^T\bar{\mathbf{Q}}_f(\omega)$ are symmetric and defined as follows:

$$\mathbf{B}_{\Psi z}(\omega) = \mathbf{\Psi}^T\mathbf{Q}_z(\omega) = \begin{bmatrix} B_{11}(\omega) & B_{12}(\omega) & ..... & B_{1J}(\omega) \\ B_{21}(\omega) & B_{22}(\omega) & ..... & B_{2J}(\omega) \\ \vdots & \vdots & \vdots & \vdots \\ B_{J1}(\omega) & B_{J2}(\omega) & ..... & B_{JJ}(\omega) \end{bmatrix} \qquad \text{(C.22)}$$

$$\mathbf{B}_{Rf}(\omega) = \mathbf{R}^T \bar{\mathbf{Q}}_f(\omega) = \begin{bmatrix} B_{00}(\omega) & 0 & B_{0\theta}(\omega) \\ 0 & 0 & 0 \\ B_{\theta 0}(\omega) & 0 & B_{\theta\theta}(\omega) \end{bmatrix} \tag{C.23}$$

2. The matrix $\mathbf{B}_{\Psi f}(\omega) = \mathbf{\Psi}^T \bar{\mathbf{Q}}_f(\omega)$ is the transpose of matrix $\mathbf{B}_{Rz}(\omega) = \mathbf{R}^T \bar{\mathbf{Q}}_z(\omega)$. These matrices are defined as follows:

$$\mathbf{B}_{\Psi f}(\omega) = \mathbf{\Psi}^T \bar{\mathbf{Q}}_f(\omega) = \begin{bmatrix} B_{01}(\omega) & 0 & B_{\theta 1}(\omega) \\ B_{02}(\omega) & 0 & B_{\theta 2}(\omega) \\ \vdots & \vdots & \vdots \\ B_{0J}(\omega) & 0 & B_{\theta J}(\omega) \end{bmatrix} \tag{C.24}$$

$$\mathbf{B}_{Rz}(\omega) = \mathbf{R}^T \bar{\mathbf{Q}}_z(\omega) = \begin{bmatrix} B_{01}(\omega) & B_{02}(\omega) & ..... & B_{0J}(\omega) \\ 0 & 0 & ..... & 0 \\ B_{\theta 1}(\omega) & B_{\theta 2}(\omega) & ..... & B_{\theta J}(\omega) \end{bmatrix} \tag{C.25}$$

3. The other hydrodynamic terms are:

$$\mathbf{B}_{\Psi g}(\omega) = \mathbf{\Psi}^T \bar{\mathbf{Q}}_g(\omega) = \begin{bmatrix} B_{01}(\omega) & B_{y1}(\omega) & 0 \\ B_{02}(\omega) & B_{y2}(\omega) & 0 \\ \vdots & \vdots & \vdots \\ B_{0J}(\omega) & B_{yJ}(\omega) & 0 \end{bmatrix} \tag{C.26}$$

$$\mathbf{B}_{Rg}(\omega) = \mathbf{R}^T \bar{\mathbf{Q}}_g(\omega) = \begin{bmatrix} B_{00}(\omega) & B_{y0}(\omega) & 0 \\ 0 & 0 & 0 \\ B_{0\theta}(\omega) & B_{y\theta}(\omega) & 0 \end{bmatrix} \tag{C.27}$$

$$\mathbf{B}_{\Psi s}(\omega) = \mathbf{\Psi}^T \bar{\mathbf{Q}}_s(\omega) = \begin{bmatrix} B_{01}(\omega) & 0 & 0 \\ B_{02}(\omega) & 0 & 0 \\ \vdots & \vdots & \vdots \\ B_{0J}(\omega) & 0 & 0 \end{bmatrix} \tag{C.28}$$

$$\mathbf{B}_{Rs}(\omega) = \mathbf{R}^T \tilde{\mathbf{Q}}_s(\omega) = \begin{bmatrix} B_{00}(\omega) & 0 & 0 \\ 0 & 0 & 0 \\ B_{0\theta}(\omega) & 0 & 0 \end{bmatrix} \tag{C.29}$$

The individual hydrodynamic terms can be computed from equations C.11 to C.14 after application of the transformation matrices for horizontal ground motion. The terms are:

$$B_{0a}(\omega) = -2\rho H^2 \sum_{n=1}^{\infty} A_n(\omega) I_{on}(\omega) I_{an}(\omega) \tag{C.30}$$

$$B_{\theta a}(\omega) = -2\rho H^2 \sum_{n=1}^{\infty} A_n(\omega) I_{\theta n}(\omega) I_{an}(\omega) \tag{C.31}$$

$$B_{ik}(\omega) = -2\rho H^2 \sum_{n=1}^{\infty} A_n(\omega) I_{in}(\omega) I_{kn}(\omega) \tag{C.32}$$

where $a = 0, \theta, j$, and i and $k = 1, 2, ...J$. $A_n(\omega)$ is defined as:

$$A_n(\omega) = \frac{\mu_n^2(\omega)}{H[\mu_n^2(\omega) - (\omega q)^2] + i(\omega q)} \frac{1}{\sqrt{\mu_n^2(\omega) - \omega^2/C^2}} \tag{C.33}$$

The hydrodynamic terms associated with vertical ground acceleration are:

$$B_{ay}(\omega) = \rho H A_y(\omega) J_a(\omega) \tag{C.34}$$

where $a = 0, \theta, j$, and:

$$A_y(\omega) = \frac{1}{\frac{\omega H}{C}} \frac{1}{\frac{\cos \omega H}{C} + iqC \frac{\sin \omega H}{C}} \tag{C.35}$$

the coefficients $J_o(\omega)$, $J_\theta(\omega)$, and $J_j(\omega)$ are:

$$J_o(\omega) = \int_0^H \sin \frac{\omega}{C}(H - y) dy \tag{C.36}$$

$$J_\theta(\omega) = \int_0^H h(y) \sin \frac{\omega}{C}(H-y)dy \tag{C.37}$$

$$J_j(\omega) = \int_0^H \Psi_j^x(y) \sin \frac{\omega}{C}(H-y)dy \tag{C.38}$$

As an example, Figure C.1 shows the plots of the response functions B_{00} and B_{y0} for translational rigid body motion due to x- and y-components of ground motion.

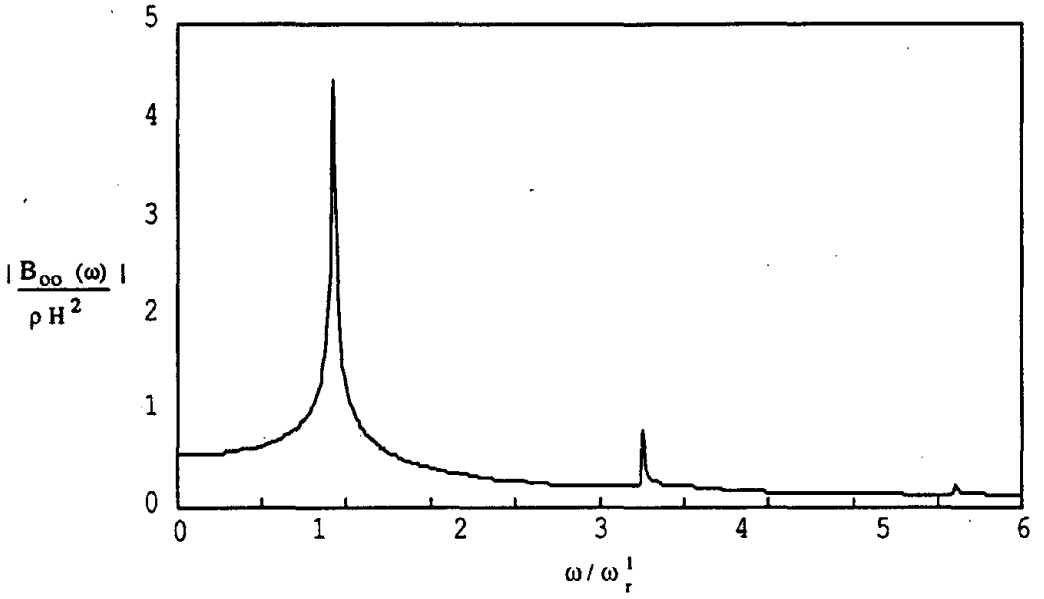

(a) HYDRODYNAMIC FUNCTION ASSOCIATED WITH HORIZONTAL FRRE-FIELD GROUND ACCELERATION

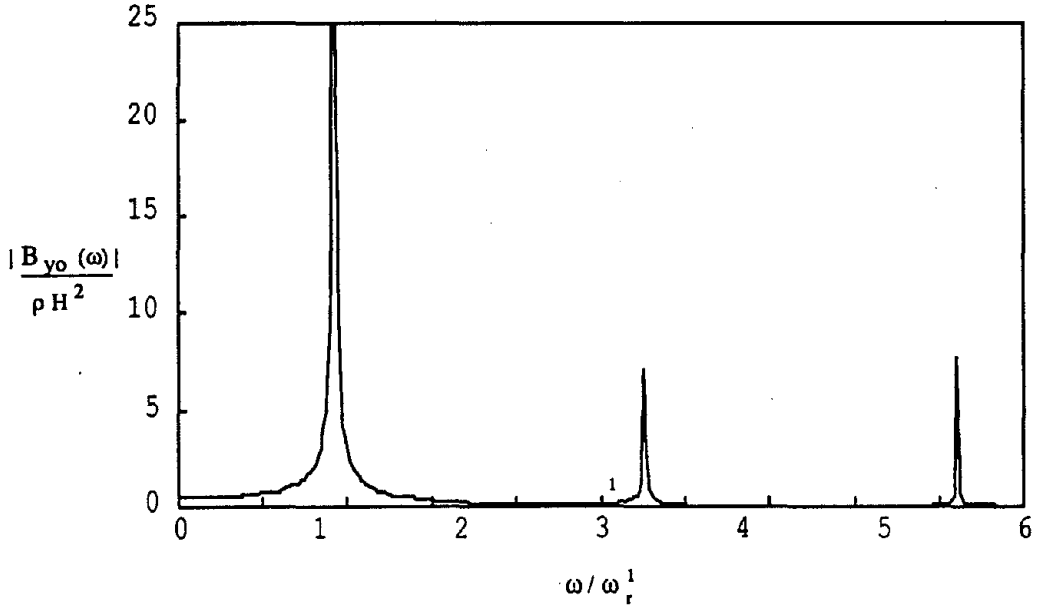

(b) HYDRODYNAMIC FUNCTION ASSOCIATED WITH VERTICAL FREE-FIELD GROUND ACCELERATION

Figure C.1. Frequency-dependent hydrodynamic functions for rigid body motion.

Appendix D

INTERPOLATION OF FREQUENCY RESPONSE FUNCTIONS

The interpolation scheme for the frequency response functions minimizes the storage and computational effort in solving the equations of motion in the frequency domain. The same approach is used for interpolating frequency-dependent hydrodynamic terms.

The interpolation scheme presented in this appendix was developed for soil-structure problems [Tajirian, 1981] and it has been used for dam analysis [Fok and Chopra, 1985]. The frequency response function is divided into frequency ranges with no more than two resonant peaks in each range. An interpolation function based on a two degree-of-freedom system is used to interpolate within a frequency range.

D.1 Formulation of Interpolation Scheme

The frequency domain equations for response to unit harmonic base accelerations at the base of the dam due to horizontal and vertical free-field ground acceleration and base sliding acceleration are:

$$\bar{\mathbf{S}}(\bar{\omega})\bar{\mathbf{Y}}^{l}(\bar{\omega}) = \mathbf{L}^{l}(\bar{\omega}) \qquad l = x, y, s \qquad \text{(D.1)}$$

where $\bar{\mathbf{S}}(\bar{\omega})$ is the dynamic stiffness matrix; and $\bar{\mathbf{Y}}^l(\bar{\omega})$ are the frequency response functions; $\mathbf{L}^l(\bar{\omega})$ are the load vector. Including two modes, a frequency response function, $\bar{Y}_j^l(\bar{\omega})$, can be expressed as:

$$\bar{Y}_j^l(\bar{\omega}) = \frac{C_{1j}\bar{\omega}^2 + C_{2j}}{\bar{\omega}^4 + C_{3j}\bar{\omega}^2 + C_{4j}} \tag{D.2}$$

The constants C_{1j}, C_{2j}, C_{3j} and C_{4j} are determined for each frequency range by solving equation D.2 at four frequencies:

$$\begin{bmatrix} \Omega_1^2 & 1 & -\bar{Y}_{j1}\Omega_1^2 & -\bar{Y}_{j1} \\ \Omega_2^2 & 1 & -\bar{Y}_{j2}\Omega_2^2 & -\bar{Y}_{j2} \\ \Omega_3^2 & 1 & -\bar{Y}_{j3}\Omega_3^2 & -\bar{Y}_{j3} \\ \Omega_4^2 & 1 & -\bar{Y}_{j4}\Omega_4^2 & -\bar{Y}_{j4} \end{bmatrix} \begin{Bmatrix} C_{1j} \\ C_{2j} \\ C_{3j} \\ C_{4j} \end{Bmatrix} = \begin{Bmatrix} \bar{Y}_{j1}\Omega_1^4 \\ \bar{Y}_{j2}\Omega_2^4 \\ \bar{Y}_{j3}\Omega_3^4 \\ \bar{Y}_{j4}\Omega_4^4 \end{Bmatrix} \tag{D.3}$$

where $\bar{Y}_{ji} = \bar{Y}_j(\Omega_i)$ and Ω_i, are selected frequencies within the range. The response for other frequencies within the range is computed from the interpolation function in equation D.2.

D.2 Selection of Frequencies

The frequencies for interpolating the frequency response function are determined as follows [Fok and Chopra, 1985]:

$$(\Delta\bar{\omega})_i = (\Delta\bar{\omega})_{i-1} \frac{b}{max \frac{|\Delta\bar{Y}_{j,i-1}|}{|\bar{Y}_{ji}|}} \tag{D.4}$$

where the recommended values for b, $\Delta\bar{\omega}_{min}$ and $\Delta\bar{\omega}_{max}$ are:

$$b = 0.5 \qquad \Delta\bar{\omega}_{min} = 0.01\omega_f \qquad \Delta\bar{\omega}_{max} = 0.20\omega_f \tag{D.5}$$

and ω_f is computed from:

$$\omega_f = min(\frac{\pi}{2}\frac{C}{H}, \omega_1)$$

in which $\frac{\pi}{2}\frac{C}{H}$ is the fundamental frequency of the impounded water and ω_1 is the fundamental frequency of the dam. In equation D.4, the values of $\Delta\bar{Y}^l_{i-1}$ and $\Delta\bar{Y}^l_{ij}$ are determined for all three components of l. This approximation assumes that the peaks of the frequency response functions due to x-ground acceleration, y-ground acceleration, and sliding acceleration occur at approximately the same frequencies. This is a modification from the original approach, which considers different limits for each component of ground motion.

D.3 Definition of Interpolation Functions

The interpolation procedure is summarized as follows:

1. Initial Computations.

   (a) Determine $\Delta\bar{\omega}_{min}$ and $\Delta\bar{\omega}_{max}$

   (b) Use equation D.1 to evaluate the frequency response function, $\bar{\mathbf{Y}}^l$, for frequencies $\bar{\omega} = 0$ and $\bar{\omega} = \Delta\bar{\omega}_{min}$.

   (c) Initialize: $\bar{\omega}_0 = 0$, $\bar{\omega}_1 = \Delta\bar{\omega}_{min}$

   (d) Initialize counter: $i = 0$

2. Compute response for selected frequencies.

   (a) Increment counter: $i = i + 1$

(b) Use equation D.1 to evaluate next frequency interval, $(\Delta\bar{\omega})_i$, and evaluate current frequency for calculation.

$$\bar{\omega}_i = \bar{\omega}_{i-1} + (\Delta\bar{\omega})_i$$

(c) Solve equation D.1 to determine $Y_{ji}^l(\bar{\omega})$ at that frequency, where $l = x, y, s$.

(d) If $\bar{\omega}_i \leq \bar{\omega}_{max}$ go to step 2b.

(e) if $\bar{\omega}_i > \bar{\omega}_{max}$ go to step 3.

3. Compute interpolation functions:

(a) Maximum number of computed frequency response functions is defined from previous step, $n_{freq} = i$.

(b) Subdivide the frequencies into ranges, each containing at least four computed values of the response. For each range, at frequencies $\bar{\omega}_k$, $\bar{\omega}_{k+1}$, $\bar{\omega}_{k+2}$, $\bar{\omega}_{k+3}$: compute C_{1j}, $j = k, k+1, k+2, k+3$, from equation D.3, and compute interpolated frequencies using equation. D.2.

(c) Repeat 3b for all frequency range, $k + 3 \leq n_{freq}$.

Appendix E

EQUATIONS FOR COMPUTING ENERGY BALANCE

One measure of the damage in a structure is the dissipated energy during an earthquake. This concept and the corresponding energy equations were introduced by Uang and Bertero [1988]. In this appendix, the energy equations are extended for the dam-water-foundation rock system, considering the foundation, hydrodynamic, and sliding effects. The energy balance of the system is also used to verify the accuracy of the solution by the HFTD procedure.

E.1 Equations of Motion for System

The equations of motion for the dam-water-foundation rock system, equations 3.1 and 3.2, can be written as follows:

$$\begin{Bmatrix} \mathbf{M} \\ \mathbf{R}^T\mathbf{M} \end{Bmatrix} \ddot{\mathbf{U}} + \begin{Bmatrix} \mathbf{C} \\ \mathbf{0} \end{Bmatrix} \dot{\mathbf{U}} + \begin{Bmatrix} \mathbf{K} \\ \mathbf{0} \end{Bmatrix} \mathbf{U} + \begin{Bmatrix} \mathbf{MR} \\ \mathbf{M}_t \end{Bmatrix} \ddot{\mathbf{U}}_b + \begin{Bmatrix} \mathbf{0} \\ \mathbf{F}_f(t) \end{Bmatrix} = \begin{Bmatrix} \mathbf{P}(t) \\ \mathbf{R}^T\mathbf{P}(t) \end{Bmatrix} + \begin{Bmatrix} -\mathbf{MR} \\ -\mathbf{M}_t \end{Bmatrix} \ddot{\mathbf{U}}_g(t) \qquad \text{(E.1)}$$

where $\mathbf{U}_b$ is the rigid body displacement of the dam base relative to the free-field ground motion:

$$\mathbf{U}_b = \mathbf{U}_f + \mathbf{T}_\beta \ddot{U}_{s\beta} \qquad \text{(E.2)}$$

The hydrodynamic force can be partitioned as:

$$\mathbf{P}(t) = \mathbf{P}(\ddot{\mathbf{U}}, \ddot{\mathbf{U}}_b) + \mathbf{P}(\ddot{\mathbf{U}}_g) \qquad \text{(E.3)}$$

where $\mathbf{P}(\ddot{\mathbf{U}}, \ddot{\mathbf{U}}_b)$ is the hydrodynamic force due to dam acceleration and base accelerations, and $\mathbf{P}(\ddot{\mathbf{U}}_g)$ is the hydrodynamic force due to the free-field ground acceleration.

E.2 Integration of Equations of Motion

Integrating the equations of motion with respect to dam displacements, $\mathbf{U}$, and base displacements, $\mathbf{U}_b$, and using the partitioned form of $\mathbf{P}(t)$ from equation E.3, gives:

$$\begin{aligned}
&\int_0^t \begin{Bmatrix} \mathbf{M}\ddot{\mathbf{U}} \\ \mathbf{R}^T\mathbf{M}\ddot{\mathbf{U}} \end{Bmatrix}^T d\begin{Bmatrix} \mathbf{U} \\ \mathbf{U}_b \end{Bmatrix} + \int_0^t \begin{Bmatrix} \mathbf{C}\dot{\mathbf{U}} \\ \mathbf{0} \end{Bmatrix}^T d\begin{Bmatrix} \mathbf{U} \\ \mathbf{U}_b \end{Bmatrix} + \int_0^t \begin{Bmatrix} \mathbf{K}\mathbf{U} \\ \mathbf{0} \end{Bmatrix}^T d\begin{Bmatrix} \mathbf{U} \\ \mathbf{U}_b \end{Bmatrix} \\
&\quad + \int_0^t \begin{Bmatrix} \mathbf{M}\mathbf{R}\ddot{\mathbf{U}}_b \\ \mathbf{M}_t\ddot{\mathbf{U}}_b \end{Bmatrix}^T d\begin{Bmatrix} \mathbf{U} \\ \mathbf{U}_b \end{Bmatrix} + \int_0^t \begin{Bmatrix} \mathbf{0} \\ \mathbf{F}_f(t) \end{Bmatrix}^T d\begin{Bmatrix} \mathbf{U} \\ \mathbf{U}_b \end{Bmatrix} \\
&\quad = \int_0^t \begin{Bmatrix} \mathbf{P}(\ddot{\mathbf{U}}, \ddot{\mathbf{U}}_b) \\ \mathbf{R}^T\mathbf{P}(\ddot{\mathbf{U}}, \ddot{\mathbf{U}}_b) \end{Bmatrix}^T d\begin{Bmatrix} \mathbf{U} \\ \mathbf{U}_b \end{Bmatrix} + \int_0^t \begin{Bmatrix} \mathbf{P}(\ddot{\mathbf{U}}_g) \\ \mathbf{R}^T\mathbf{P}(\ddot{\mathbf{U}}_g) \end{Bmatrix}^T d\begin{Bmatrix} \mathbf{U} \\ \mathbf{U}_b \end{Bmatrix} \\
&\quad + \int_0^t \begin{Bmatrix} -\mathbf{M}\mathbf{R}\ddot{\mathbf{U}}_g(t) \\ -\mathbf{M}_t\ddot{\mathbf{U}}_g(t) \end{Bmatrix}^T d\begin{Bmatrix} \mathbf{U} \\ \mathbf{U}_b \end{Bmatrix}
\end{aligned} \tag{E.4}$$

Expressing the dam displacements in terms of the generalized displacements, $\mathbf{U} = \mathbf{\Psi}\mathbf{Z}$ in equation E.4 gives:

$$\begin{aligned}
&\int_0^t \begin{Bmatrix} \mathbf{M}^*\ddot{\mathbf{Z}} \\ \mathbf{L}^T\ddot{\mathbf{Z}} \end{Bmatrix}^T \begin{Bmatrix} d\mathbf{Z} \\ d\mathbf{U}_b \end{Bmatrix} + \int_0^t \begin{Bmatrix} \mathbf{C}^*\dot{\mathbf{Z}} \\ \mathbf{0} \end{Bmatrix}^T \begin{Bmatrix} d\mathbf{Z} \\ d\mathbf{U}_b \end{Bmatrix} + \int_0^t \begin{Bmatrix} \mathbf{K}^*\mathbf{Z} \\ \mathbf{0} \end{Bmatrix}^T \begin{Bmatrix} d\mathbf{Z} \\ d\mathbf{U}_b \end{Bmatrix} \\
&\quad + \int_0^t \begin{Bmatrix} \mathbf{L}\ddot{\mathbf{U}}_b \\ \mathbf{M}_t\ddot{\mathbf{U}}_b \end{Bmatrix}^T \begin{Bmatrix} d\mathbf{Z} \\ d\mathbf{U}_b \end{Bmatrix} + \int_0^t \begin{Bmatrix} \mathbf{0} \\ \mathbf{F}_f(t) \end{Bmatrix}^T \begin{Bmatrix} d\mathbf{Z} \\ d\mathbf{U}_b \end{Bmatrix} \\
&\quad = \int_0^t \begin{Bmatrix} \mathbf{\Psi}\mathbf{P}(\ddot{\mathbf{Z}}, \ddot{\mathbf{U}}_\mathbf{b}) \\ \mathbf{R}^T\mathbf{P}(\ddot{\mathbf{Z}}, \ddot{\mathbf{U}}_b) \end{Bmatrix}^T \begin{Bmatrix} d\mathbf{Z} \\ d\mathbf{U}_b \end{Bmatrix} \int_0^t \begin{Bmatrix} \mathbf{\Psi}\mathbf{P}(\ddot{\mathbf{U}}_\mathbf{g}) \\ \mathbf{R}^T\mathbf{P}(\ddot{\mathbf{U}}_g) \end{Bmatrix}^T \begin{Bmatrix} d\mathbf{Z} \\ d\mathbf{U}_b \end{Bmatrix} \\
&\quad + \int_0^t \begin{Bmatrix} -\mathbf{L}\ddot{\mathbf{U}}_g(t) \\ -\mathbf{M}_t\ddot{\mathbf{U}}_g(t) \end{Bmatrix}^T \begin{Bmatrix} d\mathbf{Z} \\ d\mathbf{U}_b \end{Bmatrix}
\end{aligned} \tag{E.5}$$

Evaluating the matrix inner products in equation E.5 gives the energy balance for the system:

$$\begin{aligned}
&\int_0^t \{\mathbf{M}^*\ddot{\mathbf{Z}}\}^T d\mathbf{Z} + \int_0^t \{\mathbf{L}\ddot{\mathbf{U}}_b\}^T d\mathbf{Z} + \int_0^t \{\mathbf{L}^T\ddot{\mathbf{Z}}\}^T d\mathbf{U}_b + \int_0^t \{\mathbf{M}_t\ddot{\mathbf{U}}_b\}^T d\mathbf{U}_b \\
&\quad + \int_0^t \{\mathbf{C}^*\dot{\mathbf{Z}}\}^T d\mathbf{Z} + \int_0^t \{\mathbf{K}^*\mathbf{Z}\}^T d\mathbf{Z} + \int_0^t \{\mathbf{F}_f(t)\}^T d\mathbf{U}_b \\
&\quad + \int_0^t \{-\mathbf{\Psi}^T\mathbf{P}(\ddot{\mathbf{Z}}, \ddot{\mathbf{U}}_b)\}^T d\mathbf{Z} + \int_0^t \{-\mathbf{R}^T\mathbf{P}(\ddot{\mathbf{Z}}, \ddot{\mathbf{U}}_b)\}^T d\mathbf{U}_b \\
&\quad = \int_0^t \{\mathbf{\Psi}^T\mathbf{P}(\ddot{\mathbf{U}}_g)\}^T d\mathbf{Z} + \int_0^t \{\mathbf{R}^T\mathbf{P}(\ddot{\mathbf{U}}_g)\}^T d\mathbf{U}_b \\
&\quad + \int_0^t -\{\mathbf{L}\ddot{\mathbf{U}}_g(t)\}^T d\mathbf{Z} + \int_0^t -\{\mathbf{M}_t\ddot{\mathbf{U}}_g(t)\}^T d\mathbf{U}_b
\end{aligned} \tag{E.6}$$

E.3 Energy Balance Equation

The energy balance equation is obtained by rearranging equation E.6 to consider the work due to dam deformation, foundation displacement, and sliding displacement, as follows:

$$E_i = E_d + E_f + E_s \tag{E.7}$$

E_i is the input energy due to ground motion. It represents the work done by the forces produced by the free-field ground motion:

$$\begin{aligned}
E_i \;=\; &\int_0^t \{\mathbf{\Psi}^T\mathbf{P}(\ddot{\mathbf{U}}_g)\}^T d\mathbf{Z} + \int_0^t \{\mathbf{R}^T\mathbf{P}(\ddot{\mathbf{U}}_g)\}^T d\mathbf{U}_b \\
&+ \int_0^t -\{\mathbf{L}\ddot{\mathbf{U}}_g(t)\}^T d\mathbf{Z} + \int_0^t -\{\mathbf{M}_t\ddot{\mathbf{U}}_g(t)\}^T d\mathbf{U}_b
\end{aligned} \tag{E.8}$$

E_d represents a number of energy terms in the dam model and impounded water due to deformation of the dam. It contains the conservative kinetic and strain energy in the dam and the work dissipated by hysteretic damping. For convenience, E_d also

contains the work performed by the hydrodynamic forces acting through the dam displacements:

$$\begin{aligned} E_d &= \int_0^t \{\mathbf{M}^*\ddot{\mathbf{Z}}\}^T d\mathbf{Z} + \int_0^t \{\mathbf{L}\ddot{\mathbf{U}}_b\}^T d\mathbf{Z} \\ &+ \int_0^t \{\mathbf{C}^*\dot{\mathbf{Z}}\}^T d\mathbf{Z} + \int_0^t \{\mathbf{K}^*\mathbf{Z}\}^T \, d\mathbf{Z} \\ &+ \int_0^t [-\mathbf{\Psi}^T\mathbf{P}(\ddot{\mathbf{Z}}, \ddot{\mathbf{U}}_b)]^T d\mathbf{Z} \end{aligned} \tag{E.9}$$

E_f is the work performed by the forces acting through the foundation rock displacement:

$$\begin{aligned} E_f &= \int_0^t \{\mathbf{L}^T\ddot{\mathbf{Z}}\}^T d\mathbf{U}_f + \int_0^t \{\mathbf{M}_t\ddot{\mathbf{U}}_b\}^T d\mathbf{U}_f \\ &+ \int_0^t [-\mathbf{R}^T\mathbf{P}(\ddot{\mathbf{Z}}, \ddot{\mathbf{U}}_b)]^T d\mathbf{U}_f + \int_0^t \{\mathbf{F}_f(t)\}^T d\mathbf{U}_f \end{aligned} \tag{E.10}$$

E_s is the energy associated with the sliding displacement at the base of the dam:

$$\begin{aligned} E_s &= \int_0^t \{\mathbf{L}^T\ddot{\mathbf{Z}}\}^T \mathbf{T} dU_{s,\beta} + \int_0^t \{\mathbf{M}_t\ddot{\mathbf{U}}_b\}^T \mathbf{T} dU_{s,\beta} \\ &+ \int_0^t [-\mathbf{R}^T\mathbf{P}(\ddot{\mathbf{Z}}, \ddot{\mathbf{U}}_b)]^T \mathbf{T} \, dU_{s,\beta} + \int_0^t \{\mathbf{F}_f(t)\}^T \mathbf{T} \, dU_{s,\beta} \end{aligned} \tag{E.11}$$

EARTHQUAKE ENGINEERING RESEARCH CENTER REPORT SERIES

EERC reports are available from the National Information Service for Earthquake Engineering (NISEE) and from the National Technical Information Service (NTIS). Numbers in parentheses are Accession Numbers assigned by the National Technical Information Service; these are followed by a price code. Contact NTIS, 5285 Port Royal Road, Springfield Virginia, 22161 for more information. Reports without Accession Numbers were not available from NTIS at the time of printing. For a current complete list of EERC reports (from EERC 67-1) and availablity information, please contact University of California, EERC, NISEE, 1301 South 46th Street, Richmond, California 94804.

UCB/EERC-83/01 "The Economic Feasibility of Seismic Rehabilitation of Buildings by Base Isolation," by Kelly, J.M., January 1983, (PB83 197 988)A05.

UCB/EERC-83/02 "Seismic Moment Connections for Moment-Resisting Steel Frames.," by Popov, E.P., January 1983, (PB83 195 412)A04.

UCB/EERC-83/03 "Design of Links and Beam-to-Column Connections for Eccentrically Braced Steel Frames," by Popov, E.P. and Malley, J.O., January 1983, (PB83 194 811)A04.

UCB/EERC-83/04 "Numerical Techniques for the Evaluation of Soil-Structure Interaction Effects in the Time Domain," by Bayo, E. and Wilson, E.L., February 1983, (PB83 245 605)A09.

UCB/EERC-83/05 "A Transducer for Measuring the Internal Forces in the Columns of a Frame-Wall Reinforced Concrete Structure," by Sause, R. and Bertero, V.V., May 1983, (PB84 119 494)A06.

UCB/EERC-83/06 "Dynamic Interactions Between Floating Ice and Offshore Structures," by Croteau, P., May 1983, (PB84 119 486)A16.

UCB/EERC-83/07 "Dynamic Analysis of Multiply Tuned and Arbitrarily Supported Secondary Systems," by Igusa, T. and Der Kiureghian, A., July 1983, (PB84 118 272)A11.

UCB/EERC-83/08 "A Laboratory Study of Submerged Multi-body Systems in Earthquakes," by Ansari, G.R., June 1983, (PB83 261 842)A17.

UCB/EERC-83/09 "Effects of Transient Foundation Uplift on Earthquake Response of Structures," by Yim, C.-S. and Chopra, A.K., June 1983, (PB83 261 396)A07.

UCB/EERC-83/10 "Optimal Design of Friction-Braced Frames under Seismic Loading," by Austin, M.A. and Pister, K.S., June 1983, (PB84 119 288)A06.

UCB/EERC-83/11 "Shaking Table Study of Single-Story Masonry Houses: Dynamic Performance under Three Component Seismic Input and Recommendations," by Manos, G.C., Clough, R.W. and Mayes, R.L., July 1983, (UCB/EERC-83/11)A08.

UCB/EERC-83/12 "Experimental Error Propagation in Pseudodynamic Testing," by Shing, P.B. and Mahin, S.A., June 1983, (PB84 119 270)A09.

UCB/EERC-83/13 "Experimental and Analytical Predictions of the Mechanical Characteristics of a 1/5-scale Model of a 7-story R/C Frame-Wall Building Structure," by Aktan, A.E., Bertero, V.V., Chowdhury, A.A. and Nagashima, T., June 1983, (PB84 119 213)A07.

UCB/EERC-83/14 "Shaking Table Tests of Large-Panel Precast Concrete Building System Assemblages," by Oliva, M.G. and Clough, R.W., June 1983, (PB86 110 210/AS)A11.

UCB/EERC-83/15 "Seismic Behavior of Active Beam Links in Eccentrically Braced Frames," by Hjelmstad, K.D. and Popov, E.P., July 1983, (PB84 119 676)A09.

UCB/EERC-83/16 "System Identification of Structures with Joint Rotation," by Dimsdale, J.S., July 1983, (PB84 192 210)A06.

UCB/EERC-83/17 "Construction of Inelastic Response Spectra for Single-Degree-of-Freedom Systems," by Mahin, S. and Lin, J., June 1983, (PB84 208 834)A05.

UCB/EERC-83/18 "Interactive Computer Analysis Methods for Predicting the Inelastic Cyclic Behaviour of Structural Sections," by Kaba, S. and Mahin, S., July 1983, (PB84 192 012)A06.

UCB/EERC-83/19 "Effects of Bond Deterioration on Hysteretic Behavior of Reinforced Concrete Joints," by Filippou, F.C., Popov, E.P. and Bertero, V.V., August 1983, (PB84 192 020)A10.

UCB/EERC-83/20 "Correlation of Analytical and Experimental Responses of Large-Panel Precast Building Systems," by Oliva, M.G., Clough, R.W., Velkov, M. and Gavrilovic, P., May 1988, (PB90 262 692)A06.

UCB/EERC-83/21 "Mechanical Characteristics of Materials Used in a 1/5 Scale Model of a 7-Story Reinforced Concrete Test Structure," by Bertero, V.V., Aktan, A.E., Harris, H.G. and Chowdhury, A.A., October 1983, (PB84 193 697)A05.

UCB/EERC-83/22 "Hybrid Modelling of Soil-Structure Interaction in Layered Media," by Tzong, T.-J. and Penzien, J., October 1983, (PB84 192 178)A08.

UCB/EERC-83/23 "Local Bond Stress-Slip Relationships of Deformed Bars under Generalized Excitations," by Eligehausen, R., Popov, E.P. and Bertero, V.V., October 1983, (PB84 192 848)A09.

UCB/EERC-83/24 "Design Considerations for Shear Links in Eccentrically Braced Frames," by Malley, J.O. and Popov, E.P., November 1983, (PB84 192 186)A07.

UCB/EERC-84/01 "Pseudodynamic Test Method for Seismic Performance Evaluation: Theory and Implementation," by Shing, P.-S.B. and Mahin, S.A., January 1984, (PB84 190 644)A08.

UCB/EERC-84/02 "Dynamic Response Behavior of Kiang Hong Dian Dam," by Clough, R.W., Chang, K.-T., Chen, H.-Q. and Stephen, R.M., April 1984, (PB84 209 402)A08.

UCB/EERC-84/03 "Refined Modelling of Reinforced Concrete Columns for Seismic Analysis," by Kaba, S.A. and Mahin, S.A., April 1984, (PB84 234 384)A06.

UCB/EERC-84/04 "A New Floor Response Spectrum Method for Seismic Analysis of Multiply Supported Secondary Systems," by Asfura, A. and Der Kiureghian, A., June 1984, (PB84 239 417)A06.

UCB/EERC-84/05 "Earthquake Simulation Tests and Associated Studies of a 1/5th-scale Model of a 7-Story R/C Frame-Wall Test Structure," by Bertero, V.V., Aktan, A.E., Charney, F.A. and Sause, R., June 1984, (PB84 239 409)A09.

UCB/EERC-84/06 "Unassigned," by Unassigned, 1984.

UCB/EERC-84/07 "Behavior of Interior and Exterior Flat-Plate Connections Subjected to Inelastic Load Reversals," by Zee, H.L. and Moehle, J.P., August 1984, (PB86 117 629/AS)A07.

UCB/EERC-84/08 "Experimental Study of the Seismic Behavior of a Two-Story Flat-Plate Structure," by Moehle, J.P. and Diebold, J.W., August 1984, (PB86 122 553/AS)A12.

UCB/EERC-84/09 "Phenomenological Modeling of Steel Braces under Cyclic Loading," by Ikeda, K., Mahin, S.A. and Dermitzakis, S.N., May 1984, (PB86 132 198/AS)A08.

UCB/EERC-84/10 "Earthquake Analysis and Response of Concrete Gravity Dams," by Fenves, G.L. and Chopra, A.K., August 1984, (PB85 193 902/AS)A11.

UCB/EERC-84/11 "EAGD-84: A Computer Program for Earthquake Analysis of Concrete Gravity Dams," by Fenves, G.L. and Chopra, A.K., August 1984, (PB85 193 613/AS)A05.

UCB/EERC-84/12 "A Refined Physical Theory Model for Predicting the Seismic Behavior of Braced Steel Frames," by Ikeda, K. and Mahin, S.A., July 1984, (PB85 191 450/AS)A09.

UCB/EERC-84/13 "Earthquake Engineering Research at Berkeley - 1984," by EERC, August 1984, (PB85 197 341/AS)A10.

UCB/EERC-84/14 "Moduli and Damping Factors for Dynamic Analyses of Cohesionless Soils," by Seed, H.B., Wong, R.T., Idriss, I.M. and Tokimatsu, K., September 1984, (PB85 191 468/AS)A04.

UCB/EERC-84/15 "The Influence of SPT Procedures in Soil Liquefaction Resistance Evaluations," by Seed, H.B., Tokimatsu, K., Harder, L.F. and Chung, R.M., October 1984, (PB85 191 732/AS)A04.

UCB/EERC-84/16 "Simplified Procedures for the Evaluation of Settlements in Sands Due to Earthquake Shaking," by Tokimatsu, K. and Seed, H.B., October 1984, (PB85 197 887/AS)A03.

UCB/EERC-84/17 "Evaluation of Energy Absorption Characteristics of Highway Bridges Under Seismic Conditions - Volume I (PB90 262 627)A16 and Volume II (Appendices) (PB90 262 635)A13," by Imbsen, R.A. and Penzien, J., September 1986.

UCB/EERC-84/18 "Structure-Foundation Interactions under Dynamic Loads," by Liu, W.D. and Penzien, J., November 1984, (PB87 124 889/AS)A11.

UCB/EERC-84/19 "Seismic Modelling of Deep Foundations," by Chen, C.-H. and Penzien, J., November 1984, (PB87 124 798/AS)A07.

UCB/EERC-84/20 "Dynamic Response Behavior of Quan Shui Dam," by Clough, R.W., Chang, K.-T., Chen, H.-Q., Stephen, R.M., Ghanaat, Y. and Qi, J.-H., November 1984, (PB86 115177/AS)A07.

UCB/EERC-85/01 "Simplified Methods of Analysis for Earthquake Resistant Design of Buildings," by Cruz, E.F. and Chopra, A.K., February 1985, (PB86 112299/AS)A12.

UCB/EERC-85/02 "Estimation of Seismic Wave Coherency and Rupture Velocity using the SMART 1 Strong-Motion Array Recordings," by Abrahamson, N.A., March 1985, (PB86 214 343)A07.

UCB/EERC-85/03 "Dynamic Properties of a Thirty Story Condominium Tower Building," by Stephen, R.M., Wilson, E.L. and Stander, N., April 1985, (PB86 118965/AS)A06.

UCB/EERC-85/04 "Development of Substructuring Techniques for On-Line Computer Controlled Seismic Performance Testing," by Dermitzakis, S. and Mahin, S., February 1985, (PB86 132941/AS)A08.

UCB/EERC-85/05 "A Simple Model for Reinforcing Bar Anchorages under Cyclic Excitations," by Filippou, F.C., March 1985, (PB86 112 919/AS)A05.

UCB/EERC-85/06 "Racking Behavior of Wood-framed Gypsum Panels under Dynamic Load," by Oliva, M.G., June 1985, (PB90 262 643)A04.

UCB/EERC-85/07 "Earthquake Analysis and Response of Concrete Arch Dams," by Fok, K.-L. and Chopra, A.K., June 1985, (PB86 139672/AS)A10.

UCB/EERC-85/08 "Effect of Inelastic Behavior on the Analysis and Design of Earthquake Resistant Structures," by Lin, J.P. and Mahin, S.A., June 1985, (PB86 135340/AS)A08.

UCB/EERC-85/09 "Earthquake Simulator Testing of a Base-Isolated Bridge Deck," by Kelly, J.M., Buckle, I.G. and Tsai, H.-C., January 1986, (PB87 124 152/AS)A06.

UCB/EERC-85/10 "Simplified Analysis for Earthquake Resistant Design of Concrete Gravity Dams," by Fenves, G.L. and Chopra, A.K., June 1986, (PB87 124 160/AS)A08.

UCB/EERC-85/11 "Dynamic Interaction Effects in Arch Dams," by Clough, R.W., Chang, K.-T., Chen, H.-Q. and Ghanaat, Y., October 1985, (PB86 135027/AS)A05.

UCB/EERC-85/12 "Dynamic Response of Long Valley Dam in the Mammoth Lake Earthquake Series of May 25-27, 1980," by Lai, S. and Seed, H.B., November 1985, (PB86 142304/AS)A05.

UCB/EERC-85/13 "A Methodology for Computer-Aided Design of Earthquake-Resistant Steel Structures," by Austin, M.A., Pister, K.S. and Mahin, S.A., December 1985, (PB86 159480/AS)A10 .

UCB/EERC-85/14 "Response of Tension-Leg Platforms to Vertical Seismic Excitations," by Liou, G.-S., Penzien, J. and Yeung, R.W., December 1985, (PB87 124 871/AS)A08.

UCB/EERC-85/15 "Cyclic Loading Tests of Masonry Single Piers: Volume 4 - Additional Tests with Height to Width Ratio of 1," by Sveinsson, B., McNiven, H.D. and Sucuoglu, H., December 1985, (PB87 165031/AS)A08.

UCB/EERC-85/16 "An Experimental Program for Studying the Dynamic Response of a Steel Frame with a Variety of Infill Partitions," by Yanev, B. and McNiven, H.D., December 1985, (PB90 262 676)A05.

UCB/EERC-86/01 "A Study of Seismically Resistant Eccentrically Braced Steel Frame Systems," by Kasai, K. and Popov, E.P., January 1986, (PB87 124 178/AS)A14.

UCB/EERC-86/02 "Design Problems in Soil Liquefaction," by Seed, H.B., February 1986, (PB87 124 186/AS)A03.

UCB/EERC-86/03 "Implications of Recent Earthquakes and Research on Earthquake-Resistant Design and Construction of Buildings," by Bertero, V.V., March 1986, (PB87 124 194/AS)A05.

UCB/EERC-86/04 "The Use of Load Dependent Vectors for Dynamic and Earthquake Analyses," by Leger, P., Wilson, E.L. and Clough, R.W., March 1986, (PB87 124 202/AS)A12.

UCB/EERC-86/05 "Two Beam-To-Column Web Connections," by Tsai, K.-C. and Popov, E.P., April 1986, (PB87 124 301/AS)A04.

UCB/EERC-86/06 "Determination of Penetration Resistance for Coarse-Grained Soils using the Becker Hammer Drill," by Harder, L.F. and Seed, H.B., May 1986, (PB87 124 210/AS)A07.

UCB/EERC-86/07 "A Mathematical Model for Predicting the Nonlinear Response of Unreinforced Masonry Walls to In-Plane Earthquake Excitations," by Mengi, Y. and McNiven, H.D., May 1986, (PB87 124 780/AS)A06.

UCB/EERC-86/08 "The 19 September 1985 Mexico Earthquake: Building Behavior," by Bertero, V.V., July 1986.

UCB/EERC-86/09 "EACD-3D: A Computer Program for Three-Dimensional Earthquake Analysis of Concrete Dams," by Fok, K.-L., Hall, J.F. and Chopra, A.K., July 1986, (PB87 124 228/AS)A08.

UCB/EERC-86/10 "Earthquake Simulation Tests and Associated Studies of a 0.3-Scale Model of a Six-Story Concentrically Braced Steel Structure," by Uang, C.-M. and Bertero, V.V., December 1986, (PB87 163 564/AS)A17.

UCB/EERC-86/11 "Mechanical Characteristics of Base Isolation Bearings for a Bridge Deck Model Test," by Kelly, J.M., Buckle, I.G. and Koh, C.-G., November 1987, (PB90 262 668)A04.

UCB/EERC-86/12 "Effects of Axial Load on Elastomeric Isolation Bearings," by Koh, C.-G. and Kelly, J.M., November 1987.

UCB/EERC-87/01 "The FPS Earthquake Resisting System: Experimental Report," by Zayas, V.A., Low, S.S. and Mahin, S.A., June 1987, (PB88 170 287)A06.

UCB/EERC-87/02 "Earthquake Simulator Tests and Associated Studies of a 0.3-Scale Model of a Six-Story Eccentrically Braced Steel Structure," by Whittaker, A., Uang, C.-M. and Bertero, V.V., July 1987, (PB88 166 707/AS)A18.

UCB/EERC-87/03 "A Displacement Control and Uplift Restraint Device for Base-Isolated Structures," by Kelly, J.M., Griffith, M.C. and Aiken, I.D., April 1987, (PB88 169 933)A04.

UCB/EERC-87/04 "Earthquake Simulator Testing of a Combined Sliding Bearing and Rubber Bearing Isolation System," by Kelly, J.M. and Chalhoub, M.S., December 1990.

UCB/EERC-87/05 "Three-Dimensional Inelastic Analysis of Reinforced Concrete Frame-Wall Structures," by Moazzami, S. and Bertero, V.V., May 1987, (PB88 169 586/AS)A08.

UCB/EERC-87/06 "Experiments on Eccentrically Braced Frames with Composite Floors," by Ricles, J. and Popov, E., June 1987, (PB88 173 067/AS)A14.

UCB/EERC-87/07 "Dynamic Analysis of Seismically Resistant Eccentrically Braced Frames," by Ricles, J. and Popov, E., June 1987, (PB88 173 075/AS)A16.

UCB/EERC-87/08 "Undrained Cyclic Triaxial Testing of Gravels-The Effect of Membrane Compliance," by Evans, M.D. and Seed, H.B., July 1987, (PB88 173 257)A19.

UCB/EERC-87/09 "Hybrid Solution Techniques for Generalized Pseudo-Dynamic Testing," by Thewalt, C. and Mahin, S.A., July 1987, (PB 88 179 007)A07.

UCB/EERC-87/10 "Ultimate Behavior of Butt Welded Splices in Heavy Rolled Steel Sections," by Bruneau, M., Mahin, S.A. and Popov, E.P., September 1987, (PB90 254 285)A07.

UCB/EERC-87/11 "Residual Strength of Sand from Dam Failures in the Chilean Earthquake of March 3, 1985," by De Alba, P., Seed, H.B., Retamal, E. and Seed, R.B., September 1987, (PB88 174 321/AS)A03.

UCB/EERC-87/12 "Inelastic Seismic Response of Structures with Mass or Stiffness Eccentricities in Plan," by Bruneau, M. and Mahin, S.A., September 1987, (PB90 262 650/AS)A14.

UCB/EERC-87/13 "CSTRUCT: An Interactive Computer Environment for the Design and Analysis of Earthquake Resistant Steel Structures," by Austin, M.A., Mahin, S.A. and Pister, K.S., September 1987, (PB88 173 339/AS)A06.

UCB/EERC-87/14 "Experimental Study of Reinforced Concrete Columns Subjected to Multi-Axial Loading," by Low, S.S. and Moehle, J.P., September 1987, (PB88 174 347/AS)A07.

UCB/EERC-87/15 "Relationships between Soil Conditions and Earthquake Ground Motions in Mexico City in the Earthquake of Sept. 19, 1985," by Seed, H.B., Romo, M.P., Sun, J., Jaime, A. and Lysmer, J., October 1987, (PB88 178 991)A06.

UCB/EERC-87/16 "Experimental Study of Seismic Response of R. C. Setback Buildings," by Shahrooz, B.M. and Moehle, J.P., October 1987, (PB88 176 359)A16.

UCB/EERC-87/17 "The Effect of Slabs on the Flexural Behavior of Beams," by Pantazopoulou, S.J. and Moehle, J.P., October 1987, (PB90 262 700)A07.

UCB/EERC-87/18 "Design Procedure for R-FBI Bearings," by Mostaghel, N. and Kelly, J.M., November 1987, (PB90 262 718)A04.

UCB/EERC-87/19 "Analytical Models for Predicting the Lateral Response of R C Shear Walls: Evaluation of their Reliability," by Vulcano, A. and Bertero, V.V., November 1987, (PB88 178 983)A05.

UCB/EERC-87/20 "Earthquake Response of Torsionally-Coupled Buildings," by Hejal, R. and Chopra, A.K., December 1987.

UCB/EERC-87/21 "Dynamic Reservoir Interaction with Monticello Dam," by Clough, R.W., Ghanaat, Y. and Qiu, X-F., December 1987, (PB88 179 023)A07.

UCB/EERC-87/22 "Strength Evaluation of Coarse-Grained Soils," by Siddiqi, F.H., Seed, R.B., Chan, C.K., Seed, H.B. and Pyke, R.M., December 1987, (PB88 179 031)A04.

UCB/EERC-88/01 "Seismic Behavior of Concentrically Braced Steel Frames," by Khatib, I., Mahin, S.A. and Pister, K.S., January 1988, (PB91 210 898/AS)A11.

UCB/EERC-88/02 "Experimental Evaluation of Seismic Isolation of Medium-Rise Structures Subject to Uplift," by Griffith, M.C., Kelly, J.M., Coveney, V.A. and Koh, C.G., January 1988, (PB91 217 950/AS)A09.

UCB/EERC-88/03 "Cyclic Behavior of Steel Double Angle Connections," by Astaneh-Asl, A. and Nader, M.N., January 1988, (PB91 210 872)A05.

UCB/EERC-88/04 "Re-evaluation of the Slide in the Lower San Fernando Dam in the Earthquake of Feb. 9, 1971," by Seed, H.B., Seed, R.B., Harder, L.F. and Jong, H.-L., April 1988, (PB91 212 456/AS)A07.

UCB/EERC-88/05 "Experimental Evaluation of Seismic Isolation of a Nine-Story Braced Steel Frame Subject to Uplift," by Griffith, M.C., Kelly, J.M. and Aiken, I.D., May 1988, (PB91 217 968/AS)A07.

UCB/EERC-88/06 "DRAIN-2DX User Guide.," by Allahabadi, R. and Powell, G.H., March 1988, (PB91 212 530)A12.

UCB/EERC-88/07 "Theoretical and Experimental Studies of Cylindrical Water Tanks in Base-Isolated Structures," by Chalhoub, M.S. and Kelly, J.M., April 1988, (PB91 217 976/AS)A05.

UCB/EERC-88/08 "Analysis of Near-Source Waves: Separation of Wave Types Using Strong Motion Array Recording," by Darragh, R.B., June 1988, (PB91 212 621)A08.

UCB/EERC-88/09 "Alternatives to Standard Mode Superposition for Analysis of Non-Classically Damped Systems," by Kusainov, A.A. and Clough, R.W., June 1988, (PB91 217 992/AS)A04.

UCB/EERC-88/10 "The Landslide at the Port of Nice on October 16, 1979," by Seed, H.B., Seed, R.B., Schlosser, F., Blondeau, F. and Juran, I., June 1988, (PB91 210 914)A05.

UCB/EERC-88/11 "Liquefaction Potential of Sand Deposits Under Low Levels of Excitation," by Carter, D.P. and Seed, H.B., August 1988, (PB91 210 880)A15.

UCB/EERC-88/12 "Nonlinear Analysis of Reinforced Concrete Frames Under Cyclic Load Reversals," by Filippou, F.C. and Issa, A., September 1988, (PB91 212 589)A07.

UCB/EERC-88/13 "Implications of Recorded Earthquake Ground Motions on Seismic Design of Building Structures," by Uang, C.-M. and Bertero, V.V., November 1988, (PB91 212 548)A06.

UCB/EERC-88/14 "An Experimental Study of the Behavior of Dual Steel Systems," by Whittaker, A.S. , Uang, C.-M. and Bertero, V.V., September 1988, (PB91 212 712)A16.

UCB/EERC-88/15 "Dynamic Moduli and Damping Ratios for Cohesive Soils," by Sun, J.I., Golesorkhi, R. and Seed, H.B., August 1988, (PB91 210 922)A04.

UCB/EERC-88/16 "Reinforced Concrete Flat Plates Under Lateral Load: An Experimental Study Including Biaxial Effects," by Pan, A. and Moehle, J.P., October 1988, (PB91 210 856)A13.

UCB/EERC-88/17 "Earthquake Engineering Research at Berkeley - 1988," by EERC, November 1988, (PB91 210 864)A10.

UCB/EERC-88/18 "Use of Energy as a Design Criterion in Earthquake-Resistant Design," by Uang, C.-M. and Bertero, V.V., November 1988, (PB91 210 906/AS)A04.

UCB/EERC-88/19 "Steel Beam-Column Joints in Seismic Moment Resisting Frames," by Tsai, K.-C. and Popov, E.P., November 1988, (PB91 217 984/AS)A20.

UCB/EERC-88/20 "Base Isolation in Japan, 1988," by Kelly, J.M., December 1988, (PB91 212 449)A05.

UCB/EERC-89/01 "Behavior of Long Links in Eccentrically Braced Frames," by Engelhardt, M.D. and Popov, E.P., January 1989, (PB92 143 056)A18.

UCB/EERC-89/02 "Earthquake Simulator Testing of Steel Plate Added Damping and Stiffness Elements," by Whittaker, A., Bertero, V.V., Alonso, J. and Thompson, C., January 1989, (PB91 229 252/AS)A10.

UCB/EERC-89/03 "Implications of Site Effects in the Mexico City Earthquake of Sept. 19, 1985 for Earthquake-Resistant Design Criteria in the San Francisco Bay Area of California," by Seed, H.B. and Sun, J.I., March 1989, (PB91 229 369/AS)A07.

UCB/EERC-89/04 "Earthquake Analysis and Response of Intake-Outlet Towers," by Goyal, A. and Chopra, A.K., July 1989, (PB91 229 286/AS)A19.

UCB/EERC-89/05 "The 1985 Chile Earthquake: An Evaluation of Structural Requirements for Bearing Wall Buildings," by Wallace, J.W. and Moehle, J.P., July 1989, (PB91 218 008/AS)A13.

UCB/EERC-89/06 "Effects of Spatial Variation of Ground Motions on Large Multiply-Supported Structures," by Hao, H., July 1989, (PB91 229 161/AS)A08.

UCB/EERC-89/07 "EADAP - Enhanced Arch Dam Analysis Program: Users's Manual," by Ghanaat, Y. and Clough, R.W., August 1989, (PB91 212 522)A06.

UCB/EERC-89/08 "Seismic Performance of Steel Moment Frames Plastically Designed by Least Squares Stress Fields," by Ohi, K. and Mahin, S.A., August 1989, (PB91 212 597)A05.

UCB/EERC-89/09 "Feasibility and Performance Studies on Improving the Earthquake Resistance of New and Existing Buildings Using the Friction Pendulum System," by Zayas, V., Low, S., Mahin, S.A. and Bozzo, L., July 1989, (PB92 143 064)A14.

UCB/EERC-89/10 "Measurement and Elimination of Membrane Compliance Effects in Undrained Triaxial Testing," by Nicholson, P.G., Seed, R.B. and Anwar, H., September 1989, (PB92 139 641/AS)A13.

UCB/EERC-89/11 "Static Tilt Behavior of Unanchored Cylindrical Tanks," by Lau, D.T. and Clough, R.W., September 1989, (PB92 143 049)A10.

UCB/EERC-89/12 "ADAP-88: A Computer Program for Nonlinear Earthquake Analysis of Concrete Arch Dams," by Fenves, G.L., Mojtahedi, S. and Reimer, R.B., September 1989, (PB92 139 674/AS)A07.

UCB/EERC-89/13 "Mechanics of Low Shape Factor Elastomeric Seismic Isolation Bearings," by Aiken, I.D., Kelly, J.M. and Tajirian, F.F., November 1989, (PB92 139 732/AS)A09.

UCB/EERC-89/14 "Preliminary Report on the Seismological and Engineering Aspects of the October 17, 1989 Santa Cruz (Loma Prieta) Earthquake," by EERC, October 1989, (PB92 139 682/AS)A04.

UCB/EERC-89/15 "Experimental Studies of a Single Story Steel Structure Tested with Fixed, Semi-Rigid and Flexible Connections," by Nader, M.N. and Astaneh-Asl, A., August 1989, (PB91 229 211/AS)A10.

UCB/EERC-89/16 "Collapse of the Cypress Street Viaduct as a Result of the Loma Prieta Earthquake," by Nims, D.K., Miranda, E., Aiken, I.D., Whittaker, A.S. and Bertero, V.V., November 1989, (PB91 217 935/AS)A05.

UCB/EERC-90/01 "Mechanics of High-Shape Factor Elastomeric Seismic Isolation Bearings," by Kelly, J.M., Aiken, I.D. and Tajirian, F.F., March 1990.

UCB/EERC-90/02 "Javid's Paradox: The Influence of Preform on the Modes of Vibrating Beams," by Kelly, J.M., Sackman, J.L. and Javid, A., May 1990, (PB91 217 943/AS)A03.

UCB/EERC-90/03 "Earthquake Simulator Testing and Analytical Studies of Two Energy-Absorbing Systems for Multistory Structures," by Aiken, I.D. and Kelly, J.M., October 1990, (PB92 192 988)A13.

UCB/EERC-90/04 "Damage to the San Francisco-Oakland Bay Bridge During the October 17, 1989 Earthquake," by Astaneh-Asl, A., June 1990.

UCB/EERC-90/05 "Preliminary Report on the Principal Geotechnical Aspects of the October 17, 1989 Loma Prieta Earthquake," by Seed, R.B., Dickenson, S.E., Riemer, M.F., Bray, J.D., Sitar, N., Mitchell, J.K., Idriss, I.M., Kayen, R.E., Kropp, A., Harder, L.F., Jr. and Power, M.S., April 1990, (PB 192 970)A08.

UCB/EERC-90/06 "Models of Critical Regions in Reinforced Concrete Frames Under Seismic Excitations," by Zulfiqar, N. and Filippou, F.C., May 1990.

UCB/EERC-90/07 "A Unified Earthquake-Resistant Design Method for Steel Frames Using ARMA Models," by Takewaki, I., Conte, J.P., Mahin, S.A. and Pister, K.S., June 1990.

UCB/EERC-90/08 "Soil Conditions and Earthquake Hazard Mitigation in the Marina District of San Francisco," by Mitchell, J.K., Masood, T., Kayen, R.E. and Seed, R.B., May 1990. (PB 193 267/AS)A04.

UCB/EERC-90/09 "Influence of the Earthquake Ground Motion Process and Structural Properties on Response Characteristics of Simple Structures," by Conte, J.P., Pister, K.S. and Mahin, S.A., July 1990, (PB92 143 064)A15.

UCB/EERC-90/10 "Experimental Testing of the Resilient-Friction Base Isolation System," by Clark, P.W. and Kelly, J.M., July 1990, (PB92 143 072)A08.

UCB/EERC-90/11 "Seismic Hazard Analysis: Improved Models, Uncertainties and Sensitivities," by Araya, R. and Der Kiureghian, A., March 1988.

UCB/EERC-90/12 "Effects of Torsion on the Linear and Nonlinear Seismic Response of Structures," by Sedarat, H. and Bertero, V.V., September 1989, (PB92 193 002/AS)A15.

UCB/EERC-90/13 "The Effects of Tectonic Movements on Stresses and Deformations in Earth Embankments," by Bray, J. D., Seed, R. B. and Seed, H. B., September 1989.

UCB/EERC-90/14 "Inelastic Seismic Response of One-Story, Asymmetric-Plan Systems," by Goel, R.K. and Chopra, A.K., October 1990, (PB93 114 767)A11.

UCB/EERC-90/15 "Dynamic Crack Propagation: A Model for Near-Field Ground Motion.," by Seyyedian, H. and Kelly, J.M., 1990.

UCB/EERC-90/16 "Sensitivity of Long-Period Response Spectra to System Initial Conditions," by Blasquez, R., Ventura, C. and Kelly, J.M., 1990.

UCB/EERC-90/17 "Behavior of Peak Values and Spectral Ordinates of Near-Source Strong Ground-Motion over a Dense Array," by Niazi, M., June 1990, (PB93 114 833)A07.

UCB/EERC-90/18 "Material Characterization of Elastomers used in Earthquake Base Isolation," by Papoulia, K.D. and Kelly, J.M., 1990.

UCB/EERC-90/19 "Cyclic Behavior of Steel Top-and-Bottom Plate Moment Connections," by Harriott, J.D. and Astaneh-Asl, A., August 1990, (PB91 229 260/AS)A05.

UCB/EERC-90/20 "Seismic Response Evaluation of an Instrumented Six Story Steel Building," by Shen, J.-H. and Astaneh-Asl, A., December 1990, (PB91 229 294/AS)A04.

UCB/EERC-90/21 "Observations and Implications of Tests on the Cypress Street Viaduct Test Structure," by Bollo, M., Mahin, S.A., Moehle, J.P., Stephen, R.M. and Qi, X., December 1990, (PB93 114 775)A13.

UCB/EERC-91/01 "Experimental Evaluation of Nitinol for Energy Dissipation in Structures," by Nims, D.K., Sasaki, K.K. and Kelly, J.M., 1991.

UCB/EERC-91/02 "Displacement Design Approach for Reinforced Concrete Structures Subjected to Earthquakes," by Qi, X. and Moehle, J.P., January 1991, (PB93 114 569/AS)A09.

UCB/EERC-91/03 "A Long-Period Isolation System Using Low-Modulus High-Damping Isolators for Nuclear Facilities at Soft-Soil Sites," by Kelly, J.M., March 1991, (PB93 114 577/AS)A10.

UCB/EERC-91/04 "Dynamic and Failure Characteristics of Bridgestone Isolation Bearings," by Kelly, J.M., April 1991, (PB93 114 528)A05.

UCB/EERC-91/05 "Base Sliding Response of Concrete Gravity Dams to Earthquakes," by Chopra, A.K. and Zhang, L., May 1991, (PB93 114 544/AS)A05.

UCB/EERC-91/06 "Computation of Spatially Varying Ground Motion and Foundation-Rock Impedance Matrices for Seismic Analysis of Arch Dams," by Zhang, L. and Chopra, A.K., May 1991, (PB93 114 825)A07.

UCB/EERC-91/07 "Estimation of Seismic Source Processes Using Strong Motion Array Data," by Chiou, S.-J., July 1991, (PB93 114 551/AS)A08.

UCB/EERC-91/08 "A Response Spectrum Method for Multiple-Support Seismic Excitations," by Der Kiureghian, A. and Neuenhofer, A., August 1991, (PB93 114 536)A04.

UCB/EERC-91/09 "A Preliminary Study on Energy Dissipating Cladding-to-Frame Connection," by Cohen, J.M. and Powell, G.H., September 1991, (PB93 114 510)A05.

UCB/EERC-91/10 "Evaluation of Seismic Performance of a Ten-Story RC Building During the Whittier Narrows Earthquake," by Miranda, E. and Bertero, V.V., October 1991, (PB93 114 783)A06.

UCB/EERC-91/11 "Seismic Performance of an Instrumented Six-Story Steel Building," by Anderson, J.C. and Bertero, V.V., November 1991, (PB93 114 809)A07.

UCB/EERC-91/12 "Performance of Improved Ground During the Loma Prieta Earthquake," by Mitchell, J.K. and Wentz, Jr., F.J., October 1991, (PB93 114 791)A06.

UCB/EERC-91/13 "Shaking Table - Structure Interaction," by Rinawi, A.M. and Clough, R.W., October 1991, (PB93 114 917)A13.

UCB/EERC-91/14 "Cyclic Response of RC Beam-Column Knee Joints: Test and Retrofit," by Mazzoni, S., Moehle, J.P. and Thewalt, C.R., October 1991, (PB93 120 277)A03.

UCB/EERC-91/15 "Design Guidelines for Ductility and Drift Limits: Review of State-of-the-Practice and State-of-the-Art in Ductility and Drift-Based Earthquake-Resistant Design of Buildings," by Bertero, V.V., Anderson, J.C., Krawinkler, H., Miranda, E. and The CUREe and The Kajima Research Teams, July 1991, (PB93 120 269)A08.

UCB/EERC-91/16 "Evaluation of the Seismic Performance of a Thirty-Story RC Building," by Anderson, J.C., Miranda, E., Bertero, V.V. and The Kajima Project Research Team, July 1991, (PB93 114 841)A12.

UCB/EERC-91/17 "A Fiber Beam-Column Element for Seismic Response Analysis of Reinforced Concrete Structures," by Taucer, F., Spacone, E. and Filippou, F.C., December 1991.

UCB/EERC-91/18 "Investigation of the Seismic Response of a Lightly-Damped Torsionally-Coupled Building," by Boroschek, R. and Mahin, S.A., December 1991, (PB93 120 335)A13.

UCB/EERC-92/01 "Studies of a 49-Story Instrumented Steel Structure Shaken During the Loma Prieta Earthquake," by Chen, C.-C., Bonowitz, D. and Astaneh-Asl, A., February 1992, (PB93 221 778)A08.

UCB/EERC-92/02 "Response of the Dumbarton Bridge in the Loma Prieta Earthquake," by Fenves, G.L., Filippou, F.C. and Sze, D.T., January 1992, (PB93 120 319)A09.

UCB/EERC-92/03 "Models for Nonlinear Earthquake Analysis of Brick Masonry Buildings," by Mengi, Y., McNiven, H.D. and Tanrikulu, A.K., March 1992, (PB93 120 293)A08.

UCB/EERC-92/04 "Shear Strength and Deformability of RC Bridge Columns Subjected to Inelastic Cyclic Displacements," by Aschheim, M. and Moehle, J.P., March 1992, (PB93 120 327)A06.

UCB/EERC-92/05 "Parameter Study of Joint Opening Effects on Earthquake Response of Arch Dams," by Fenves, G.L., Mojtahedi, S. and Reimer, R.B., April 1992, (PB93 120 301)A04.

UCB/EERC-92/06 "Seismic Behavior and Design of Semi-Rigid Steel Frames," by Nader, M.N. and Astaneh-Asl, A., May 1992.

UCB/EERC-92/07 "A Beam Element for Seismic Damage Analysis," by Spacone, E., Ciampi, V. and Filippou, F.C., August 1992.

UCB/EERC-92/08 "Nonlinear Static and Dynamic Analysis of Reinforced Concrete Subassemblages," by Filippou, F.C., D'Ambrisi, A. and Issa, A., August 1992.

UCB/EERC-92/09 "Evaluation of Code Accidental-Torsion Provisions Using Earthquake Records from Three Nominally Symmetric-Plan Buildings," by De la Llera, J.C. and Chopra, A.K., September 1992, (PB94 117 611)A08.

UCB/EERC-92/10 "Slotted Bolted Connection Energy Dissipators," by Grigorian, C.E., Yang, T.-S. and Popov, E.P., July 1992, (PB92 120 285)A03.

UCB/EERC-92/11 "Mechanical Characteristics of Neoprene Isolation Bearings," by Kelly, J.M. and Quiroz, E., August 1992, (PB93 221 729)A07.

UCB/EERC-92/12 "Application of a Mass Damping System to Bridge Structures," by Hasegawa, K. and Kelly, J.M., August 1992, (PB93 221 786)A06.

UCB/EERC-92/13 "Earthquake Engineering Research at Berkeley - 1992," by EERC, October 1992.

UCB/EERC-92/14 "Earthquake Risk and Insurance," by Brillinger, D.R., October 1992, (PB93 223 352)A03.

UCB/EERC-92/15 "A Friction Mass Damper for Vibration Control," by Inaudi, J.A. and Kelly, J.M., October 1992, (PB93 221 745)A04.

UCB/EERC-92/16 "Tall Reinforced Concrete Buildings: Conceptual Earthquake-Resistant Design Methology," by Bertero, R.D. and Bertero, V.V., December 1992, (PB93 221 695)A12.

UCB/EERC-92/17 "Performance of Tall Buildings During the 1985 Mexico Earthquakes," by Terán-Gilmore, A. and Bertero, V.V., December 1992, (PB93 221 737)A11.

UCB/EERC-92/18 "Dynamic Analysis of Nonlinear Structures using State-Space Formulation and Partitioned Integration Schemes," by Inaudi, J.A. and De la Llera, J.C., December 1992.

UCB/EERC-93/01 "Seismic Performance of an Instrumented Six-Story Reinforced-Concrete Building," by Anderson, J.C. and Bertero, V.V., 1993.

UCB/EERC-93/02 "Evaluation of an Active Variable-Damping-Structure," by Polak, E., Meeker, G., Yamada, K. and Kurata, N., 1993, (PB93 221 711)A05.

UCB/EERC-93/03 "An Experimental Study of Flat-Plate Structures under Vertical and Lateral Loads," by Hwang, S.-H. and Moehle, J.P., February 1993.

UCB/EERC-93/04 "Seismic Performance of a 30-Story Building Located on Soft Soil and Designed According to UBC 1991," by Terán-Gilmore, A. and Bertero, V.V., 1993, (PB93 221 703)A17.

UCB/EERC-93/05 "Multiple-Support Response Spectrum Analysis of the Golden Gate Bridge," by Nakamura, Y., Der Kiureghian, A. and Liu, D., May 1993, (PB93 221 752)A05.

UCB/EERC-93/06 "On the Analysis of Structures with Viscoelastic Dampers," by Inaudi, J.A., Zambrano, A. and Kelly, J.M., August 1993.

UCB/EERC-93/07 "Earthquake Analysis and Response of Concrete Gravity Dams Including Base Sliding," by Chávez, J.W. and Fenves, G.L., December 1993.

UCB/EERC-93/08 "Model for Anchored Reinforcing Bars under Seismic Excitations," by Monti, G., Spacone, E. and Filippou, F.C., December 1993.

UCB/EERC-94/01 "Preliminary Report on the Seismological and Engineering Aspects of the January 17, 1994 Northridge Earthquake," by EERC, January 1994.